Aix*Marseille université
Socialement engagée

NNT : 0000AIXM0000

THÈSE DE DOCTORAT

Soutenue à Aix-Marseille Université
le 18 octobre 2024 par

Vinicius LIMA CORDEIRO

Emergence auto-organisée du traitement distribué de l'information chez les primates non-humains

Self-organized emergence of distributed information processing in non-human primates

Discipline
Biologie santé

Spécialité
Neurosciences

École doctorale
Sciences de la vie et de la santé / ED 62

Laboratoire/Partenaires de recherche
Institut de Neurosciences des Systèmes
Institut de Neurosciences de la Timone

Composition du jury

Emmanuel PROCYK INSERM, Lyon	Rapporteur
Martin VINCK Ernst Strüngmann Institute, Francfort, Allemagne	Rapporteur
Kari HOFFMAN Vanderbilt University, Nashville, États-Unis	Examinatrice
Laurent PERRINET Aix-Marseille Université	Président du jury
Andrea BROVELLI Aix-Marseille Université	Directeur de thèse
Demian BATTAGLIA Aix-Marseille Université	Co-directeur de thèse
Charles GRAY Montana University, Bozeman, États-Unis	Membre invité

European Commission
MARIE CURIE ACTIONS
Institut de Neurosciences des Systèmes
int institut de neurosciences de la timone

Affidavit

Je soussigné, Vinicius Lima, déclare par la présente que le travail présenté dans ce manuscrit est mon propre travail, réalisé sous la direction scientifique de Andrea Brovelli et Demian Battaglia, dans le respect des principes d'honnêteté, d'intégrité et de responsabilité inhérents à la mission de recherche. Les travaux de recherche et la rédaction de ce manuscrit ont été réalisés dans le respect à la fois de la charte nationale de déontologie des métiers de la recherche et de la charte d'Aix-Marseille Université relative à la lutte contre le plagiat.

Ce travail n'a pas été précédemment soumis en France ou à l'étranger dans une version identique ou similaire à un organisme examinateur.

Fait à Marseille le 12 Juillet 2024



Cette œuvre est mise à disposition selon les termes de la Licence Creative Commons Attribution - Pas d'Utilisation Commerciale - Pas de Modification 4.0 International.

Liste de publications et participation aux conférences

Liste des publications et/ou brevets réalisées dans le cadre du projet de thèse:

1. Hoffman, S. J., Dotson, N. M., **Lima, V.**, Gray, C. M. (2024). The Primate Cortical LFP Exhibits Multiple Spectral and Temporal Gradients and Widespread Task-Dependence During Visual Short-Term Memory. Journal of Neurophysiology.

2. Voges, N.*, **Lima, V.***, Hausmann, J., Brovelli, A., Battaglia, D. (2024). Decomposing neural circuit function into information processing primitives. Journal of Neuroscience, 44(2). (*shared first authorship).

3. Karittevlis, C., Papadopoulos, M., **Lima, V.**, Orphanides, G. A., Tiwari, S., Antonakakis, M., ... Ioannides, A. A. (2024). First activity and interactions in thalamus and cortex using raw single-trial EEG and MEG elicited by somatosensory stimulation. Frontiers in Systems Neuroscience, 17, 1305022.

4. Voutsa, V., Battaglia, D., Bracken, L. J., Brovelli, A., Costescu, J., Diaz Munoz, M., ... **Lima, V.**, ..., & Hütt, M. T. (2021). Two classes of functional connectivity in dynamical processes in networks. Journal of the Royal Society Interface, 18(183), 20210486.

Autres publications:

1. **Lima, V.**, Shimoura, R. O., Kamiji, N. L., Battaglia, D., & Roque, A. C. (2023). Propagation in a Large-Scale Circuit Model of the Primate Cortex. ReScience.

2. Combrisson, E., Basanisi, R., **Cordeiro, V. L.**, Ince, R. A., & Brovelli, A. (2022). Frites: A Python package for functional connectivity analysis and group-level statistics of neurophysiological data. Journal of Open Source Software, 7(79), 3842.

Participation aux conférences et écoles d'été au cours de la période de thèse:

1. CSCS-USI SUMMER SCHOOL 2021 Effective High-Performance Computing & Data Analytics with GPUs Online.

2. **Cordeiro, V. L.**; Hoffman, S.J.; Dotson, N.; Gray, C.M.; Brovelli, A., Battaglia, D.; Large-scale dynamic network and information theory analyses of coherent activity during a working memory task (**poster**). In: Brain Criticality workshop, 2022.

3. **Cordeiro, V. L.**; Hoffman, S.J.; Dotson, N.; Gray, C.M.; Brovelli, A., Battaglia, D.; Large-scale dynamic network and information theory analyses of coherent activity during a working memory task (**poster**). In: Society for Neuroscience (SfN), 2022.

4. **Cordeiro, V. L.**; Hoffman, S.J.; Dotson, N.; Gray, C.M.; Brovelli, A., Battaglia, D.; Working memory content is encoded in transient functional network dynamics (**poster**) In: NetSci, 2023 and GDR NeuralNets, 2023

5. **Cordeiro, V. L.**; Hoffman, S.J.; Dotson, N.; Gray, C.M.; Brovelli, A., Battaglia, D.; Working memory content is encoded in transient functional network dynamics (**poster**) In: Society for Neuroscience (SfN), 2023.

6. **Cordeiro, V. L.**; Gray, C.M.; Voges, N.; Brovelli, A., Battaglia, D.; Self-organized emergence of multi-areal information processing in a non human primate connectome-based model (**talk**) In: Computational Neuroscience (CNS), 2023.

Résumé et mots clés

Le fonctionnement du cerveau nécessite le maintien, la modification et le transfert d'information vers diverses régions cérébrales. Cet échange d'information serait en partie réalisé par la coordination de leurs activités neuronales. La structure cérébrale contraint les chemins de l'information, mais ne détermine pas strictement son flux, permettant une flexibilité afin de s'adapter aux changements environnementaux. De plus, les dynamiques de réseaux relient structure et fonctions, et reflètent le traitement de l'information nécessaire aux fonctions cognitives. Ainsi, l'objectif de ma thèse est d'explorer les régimes dynamiques supportant la mémoire de travail (MT), une fonction cognitive clé impliquant un traitement distribué de l'information. Dans la première étude, j'ai analysé des données enregistrées dans plus de 50 aires corticales chez deux primates non humains effectuant une tâche de MT. Nous avons constaté que durant la tâche, des aires cérébrales se coordonnent pour former des activités transitoires ininterrompues, que nous avons définies comme des "assemblées co-crackles" (CrAs). La fréquence avec laquelle une aire s'engage avec les autres dans les CrAs prédit de façon plus précise si elle contient des informations de MT plutôt que des caractéristiques locales, comme la puissance oscillatoire absolue. Si les CrAs trouvées dans cette étude peuvent être une empreinte générale du traitement distribué de l'information, est-ce que les opérations de traitement de l'information, telles que le stockage, la modification et le transfert d'information, via ces CrAs peuvent être quantifiées ? Pour répondre à cette question j'ai appliqué des outils de la théorie de l'information aux dynamiques des modèles computationnels. Ces outils ont capturé les opérations algorithmiques reflétant les dynamiques de réseau et ont révélé les propriétés émergentes du système étudié. Ce travail met en évidence que les dynamiques neuronales des aires cérébrales individuelles et des réseaux exécutent des opérations computationnelles complexes, et les différents motifs produits peuvent porter différentes fonctions de traitement de l'information. Par conséquent, ces résultats ont des implications théoriques importantes pour la première étude. Dans la troisième étude, j'ai cherché à comprendre le rôle computationnel des activités en "bursts", qui sont liés à un ensemble de fonctions et servent d'élément de base aux CrAs. Pour ce faire, j'ai utilisé des données d'hippocampes provenant de deux singes enregistrés pendant une tâche visuelle et durant leur sommeil. Plus précisément, j'ai développé des méthodes pour caractériser les "bursts" définis dans le domaine temps-fréquence. Pour conclure, le travail réalisé durant ma thèse propose un mécanisme général par lequel l'activité transitoire, en "bursts", s'auto-organise pour fournir une diversité d'états pour le traitement de l'information lors de tâches cognitives. Plus spécifiquement, nous proposons trois scénarios sur le rôle des "crackles" dans l'intégration à longue distance : (1) Un "crackle" correspond à un "burst" d'activité neuronale

synchronisée dans la zone enregistrée, permettant d'implémenter la communication par la cohérence ; (2) les "crackles" sont plus faibles et reflètent possiblement des réverbérations d'activité neuronale dans l'aire "source" sous forme de potentiels synaptiques. Bien qu'ils ne reflètent pas une véritable oscillation, leurs statistiques capturent néanmoins les communications sous-jacentes entre deux aires ; (3) les "crackles" peuvent être plus faibles, mais si le système entre dans un état où ils peuvent se coordonner (via le "co-crackling"), leur activité conjointe peut être suffisante pour exciter les zones cibles. Dans ce cadre général, le traitement de l'information est réalisé par la cohérence interne du système, tandis que les calculs de haut niveau soutenant les fonctions cognitives sont représentés par les états observés du système.

Mots clés: neurosciences des systèmes, neurosciences cognitives, mémoire de travail, neurosciences computationnelles, dynamique de l'information.

Abstract and keywords

Brain function requires the maintenance, exchange, and merging of information conveyed by multiple brain regions, achieved through the coordination of distributed neural activity. While brain structure constrains the pathways through which information can flow, it does not determine them in a fully hardwired manner. In fact, flexibility in information processing is essential to behavior, allowing for rapid adaptation to environmental changes. Hence, dynamics not only links structure and function but also reflect the information processing operations that support those functions. The main goal of my thesis is to probe the types of dynamical regimes that support working memory (WM), a key cognitive function involving distributed information processing. I have done this by analyzing large-scale datasets and employing computational modeling. In the first study, we analyze a dataset recording up to 50 cortical areas in two non-human primates performing a WM task. During the task, groups of areas coordinate to form packets of uninterrupted transient activity, which we define as "co-crackle assemblies" (CrAs). Interestingly, the frequency with which an area engages in CrAs better predicts whether it holds WM information than local features, such as absolute oscillatory power. While the CrAs found in this study might be a fingerprint of distributed information processing, can the actual computations performed by areas participating in it be quantified? In the second study, we explore this question using two computational models. Specifically, by applying tools from information theory to the models' dynamics, we could quantify information processing operations, such as information storage, transfer, and modification. The tools from information theory correctly capture the algorithmic operations reflected in neuronal dynamics and revealed emergent properties of the studied systems. This work suggests that the neuronal dynamics of single areas and the networks they form implement complex computational operations, and possibly different motifs in this network may carry different coexisting information processing functions. Consequently, these findings have theoretical implications that might be important for the first study. In the third study, we sought to better understand the computational role of burst activity, which is related to a range of cognitive functions and serves as the building blocks of the CrAs from the first study. We used hippocampal recordings from two monkeys during task and sleep conditions. Lastly, in the third chapter we present a preliminary study where we sought to deepen the understanding of the computational role of burst activity. In particular, we developed methods for the characterization of bursts defined in the time-frequency domain across recording channels implanted in the hippocampus of freely behaving monkeys doing a visual search task. To conclude, this thesis proposes a general mechanism by which transient activity, occurring in bursts, self-organizes to provide a substrate of states for information processing during cognitive tasks.

Specifically, we speculate on the role of crackling activity in promoting long-range integration by proposing three scenarios: (1) crackles correspond to bursts of synchronous spiking in the recorded regions, capable of mediating communication via coherence; (2) crackles are weaker and might reflect reverberations of activity in source areas in the form of synaptic potentials. While not reflecting a genuine oscillation, their statistics still capture the underlying communications between two areas; (3) crackles may be weaker, but if the system enters a state in which they can coordinate (via co-crackling), their joint activity may be sufficient to excite target areas. In this framework, information processing is carried out by the internal congruence of the system, while high-level computations supporting cognitive functions are mirrored in the observed system's states.

Keywords: systems neuroscience, cognitive neuroscience, working memory, computational neuroscience, information dynamics.

Je dédie cette thèse,

à Sofia, pour toutes les heures que nous avons passées à étudier ensemble.

Remerciements

This thesis work finds its seeds in one of the most fundamental desires of man, the one of learning. This desire, finding in me a habitat, moved me forward in the path leading to the wonderful years I have passed learning and creating knowledge, even if modest, in Marseille. But I would lie if this desire alone led me here, as it is said “no man is an island”, and this could not be closer to the truth when referring to myself. I am not particularly bright or skillful, so I had to count on several people along the way. Therefore, here I dedicate a few words to these people.

First, I would like to thank my two supervisors, Dr. Demian Battaglia and Dr. Andrea Brovelli, from whom I not only received guidance and learned a great deal but was also granted the freedom to use my time to explore subjects that captured my interest. Without the confidence they placed in me as their PhD student, none of this would have been possible. I would also like to thank Dr. Charles Gray for his support during the many instructive meetings we had and for the constructive criticism he provided, which enabled me to learn a great deal. Finally, I would like to thank Dr. Antonio Roque, my undergraduate and master’s supervisor, who set me on the path of computational neuroscience, for which I am deeply grateful.

I would like to extend my heartfelt gratitude to the jury members for agreeing to be part of this very important and celebratory day for me. I am deeply thankful for their contributions in helping to improve the quality of my thesis manuscript and for providing valuable and constructive feedback on the day of my defense. Thank you very much, Dr. Laurent Perrinet, Dr. Martin Vinck, Dr. Emmanuel Procyk, and Dr. Kari Hoffman.

Next, I would like to thank the numerous friends and colleagues I met along the way at the Institut de Neurosciences des Systèmes (INS) and the Institut de Neurosciences de La Timone (INT). In particular, I extend my heartfelt thanks to my colleagues from the TNG and PhysioNet teams at INS and to those from the BranNets group at INT. Of course, I am also deeply indebted to my old friends, who continue to be supportive to this day. From all these people, I have learned a great deal about both scientific and non-scientific matters. Additionally, I truly appreciated the time I spent with the colleagues and PIs from the Marie Skłodowska-Curie Training Network (I-CONN). Finally, I owe a special thanks to those whose discussions were especially helpful when scientific and delightfully entertaining when non-scientific : Pierpaolo Sorrentino, Etienne Combrisson, Sammy Castro, Mariana Angiolelli, Gianmarco Cafaro, Damian Depannemaecker, Viktor Sip, Michalis Papadopoulos, Christodoulos Karittevlis, Yan-

hua Shi, Selim Ali, Rodrigo Pena, Renan Shimoura, Nilton Kamiji, Mauricio Schappo, and countless others.

À ce moment-là, je change de langue pour remercier ceux qui ont été ma deuxième famille à Marseille, et sans le soutien desquels je n'aurais jamais pu réussir dans cette odyssée appelée thèse. (Pour être un peu dramatique, je n'aurais probablement même pas survécu jusqu'à la fin sans l'aide qu'ils m'ont apportée lors de l'infection pulmonaire que j'ai eue au début de l'année 2024). Je suis conscient que ces quelques lignes de remerciements sont bien en-deçà de ce que vous méritez, mais sachez que vous avez tout mon amour, ma reconnaissance et mon soutien pour quoi que ce soit : Elisabeth, Patrick, Raphaël et Myriam Azzarelli. Et ne pensez surtout pas que j'ai oublié les grands-parents, un immense merci également à Angèle, Consuelo et Antoine.

Uma última mudança de língua para agradecer à minha família, sem a qual não só esta tese, mas a vida, não seriam possíveis. Um obrigado repleto de amor à minha mãe Valéria, à minha irmã Mariana e à minha sobrinha, a quem desejo um futuro luminoso e repleto de alegria – como o que tive a sorte e o prazer de trilhar e espero continuar trilhando – Alice.

I am truly grateful with all my heart to all these people, and to many others who, in one way or another, have influenced me up to this point. To quote Borges : "As the end approaches, there are no longer any images from memory — there are only words". The following are the words — that we have constructed together — remaining from the past four years!

Table des matières

Affidavit 3

Liste de publications et participation aux conférences 4

Résumé et mots clés 6

Abstract and keywords 8

Remerciements 11

Table des matières 13

1. GENERAL INTRODUCTION 17
- 1.1. Initial considerations . . . 17
- 1.2. Thesis main objectives . . . 21
- 1.3. The working memory system . . . 22
  - 1.3.1. The classical model . . . 23
  - 1.3.2. In search of the correlates . . . 24
  - 1.3.3. Concluding remarks . . . 27
- 1.4. Neural oscillations . . . 28
  - 1.4.1. The local-field potential . . . 30
  - 1.4.2. Cellular and network mechanisms of rhythmogenesis . . . 31
  - 1.4.3. From neural oscillations to brain function . . . 36
  - 1.4.4. Persistent *versus* transient oscillations . . . 41
  - 1.4.5. Concluding remarks . . . 44
- 1.5. From dynamics to computation . . . 45
  - 1.5.1. Complexity and computation . . . 46
  - 1.5.2. Computation and information dynamics . . . 50
  - 1.5.3. Computation and the brain . . . 54
  - 1.5.4. Concluding remarks . . . 60

2. WORKING MEMORY CONTENT IS ENCODED IN TRANSIENT FUNCTIONAL NETWORK DYNAMICS 64
- 2.1. Introduction . . . 65
- 2.2. Methods . . . 66
  - 2.2.1. Behavior, implantation and recordings . . . 66
  - 2.2.2. Estimating single-trial power . . . 66
  - 2.2.3. Single-trial coherence . . . 67
  - 2.2.4. Gaussian-Copula mutual information and stimuli encoding . . . 68

2.2.5. Detecting crackles . . . 68
2.2.6. Flattened spacetime graph representation and crackle assemblies 68
2.3. Results . . . 70
2.3.1. Power time-series are stochastic and emits burst-like events . . 70
2.3.2. Power crackles dynamics are task modulated . . . 73
2.3.3. Power time-series contains stimulus related information . . . 77
2.3.4. Crackles' assemblies predicts stimulus encoding . . . 79
2.3.5. Crackles' assemblies unveils how information is transferred across cortical areas . . . 82
2.3.6. Crackles' assemblies are mainly from functional origin and predict pairwise coherence . . . 84
2.3.7. Interplay between local recurrent connections and connection delays gives rise to co-crackling activity . . . 88
2.4. Discussion . . . 91

3. DECOMPOSING NEURAL CIRCUIT FUNCTION INTO INFORMATION PROCESSING PRIMITIVES 113
3.1. Introduction . . . 114
3.2. Model and methods . . . 116
3.2.1. Computational model of one region : ring network model . . . 117
3.2.2. Dynamical regimes of the ring model and properties of stimulus response . . . 118
3.2.3. Multi-regional architectures : coupled ring networks . . . 119
3.2.4. Task simulations with the ring models . . . 119
3.2.5. Estimating information-theoretical quantities . . . 120
3.2.6. Tracking Information Processing Primitives (IPPs) . . . 122
3.2.7. Large-scale connectome-based model . . . 125
3.3. Results . . . 127
3.3.1. Two dynamic regimes of response to stimulus . . . 127
3.3.2. IPP analysis can track the representation of a stimulus . . . 130
3.3.3. IPP analysis can track the loading and maintenance of a representation in working memory . . . 133
3.3.4. IPP analysis can track the propagation of representations through a multi-regional hierarchy . . . 134
3.3.5. IPP analysis can track the integration of bottom-up and top-down information flows . . . 137
3.3.6. Information dynamics in a large-scale model of cerebral cortex 142
3.4. Discussion . . . 146

4. HIPPOCAMPAL BURST VARIETY IN A FREELY EXPLORING NON-HUMAN PRIMATE 159
4.1. Introduction . . . 159
4.2. Methods . . . 166
4.2.1. Empirical Mode Decomposition . . . 166

4.2.2. Estimation of the composite time-series 167
4.2.3. Burst-detection and feature extraction 168
4.3. Results 168
4.3.1. Decomposing the LFPs into oscillatory modes 169
4.3.2. Estimating the composite signals 169
4.3.3. Bursts' features extraction 172
4.4. Future steps and directions 173

5. GENERAL DISCUSSION **179**
5.1. Computation... but why? 180
5.2. Bursting activity and computation 185
5.3. Future directions 187
5.4. Conclusion 190

Bibliographie **192**

APPENDICES **241**

A. [Replication] Inter-areal Balanced Amplification Enhances Signal Propagation in a Large-Scale Circuit Model of the Primate Cortex **242**

B. Frites : A Python package for functional connectivity analysis and group-level statistics of neurophysiological data **260**

Down how many roads among the stars must man propel himself in search of the final secret? The journey is difficult, immense, at times impossible, yet that will not deter some of us from attempting it . . . we will travel as far as we can, but we cannot in one lifetime see all that we would like to see or learn all that we hunger to know.

Loren Eiseley
(The Immense Journey)

1. GENERAL INTRODUCTION

In this chapter, I provide a review of the literature, focusing on the topics that are fundamental for the research comprised in this dissertation. More specifically, I present the concept, the classical model, and the neurobiological basis of the working memory system. Next, we review the role of oscillatory activity in the brain, from its generating mechanisms, to its functions. To support the role of oscillatory activity as the basic markers of computation in the nervous system, I present the theoretical basis on how dynamics can be used to implement computation, and give examples to illustrate how it is achieved in the brain. I finalize this chapter, by briefly reviewing the current techniques used to explore the brain[1].

1.1. Initial considerations

Modern neuroscience research programs aim to map distinct brain phenomena to their neuronal substrates (or correlates). One successful example of this program is the discovery made by John O'Keefe of "place cells" located in the hippocampus (O'KEEFE 1976). This discovery revealed how the environment is internally represented through the activity of these cells (O'KEEFE et al. 1993). In other words, place cells' activity is the neural correlate of spatial representation. In his book entitled "The Brain from Inside Out" (BUZSÁKI et al. 2023), Gyorgy Buzsaki points out that while this *modus operandi* has allowed incredible advancements in neuroscience, most of the concepts for which we search for neuronal correlates originated in late 19th-century psychology. More specifically, Buzsaki claims that modern neuroscience has a strong reliance on the vocabulary originating from those influential works, such as those of William James (JAMES 1890). Since these concepts that originated from the field of psychology, are not rooted in neurobiological observations, and we have no means to verify the existence of the concepts this vocabulary comprises, Buzsaki suggests that one should consider these problems without preconceived ideas and interpret brain phenomena in light of what the brain evolved to do, i.e., maximizing the prediction of the outcome of one's actions. In Buzsaki's proposed framework, the activity of a group of neurons is only meaningful if it can create an effect on downstream "reader" neurons, and not by being correlated with an external variable defined by the experimenter (BUZSÁKI 2010; PANZERI et al. 2017; PANZERI et al. 2022; BUZSÁKI et al. 2023). He refers to these two contrasting views as "outside-in" and "inside-out", respectively.

The development of top-notch technology for recording brain activity at different spatial and temporal scales, such as neuropixel probes (STEINMETZ et al. 2021), dis-

[1]Throughout this chapter, I adopt a "Pratchettian" style, and use footnotes to offer complementary information and general comments, so in some sense, they can be skipped if wished.

tributed recording systems (DOTSON et al. 2017), and new powerful MRI scanners[2], provides investigators with an unprecedented amount of high-quality data, which is very favorable for the "inside-out" program. Additionally, state-of-the-art data analysis techniques, now available to the neuroscience community due to the migration of physicists, mathematicians, and computer scientists into the neuroscience field, as well as ready-to-use software for performing complex analyses, allow a range of new aspects of these datasets to be explored. The confluence of technological and technical development has led to advancements enabling the measurement of neural activity from widespread regions of a cortical hemisphere of non-human primates during a working memory task (DOTSON et al. 2017; DOTSON et al. 2018; HOFFMAN et al. 2024) and hippocampal activity in monkeys that are free to explore and perform a task in a 3D cage (SAMAN et al. 2023). The datasets resulting from those experiments are the ones analyzed here in Chapters 2 and 4.

If on one hand the recent years have seen an incredible technological and theoretical development, on the other the conceptual dichotomy pointed out by Buzsaki, is reflected on inherited methodological practices of the neuroscience field. Just to cite one example, in PESSOA (2022), the author discusses how the practice of dividing the cortex in multiple functional areas is also an inheritance from the work of 20th century neuroscientist Korbinian Broadmann, that created the "Broadmann map". I quote Pessoa's words on the subject :

> "*Historically, two winners in the search for rightful units have been the neurons and the individual brain area. At the cellular level, the neuron reigns supreme . . . At the supra-cellular level, the chief unit is the area. But what constitutes an area?*".

Regarding the last question, he recognizes that those divisions were founded in anatomical studies, these questions remain far from being trivial :

> "*All subcortical areas have multiple sub-divisions, and some have boundaries that are more like fuzzy zones than clearly defined lines*".

This example serves to illustrate how one should be aware of the processes that lead to certain scientific conventions and their consequences in hypothesis testing. As a matter of fact, the search for the basis of cognition has pushed towards a more collectivist view of the nervous system, in which cognitive functions are believed to arise from the collaboration of widespread brain regions (VARELA 1989; VARELA et al. 2001; BRESSLER et al. 2010; VON DER MALSBURG et al. 2010; DECO et al. 2021). In this context, the functional delimitation's of cortical areas can be context dependent. For example, in ANDERSON et al. (2013), the authors showed that areas can engage in multiple activities ranging from language to motor learning, language, and fear with different extents.

[2] Such as the newly developed 11.7 Tesla scanner https://www.cea.fr/presse/Pages/actualites-communiques/sante-sciences-du-vivant/iseult-IRM-record-11-7-teslas.aspx.

The state, where inherited research practices coexist with new conceptual and technical advancements suggests that neuroscience as a field is undergoing a transition (pretty much like water, that when sitting at its triple point coexists as liquid, solid, and gas). In fact, one could say that the discussions carried in PESSOA (2022) et BUZSÁKI et al. (2023) are a natural evolution of years of research indicating that information processing in the brain is conducted by a system of distributed dynamic networks (MOUNTCASTLE 1978). Today, this understanding relies on novel graph theory methods, which create new and useful interpretations (SPORNS 2016; and even this approach is limited since it is restricted to pairwise interactions). Analogously, the introduction of frameworks such as information theory by Rieke, Bialek and others (BIALEK et al. 1989; RIEKE et al. 1999) allowed to conceptualize neuronal activity as a form of encoded representation of stimuli [3], which is transmitted across neurons as if they worked as communication channels[4].

In fact, recent developments in information theory (WIBRAL et al. 2017; LUPPI et al. 2024a; LUPPI et al. 2024b) and network science provided frameworks to explore the brain as a complex system where interactions are not constrained to being pairwise (or dyadic), i.e., allowing high-order interactions (GIUSTI et al. 2016; BETZEL et al. 2023) to be investigated. From the information theoretical side approaches such as the partial-information decomposition (WILLIAMS et al. 2010; LIZIER et al. 2018) and metrics as the O-information (ROSAS et al. 2019; VARLEY et al. 2023a; VARLEY 2024) allow to characterize not only if information is stored in the system, but how its multiple parts exchange and interact to transform it, revealing that the interaction between neurons or brain regions goes beyond correlation (VOGES et al. 2024). From the network science perspective, interaction between multiple elements can be obtained on one hand by generalizations of graphs such as hyper-graphs and simplicial complexes[5] (BATTISTON et al. 2020), which allows one not only to generalize graph-theoretical metrics taking into account multiple interactions, but also to study how the dynamics of a system is influenced by those interactions.[6]

Even though the examples above illustrate how conceptual and technical advances

[3] Where the code was typically taken as being the neuron's firing rate, the precise timing of spikes (EGGERMONT 1998; DAYAN et al. 2005), or a population coding where either the firing rate is averaged over many neurons to control for noise, or the timing of spikes among a group of neurons is coordinated forming what is called cell assemblies (BUZSÁKI 2010; POMPILI et al. 2022; MAKDAH et al. 2024).

[4] This perspective can be traced back to the logical neuron of McCulloch and Pitts (MCCULLOCH et al. 1943), but information theory provides a framework allowing to quantify the amount of information carried or communicated by neuronal activity.

[5] The simplicial complexes are a way of characterizing multiple interactions by studying its topological properties. The distinction of a simplicial complex and a hyper-graph, is that the first requires that for each N-body interaction all the (N-1)-interactions composing it must also exist. For a concise introduction to complexes check (BIANCONI 2021).

[6] This approaches allowed to found redundant subsystems linked to reward and punishment (COMBRISSON et al. 2023, and that synergistic interaction in the brain are linked to cognition and integrative functions (LUPPI et al. 2022). To cite one example outside of the neuroscience domain, it was found that the epidemic threshold for contagion spread is actually lower when high-order interactions are considered (LUCAS et al. 2023).

have pushed towards a pluralistic view of the nervous system and the dynamics of its constituent parts, they are not the only points where a paradigm shift is taking place. Another example lies in the increasing relevance of transient - rather than sustained - oscillatory activity in a range of cognitive functions (EDE et al. 2018; LUNDQVIST et al. 2024). In particular, experimental works have shown that single-trial bursts not only differ from their averaged description but are also informative in decoding the position of a mouse in a maze during a task (DOUCHAMPS et al. 2024). These bursts are related to working memory (LUNDQVIST et al. 2016; LUNDQVIST et al. 2018; and see Chapter 2), and can predict behavior (SHIN et al. 2017). The short-lived nature of these transient events highlights the importance of single-trial analysis (STOKES et al. 2016), as averaging can obscure sub-threshold, weak, and/or non-trial-locked activity modulations. The correct characterization of transients at the single-trial level is another issue that we will address in Chapter 3.

Finally, another dimension of neuroscience research is computational neuroscience, which allows, via modeling or mathematical analysis, to comprehend how a network of well known neuron models interacts to give rise to different phenomena depending on the parameter values used (e.g., as network structure). Theoretical work has helped to push forward the understanding of basic principles such as rhytmogenesis, and information processing in the brain, (BRUNEL 2000; KINOUCHI et al. 2006; JOGLEKAR et al. 2018; D'ANGELO et al. 2022). Additionally, the use of computational models that profit from experimental data in order to be constructed (MARKRAM 2012; POTJANS et al. 2014; MARKRAM et al. 2015; SCHMIDT et al. 2016; SHIMOURA et al. 2021) are powerful tools that helps to better understand how the properties of neuronal networks emerges as an increasingly number of elements are added to the model.

While the confluence of the technical and theoretical advancements discussed so far are quickly expanding our neuroscientific knowledge, the conceptual shift of seeing the brain as a complex system is the most important aspect of it. This shift acknowledges the fact that brain phenomena can not be addressed using a reductionist approach, i.e., emergent phenomena such as cognition, and behavior can only be understood by studying the system and its interactions as a whole. As the microbiologist Carl Woese, discussed in his manifesto paper "A New Biology for a New Century" (WOESE 2004), the advent of molecular biology and the sequencing of the human genome created an atmosphere that all problems in biology were solved, leaving only a few details to be filled in. Well, except that later we found out that there are some problems that can not be solved in this way, and this usually indicates that deeper truths about nature are hiding somewhere else. In his words :

> "*Didn't a similar sense of a science coming to completion pervade physics at the 19th century's end—the big problems were all solved; from here on out it was just a matter of working out the details? Deja vu! Biology today is no more fully understood in principle than physics was a century or so ago. In both cases the guiding vision has (or had) reached its end, and in both, a new, deeper, more invigorating representation of reality is (or was) called for.*"

It is true the neuroscience is further from understanding the fundamental components of the brain, as physics achieved with the standard model and biology with the advent of molecular biology. But it only makes the pervasion of all the ideas discussed above more welcoming.

To finalize, the point here is not to claim that new ideas and methodological practices are better. As a matter of fact, technical and methodological advancement alone can only go as deep as a pond and left a vast ocean unexplored (as I came to learn during my own thesis). For instance, the mechanisms of emergence of high-order interactions in the brain are still poorly understood and often its results remains on a correlational level. Particularly, I believe that this is because technicality advances without corresponding theoretical advances guided by the history of the field is not enough [7]. This is why efforts to broaden neuroscience by incorporating the often-neglected philosophical component (BUCCELLA et al. 2024), as well as more clarity in the ideas proposed and discussed in order to (BAKER et al. 2022), are so of utmost importance to develop a deeper understanding of the brain and the causal process underlying behavior (KRAKAUER et al. 2017).

With the discussion above I wished to provide my "first-person" view of the movements happening in the neuroscience field. Those are the views of someone that landed in this field by accident, and I am aware that it may be naive (and not completely precise). But hopefully, they give an overview of the context in which the research carried during this thesis was done, and how the amalgamation of those ideas influenced it consciously or unconsciously.

1.2. Thesis main objectives

To state it simply, the main scientific question that puts the works compiled in this dissertation "under the same hood" is, to understand how function emerges from neuronal dynamics, and how this dynamics may reflect information processing in the brain. In particular, we explore this question in each result chapter as follows :

Chapter 2 : In this study, we sought to understand the network mechanisms underlying working memory (WM) by using an extensive dataset of local-field recordings from the entire cortical hemisphere of two non-human primates, which makes it ideal for studying the distributed mechanisms of memory maintenance across networks formed by widespread cortical areas. Specifically, we relied on increasing empirical evidence showing that burst activity underlies memory maintenance during WM. We examined the network interactions established by the co-occurrence of oscillatory bursts in single-trial activity across multiple frequency bands. We found that stimulus "encodability" is better predicted by the rate at which areas tend to co-burst together. We propose a general mechanism in which the coordination of burst activity provides

[7] To cite Captain Jean-Luc Picard word's : "*Open your mind to the past ... to history, art, philosophy. And then ... this will mean something*"

short windows for information integration in the cortex, supporting memory maintenance by enabling information transfer across areas and modification from a local to a distributed representation.

Chapter 3 : While in Chapter 2 we found evidence supporting the coordinated activity is a fingertip of the neuronal computation supporting WM, we did not access directly what those computations are. Here, we used two computational models with the goal of quantifying how neuronal dynamics gives rise to the information primitives of information storage, transfer and modification. We found that dynamics not only can be decomposed in terms of the "algorithmic" operations it comprises, but also that this quantification can put in evidence important emergent properties of the system. The conjunction of this study with the one in Chapter 3 suggests that collective activity dynamics might carry multiplexed information processing properties, going beyond simple correlations.

Chapter 4 : Here I present the preliminary analysis of a work in which we aim to deepen the understanding concerning the computational role of bursts, this time in the hippocampus. The data analyzed in this chapter was recorded from two non-human primates during a task which involved freely-exploring behavior in a 3D cage alternated by periods of sleep. In this chapter I present the method we developed for extracting and characterizing bursts in single-trial activity, and I discuss the future steps of the analysis we plan to carry.

In the following sections, I will develop a more traditional review of the literature necessary to support the research conducted in my thesis and to address our scientific questions. I begin by providing a review of the WM system, the cognitive function in which our studies focused on. Next, I discuss oscillations in the cortex, which are the basic markers of neuronal processing at this scale, akin to action potentials at the neuronal level. Following this, I examine transient events, usually referred to as bursts. This type of transient activity is gaining increasing relevance due to its apparent relationship with many brain phenomena and is of particular importance for this dissertation. Finally, I will conclude the literature review by discussing how oscillations and transient activity subserve their functions and briefly explore how dynamics are thought to implement computation and, consequently, function from a theoretical perspective.

1.3. The working memory system

Working memory (WM) is the ability we have not only to temporarily "keep in mind" a representation of the world around us but also to mentally manipulate it, making WM essential for behavior (BADDELEY 2012; D'ESPOSITO et al. 2015). For example, consider a situation where you need to memorize a phone number and then tap it on a phone keyboard. This task requires not only holding the sequence of numbers in

your memory but also correctly matching each number with the numerical keys on the phone in order to press the correct ones. Another example is the card matching memory game, where you must remember the image and position of cards initially facing down to identify the matching ones.

A common factor in both examples is : (i) When the call or the game (or more generally the task) is over, you completely forget the numbers and card positions. In other words, the information was only retained while it was relevant for performing the task. (ii) If you had to memorize a long stream of numbers or there were too many cards in the memory game, it would become increasingly difficult to remember all of them correctly.

The examples above serve to illustrate two important properties of WM. First, it is very flexible, meaning that it can store a variety of stimulus categories (e.g., numbers, images, sounds, etc.). Second, WM has a very limited storage capacity, typically constrained to an average of four items at a time (MILLER 1956 ; COWAN 2010). Thus, WM is not only essential for performing goal-directed behavior but also for internal processing (e.g., transforming numerical inputs via mental arithmetic operations) that gives rise to higher cognitive functions, such as learning, language comprehension, and reasoning (BADDELEY 1992 ; ENGLE et al. 1999 ; POSTLE 2006).

But how exactly does this system work, and what are its neuronal bases ? Answers to these questions began to emerge from the confluence of empirical studies that reported persistent neuronal activity in the prefrontal cortex during WM tasks (FUSTER et al. 1971 ; FUSTER 1973), and the influential formulation of WM proposed by the psychologists Baddeley and Hitch (BADDELEY 1992). In what follows, I briefly describe those developments. I start by presenting the WM model proposed by BADDELEY (ibid.), and then I move to the neurobiological correlates associated with the components of their model.

1.3.1. The classical model

The model proposed by Baddeley and Hitch (ibid.) postulated that WM is a system composed of multiple components, including a central executive that coordinates and biases the selective attention of two sensory sub-systems : the phonological loop and the visuospatial sketchpad. The phonological loop is responsible for processing auditory information (e.g., speech), while the visuospatial sketchpad handles visual information. In later models, they also introduced an episodic buffer, which gathers information from these sub-systems and consolidates it into long-term memories (BADDELEY 2000 ; BADDELEY et al. 2001 ; BADDELEY 2012).

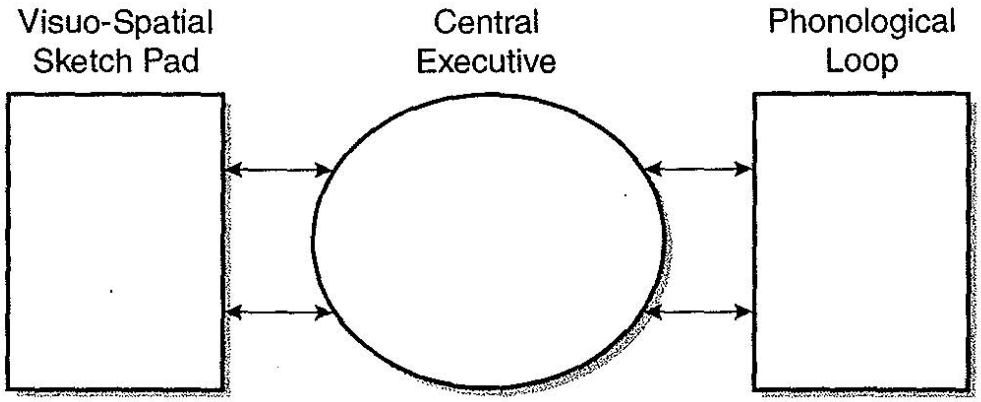

FIGURE 5.1 Baddeley Model of Working Memory

Source: Baddeley, 1986

FIGURE 1.1. : Screen capture from the paper where Baddeley and Hitch (BADDELEY 1992), proposed their original WM model. In this iteration of the model, the episodic buffer was still not present.

Notice that in this model, WM is required to be dynamic to allow the subsystems to properly coordinate their information under the central executive's orchestration. In particular, the central executive coordinates which information should be attended to and which subsystem it should be conveyed to, i.e., either the phonological loop or the visuospatial sketchpad. Additionally, the central executive is responsible for monitoring the operations carried out in those subsystems to integrate information distributed across the WM system. Altogether, this makes the central executive the most important component of the model.

While this model conceptualizes the WM system, neuroscientific research aims to probe the neurobiological basis of its concepts. The main interest is to answer questions such as : Which brain regions perform executive control ? What are the neuronal dynamics of those regions during a WM task ? By what means do the executive areas coordinate their subsystems (the sensory areas) ? For the remainder of this section, I will review some of the experimental findings that have addressed these questions.

1.3.2. In search of the correlates

Experimentally, WM is tested in tasks where the subject is required to hold one or more items (or cues) in memory (the number of items corresponds to the "memory load" of the task). These items must be retained during a "delay" period, during which the cue is not displayed. After this interval, the subject is asked to choose between the correct item and one or more distractor cues. If the correct cue is chosen, it is considered that information was successfully maintained in WM.

An example of such a task is the visual delayed-match-to-sample task (DMTS). In the DMTS task, one out of several images is randomly selected and shown to the subject during a sample period, followed by the delay period where the cue is suppressed, and finally a match period when the subject has to choose between the correct and an incorrect image (BLOUGH 1959; DANIEL et al. 2016).

During these tasks, neuronal activity is recorded in one or more regions of interest. The rationale behind this is that while neuronal activity during the sample period is mostly elicited by the stimulus, during the delay period, it should reflect working memory (WM) processes related to executive control and memory maintenance.

Early observations of sustained activity of neurons in the prefrontal cortex (PFC) during the delay period (in both monkeys and humans; MILLER et al. 1996; COURTNEY et al. 1998; CURTIS et al. 2003) led to the attribution of the executive role to this region (FUSTER et al. 1971; GOLDMAN-RAKIC 1987; FUNAHASHI et al. 1993). Specifically, this persistent activity is thought to encode the cue identity (FUSTER 1973; FUNAHASHI et al. 1993; PROCYK et al. 2006), as it is stimulus-dependent and resistant against distractors, allowing for the filtering of irrelevant information for task performance (MILLER et al. 1996; RAINER et al. 1998). In parallel, the relevance of the PFC for WM was demonstrated in studies where performance during WM tasks decreased after lesioning this region (FUSTER et al. 1971; FUNAHASHI et al. 1993; CURTIS et al. 2004).

Additionally, work in computational neuroscience has proposed several mechanisms by which persistent activity may be achieved in the PFC during the delay period. For instance, AMIT et al. (1997) demonstrated that in a network of leaky integrate-and-fire neurons with sparse spiking activity and balanced excitation and inhibition, persistent delay activity can be achieved through attractor states, created via long-term potentiation between neurons whose spiking is correlated during stimulus presentation. Contrary to the proposals of WM as being represented by attractor states of persistent firing created by means of (AMIT 1995; WANG 2001; BRUNEL 2003). In MONGILLO et al. (2008) based on observations that sometimes delay activity increase is mild or even intermittent (NAYA et al. 1996; SHAFI et al. 2007; RAINER et al. 2002) the authors proposed a synaptic theory of WM, in which short-term synaptic facilitation (STP) would allow an item to be maintained by WM. In particular, STP would be mediated by an increasing residual calcium concentration on the synapses of encoding neurons. The slow process of removal of these residuals would favor memory to be held for long transients (ZUCKER et al. 2002). The authors demonstrated this principle in a recurrent network of integrate-and-fire neurons.

In a later discovery, it was found that while prefrontal cortex (PFC) neurons displayed persistent spiking activity during the delay period, this activity did not encode stimulus-specific information (CURTIS et al. 2003). Instead, stimulus encoding was observed in the activity of sensory areas (CURTIS et al. 2003; RIGGALL et al. 2012; HALLENBECK et al. 2021). But if PFC activity does not encode the stimulus identity, what is its role?

An alternative hypothesis is that the persisted spiking in the PFC reflects top-down control over sensory regions (CURTIS et al. 2003; PASTERNAK et al. 2005; LARA et al. 2015; MILLER et al. 2018), responsible for mediating interference and distraction,

attentional selection, response preparation, and other functions (POSTLE 2006). This hypothesis was corroborated by experimental evidence showing that the PFC actually encodes general information related to the task (e.g., whether a stimulus is a distractor, passage of time, and spatial location of the stimuli, etc.) corroborated the view that it may support alternative WM functions (LEBEDEV et al. 2004; STOKES et al. 2013; LARA et al. 2014).

In another modeling work by ARDID et al. (2007), frontal top-down modulation, is achieved in a model with two areas with a ring topology, reflecting the stimulus selectivity of each neuronal population. Specifically, in the sensory area, lateral inhibition favors the maintenance of stimuli in areas with matching orientation preference, while in the WM area, stronger excitation favors stimulus maintenance. This allows stimulus-specific activity in WM areas to be sent top-down, and confronted with information about new stimuli that may be in the sensory areas. [8] We have used this model in Chapter 3, in order to understand how the specific operations of WM and selective attention can be decomposed into information processing primitives.

However, the aforementioned hypotheses are confronted by other studies. For instance, in a study using BOLD signals from humans (ESTER et al. 2015), the authors were able to reconstruct remembered orientation from occipital, frontal, and parietal cortices. Additionally, in HERNÁNDEZ et al. (2010), the authors found that encoding is distributed across many cortical areas throughout the WM task, but that frontal areas also play a role in reading out from WM to compare past information with new stimuli and guide the animals' choices.

Indeed, working memory appears to be a distributed system, and traces of stimulus encoding are found across many cortical areas, depending on the task at hand (CHRISTOPHEL et al. 2017). Additionally, in a study recording multiple cortical areas of non-human primates (DOTSON et al. 2018), researchers found that multi-unit activity modulations, measured as the fraction of channels for which the firing rate differed between the task and control condition (where no memory was required from the animals), are widespread and observed across many cortical areas.

But what does it mean for WM, to be a distributed system? First of all, that information is not necessarily contained in a single region, but in multi-regional interactions. Additionally, they may not all carry the same stimuli representation.

More specifically, stimulus-related information present in sensory areas, can be either directly copied into frontal regions, or some abstract representation of it (CHRISTOPHEL et al. 2017). In the latter case, the compressed representation could be a low-level visual feature of the input (as color, or contour), or a semantic categorical representation[9].

Consequently, the information sent from sensory to frontal areas, would keep different stimuli features, ranging from high to low abstraction level (e.g., in frontal areas,

[8] In these network models, the concepts of WM and selective attention are somewhat blurred, encompassing functions that are traditionally considered distinct (DESIMONE et al. 1995; BADDELEY 1996; FOCKERT et al. 2001).

[9] Experimentally, the reliance of WM in visual or verbal categories can be tested, for instance, by using complex images for which there is no verbal counterpart (CERMAK 1971), or images that gradually morph from one animal to another (FREEDMAN et al. 2001).

information about the picture of a zebra would consist of low-level information, of whether the seen animal has stripes or not). This low-level representation would then be conveyed back to sensory areas, so that the initially stored information can be confronted with new stimuli (so now if the picture of an elephant is being shown we could decide whether it was the same animal as before). In this scenario, the PFC would not only store a compressed version of the cue presented to the subject, but also would allow matching this information with new incoming stimuli, avoiding interference between information present in sensory areas and guiding the behavioral response by biasing selective attention (CHRISTOPHEL et al. 2017; JACOB et al. 2014).

Another aspect of carrying a multi-regional representation of the stimulus, is that its encoding may be segregated across regions in a complementary fashion, meaning that while stimulus-specific information can be recovered from each region, some information could only be retrieved by inspecting their collective activity. As a matter of fact, in our own research (present in Chapter 2 of this dissertation), we found encoding of the identity of a visual stimulus, across multiple cortical regions in non-human primates. Most interestingly, we found that areas tend to form spatio-temporal coalitions, and that the prediction of areas carrying stimulus information, was enhanced if the frequency in which areas participated on them was considered instead of their local activity.

Finally, if WM is a distributed system, there should be a mechanism allowing sensory information to be sent to higher areas. One of the most prominent hypothesis is that this information between cortical areas is exchanged via the synchronization of their oscillatory activity (FRIES 2009; CANOLTY et al. 2010). In fact, there are experimental evidences supporting the role of oscillatory activity in WM. For example, increased oscillatory activity in monkeys' intra-parietal (PESARAN et al. 2002), V4 (TALLON-BAUDRY et al. 2004; LEE et al. 2005), and PFC (SIEGEL et al. 2009; LARA et al. 2014), was observed during DMTS tasks. Furthermore, in a study by Salazar and colleagues, (SALAZAR et al. 2012), fronto-parietal beta band (12 – 30 Hz) coherence was shown to encode stimulus identity. In LIEBE et al. (2012), the authors found that spikes in V4 were modulated by delta band (0.5 – 4 Hz) oscillations in PFC, and that an increased synchrony in theta band (4 – 8 Hz), between those areas was observed, in trials where the animals successfully remembered the cue stimulus.

1.3.3. Concluding remarks

The working memory (WM) is a highly distributed system that engages many cortical regions as a task unfolds (CHRISTOPHEL et al. 2017; DOTSON et al. 2018). Experimental evidence suggests that the interplay between frontal and sensory areas' oscillatory activity plays an important role in memory maintenance. There is an increasing consensus that the prefrontal cortex (PFC) not only encodes stimulus-related information with different abstraction levels but also information related to the task structure and plays an important role in biasing attentive selection via top-down modulation of sensory areas. Additionally, stimulus representation in distributed circuits was found to be sustained by phase synchrony in fronto-parietal networks (SALAZAR et al. 2012). And

more generally, by the coordination of transient oscillatory events across multiple cortical areas, as I will show in the study in Chapter 2. Therefore, given the relevance of oscillatory activity in implementing local and distributed mechanisms of memory maintenance during WM, in the next section, I present aspects of oscillatory activity in field potentials. More specifically, in Sections 1.4.3-1.4.4, I define the typical oscillatory bands found in these signals and cognitive functions, among them WM, related to them. Finally, I also discuss the role of transient oscillations for those functions.

1.4. Neural oscillations

Oscillations in the cortical electrical activity of humans were first observed by Berger and Lord Adrian (BERGER 1934; ADRIAN 1934). Berger described an oscillation of about 12 cycles per second, now known as an "alpha oscillation", which typically increased after the subject closed their eyes. While recording scalp electrical activity had been practiced in animal studies for about half a century (CATON 1970; BISHOP et al. 1936; BARTLEY et al. 1931), it was Berger's observation that initiated investigations into the relationship between field potential rhythms and brain functions, as is done today (BUZSÁKI et al. 2004; BUZSÁKI 2006; BUZSÁKI et al. 2023).

The study of neural oscillations owes much to advancements in technology that allow the registration of neuronal activity with high temporal resolution, such as EEG, MEG, and LFP. The latter, in particular, benefits from high spatial resolution, enabling researchers to simultaneously relate neuronal activity to ongoing mesoscopic recordings (BUZSÁKI et al. 2004; WANG 2010). Understanding the relationship between the underlying spiking activity and the rhythms present in field potentials is crucial, given the highly nonlinear behavior of neurons. This behavior provides neurons with properties like bursting, sub-threshold oscillations, resonance, and rebound action potentials, which are believed to shape brain rhythms (IZHIKEVICH 2007; HUTCHEON et al. 2000; IZHIKEVICH 2000; IZHIKEVICH 2001; PENA et al. 2018; PENA et al. 2019).

These advancements, coupled with increasing experimental evidence linking these rhythms to various brain functions, have positioned the field of neural oscillations as a central axis in describing brain activity in both healthy and pathological states (BAŞAR et al. 2008; BAŞAR 2013; BAŞAR et al. 2016; SILVA 2013).

Since Berger's initial descriptions of alpha and beta oscillations, numerous other brain rhythms spanning frequencies from less than 1 Hz to over 200 Hz have been discovered. Typically, these rhythms are categorized by adopting typical frequency bands. Commonly recognized brain oscillations and their respective frequency ranges include slow (< 1 Hz), delta (1.5-4 Hz), theta (4-8 Hz), alpha (8-12 Hz), beta (12-30 Hz), gamma (30-80 Hz), fast, and ultra-fast gamma (>80 Hz) rhythms (PENTTONEN et al. 2003). In particular, for the gamma rhythm there exists a distinction between narrowband gamma *oscillation* and broadband gamma *activity* that have distinct involvements in cognitive processes (PESARAN et al. 2002; BROVELLI et al. 2005; LACHAUX et al. 2012; BOSMAN et al. 2012; BROVELLI et al. 2015). However, these bands are loosely defined and are likely to vary across subjects, and cortical areas (HOFFMAN et al.

2024), due to differences in biophysical properties such as cellular membrane and synaptic characteristic times (GEISLER et al. 2005), neurons' resonant properties, and the degree of recurrent inhibition in local circuits which is reflected in the laminar dependence of peak frequency across the primate cortex (MENDOZA-HALLIDAY et al. 2024).

Detecting these rhythms in field potentials involves decomposing them into the frequency domain using Fourier-based techniques. Subsequently, their frequency content (i.e., their oscillatory components) can be correlated with a given function by comparing a control condition, where the subject or animal is at "rest", with a condition where a task is performed. Therefore, in addition to the technical procedures used to analyze field potentials, it is essential to carefully design experimental protocols that allow hypotheses to be tested while eliminating as many confounding factors as possible.

Following these procedures, each of these rhythms has been identified as a major marker of information processing in both local and distributed neuronal populations. Specifically, they are associated with various functions such as spatial navigation (O'KEEFE 1976; HASSELMO et al. 2002; BUZSÁKI 2005), memory consolidation (BUZSÁKI 1998), selective attention, and working memory. Furthermore, alterations in their properties are often linked to pathological conditions. Rhythms are also believed to play a crucial role in implementing distributed processing in the brain. In particular, the communication-through-coherence hypothesis (CTC) suggests that long-range communication is established when the oscillatory activity of different areas maintains a fixed phase relationship (GRAY et al. 1989; FRIES 2015). I will further elaborate on these relationships in Sections 1.4.3 and 1.4.3.

For now, as I hinted to the relevance of brain oscillations[10], I will provide a brief discussion concerning three questions researchers aiming to unveil the relation between neuronal oscillations and function, should try to address : What are their origin? How they work? What is the correct description of brain oscillations? (here in a different order, and context, than the one mentioned in BULLOCK (2002)). Since a complete answer to those questions would be a task beyond my competences, and also not possible at the time this dissertation was written, I will discuss them in a way that allows me to focus on the topics here enclosed. In particular, I will begin by describing the possible generating mechanisms of prevalent cortical rhythms, i.e., from the delta to the gamma range; describe their workings by presenting which phenomena they are most related to, and their possible role in long-range communication; and finally, I will discuss what would correspond to a correct description of brain oscillations by focusing on the debate of whether they are sustained or transient oscillations (which

[10] I avoid the discussion of whether or not oscillations are epiphenomenal (BREE et al. 2024). First, due to the amount of experimental evidence relating oscillations to different neuronal and cognitive functions (even though I come back to it in Chapter 1 discussion). Second, being epiphenomenal poses a problem when formulating mechanistic causal models concerning the involvement of oscillations in a given function, however, it does not mean they can not provide a useful description. One practical example is the technology of brain-machine interfaces that can infer subjects' intents by "learning"to read brain states from EEG/MEG signals (LOTTE et al. 2015).

is particularly relevant for Chapters 2 and 4). But before, I will make a brief detour to describe the field recordings (focusing on the local-field potentials, since they are the eletrophysiological recordings we used in both Chapters 2 and 4) from which those oscillations are detected.

1.4.1. The local-field potential

The local field potential (LFP) is recorded by implanting electrodes directly into the brain to capture the activity of neurons in its vicinity. The biophysical origin of the recorded potential is believed to be the summed transmembrane currents in a given neuronal population resulting from synaptic communication (BUZSÁKI et al. 2012a; EINEVOLL et al. 2013; PESARAN et al. 2018; VINCK et al. 2023). This is because, while action potentials (spikes) are brief "all-or-none" events, the excitatory and inhibitory post-synaptic potentials (EPSPs/IPSPs) caused by spikes arriving at a neuron are slower and more susceptible to synchronization due to the passive properties of the neuronal membrane. Consequently, their contribution to the field potential detected by the electrode is more significant (BUZSÁKI 2006), although spiking activity (usually multi-unit activity) can be extracted by applying a technique called "spike sorting" to the high-frequency component (> 500 Hz) of the LFP (QUIROGA 2012).

In addition to this textbook definition of the LFP's origins, various other factors may contribute to it, such as the active (LLINÁS 1988) and resonant properties of neurons (HUTCHEON et al. 2000), the contribution of action potentials (BUZSÁKI et al. 2003), and even the still poorly understood role of glial cells. In VINCK et al. (2023), the author provides a concise summary of the genesis of the LFP, in which the richness contained in this electrophysiological signal is nicely summarized :

> "*... Because synaptic currents also cause changes in membrane potential (i.e., synaptic potentials), LFPs are closely related to the summed neural membrane potentials in an area. These membrane potentials also give rise to spikes such that the LFP is both a proxy of the causes of neural spiking activity and a consequence of neural spiking activity.*"

The amount of sources influencing the LFP, make it not only difficult to interpret, but also dependable on several factors such as the electrode position relative to the neurons' recorded (i.e., the geometric configuration of the neurons-electrode system), and the overall correlation of the activity registered. The influence of this factors can be further elucidated by applying the better understood physical principles generating the field-potentials, together with the aid of computational modeling, to infer how the recorded signal depend on those factors. This constitutes the so-called LFP's "forward-modeling"(PESARAN et al. 2018).

In practice, the propagation of transmembrane currents along the neuronal membrane creates regions where there is a predominant influx (sinks) and others where outflux (sources) of currents dominate. This causes the cell to behave like a dipole, from which the potential is detected by the electrode. Using multi-compartmental

neuron models, researchers can simulate the field potential generated by a single cell to understand how the LFP changes when recorded closer or farther from the soma (EINEVOLL et al. 2013), as well as to understand the reach of the LFP by simulating a population of neurons (LINDÉN et al. 2011). Additionally, forward modeling can be a powerful tool to elucidate the relationship between spiking activity and field potentials (GŁKABSKA et al. 2016). Overall, this framework can aid in increasing the interpretability of LFPs by providing a better understanding of how local the recorded signal is, the extent of volume conduction effects, and linking findings based on mesoscale signals to their neuronal substrate.

Despite being an invasive recording method, LFPs benefit from better spatial resolution since they are not subject to the spatial smoothing caused by the scalp, as seen in EEG/MEG signals, and are thought to be highly local (GRAY et al. 1989; DUBEY et al. 2019; SPAAK et al. 2012). Despite the challenges mentioned above, LFPs have proven to be a powerful signal for understanding the brain. For example, they have been shown to correlate with aspects of motor preparation (SCHERBERGER et al. 2005; ROUX et al. 2006), processing of sensory stimuli (DI et al. 1990; VICTOR et al. 1994; MAZZONI et al. 2011; SZYMANSKI et al. 2011), and several cognitive functions (PESARAN et al. 2002; LIU et al. 2006; WOMELSDORF et al. 2006; LIEBE et al. 2012).

After this brief presentation of the local-field potential we can go back to the original track, i.e., discussing brain oscillations.

1.4.2. Cellular and network mechanisms of rhythmogenesis

The origin of neuronal rhythms can be traced back to the properties of single neurons and their synaptic interactions at the mesoscopic level. At the single-neuron level, the emergence of rhythmic spiking depends on biophysical properties that give rise to resonance, bursting, and sub-threshold oscillations. Additionally, the non-linear nature of neuronal responses allows them to adapt to synaptic inputs (e.g., by adjusting their phase) in ways that might lead to coherent spiking activity in local populations. At the mesoscopic scale, the emergence of oscillatory activity depends on the properties of the synapses through which these neurons communicate. For instance, local inhibition has been shown to generate local gamma activity. An understanding of how these micro- and mesoscopic properties contribute to the emergence of collective synchronous activity has been achieved through the collaborative efforts of experimental and computational research (WANG et al. 1996; BRUNEL 2000; BARTOS et al. 2002; BRUNEL et al. 2003; BATTAGLIA et al. 2007; BRUNEL et al. 2008; BATTAGLIA et al. 2011). In what follows, I will briefly describe a few neuronal features related to the emergence of neuronal oscillations, going from the micro- to the mesoscopic level.

Neuronal mechanisms of rhytmogenesis

Neurons generate rhythmic spiking activity, behaving as oscillators. Consequently, the phase at which action potentials are emitted can be influenced by external stimulation, that causes either phase delays or advances. A general mechanism through which

neurons synchronize their activity involves adjusting the phase of their spiking times relative to incoming synaptic inputs (ERMENTROUT et al. 1991). Whether a neuron delays or advances its spiking times in response to the phase of a stimulus is characterized by the "phase response curve" (PRC; CUI et al. 2009). Neurons that exhibit only phase advances are designated as "type I" cells, while those that exhibit both delays and advances are termed "type II" cells. The neuronal PRC type depends on the predominance of specific ion channels in its cellular membrane (CROOK et al. 1998; GOLDBERG et al. 2007). Typically, both types of neurons coexist within a neuronal population (TSUBO et al. 2007; WANG 2010), contributing to complex network dynamics. Specifically, this complexity is illustrated by the fact that type II neurons can achieve synchronization through mutual excitation, whereas type I neurons can achieve synchrony via mutual inhibition (UHLHAAS et al. 2010).

Additionally, the interplay between the low-pass filtering of the neuronal membrane, and the high-pass filtering properties of certain ionic currents, as the I_H current (IZHIKEVICH 2007; GE et al. 2016), equip neurons with band-pass filtering properties (HUTCHEON et al. 2000; PENA et al. 2018). In practice, this means that voltage responses will be enhanced for a certain range of frequencies. To determine the frequency preferences of a neuron, usually an oscillatory signal with increasing frequency (called ZAP; PUIL et al. 1986; CALÌ et al. 2008) is applied to the neuron. Next, the neuron's impedance is characterized as a function of the input frequency, in the what is called its "impedance amplitude profile". The impedance profile of resonant neurons exhibits a peak around the preferred frequency. The dependence of preferred frequency on cell type hints at distinct functional roles for them, for instance, hippocampus cells tend to fire with a rate very close to their preferred frequency (in the theta range; PIKE et al. 2000). Additionally, its been shown, computationally, that the preferred frequency of neurons can directly impact the frequency of network oscillations (CHEN et al. 2016).

Apart from the resonant effects due to the interaction of passive membrane properties, and ionic current dynamics. Neurons can display preferred frequencies due to damped sub-threshold oscillations (RICHARDSON et al. 2003). An interesting example on the possible role of this kind of sub-threshold dynamics in network oscillations, are the GABAergic neurons in the nucleus basalis and medial septum (WANG 2010). Those cells exhibit sub-threshold oscillations in the theta frequency range, that are interleaved by spiking activity lying in the gamma range (phenomenon refereed to as "mixed-mode oscillations"; WANG (ibid.)). Interestingly, the existence of theta-gamma coupling in some brain structures, such as the hippocampus in rodents (STUMPF 1965; SOLTESZ et al. 1993), and the neocortex in humans (CANOLTY et al. 2006), is a known phenomenon that might be influenced by this single-cell behavior, and morphology as hinted by computational studies in which the presence of both soma and dendrites are essential for achieving cross-frequency coupling (KEELEY et al. 2017).

Finally, Some cortical cells exhibits a type of "explosive"activity, characterized by the emission of a packet of spikes, refereed to as bursts. The frequency of emitted bursts depends on several factors, such as cell type, brain region, and ionic-currents involved on its generation. As an example, neocortical neurons displaying fast rhythmic bursting (or "chattering neurons") have been shown to influence gamma oscillations in

visual related activity (GRAY et al. 1996), and the same effect was observed in *in vitro* experiments (CUNNINGHAM et al. 2004).

With this, it is demonstrated not only how properties of single-cells are crucial for rhythmogenesis, but also that their interaction can yield complex oscillatory dynamics when they are put together. Next, it is also possible to think of synaptic and network mechanisms capable of generating neuronal oscillations. They can be understood from the level of a local-circuit (with a couple of connected neurons), to the level of network architecture as the number of interacting neurons increase (WANG 2010). In what follows, I will go over both of them.

Synaptic and network mechanisms of rhytmogenesis

Even though at a first moment, synchronization was thought to be due excitatory coupling (BREMER 1958), inhibition is essential in order to achieve neuronal synchronization (VAN VREESWIJK et al. 1994; WHITTINGTON et al. 1995; TRAUB et al. 1996; FISAHN et al. 1998; TIESINGA et al. 2009; BARTOS et al. 2007). While mutual excitation can generate epileptic-like synchronous activity, feedback inhibition can provide a resetting mechanism for the ongoing neuronal activity, defining the temporal scale of the entrained oscillation. This type of excitatory-inhibitory feedback loop was demonstrated in WILSON et al. (1972). More specifically, it poses that oscillations emerge naturally in a system where excitation is counterbalanced by either a slow or delayed inhibitory feedback loop. The characteristic time-scale of the inhibitory activity jointly with the inhibitory to excitatory delay transmission would set the phase relation between the two populations, and consequently, the period of the generated oscillations.

The model proposed by WILSON et al. (ibid.), and later the one by Kuramoto (KURAMOTO et al. 1984) provides a general mechanism to describe the emergence of synchrony between an excitatory and inhibitory oscillatory neurons (or the rate of populations of neurons, obtained in the mean-field limit). More specifically, synchrony between a couple of oscillators can be described by their phase-relation (ROSENBLUM et al. 2001; STROGATZ 2000). Using this framework one can devise the condition in which synchrony can arise from mutual-excitation, in particular in the condition where the neuron pair is weakly connected, and behave as "type II" neurons (as defined above). Analogously, synchronization between mutually inhibitory cells can be obtained for "type I" neurons, when inhibition is slow (WANG et al. 1993). More specifically, the description of oscillations in neuronal populations consisting of oscillator neurons and their phase-response curve belongs to a class of models based on the coupled oscillators theory (KOPELL et al. 1986; HANSEL et al. 1995; WANG et al. 1996; PANCHUK et al. 2013). Models of oscillations based on this theory fall into the category of the "spike-to-spike" regime (WHITTINGTON et al. 2000; KOPELL et al. 2002), where the mechanism of oscillogenesis relies on tonic drive input and synaptic decay time (TRAUB et al. 1996; WANG et al. 1992; WANG et al. 1996; ERMENTROUT et al. 1998; BÖRGERS et al. 2003).

A major drawback of the coupled oscillators theory lies in the experimental obser-

vation that even at moments of synchronous firing, neurons fire irregularly in vivo (SOFTKY et al. 1993; GEISLER et al. 2005; BUZSÁKI et al. 2012b). Another class of models, pioneered by Brunel, Wang, and others (BRUNEL et al. 1999; BRUNEL et al. 2003; GEISLER et al. 2005; ARDID et al. 2010), attempts to reconcile the emergence of gamma oscillations with irregular firing. In these models, neurons fire stochastically due to a fluctuating driving input, and oscillations emerge when the inhibition is sufficiently strong to inhibit a subset of neurons, which subsequently fire coherently when inhibition decays. Notice that these models rely on mutual inhibition, and oscillations are achieved in the firing rate limit, not at the single-neuron level, in contrast to the "spike-to-spike" models. Both models provide important insights into the descriptions of the ING (driven by interneurons inhibition) and PING (relying on both interneuron inhibition and pyramidal neuron excitation) models of gamma oscillations (BARTOS et al. 2007), and may even be useful for describing the mechanisms underlying other rhythms (BUZSÁKI et al. 2012b).

While the study of synchronization for a couple of neurons (or neuronal populations) is useful to understand the synaptic mechanisms leading to synchronization, and sometimes allows describing the resulting oscillatory regimes, via the mathematical analysis of the equations of the coupled oscillations, using non-linear dynamics theory (IZHIKEVICH 2007; STROGATZ 2018). As the size of the neuronal population analysed increases, another important factor influencing the appearance of synchronous activity is the way in which those neurons are wired together, i.e., the network topology. In this context, computational modeling is a powerful tool, since one can build models allowing the interplay of single-neuron, synaptic and network features affects rhythmogenesis.

Usually, studies consider network structures such as, fully-connected, "Erdős-Rényi" (or random; ERDŐS et al. 1960), "small-world" (WATTS et al. 1998) or even empirically estimated graphs (POTJANS et al. 2014; JOGLEKAR et al. 2018; MEJIAS et al. 2022). Studies considering fully-connected graphs showed that networks oscillations are present if the constituent neurons hold a zero-lag phase-relation when connected in pairs, otherwise they either manifest other types of synchronous dynamics, as the formation of clustering patterns, or asynchrony (WANG 2010).

Moving to random graphs, the work by BRUNEL (2000) showed that sparsely connected "leaky integrate-and-fire" (LIF) neurons driven by noise, are capable of producing regimes where synchrony is obtained. Interestingly, at single-neuron level neurons exhibit firing with Poisson statistics, but inputs can drive subthreshold activity, making it float around the spiking threshold. In this way, groups of interconnected neurons can drive each other without leading to super-synchronous activity, if excitation and inhibition are balanced. This work suggests that the emergence of oscillations depends on synaptic properties, and also requires a minimum degree of connected elements. For instance, in a study by WANG et al. (1996), they showed that the minimal number of required connections vary when conductance-based or LIF neurons are used as the network's building blocks. Additionally, only the first correctly predicts the emergence of hippocampal gamma oscillations in random graphs with sparsely connected elements (WANG 2010), evidencing the relevance of the interactions of single-neuron

and network properties in rhythmogenesis.

It is conjectured that neuronal circuits may exploit architectures, as those of "small-world" graphs (YU et al. 2008), that drastically reduce the distance between clusters of interconnected neurons by drawing a few connections among them. A practical way of obtaining "small-world" networks, is by converting (with a given probability p) local connections (belonging to a densely connected community of neurons), into long-range connections (between two distinct communities). By following this procedure, and evaluating the impact of the rewiring probability on the dynamics of a computational model (BUZSÁKI et al. 2004), the authors showed for an optimal value of this probability ($p = 0.25$), neurons showed an increased level of synchrony. Additionally, their model suggests that, a general organizational principle in this kind of networks may involve the optimization of the quantity of long-range connections used for achieve synchronizations, given that those are costly.

Brain structure and oscillations

We have seen that rhythms emerge from the interaction of neuronal, synaptic and network forming a hierarchical organization from which brain rhythms can be understood. At a systems level, the interaction between these three levels is dictated by the brain structure. Therefore the relation between structure and oscillatory activity is essential for understanding the cognitive functions it supports.

In particular, brain structure is the end result of millennia of evolution. Natural selection, has shaped the brain to enable organisms not only to create representations of the environment and interact with it but also to infer the outcome of their actions (FRISTON 2003; BUZSÁKI et al. 2023). As organisms developed increasingly complex traits, their brains evolved specialized structures for processing stimuli from different sensory categories, along with diverse cell types from both morphological and functional perspectives (NIEUWENHUYS 1994; SCHMITZ et al. 2022). With the increase in brain size, strategies for communication among its regions became necessary (BUZSÁKI 2006), as evidenced by intricate structural connectivity (SC) measured through diffusion imaging, tractography (TAYLOR et al. 2017; ZHANG et al. 2022), and retrograde tracing (MARKOV et al. 2013).

From the mesoscopic scale, the cortex is organized in five layers (MOUNTCASTLE 1997). Each layer has a predominant class of neuron types. The smallest functional division of the cortical mesh capable of performing all cortical functions is estimated to be a micro-column of around one millimeter squared (HUBEL et al. 1974), containing tens of thousands of neurons (ROCKEL et al. 1980), of all the "main" neuron types (SZENTAGOTHAI 1975). Even though a connectome can not be devised at this level due to the baffling number of synapses among neurons (in the order of billions inside a micro-column), it is believed that the connections between neurons are cell-type specific (THOMSON et al. 2002; BINZEGGER et al. 2004; POTJANS et al. 2014).

At the macroscopic scale, studies estimating the brain's SC have revealed a division into functional modules embedded in a hierarchical structure (FELLEMAN et al. 1991; YOUNG 1993; MEUNIER et al. 2010; SPORNS et al. 2016). Despite the considerable

cost of obtaining such a structure, the maximization of efficiency and robustness of the network, when compared to a randomly wired connectome, provides significant benefits (BASSETT et al. 2010; BULLMORE et al. 2012). Alongside this modular structure, the brain may exhibit a "small-world" structure characterized by communities where elements are highly connected internally but send few projections to other communities. This organization allows for short characteristic path lengths among elements, facilitating faster information spread across communities, a phenomenon known as the "six degrees of separation" effect (BASSETT et al. 2006).

Hierarchically organized modules often exhibit a "scale-free" structure, which implies that while local dynamics can be orchestrated by modules at higher hierarchy levels, the dynamics of these higher-level modules can also be impacted by their sub-modules. Scale-free networks are typically characterized by power laws, where the probability of an area making K connections scales linearly with K when plotted on a log-log scale ($P(K) \propto K^{-b}$). A consequence of this scaling law is the observation of similar structures as one moves from macro to microscopic scales, often displaying a fractal or self-similar architecture (BARABÁSI et al. 1999).

Interestingly, experimental evidence shows that the oscillatory power of field potentials tend to decrease as frequency increases, also following a power-law (typically refereed to $1/f$ decay of the power spectrum; FREEMAN et al. 2000). This observation not only hints on the intrinsic relation of structure and function (BUZSÁKI 2006; STEINKE et al. 2011), but also unveils an organized system of oscillatory classes that spans frequencies going from less than 1 to more than 600 Hz (PENTTONEN et al. 2003). For instance, experimental evidence points alpha and theta oscillations as global pacemakers responsible for engaging neuronal populations across the cortex and consequently establishing long-range communication, while faster rhythms are associated with local processing (SILVA 1991; VON STEIN et al. 2000; SAUSENG et al. 2005). Altogether, the interplay of brain rhythms embedded in the cortical architecture allow information processing to be multiplexed across spatial, temporal and spectral scales (BUZSÁKI et al. 2004; BUZSAKI et al. 2004; VEZOLI et al. 2021). The mechanisms by which this is achieved remains an open question, and it is one of the motivation question that we tried to partially address in the projects presented in this dissertation.

To close this section, while I provided a non-exhaustive overview about the mechanisms of rhythmogenesis, the ones discussed above provide a general view of the number of interacting scales involved on observed neuronal rhythms. In particular, it illustrates how the appearance of oscillations depends on the interaction of many spatial and temporal scales of the brain.

1.4.3. From neural oscillations to brain function

In this section, I will shortly describe each rhythm ranging in an order of increasing frequency (and decreasing power due to their $1/f$ dependence; see Section 1.4.2), i.e., from delta to gamma. I give an specific focus on the cognitive functions they were found to support.

Delta rhythm (0.5-4 Hz)

The delta rhythm was first reported by William Grey Walter (GREY 1961), not long after Berger's description of the alpha and beta oscillations. This rhythm is usually associate with sleep, manifesting during the slow-wave-sleep (SWS) stage and characterized by cortex-wide activity that switches between moments of high hyperpolarization and depolarization (STERIADE et al. 1993; NESKE 2016). While this rhythm can be generated by the neocortex (SANCHEZ-VIVES et al. 2000), it also engages other subcortical structures (MAHON et al. 2006; SHEROZIYA et al. 2014; HEADLEY et al. 2017).

Besides its contribution to a variety of cognitive tasks (HARMONY 2013), it has also been related to motivation due to the overlap of sites in which delta waves propagates, and the one corresponding to the dopaminergic circuits (ALPER et al. 2006; KNYAZEV 2007). Even though there is little consensus about the origin of delta waves during cognitive processes, it has been demonstrated that modulations in delta power are also associate to attention and working memory, and are thought to provide inhibition to suppress all internal interference during those processes (FERNÁNDEZ et al. 1995; HARMONY et al. 1996).

Theta rhythm (4-8 Hz)

In the hippocampus the theta rhythm display a variate of behavioral correlates. In particular, the firing activity of "place cells"(O'KEEFE 1976) responds preferentially to specific locations as a rat navigate through a maze (defining their "place field"). Interestingly, in O'KEEFE et al. (1993), it was found that as the rat moved along a cell's place field, its place cells' spiking times receded towards an earlier phase of the ongoing theta oscillation. Additionally, theta activity is prominent during REM sleep, and sniffing (VANDERWOLF 1969; HEADLEY et al. 2017), and is thought responsible for consolidation and retrieval of episodic memory (HASSELMO et al. 2005; HASSELMO 2005). Finally, it is also know that gamma activity is modulated by theta oscillations, suggesting that it carries a role of coordinating local processing in the hippocampus (BRAGIN et al. 1995), and also in the pre-frontal cortex during exploration tasks (LUBENOV et al. 2009).

While the theta rhythm carries a strong link to the hippocampus, experimental evidence suggests that increased theta activity originated in the neocortex (CANOLTY et al. 2006), is related to working memory in humans (RAGHAVACHARI et al. 2001), and modulations in theta power carry a relation with the memory load associated with the task, that is spatially dependent (MELTZER et al. 2008). In non-human primates and humans, spiking activity showed to be modulated by the theta frequency component of the LFP, during working memory (LEE et al. 2005; JACOBS et al. 2007). Evidence that theta acts to promote long-range integration, due to observations of increased phase-synchrony in the theta range, both within V4, and between V4 and the pre-frontal cortex, in monkeys performing memory task (HOERZER et al. 2010; LIEBE et al. 2012), most interestingly, the entertainment between those areas seems to predict the animals' performance.

Alpha rhythm (8-12 Hz)

As previously mentioned, the alpha rhythm, was first reported by Berger (BERGER 1934; see Section 1.4), and is thought to have thalamic origin (RENNIE et al. 2002; HINDRIKS et al. 2013), even though there are pacemaker cells, with rhythmic firing within the alpha frequency range, present in cortical layer 5 (SILVA et al. 1991). Due to the observations of alpha power increase while subjects kept their eyes closed (BERGER 1934; ADRIAN 1934; KLIMESCH et al. 1996), it has traditionally being associated to a cortical "default state", present when no sensory processing was taking place in the brain (BUZSÁKI 2006). Oftentimes, alpha oscillations have been regarded as random neural activity, however analysis founded on non-linear dynamics theory showed that they show deterministic-chaos behavior (BAŞAR 1990; DA SILVA et al. 1997), oscillating between regimes of low- and high-amplitude fluctuations, akin to what would be expected in systems tuned close to a Hopf bifurcation (FREYER et al. 2009; FREYER et al. 2011). Furthermore, it has later been associate to diverse brain functions (BAŞAR et al. 1997), such as, visual attention (PALVA et al. 2007; BABILONI et al. 2006; BOLLIMUNTA et al. 2011), movement, and memory (PFURTSCHELLER et al. 1992). Interestingly, contrary to one would expect from a "default state", increases in alpha power are known to correlate with working memory (JENSEN et al. 2002; SCHEERINGA et al. 2009; TULADHAR et al. 2007).

How to resolve this apparent paradoxical nature of alpha oscillations? Given that alpha power was found to increase during tasks that were mental operation were required (SCHUPP et al. 1994; PALVA et al. 2005; COOPER et al. 2006), theories suggesting a mechanism of active inhibition for the alpha rhythm were proposed. For instance, during working memory tasks, alpha power would increase in areas not related to memory maintenance to "silence" distractors (KLIMESCH et al. 2007; JENSEN et al. 2010; BONNEFOND et al. 2012). Even so, it is difficult to disentangle a role of inhibitor from a possible active mechanism of memory maintenance during memory tasks, since those areas engage many areas and the extent of their relevance is difficult to determine (PALVA et al. 2007). Finally, the association of alpha activity with active inhibition, has been used to propose mechanisms in which alpha would long-range integration. In this framework, alpha oscillations would actively inhibit pathways that are not used for a particular task, allowing the task-related regions to establish communication (the "gating by inhibition"hypothesis; BONNEFOND et al. 2017)

Beta rhythm (12-30 Hz)

The beta rhythm was first reported in the motor cortex by Berger (BERGER 1934). This early association with sensorimotor regions was deepened when JASPER et al. (1949), reported a reset of beta activity related to just prior movement onset and execution, and as soon as the movement ceased, beta power started to increase (PFURTSCHELLER et al. 1977; PFURTSCHELLER et al. 1999; ERBIL et al. 2007; WHEATON et al. 2009). The same effect is observed if a a prepared movement is not executed (ALEGRE et al. 2004; ZHANG et al. 2008). Those observations led to the idea that beta activity, is not

only related to movement preparation, but also act for commanding its inhibition (PFURTSCHELLER et al. 1996; LEOCANI et al. 1997). Apart from its involvement with motor functions, beta activity is also implied to support a range of cognitive processes (KILAVIK et al. 2013). For instance, during visual working memory tasks, significant coherence is observed in the beta band between sensory and cognitive areas (SAALMANN et al. 2007; BUSCHMAN et al. 2007). These observations, accompanied of experimental evidences that most feedback pathways originate on deep cortical layers, known to be generators of beta activity (BARBAS et al. 1997; DOUGLAS et al. 2004; ROOPUN et al. 2006), suggests that this rhythm is related to "top-down" signaling (FRIES 2005; SIEGEL et al. 2012; BASTOS et al. 2015; FRIES 2015). This role of beta activity, in routing "top-down"information, make it one of the prominent rhythms candidate to mediate and establish long-range communication in the "communication-through-coherence" (CTC) framework. As a matter of fact, in a experiment where humans had to keep a visual cue in mind, increased beta coherence was observed in regions separated by several centimeters in visual areas (TALLON-BAUDRY et al. 1997), a similar effect was observed in the temporal lobe (TALLON-BAUDRY et al. 1998), where it was also related to information routing (BROVELLI et al. 2004). In non-human primates experiments, it was shown that stimulus encoding may depend on the phase of the ongoing beta activity in the PFC, when the animals have to hold multiple objects in mind (SIEGEL et al. 2009). Finally, fronto-parietal beta coherence during the delay period of a visual task was shown to encode stimulus identity (SALAZAR et al. 2012), and within the PFC beta modulations were shown to depend on whether the monkey had to respond to color or the orientation of a visual cue, i.e., from the task rule adopted (BUSCHMAN et al. 2012). In summary, in addition to beta's involvement in motor tasks, beta coupling is also thought to promote sensorimotor integration (LALO et al. 2007; SPINKS et al. 2008) and serve cognitive processes. For example, beta activity before cue presentation in tasks is thought to reflect task-related information (SALEH et al. 2010; JENKINSON et al. 2011).

Gamma rhythm (30-80 Hz)

The gamma rhythm was first described in the olfactory bulb by Lord Adrian (ADRIAN 1942; ADRIAN 1950). Its relation with odor processing was later extended by the works of Freeman (BRESSLER et al. 1980; FREEMAN 1987). In particular, he suggested that the synaptic interaction between bursting neurons would bind them, creating chaotic[11] alternating spatio-temporal patterns (as "movie frames"), carrying stimulus related information (BRESSLER 1984; FREEMAN 1991; FREEMAN III et al. 2010). In parallel, recordings from cats' fronto-parietal regions, carried by BOUYER et al. (1981), associated gamma activity to a state of "hyper-vigilance", and led to the current ideas of the gamma rhythm being linked to attention (FRIES 2009). In a series of studies, it was found that attention is typically followed by an increase in gamma, and a decrease in alpha power (TULADHAR et al. 2007; SCHROEDER et al. 2009; RICHTER et al. 2017; XIONG et al. 2023) in a range of sensory modalities (TIITINEN et al. 1993; TAYLOR et al.

[11] Chaotic as it is used in the context of non-linear dynamics theory.

2005; HAUCK et al. 2007). This effect was demonstrated, in FRIES et al. (2001b), where monkeys had to attend to, either a visual cue lying at the receptive field of neurons in V4, or another one (that was shown simultaneously) outside of the receptive field. By analyzing both LFP, and multi-unit activity, they show that attention directed to the cue inside the receptive field was accompanied with a reduction of power in alpha, and enhanced gamma bands.

Investigations concerning spatial patters generated by gamma in the visual cortex (FREEMAN et al. 1987), would culminate in the groundbreaking finding, by GRAY et al. (1989) et ECKHORN et al. (1988), that seemingly distant sites (possessing similar receptive fields), in the cat visual cortex, would synchronize their gamma activity when being stimulated with light bars moving in the same direction. Most interestingly, this finding provided a possible neural correlate for the "binding problem" that roughly consisted in understanding how the image of a "whole" object is formed by the the representation of its parts, scattered across a population of neurons, i.e., how those areas bind together features of an object (TREISMAN 1996). The mechanism for binding was explained under the "temporal correlation hypothesis" (SINGER et al. 1995), which today, with the conceptual addition that phase-synchronization can mediate routing of information, is known as "communication-through-coherence" hypothesis (VOLGUSHEV et al. 1998; AZOUZ et al. 2003; WOMELSDORF et al. 2007b; WOMELSDORF et al. 2007a; FRIES 2005; FRIES 2015). Additionally, when dealing with multiple items during WM, the interplay between gamma and theta rhythms is thought to guide attention via a mechanism named "Rhythmic Attentional Scanning" (FRIES 2023), where each attended item is processed in a distinct theta cycles containing nested gamma cycles. In this mechanism, attention is propagate in the form of traveling theta waves that helps to consolidate cue representation by means of gamma-synchronized neuronal populations. Finally, in an investigation of the relation between the relation structure-function and its dependence on cortical rhythms, Vezoli and colleagues (VEZOLI et al. 2021) found that directed interactions in the gamma-rhythm (measure by means of Granger Causality) are most predictive of the macaque connectome.

Oscillations and long-range communication

During this brief description of the neuronal oscillations, the role of synchronization of oscillations as a way of establishing long-range communication came up a couple of times. In particular, the alpha, beta and gamma rhythms play an important role, since they provide ways of actively inhibit sensory areas, to do "top-down" signaling, and assemblies formation (among other functionalities). Therefore, it is tempting, given this system of oscillators present in the brain, to formulate hypothesis in which they are the main actors creating (or suppressing) routes for communication. As a matter of fact, oscillatory activity is a perfect candidate for that, since it not only create windows where synaptic inputs provident from a sender region can impact the receiver (the up phase of an oscillatory cycle), but also the contrary (the down phase of an oscillatory cycle). In this case, efficient communication would only depend on conduction delays between a pair of areas, and the phase of the oscillatory activity in the receiver

region relative to the spike discharges in the sender. This, together with the "temporal correlation hypothesis", that proposes a mechanism for the "binding problem", allows to the system of rhythms of the brain to be under a common framework of neuronal communication, i.e., the "communication-through-coherence" hypothesis.

Given that the interplay between brain-wide integration and segregation is thought to support a range of cognitive functions (TONONI et al. 1994; BASSETT et al. 2011; SPORNS 2013; COHEN et al. 2016; DOTSON et al. 2018), correctly addressing the mechanism(s) by which long-range communication among brain areas is established, is of utmost relevance. This question is particularly challenging, since (i) oscillatory activity may be transient which puts in question the feasibility of CTC (BURNS et al. 2011; XING et al. 2012; PALMIGIANO et al. 2017); (ii) multiple mechanisms of integration could exist some that profit of oscillatory activity other from transient bursts in order to implement non-linear integration (VINCK et al. 2023); (iii) in the case of transient events their characterization may be technically difficult and standard methods based on Fourier-theory (e.g., coherence) may not faithfully capture neuronal interactions (SCHNEIDER et al. 2021; DOWDALL et al. 2023). One of the main goals of this dissertation was to properly characterize the mechanisms of cortical integration during working memory by considering events of excitability that may or may not be oscillatory, which allowed to consider the role of both oscillatory and transient activity to achieve integration without strong *a priori*.

The elaborate on this issue, in the next section, the problem of finding a "correct" representation to oscillations in the brain. In particular, I will go over the matter discussing whether they are of persistent or transient (EDE et al. 2018). In particular, will concentrate on the two major scientific questions regarding transient activity, that is, "are they implied in any brain function?", and "can they be used to establish communication (i.e., implement CTC)?".

1.4.4. Persistent *versus* transient oscillations

At a first glance, burst events may seem an unreliable candidate for implementing any function, due to their seemingly stochasticity. So, answering both questions posed above require reconciling this observation, with experimental evidence supporting functional role of transient oscillations. First of all, the fact that these events seem to arrive "randomly" (BURNS et al. 2011; XING et al. 2012), does not mean that they are not elicited by stimuli or other internal process (PALMIGIANO et al. 2017). As a matter of fact, experiments related to motor tasks have gathered evidence that beta bursts are indeed task modulated (FEINGOLD et al. 2015; LUNDQVIST et al. 2016; MIRZAEI et al. 2017), and some of this events (while not trial locked) have bigger propensity to manifest in specific moments of a task. As it is nicely put in FEINGOLD et al. (2015) :

> "*... beta synchronization and desynchronization are quantum-mechanics-like probabilistic states, reflecting the probability of much shorter bursts of oscillation rather than the strength of sustained oscillations.*"

Another evidence comes from the already mentioned study by Douchamps and colleagues (DOUCHAMPS et al. 2024). As I said before, they detected bursts resolved in time and frequency by detecting them on the spectograms of a theta and a gamma components of the recorded LFPs. Afterwards, they extracted a few features from each detected burst. Using those features as inputs to a random-forest classifiers, they were able to decode the location of the mice during exploration, suggesting that the stochastic dynamics of those bursts were modulated by (and informative about) behavior. Here, they also observed a big variety of burst frequencies (within their corresponding ranges, i.e., the theta and gamma bands), and that the averaged signals were dominated by a few strong bursts.

Even though beta bursts were detected in the motor-cortex (FEINGOLD et al. 2015; LUNDQVIST et al. 2016; MIRZAEI et al. 2017), their relation with working memory, put them in the spotlight as candidates of bursts of cognition (LUNDQVIST et al. 2024). In LUNDQVIST et al. (2016), while recording LFPs from the lateral PFC and frontal eye-field of monkeys performing a visual WM task, the authors reported that increases in the rate of beta burst were accompanied by a suppression of gamma bursting, and vice-versa. Interestingly, units carrying stimulus-specific information displayed increased activity during gamma bursting. These results suggests that beta activity act as an inhibitor of WM's central executive functions, while gamma activity supports memory maintenance. In this scenario, WM would depend on the interplay of beta activity from deep cortical layers, and superficial layers gamma. More specifically, deep beta would inhibit the superficial one, releasing gamma-related spiking, and consequently memory retrieval/maintenance (MILLER et al. 2018).

While the experiments described above give a clear evidence for the functional role of bursts, the feasibility of CTC via bursting activity came by the modeling work in PALMIGIANO et al. (2017). The authors used a network with the dynamics tuned to operate near a subcritical Hopf bifurcation (i.e., on the edge of oscillatory synchrony), which is characterized by small amplitude fluctuations interleaved by transient bursting activity. By connecting different populations, as proxies for brain areas, they showed that even though bursts were short and stochastic, they were allowed neuronal populations to transfer information to each other above chance level. In particular, they showed that the information was sent from the area in which the burst lead the phase relation.

Finally, the highly non-linear nature of those burst activity could be exploited to mediate communication (VINCK et al. 2023). Since, this form of communication allow for amplification of signals, they would be suitable for distributed integration of information (VAN VUGT et al. 2018). More specifically, the interval of occurrence of a burst would offer a window of opportunity where co-occurring bursts could form multi-area assemblies. The multi-area patterns could then be exploited to, for example, carry stimulus specific information, and support WM maintenance (IMPERATORI et al. 2019; VINCK et al. 2023; as we show in Chapter 2). Interestingly, in a recent publication by Hindriks and Tewarie (HINDRIKS et al. 2023), the authors showed that coherence (phase-relation) and co-bursting (captured by co-kurtosis; or the rate of coincident bursts), represent two orthogonal means of communications. So, besides

being compatible with the CTC framework, transient oscillations offers new means of thinking of long-range integration among brain regions.

As we have seen in the example above, uncovering the functional role of transient activity may require proper characterization that cannot be achieved by conventional methods. Using the example in DOUCHAMPS et al. (2024), the link between burst types and behaviors could not be recovered by classical trial- or time-averaged analysis. In the next section, I will present the methodological aspects related to the characterization of burst activity, as this issue is particularly relevant to the work I developed during my thesis. Some of this issue is already present in the research project in Chapter 3, but it is in the project I present in Chapter 4 that we exclusively focus on properly detecting and categorizing the features of bursts in single-trial activity, to uncover their relation to behavior and other cognitive functions.

The methodological aspects of transient activity characterization

Strictly speaking, an oscillatory signal is a pattern that repeats itself after a given interval (called its period), in its purest form one can think of them as sines and cosines. With knowledge of its period or phase in the oscillatory cycle, its future can hold no secrets. On the other hand, electrical (and spiking) activity recorded from the brain is stochastic and highly variable across recording sessions and trials (excluding examples like hippocampal theta in rats, and the activity some stages of the sleep cycle BUZSÁKI 2006). In this sense, characterizing the registered signals by means of their power spectrum is, quoting from BULLOCK (2002), "*as adequate as describing an opera in terms of its power spectrum*".

But how to account for such variability when investigating brain's rhythms? Many techniques that allows to characterize the dynamics of power modulations, such as the Hilbert-Huang (HUANG 2014; QUINN et al. 2021), wavelet (TORRENCE et al. 1998) and multitaper transforms (BABADI et al. 2014), exist. In fact, investigating brain signals with these techniques, provided evidence that oftentimes, brain oscillations are very transient, and seemingly stochastic. Due to this intrinsic stochasticity, the aforementioned methods carry the drawback of requiring either time or trial averaging[12], which can either hinder transient oscillatory events that are not trial-locked, or create an artefactual sustained oscillation (JONES 2016).

One alternative to work around those issues, would be to extract features from transient oscillations (that I shall, interchangeably, refer to as bursts), such as duration, timing, frequency, power, and others (FEINGOLD et al. 2015; KOSCIESSA et al. 2020; DOUCHAMPS et al. 2024). Additionally, a burst-triggered[13] characterization of spiking activity can be performed, which would help to connect those events to the spiking dynamics generating them (WILLIAMS et al. 2020). Of course, this would involve detecting those bursts in first place, so in the next paragraphs I will spend some words

[12] Even though LACHAUX et al. (2002) proposed a way of measuring it for single-trials, for which we proposed a fast implementation; see Chapter 3 and Appendix B.

[13] In a burst-triggered analysis data is aligned around a specific type of event, so they are not averaged-out as it happens on cue aligned trial-averages, for example.

on this issue.

As for now, several techniques to characterize whether oscillations in neuronal data are of persistent or transient nature were proposed (SCHMIDT et al. 2023). For instance, in FRANSEN et al. (2015), they develop a method that allow to quantify to which extent the phase of a signal can be predicted, based on its previous values (rhythmicity; RAYSON et al. 2022). Hence, this method allow a proper characterization of the duration of oscillatory activity compared to power. The estimated duration of the oscillatory events, can then be used as a criterion to determine whether they are of transient nature or not (SCHMIDT et al. 2023).

While techniques, as the aforementioned lagged-coherence, can determine the nature of the oscillatory activity in a given data-set. The detection of transient events, are usually done by adopting a threshold based on a given percentile or number of standard deviations (SHIN et al. 2017; LITTLE et al. 2019; SORRENTINO et al. 2023; as we do in the analysis in Chapter 3). An alternative for hard thresholding, is presented in DOUCHAMPS et al. (2024). In this paper, the authors detected bursts in single-trial LFP recordings from the rat hippocampus, by first decomposing the signals in a theta and gamma components, using the empirical mode decomposition method (HUANG 2014; STALLONE et al. 2020; QUINN et al. 2021), and then detecting "blobs" in the spectrograms of each signal component by applying an image segmentation technique called "watershed" algorithm[14] (which we further develop to apply it to recordings from monkey hippocampus; see Chapter 3). Other methods exist, as the Hidden Markov Method, that allow to detect sequences of discrete states, that could correspond to different burst types, oscillations, and non-oscillatory activity, without recurring to any thresholding of the data (BEAL et al. 2001; QUINN et al. 2018).

1.4.5. Concluding remarks

Oscillatory activity is ubiquitous in field-potential recordings, and its emergence depends on the interaction of elements across different spatial scales, from neurons to networks. Additionally, the dynamics of oscillations in a given region may be modulated by distant sites, such as in the case of oscillations generated by thalamocortical interactions. This suggests that biophysical parameters and brain structure (i.e., the way it is wired) jointly provide the necessary substrate for the emergence of observed oscillatory activity. However, while brain activity is highly dynamic, structure only changes over long time scales.

Moreover, variations in oscillatory activity, such as their presence or absence (quantified by their power), are implicated in various functions, as discussed above. Thus, brain structure constrains pathways through which information can flow, yet does not determine them in a fully hardwired manner. Flexibility in information processing is essential for behavior, as it allows for rapid adaptation to changes in the environment

[14] This method allows to detect bursts in time-frequency without recurring to a hard threshold. It does so by iteratively thresholding the spectrogram (from high to low thresholds), and checking if at any moment the boundaries of previously detected events merge, in which case the growth of those objects is refrained (SEAL et al. 2015).

(try to imagine the feasibility of CTC if signaling depended on fixed and inflexible pathways).

In summary, if oscillatory activity (regardless of it being stationary or transient) is a fundamental marker of information processing in the nervous system, our goal is to understand how and under which conditions dynamics can implement computation. Specifically, during my thesis, we aimed to address : (i) how distributed oscillatory patterns emerge and their functional role in WM ; (ii) how they support encoding at the level of networks of cortical areas ; and (iii) whether the dynamics originating from the interaction among these areas could reflect more fundamental computations of storage, transfer, and modification, which we addressed via modeling. Therefore, it is fundamental to understand the relation between complex systems' dynamics and information from a theoretical standpoint and then linking it to brain dynamics, i.e., how to go from dynamics to computation.

1.5. From dynamics to computation

Complex systems are everywhere to be seen in nature, and can take the form of insect colonies, the immune system, economics, and the brain. But what exactly characterizes a complex system? Using the definition given by Professor Melanie Mitchel in her book "complexity" (MITCHELL 2009), a complex system corresponds to a system :

> "*... in which large networks of components with no central control and simple rules of operation give rise to complex collective behavior, sophisticated information processing, and adaptation via learning or evolution.*"

These systems are said to *self-organize*, without an external controller, by means of their internal dynamics (BAK et al. 1988), and to exhibit *emergent* phenomena, i.e., behaviors that can not be trivially extrapolated from the functioning of the fundamental constituents of the system[15]. For instance, it happens that through the simple principles of natural selection, the interaction of life-forms and the environment give rise to "*endless forms most beautiful and most wonderful*" (DARWIN 2023) ; that the cooperative behavior of animal groups may create a collective cognition (COUZIN et al. 2002 ; COUZIN 2009) ; or that consciousness emerges from the network of interacting neurons in the brain (MILLER et al. 2024).

Given the astonishing variety of systems exhibiting self-organized complex behavior, it is tempting to know whether there are laws binding them together, i.e., a unified quantitative description of complex systems. As a matter of fact, this common link lies in the fact that those system can exhibit a range of qualitatively behaviors as a parameter controlling their internal dynamics is varied. The particular values of this control parameter where a phase-transition takes place (i.e., where one behavior

[15] Or equivalently, by adopting a reductionist approach to explain the system

morphs into another), is refereed to as the critical value of this parameter, or the critical point.

Most importantly, it is conjectured that at this critical point complex systems exhibits an increased information processing capability, and the requirements for implementing computation. This conjectures derives from the fact that, (i) when at the critical point, activity occasioned by a wide range of stimuli levels (KINOUCHI et al. 2006), can optimally propagates through the system; (ii) critical behavior is characterized by the formation of complex patterns spread across many spatial and temporal scales of the system, that interact in ways in which information storage, transmission and modification may be supported (MUNOZ 2018). In the next subsections, I will present the intrinsic relation between complex systems "wandering" in the vicinity of a phase-transition, and their ability to "compute". In particular, I will discuss : (1) in which conditions a complex systems can support computation; (2) how to characterize and quantify the computations carried by the system; and (3) how the brain, as a complex system, can use its rich repertoire of activity, spanning many spatial and temporal scales, to perform computation.

1.5.1. Complexity and computation

Computation is an emergent property of complex systems, and corresponds to their capability of modifying, transferring, and storing information. In SHAW (1984) et LANGTON (1990), those authors hypothesizes that computability emerges when the system's dynamics is tuned to be close to a phase-transition ("in the edge of chaos"). Intuitively, this can be better understood by considering the example of written language, as the sequence of words you are reading now. First, imagine the scenario where those symbols were unfamiliar to you, and you try to grasp their structure. You might be able to infer that this sequence of symbols carry some meaning, because they have a structure, that is, they are neither static nor completely random. More specifically, letters and words are bonded by grammatical rules and semantics. Given enough of those symbols you might even be able to create new artificial text exploiting the statistical relations and rules you have uncovered[16]. Analogously, the different states or configurations of a complex systems, provides them with their basic alphabet. However, as it is the case for written language, possessing an alphabet is not enough for computation to emerge. Only when at the edge of a phase-transition, this symbols can bond in special ways giving rise to complex patters. Only at this point, lying between regularity and randomness, the system develops the grammar dictating how its lexicon binds together.

To render this intuition graphical, Langton used a simple "celullar automata"(CA) model consisting of a single row of cells that transited from one state to another depending on its neighbor's states, by following a table of transition rules. By controlling the fraction of rules (λ) that lead to a dead state he could make the model transition from

[16] Like the statistical model of the English language explored by Shannon, based on the idea that not only letters had distinct frequencies of usage, but also that the transition between words can be modeled as a Markov chain (SHANNON 1948; SHANNON 1951).

something that generated patterns ranging from predictable to unpredictable. In this model, complexity is lying somewhere in between these two extrema. In particular, as λ increases, the transients time in which the system arrived in a static pattern got longer and longer, and as it approached a critical point, activity morphed from a repetitive pattern to a set of complex propagating structures that expanded across the grid. As λ was further increased above this critical point, complexity was replaced by chaotic propagation (Figure 1.5.1). Those distinct qualitative behaviors we observed as λ varied, were divided in four classes by Stephen Wolfram (WOLFRAM 1997; Figure 1.5.1) :

- **Class I** : The CA evolves to a homogeneous state (or to a *limit point*) ;
- **Class II** : The CA alternates between periodic structures (or to a *limit cycle*) ;
- **Class III** : The CA exhibits aperiodic chaotic patterns (as it is observed in *strange attractors*)
- **Class IV** : The CA exhibits patterns of localized structures, with long transients.

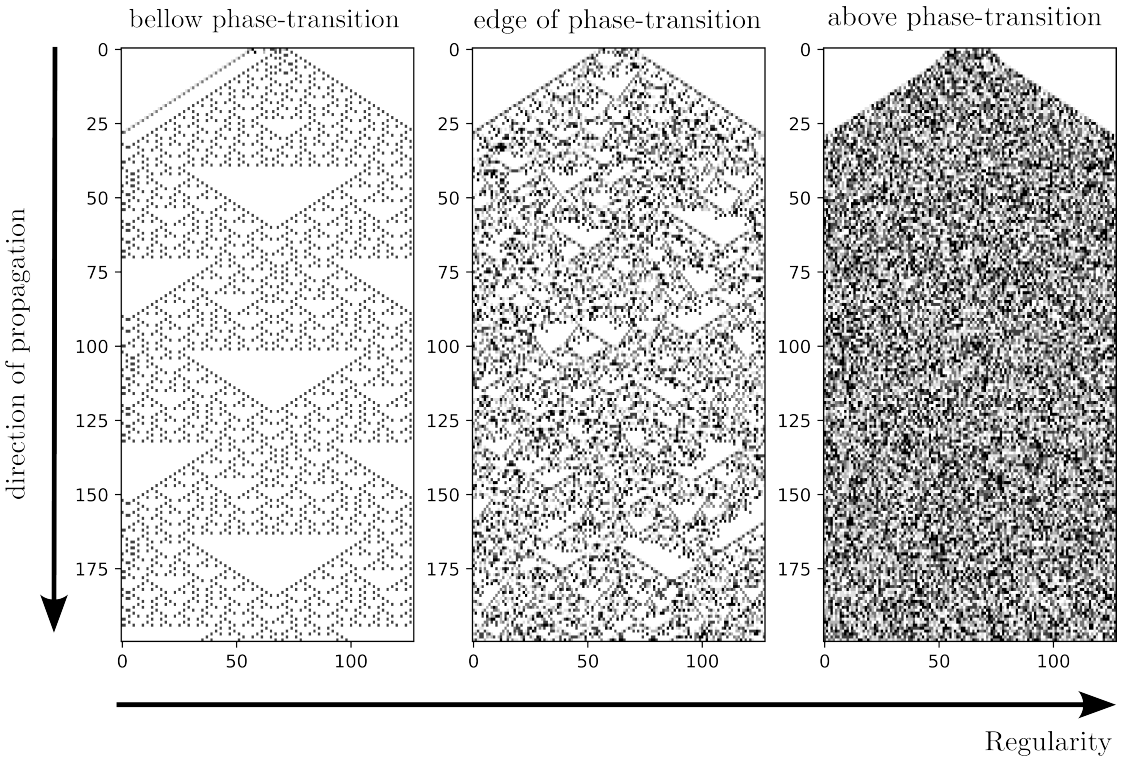

FIGURE 1.2. : Langton's 1D cellular automata. The vertical axis represents distinct generations of the cells distributed along the horizontal axis. From left to right the systems goes from an ordered state to a chaotic one, right in the middle it is at the edge of a phase-transition. Observe that while the left-side plot boring repetitive structures repeat themselves, and the right-rand side no structure can be devise whatsoever, in the middle complex patterns emerge from time-to-time.

Effectively, CAs belonging to class IV are considered capable of implementing computation, hence their complex behavior (LANGTON 1990; WOLFRAM 1997; MARTÍNEZ et al. 2013). As an illustrious example of CAs beloging to class IV, we may take Conway's game of life (GoL). In this game, each cell lives in a position of a 2D grid, and may be either "dead", or "alive", at a given moment. The transition between these two states depends from time t to $t+1$, depends on the state of its neighbors at time t. Based on those simple rules, the GoL not only can create complex patterns, such as, spaceships[17], and self-replicating patterns[18] (BROWN et al. 2023), but also be used to implement universal Turing machines (RENDELL 2011). Interestingly, by using a slightly modified version of GoL in NORDFALK et al. (1996), where the transition from the dead to alive state (and vice-versa), depended on a probability value (so it acts as a control parameter), the authors have shown that by varying the probability values, the GoL exhibit a critical region where a phase-transition takes place, and that the actual rules of the GoL lies very close, but not at, to it.

[17] Carefully categorized by GoL's geeks https://conwaylife.com/wiki/spaceship.

[18] For instance, a glider gun, capable of creating a spaceship pattern called glider https://conwaylife.com/wiki/Gosper_glider_gun.

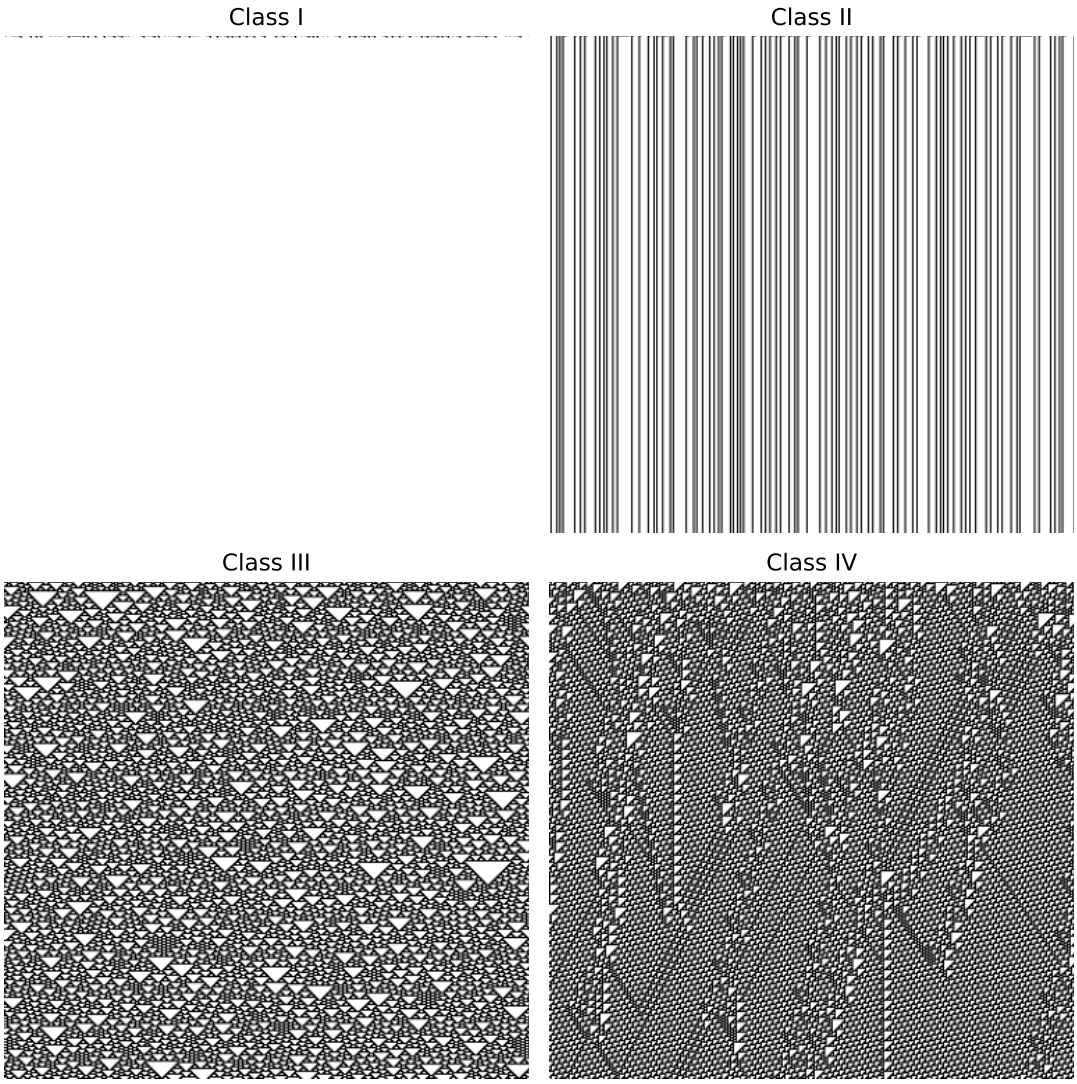

FIGURE 1.3. : Examples of each of the four Wolframs' CA classes (see titles). The initial condition was the same for every CA, and corresponded to 50% for state 0 (white dots) and state 1 (black dots). The evolution space begins with a ring of 358 cells for 344 generations, following the example in MARTÍNEZ et al. 2013.

Together, these examples drawn from the field of artificial life suggests that computation can emerge from dynamics if the following conditions are met :

1. The system analyzed is a complex system ;
2. The dynamical workpoint of the system lies in the vicinity of a phase-transition ;

But how to properly quantify the computations carried by those systems ? In the next subsection, I will briefly present the framework of information theory and how it can be used to characterize complexity and computation. Apart from the two cornerstone quantities of information theory, i.e., entropy and mutual information, I will

avoid giving a precise mathematical definition of the metrics discussed since they are carefully presented in Chapter 2 of this dissertation.

1.5.2. Computation and information dynamics

Information theory was first formalized by Claude Shannon, in his landmark publication "A mathematical theory of communication" (SHANNON 1948). While this theory was first formulated with the aim of deriving theoretical limits for the extent a message can be encoded, and then efficiently transmitted through a noisy communication channel, its generality allows it to be applied in a range of problems (PIERCE 1980; MACKAY 2003; STONE 2015).

The basic quantity of information theory, is the so-called Shannon's entropy (H), which is a measurement of the average uncertainty associated to the prediction of the outcome of a random variable X, or conversely the amount of information (measured in bits) it provides when the outcome is observed. Mathematically, it is defined as :

$$H(X) = -\sum_{x \in X} p(x) \log_2 p(x), \tag{1.1}$$

where x is an outcome from X, $p(x)$ the probability of observing it, and $\log_2$ the base-2 logarithmic function. Intuitively, $H(X)$ will be zero for the case in which X possess only one possible outcome ($p(x) = 1$), since there is no uncertainty, and maximal when X possess N equiprobable outcomes ($p(x) = 1/n$, $\forall x \in X$).

Another fundamental quantity, derived from the entropy, is the mutual information (MI), which quantifies how much the uncertainty about future outcomes of X, is reduced when knowledge about a second random variable Y is provided. Statistically, the MI can be thought as a generalized correlation metric capturing both linear and non-linear interactions, and is expressed mathematically as a function of entropy as :

$$MI(X, Y) = H(X) + X(Y) - H(X, Y). \tag{1.2}$$

where, $H(X, Y)$ is the uncertainty of X, and Y.

From these two metrics, one can derives many others that can be used to characterize complexity and computation. In particular, we search for metrics that can quantify the aforementioned "primitive operations" of information modification, transfer, and storage, proposed in LANGTON (1990). Next, I will list, focusing on their interpretation rather than their formal mathematical definitions, a few of the information-theoretical metrics that allow quantifying those operations (for formal definition of those metrics is presented in Chapter 2).

Time delayed mutual-information

By definition, mutual MI is a symmetric measurement. However, a directionality can be enforced by translating one time-series in relation to the other by τ time-steps, and is written as $MI(X, Y_{-\tau})$. The minus sign indicates that the time-series sampled from Y was *delayed* by τ time steps. Even though the delayed MI can be used as a proxy

of information transfer, it is not the ideal solution since it does not take into account information that "flows"from the past of Y to the present of X that was not in the past of X itself (SCHREIBER 2000).

Active information storage

The auto mutual-information, corresponds to the delayed MI measured between the signal and a delayed version of itself. It can provide a measurement of information storage (or buffering), being known as active information storage (AIS). Intuitively, the AIS corresponds to how much of the information contained in the past of the signal is still present in its present.

Conditional mutual information

The conditional mutual information measures the relationship between two random variables X, and Y conditioned in a third variable Z, and is written as $MI(X,Y|Z)$. The conditional MI is particularly useful in the context where one wants to verify whether correlations between the time-series of X, and Y are due to their coupling, or because they are driven by a common-source Z.

Transfer entropy

The transfer entropy (TE), is the information-theoretical formulation of Wiener's principle of causality (WIENER 1956). This principle states that, a signal Y is said to cause X if observations of the past of Y increases the predictability of X, when compared to the prediction made by the past values of X alone. The TE, is defined as the conditional MI between X, and the past of Y, conditioned on the past of X itself : $TE = MI(X, Y_{-\tau}|X_{-\tau})$. Notice that by using this definition the problem existent in using the delayed MI when measuring information transfer is corrected.

Partial information decomposition

The partial information decomposition (PID) is not a metric itself, but a framework which allows to (as the name suggests) decompose the total information shared between two random variables X, and Y have about a third variable Z, $MI(X,Y;Z)$, into information "atoms"(WILLIAMS et al. 2010; VOGES et al. 2024). The atoms composing $MI(X,Y;Z)$, corresponds to the unique information that X, and Y carries about Z, plus the redundant, and synergistic information they carry about Z. While the redundancy can be thought as the repeated information about Z, that is copied in both X, and Y[19], synergy corresponds to the information about Z that can be only retrieve by inspecting X, and Y together, i.e., by considering their interaction (BRENNER et al. 2000; LATHAM et al. 2005), and is associated to synergistic modification (LIZIER et al.

[19] Even though its mathematical definition is somewhat complicate, usually it is taken as the minimal mutual information X or Y carry about Z

2013; LIZIER et al. 2018). More specifically, synergistic modification takes place when a set of inputs, $X_1 \dots X_n$, localize (e.g., spatially), giving rise to an output Z.

O-information

The O-information, first proposed by by James, Ellison and Crutchfield (JAMES et al. 2011), allows to quantify the balance between redundancy and synergy in a system composed of N interacting elements (ROSAS et al. 2019; VARLEY et al. 2023a). In particular, $\Omega(\mathbf{X})$ is negative if the system interactions within the system are predominantly synergistic, and positive otherwise. Notice that here, $\mathbf{X}$ denoted in bold format is the state of the N constituents of the system.

Integrated information

The integrated information (ϕ; BALDUZZI et al. 2008) quantifies how much the state of a system $\mathbf{X}$, composed of N interacting elements, is better predicted by a past state of the system as a whole, when compared by the prediction made considering the system as being composed of k subsystems $\mathcal{M} = \{M^1, \dots, M^k\}$. The calculation of ϕ, consists of finding the partition of the system yielding its lowest value (MEDIANO et al. 2022), and it quantifies information shared, and transferred across the parts of the system, as well as redundant information present on them, in which case $\phi < 0$ for redundant dominated systems (MEDIANO et al. 2019)). Most importantly, integrated information was shown to capture a mixture of the system's capability to modify, transfer, and store information across its constituent parts (MEDIANO et al. 2022).

By directly applying this arsenal of metrics to the time-series recorded from the system's components, one can track the patterns generated by the dynamics of a system that give rise to emergent transformations of information (Figure 1.5.2). As a matter of fact, already in LANGTON (1990), entropy was used to characterize the complexity of the cellular automaton model he used. In particular, entropy correctly captured the transition point of the model. Additionally, he measured mutual-information between the sites in the model and found that it peaked around the critical point, as expected, since the system exhibit long-range correlations when at this point.

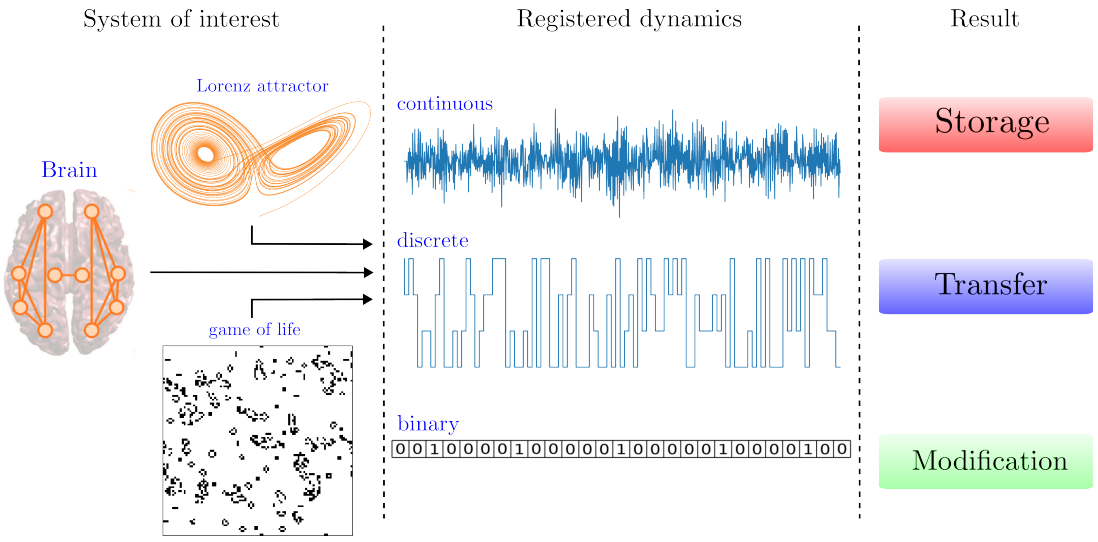

FIGURE 1.4. : Given a complex system of interest (left), and its either recorded or simulated dynamics (middle), the computational properties of the system can be estimated (right). Notice that given the generality of the information-theoretical metrics the signals used for the computation can be either discrete or continuous. This figure was adapted from Fig. 1 of MEDIANO et al. (2022).

Another interesting example, comes from the series of studies where Lizier and colleagues defined local metrics of information storage, and transfer, and modification (LIZIER et al. 2007; LIZIER et al. 2010; LIZIER 2012; LIZIER et al. 2013). The local metrics can be obtained by avoiding the averaging step when computing information theory metrics, which allows to compute them for states corresponding to a specific state of the system. They applied these metrics to different rules of Wolfram's elementary cellular automata [20]. In essence, different rules yields CAs belonging to different classes (the four classes I presented in Section 1.5.1). Interestingly, they showed that while static patterns (called "blinkers"; LIZIER 2012) stored information, propagating patterns (called "gliders"; LIZIER et al. 2007) were responsible for information transfer across the system. Conversely, the operation of information modification was carried by colliding gliders (LIZIER et al. 2010).

In MEDIANO et al. (2022), the authors investigated how the integrated information (ϕ) could be used as a marker of complexity and information-processing in different systems. In particular, still using Wolfram's CAs they showed that ϕ can correctly distinguish the four different CA classes. More specifically, ϕ increased as a function of the class, with highest value for class IV CAs, suggesting that this metric can correctly captures the emergence of distributed computation. Additionally, by applying a local version of ϕ (analogous to what Lizier and colleagues have done), the authors showed that ϕ captures information storage, transfer, and modification accordingly to what was reported in LIZIER et al. (2007), LIZIER et al. (2010) et LIZIER (2012).

Another interesting result in MEDIANO et al. (2022), was obtained by using Langton's

[20] I have not entered in details here, but how the rules of the Wolfram's CAs are set are nicely explained here : https://mathworld.wolfram.com/ElementaryCellularAutomaton.html

cellular automata model. In particular, it was shown that ϕ assumes maximal values around the around the critical λ, i.e., the region where the system can exhibit computational capabilities. As a matter of fact, other information-theoretical quantities were shown to faithfully capture phase-transitions in complex systems. For instance, in MARINAZZO et al. (2014), the authors implemented the Ising model on top of different brain connectome matrices, and showed that information transfer across unities was maximized at the critical point (in this case the control parameter is the reciprocal temperature), for four different categories of dynamics. Curiously, in another study (MARINAZZO et al. 2019) synergy and redundancy were also shown to characterize the phase-transition in an two dimensional Ising model. However, synergy peaked slightly before the critical point (i.e., in the disordered phase) being then a precursor of the transition, while redundancy was maximal at the critical point. Finally, In Chapter 3, by conceptualizing the nervous systems as consisting of a structural, algorithmic, and functional levels (MARR et al. 1976b; Figure 3.1), we could demonstrate that information metrics applied to the system's dynamics can correctly capture the computations carried at the algorithmic level.

While these examples show how those metrics can be used to characterize complexity and computation, the mechanisms generating transfer, storage and specially information modification are still poorly understood. In an effort aiming to shed light on how information modification emerges in systems with many interacting elements (i.e., high-order interactions), Thomas Varley and Joshua Bongard (VARLEY et al. 2024), evolved three sets of boolean networks using genetic algorithms. One set dominated by redundancy ($\Omega > 0$), another dominated by synergy ($\Omega < 0$), and one with high complexity, measured as the balance between segregation and integration, by means of the TSE complexity[21]. They found that the redundant networks exhibited short-transients before falling into a stable attractors, and synergistic networks the longest transients. Conversely, while redundant networks were very robust against perturbation they exhibit very low values of integrated information, the opposite trend was observed in the synergistic systems. However, networks with high complexity exhibit a balance between robustness and the capacity of integrating information, lied between the redundant and synergistic systems, suggesting that a trade-off between those two properties may be a general principle guiding the evolution of complex systems as the brain (LUPPI et al. 2022).

In the next subsection, I will explore the emergence of computation in the brain. In particular, I will aim to link the theoretical aspects we discussed so far with empirical studies in neuroscience quantifying neuronal computations that supports a range of brain functions.

1.5.3. Computation and the brain

The brain is arguably one of the most challenging complex system studied by mankind so far. In our efforts to properly describe it, we typically register neuronal activity across

[21] After Tononi, Sporns and Eldeman (TONONI et al. 1996).

many different scales, aiming to understand how it varies as external conditions or stimuli change. This is done with the hope of discovering how the world is represented in the language of neuronal activity. This neuronal representation is often referred to as the "neural code" (PERKEL et al. 1968; RIEKE et al. 1999). The existence of a code implies that the brain converts sensory and internal stimuli into spiking activity by means of an unknown *encoding* function (EGGERMONT 1998)[22]. Regardless of the codes underlying neuronal activity, the question of whether a representation of stimuli exists can be addressed through information processing by means of information theory (RIEKE et al. 1999) or by using machine learning *decoding*[23]. If the brain is to be thought of as an information processing[24] organ, two points should be addressed : under which conditions can the brain optimally do so, and how do different brain states correspond to distinct information processing regimes?

To address the first question, I will discuss the "critical brain hypothesis", which claims that the cortical activity state lies at a critical point, and as I have been discussing, this state is thought to favor information processing, supporting the emergence of computability from brain dynamics. Therefore, this is an important aspect to consider when talking about computation in the brain. Afterwards, I will tackle the second questions by means of a few empirical examples that used different techniques to quantify the repertoire of dynamical states the brain exhibits both during rest and task.

Brain criticality

Since the landmark observation of avalanches of neuronal activity in BEGGS et al. (2003), the idea that cortical activity lies at a critical point has become one of the leading hypotheses claiming that the brain is optimally tuned for information processing. In that study, the authors also observed power laws in the avalanches' size and duration, with similar exponents to those obtained for a branching ratio process. Additionally, the avalanches observed had a branching parameter approximately equal to one, indicating that the system was in a state of balanced excitation and inhibition. This balance offers enhanced information propagation and storage while preventing the system from being dominated by excitation (BEGGS et al. 2004). Following the observation of neuronal avalanches by Beggs and Plenz, this phenomenon was observed both *in vitro* (MAZZONI et al. 2007; PASQUALE et al. 2008) and *in vivo* in a range of different species (GIREESH et al. 2008; HAHN et al. 2010; RIBEIRO et al. 2010; YU et al. 2014; HAHN et al. 2017).

In addition to information propagation and stability, it was shown that cortical

[22] For instance, one widely discussed hypothesis claims that neurons encode stimuli in their average firing rates (i.e., a "rate code"; (DELGUTTE et al. 1984; GEORGOPOULOS et al. 1988)). Alternatively, a more flexible code could be achieved if information is present in neurons' precise spike timing (AINSWORTH et al. 2012) or even in distributed spatial patterns formed by co-spiking neurons (SEGUNDO et al. 1963; DAYHOFF et al. 1983; FRISTON 1997).

[23] While information theory tells you whether or not a stimulus is encoded by a given activity pattern, ML can help to retrieve which kind of activity represents which stimulus.

[24] Here information processing should be taken as synonymous of computation

activity at a critical state could favor the maximization of synchronous activity (YANG et al. 2012), essential for the emergence of cortical rhythms (see Section 1.4), enhanced information capacity and transmission (SHEW et al. 2011), dynamical range (KINOUCHI et al. 2006), and adaptability to stimuli (SHEW et al. 2015). For example, a recent study (SUÁREZ et al. 2024) showed that reservoir computing networks operating at the critical point exhibited maximal memory capacity in a simulated task. Additionally, critical avalanches were shown to be a useful cortical signature both for differentiating subjects and for improving brain-machine interface performance (SORRENTINO et al. 2023; CORSI et al. 2024). Besides the functional benefits of criticality, deviations from this state were observed in several pathological conditions, such as during epileptic seizures (HOBBS et al. 2010), and when the balance of excitation and inhibition is disrupted (VAN VREESWIJK et al. 1996; BEGGS et al. 2003; MAZZONI et al. 2007; SHEW et al. 2009; BARRAL et al. 2016), supporting the idea that criticality is the natural state of cortical activity (TETZLAFF et al. 2010).

These examples, alongside the idea that a varied range of systems and their emergent phenomena can be explained by a common framework drawing from statistical physics, illustrate why the "critical brain hypothesis" is so compelling. However, there are important caveats in the characterization of avalanche activity, such as the need to apply a threshold when studying continuous time series (PETERMANN et al. 2009), the need to time-bin the data (BEGGS et al. 2003), and the effects of sub-sampling (PRIESEMANN et al. 2009; PRIESEMANN et al. 2014). Additionally, power laws have been shown to be present in non-critical systems[25] (TOUBOUL et al. 2017). For instance, a recent publication has shown that criticality can emerge due to latent variables (MORRELL et al. 2024). Another observation that poses a contradiction is the dichotomy between overall desynchronized cortical activity (RENART et al. 2010; ECKER et al. 2010) and the states of synchronous activity occasioned by neuronal avalanches.

In general, the caveats discussed above serve to motivate research in the field of brain criticality, and solutions or possible explanations for some of these problems do not take long to emerge. For instance, it is known that adopting a time-bin equivalent to the average inter-spike interval yields robust avalanches compatible with the branching ratio process observed in BEGGS et al. (2003). Additionally, discrepancies in the values of power-law exponents across experimental conditions and species could be explained if the brain were actually slightly subcritical (FOSQUE et al. 2021). By using a model with 10^5 neurons, Tawan and colleagues (CARVALHO et al. 2021) showed that variations in the critical exponents observed could be explained by sub-sampling effects. Finally, aiming to reconcile the dichotomy of synchronous/asynchronous cortical activity, Fontenele and colleagues (FONTENELE et al. 2024) identified that critical activity was embedded in a low-dimensional subspace of cortical activity that coexists with another desynchronized space. This suggests that the cortex uses its highly dimensional space to multiplex distinct dynamical regimes.

Finally, while the critical brain hypothesis provides evidence that the brain is tuned

[25] The relation between the size and duration exponents that I showed in the previous sections is taken to be a stronger marker of criticality.

to a point where information processing is optimized and that avalanches are a general signature of cortical activity, it is important to consider the limitations and nuances in this characterization. In particular, it is of great interest to understand which patterns of activity (or brain states) map to different information processing regimes and the functions those regimes support. In the next section, I will briefly discuss a few examples showing how different activity states relate to a range of functions, hence representing different computations.

States of information processing in the brain

If brain dynamics reflects information processing, how can one characterize states that might correspond to different information processing regimes? While in statistical physics (GOODSTEIN 2014), a state (or macrostate) is related to numerous microstates (defined, for instance, by each position and momentum of an ensemble of particles), here by a state I refer to a particular dynamical regime originated from an element or by the interactions of elements of a given system. For example, a state in the brain can be defined as : (i) a given oscillatory regime of a field potential or a specific patter of phase coupling between oscillations; (ii) a cell assembly; or (iii) the configuration of spiking activity of a set of neurons or regions (with thresholds or discretized activity). Notice that this definition provides a certain degree of freedom on the spatial and temporal scales one wish to consider. The collection of one of those types of states (or mixed types) defines the dynamical repertoire that can be exploited by computation in the brain. Given that I have already discussed not only the range of oscillatory states present in the brain and their relation to cognitive functions in Section 1.4. Here I will focus on some examples related to points (ii) and (iii).

Cell assemblies consist of groups of neurons that tend to emit spikes in synchrony. Since their proposal by Donald Hebb (HEBB 1949), they have been regarded as fundamental units of information processing, contributing to the establishment of a "neuronal syntax" (BUZSÁKI 2010). Usually, to infer the type of information represented by a set of assemblies, a range of stimuli is presented to a subject, and the evoked assemblies are then related to different qualities of these stimuli (VON DER MALSBURG 1994). Whether assemblies carry a representation of external stimuli or not, can be assessed by means of mutual information analysis (see Section 1.5.2; BIALEK et al. 1989; RIEKE et al. 1999). From another perspective, instead of defining assemblies based on their representational character, one can consider that synchronous neurons effectively form an assembly if they can excite neurons in target areas. That is, they should be able to generate an output in "reader" neurons that differs for each assembly configuration (BUZSÁKI 2010). In the latter scenario, the most informative aspect of assemblies is the functional interactions they form with populations across multiple brain areas (OBERTO et al. 2022). If assemblies are characterized by their functional interactions, their temporal dynamics constitute windows where information processing can take place (VARELA et al. 2001).

In a recent study (PEDRESCHI et al. 2020), by representing neuronal interactions by means of temporal networks (HOLME et al. 2012; BIANCONI 2018), the authors

showed that the spatiotemporal dynamics responsible for sharing information in cell assemblies consisted of strongly connected neurons sending a few projections to more peripheral neurons, forming a core-periphery structure. Interestingly, neurons in the core were constantly being exchanged with neurons in the periphery, forming a "liquid" structure. Furthermore, the different configurations of the cell assemblies corresponded to distinct discrete states described by a set of features defining the core-periphery structure formed by them. The transition between states was not strongly related to the transition of the ongoing oscillatory regimes, suggesting that the information shared mediated by those assemblies follows a rich temporal dynamics.

The characterization of network configurations as discrete states, as done in PEDRESCHI et al. (2020), reveals another interesting strategy to characterize computational aspects of dynamics. This approach reduces the degrees of freedom of the system and offers robustness against noise by representing collective patterns of activity with similar features using the same "word" or symbol (PORTA et al. 2015). In some sense, this kind of symbolic analysis allows us to change the basis through which we observe the system's dynamics, enabling us to understand the transition between information processing regimes by quantifying how the relationship between these symbols changes (i.e., how their grammar changes, using the same analogy from Section 1.5.1).

In a study by Clawson and colleagues (CLAWSON et al. 2019), they described activity recorded from the rat's hippocampus and prefrontal cortex using a feature vector consisting of LFP power, single units' average firing rate, information storage, and transfer. The authors identified sub-states within the global brain states corresponding to REM and non-REM sleep activity by applying unsupervised clustering techniques to the extracted feature vectors. These sub-states exhibited dynamics that alternated among themselves in a way that was neither random nor regular, which is a marker of computation in complex systems as discussed in Section 1.5.1. Interestingly, they found that these states were characterized by hub neurons that carried out operations of information transfer and storage. In a subsequent study, they showed that the disruption of information processing characterized by these subspaces was related to epileptic behavior, suggesting that this alteration may be related the origin of neurological disorders.

Another way to track computations performed by neuronal collective dynamics is by conceptualizing them as a high-dimensional state space (**S**), with as many axes as there are recorded neurons or brain regions (see Figure 1.5; BROOME et al. 2006; BUONOMANO et al. 2009; CHURCHLAND et al. 2012; PESSOA 2019; SEBASTIAN et al. 2024). In this high-dimensional space, a set of interacting elements is associated with a state vector ($\vec{\psi}$) that moves around **S** as activity changes over time. When information processing takes place in the brain, $\vec{\psi}$ is not expected to be static nor to randomly traverse **S**. Instead, its evolution depends on how given states are interconnected, and the transitions from one state to another may not have a constant duration (i.e., $d^2\psi/dt^2$ is not constant). These constraints imposed on $\vec{\psi}$ mean that the trajectory followed by the collective activity of elements visits only a few of the theoretically possible points in **S**. If you imagine that the visited points are woven together, you would obtain a "blanket" defining the underlying geometrical structure of **S**, i.e.,

the low-dimensional manifold $\mathscr{M}$ associated with **S** (MITCHELL-HEGGS et al. 2023; CHUNG et al. 2021). The high-dimensional space, neuronal trajectory, and geometry can be explored using dimensionality reduction techniques, such as PCA (JAMES et al. 2013), UMAP (MCINNES et al. 2018), T-SNE (HINTON et al. 2002), among others (CUNNINGHAM et al. 2014)[26]. The geometrical description of neuronal activity across a range of species has revealed how collective dynamics are related to different brain functions such as navigation, encoding of task-related parameters, and discrimination of visual stimuli (CHAUDHURI et al. 2019; GALLEGO et al. 2020; NIEH et al. 2021; JAZAYERI et al. 2021).

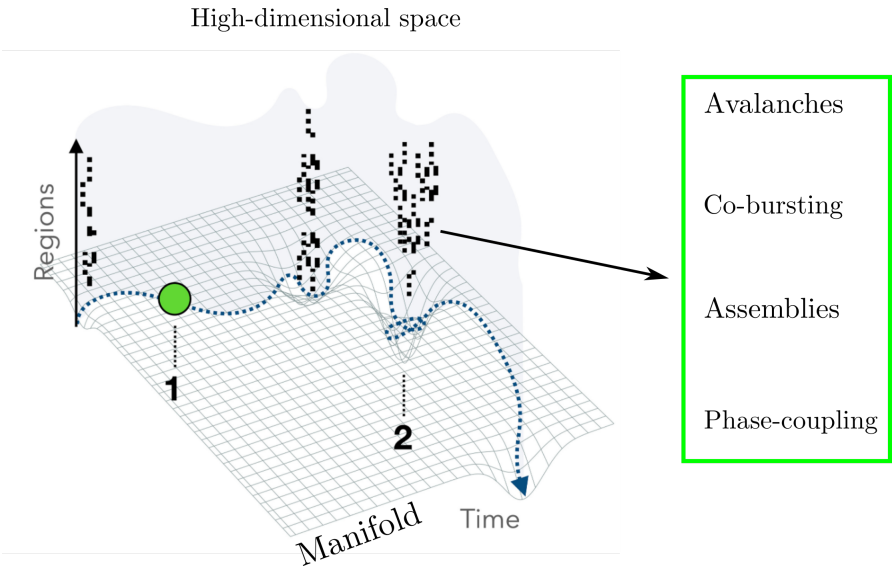

FIGURE 1.5.: The high-dimensional space defined by the activity of a set of neurons. As time evolves, the joint activity of the neuronal population wanders around the state-space, defining its underlying geometry. Moments of synchronous activity are interpreted as This figure was adapted from Fig. 1 of RABUFFO et al. (2022).

One interesting hypothesis explaining the balance between working memory flexibility and capacity was put forward by Buschman (BUSCHMAN 2021; PANICHELLO et al. 2021). This hypothesis proposes that the identity of items held in working memory is encoded in subspaces within the high-dimensional space composed of the joint activity of frontal neurons, such as distinct neuronal assemblies. Each of these subspaces forms a "coding space" for a specific item stored in working memory. In this way, the read-out of a given item is done by projecting the high-dimensional activity onto the corresponding coding space. The working memory capacity limitation would result from possible interference between the coding spaces (e.g., when many items have to be held in working memory, assemblies may display large correlations).

Last but not least, computations carried out by collective dynamics can be quantified using the framework of high-order interactions (HOI; BIANCONI 2021; BATTISTON et al. 2020; SANTORO et al. 2023). There are two approaches through which HOI can be

[26]This will also guarantee that you have at least one pretty plot in your publication.

characterized. The first one is based on information theory metrics, such as transfer entropy, active information storage, O-information, and the PID framework. As discussed in Section 1.5.2, these metrics enable the disentanglement of operations involving the transfer, storage, and modification of information from neuronal time-series data (Figure 1.5.2; STRAMAGLIA et al. 2021; SANTORO et al. 2023; VOGES et al. 2024).

The second approach relies on extensions of graph theory that consider interactions beyond pairwise (or dyadic) interactions (GIUSTI et al. 2016; BATTISTON et al. 2020). Specifically, in the context of algebraic topology, interactions involving multiple elements are represented by lines (edges, or 1-simplex), triangles (2-simplex), tetrahedrons (3-simplex), and so on. The collection of all simplices describing HOIs is referred to as a simplicial complex (BIANCONI 2018).

The comparison between simplicial complexes is conducted through their topological properties, such as homological groups. Essentially, each homological group characterizes a topology by quantifying the number of cycles, holes, cavities, and high-dimensional cavities present in the topological space defined by the complexes. More specifically, two topological spaces are considered equivalent if their homological groups match; in practice, this means that one can be shaped into the other through a series of deformations, implying that the two topologies are homeomorphic. Additionally, the relevant topological features of complexes defined by neuronal activity can be extracted by means of a filtration process called persistent homology. In this filtration process, one first constructs a connectivity matrix (e.g., the functional connectivity), and then progressively threshold the network by using a range of threshold values. By measuring the topological properties of the simplicial complex are more persistent across all thresholds used (PETRI et al. 2014; STOLZ et al. 2017; MORALES-GREGORIO et al. 2023).

Altogether, the examples used here illustrate how the high-dimensionality of neuronal recordings allows for the definition of states of information processing across a range of spatial and temporal scales. There are many complementary techniques to describe high-dimensional brain activity, which enable us to observe how it adapts to external stimuli or changes in conditions, thereby supporting information processing and computation that generate cognitive functions.

1.5.4. Concluding remarks

We have observed that complex systems exhibit a range of qualitative behaviors that characterize different dynamical regimes. In some cases, the system can self-organize into a state that lies between order and chaos, enabling information processing. The nature of the computations performed by the system can be understood at the algorithmic level (MARR et al. 1976b) by applying tools from information theory to the system's recorded dynamics. While these principles can be relatively well understood in artificial systems like cellular automata, the problem becomes more complex in the brain due to its rich repertoire of activity, which ranges from the scale of single neurons to populations of neurons and their collective oscillatory activity. Nonetheless, studying how high-dimensional neuronal activity is modulated by external

changes allows us to relate different information processing states in the brain to the representations it creates of the external world.

RESULTS

In this first research chapter, I present the results obtained from the analysis of a large data-set of local field potentials recorded from two non-human primate subjects. The recordings spanned an entire cortical hemisphere, comprising up to 50 cortical areas, and were obtained while the subjects performed a visual working memory task. Our main goal was to determine how large-scale coordination among widespread brain regions supported working memory function. More specifically, we were interested in determining by which means this coordination is established (e.g., by long-range phase-synchronization), and how the resulting cortical networks related to the memorization of the visual cue. We found that the interaction among areas is achieved by means of the coordination of transient events occurring on the areas' power time-series, that we named "crackles". Interestingly, areas that frequently co-crackle with others, forming areal coalitions we named crackle assemblies, are the ones carrying more stimulus-specific information. Overall, these results contribute to the main question of this dissertation by describing by which type of interaction, i.e. co-crackling, brain regions establish long-range integration, and show that the crackling scaffolds are related to working memory maintenance, and may reflect fingerprints of information processing in the brain.

2. WORKING MEMORY CONTENT IS ENCODED IN TRANSIENT FUNCTIONAL NETWORK DYNAMICS

Authors

Vinicius Lima[1,2], Steven Hoffman[6], Nicolas Dotson[5], Charles Gray[4], Andrea Brovelli[2], Demian Battaglia[3]

[1]Aix-Marseille Université, Institut de Neurosciences des Systèmes (INS), UMR 1106, Marseille, France
[2]Institut de Neurosciences de La Timone, UMR 7289, CNRS and Université Aix-Marseille, Marseille, France
[3]Institute for Advanced Studies (USIAS), Strasbourg, France
[4]Montana State Univ. Bozeman, Bozeman, MT
[5]SNL-R, Salk Inst. for Biol. Studies, LA JOLLA, CA
[6]Dept. of Biomedical Engineering, University of Minnesota, Minneapolis, MN 55455, United States

abstract : Working memory requires coordination among widespread brain regions. One candidate mechanism for achieving it is the synchronization of cortical oscillatory activity. Measurements such as coherence or phase-locking value, usually rely on large trial averages which "washes" away finer details present on single-trial dynamics while favoring a few strongly trial "locked" ones. However, those metrics depend on strong priors on how information is encoded and transferred by populations of neurons. Here, by conducting analysis at the single-trial level, and maintaining an agnostic view on the physiological role of oscillatory activity, we were able to detect transient events of excitability on the power time-series, that we term "crackles", and show that their coordination across most cortical areas is related to memory maintenance. We find that those areas undergo task-related modulations of crackling probability across multiple frequency bands, with a subset of frontoparietal regions exhibiting a ramping crackling probability through the delay period of the task. Furthermore, coordinated crackling

activity carries information about the identity of the visual stimulus held in working memory. Since regions whose coordinated crackling conveyed most information were not always the ones with the strongest oscillatory power, our results point towards a collective mechanism of memory maintenance, rather than a local one based on average power alone. In summary, we present evidence suggesting that visual short term memory is mediated by the emergence of a collective dynamics that favor the coordination of transient excitability events.

2.1. Introduction

Working memory (WM) relies on precise coordination among widespread cortical areas to transfer, store, and modify stimulus-related information (VANDIERENDONCK 2016; CHRISTOPHEL et al. 2017; DOTSON et al. 2018). Such coordination requires an interplay between states of cortical integration and segregation. The balance between these states is not only a general principle that enables complex systems to process information (LANGTON 1990; MEDIANO et al. 2022) but has also been suggested to support cognitive functions, as put forward by previous studies (SPORNS 2013; DECO et al. 2015; SHINE et al. 2016; FREY et al. 2016; COHEN et al. 2016; FINC et al. 2020; WANG et al. 2021). A general signature of the balance between integration and segregation is the emergence of coherent spatiotemporal patterns of activity (LIZIER et al. 2007; LIZIER et al. 2010; LIZIER 2012; LIZIER et al. 2013). In fact, cortical activity displays a rich repertoire of distributed spatiotemporally transient activity states (references). However, it remains unclear how these transient states are exploited to support cognitive functions.

Recent years have seen many other forms of neuronal and brain-wide integration being proposed (HAHN et al. 2014; VINCK et al. 2023). In particular, redundant functional interactions may appear in collective states dominated by oscillatory synchronization (FRIES et al. 2001a; VARELA et al. 2001; BUZSAKI et al. 2004; HIPP et al. 2011; FRANSEN et al. 2015) , resonance phenomena, or coincidence of non-linear upwards modulation of activity (VINCK et al. 2023). Such states may give rise to selective patterns of information flow (BUEHLMANN et al. 2010; KIRST et al. 2016; PALMIGIANO et al. 2017; BATTAGLIA et al. 2020). In particular, patterns formed by the synchronization of bursty activity have been shown to play a role in motor planning (FEINGOLD et al. 2015; SZUL et al. 2023), WM maintenance (SALAZAR et al. 2012; LUNDQVIST et al. 2016; LUNDQVIST et al. 2018), encoding of task related information (DOUCHAMPS et al. 2024), and are thought to underlie cognition (LUNDQVIST et al. 2024).

Here, we hypothesized that the coordination originating from these patterns would arise as a series of discrete states formed by areas that are co-active forming packets of spatially and temporally uninterrupted transient activity. In particular, we predict that during visual working memory, the representation of the stimulus, initially presented in lower visual areas, will propagate across cortical areas forming multi-areal assemblies carrying both control and stimulus-related information. Additionally, due

to the variability of those transient bursts of activity across time (FEINGOLD et al. 2015) single-trial based analysis (STOKES et al. 2013; JONES 2016; COLE et al. 2017), this phenomenon plays an important role in the correct characterization of those states of cortex-wide coordination. Consequently, we combine the analysis of the single-trial power estimated from LFPs with tools from network theory in order to estimate the interaction between multiple cortical areas during a visual working memory task. We found that areas forming coordinated packets of activity (which we name co-crackling scaffolds) underlying memory maintenance during a WM visual task.

2.2. Methods

2.2.1. Behavior, implantation and recordings

Two monkeys (monkey L and monkey E) performed a delayed-match-to-sample task (dMTS) (DOTSON et al. 2017). The task consisted of memorizing and later choosing the correct visual cue when it was presented next to a distractor (Figure 2.9A). The task consisted of four periods : (i) presample (P) in which the monkey fixates the center of a screen while waiting for a visual cue; (ii) sample (S) in which the cue (one out of five possible) was shown; (iii) delay (D) where the cue was removed and the monkey had to memorize it; and (iv) match (M) where the cue was shown together with a distractor and the monkey had to fixate on the right cue, in which case, the trial was considered a successful one. For both animals, a fraction of about 10% of the trials no cue was shown and the monkey had only to fixate the center of the screen. We will refer to those as "task" and "fixation" trials, respectively.

During the task, the local-field potentials (LFPs) from the two animals were recorded using an implanted Microdrive Recording System (ibid.) with grids of 252 recording channels covering 56 separate cortical areas spanning the visual, prefrontal, parietal, temporal, motor, auditory and somatosensory cortices (Figure 2.9B). The recordings from a single day consisted of many trials that, together, constituted a session. For monkey E, much of the data was lost due to a perfusion of liquid that short-circuited some recording channels (for more details on the recording check (DOTSON et al. 2017; DOTSON et al. 2018; HOFFMAN et al. 2024). In total, monkey L (E) had 62 (25) sessions. The total number of recordings used for monkey L and E was 4302 and 793. Notice that those recordings were distributed across different cortical regions with different sampling sizes (Figure 2.9C,D). Apart from differences stemming from the apparatus used for recording the LFPs, it was shown that many dynamical and spectral features are subject dependent (HOFFMAN et al. 2024). The number of recordings used per region in each animal is summarized in Table 2.1.

2.2.2. Estimating single-trial power

Time-frequency analysis was performed by applying Morlet's transforms for 10 linearly spaced frequencies from 3 to 75 Hz and time-bandwidth equals 4 Hz , the number of cycles was scaled with frequency by a factor of 1/4 in order to fix the time and

frequency resolution (39.8 ms, and 4 Hz). After decomposing the LFPs, a decimation factor of 10 was applied. For computing the crackling and propagation scaffolds, which required a better temporal resolution we used a decimation factor of 5 when estimating single-trial and time-resolved power, and later we binned the threshold power time series in windows of 15 ms, and considered a bin to be crackling if any value in the bin was one.

Applying the MT to the data-set yields one complex coefficient W per channel, time, frequency, and trial. Then, for channel i in trial T, the power is defined as $S^T_{ii}(t,f) = W_i(t,f)\tilde{W}_i(t,f)$, where $\tilde{W}$ represents complex conjugation. Using this notation, S_{ij} would represent the cross-spectrum between channels i and j. After estimating the single-trial power, a sub-sampling factor of 20 was applied to the data.

When it was necessary to pool or average data within a specific period of the task, we subdivided the trial into a pre-sample and sample periods each with 400 ms (hence from -400 to 400 ms relative to cue onset), and we divided the delay period into three components : early delay (D1), late delay (D2) and matched delay (Dm), each with 400 ms. The late delay ends at the earliest delay of a session, and the matched delay spans a period that goes from the middle of D2 hence it might contain match activity mixed into it (Figure 2.9A; Figure 2.1B).

2.2.3. Single-trial coherence

In order to estimate the frequency-resolved time-series of functional connectivity at single-trial level, we extended the metric proposed by Lachaux and colleagues (LACHAUX et al. 1999; LACHAUX et al. 2002). To do so, we replaced the standard averaging with a smoothing kernel $g = g(\delta t, \delta f)$ with δt and δf being the width of the kernel in time and frequency within each trial, respectively. This is equivalent to estimating coherence inside small windows defined by the kernel, which is analogous to using the sliding window. However, considerably more efficient computationally. The single-trial and time-resolved coherence is given by :

$$C^2_{ij}(t,f,T) = \frac{|g * S_{ij}(t,f)|^2}{[g * S_{ii}(t,f)][g * S_{jj}(t,f)]}$$

where T indicates the index of a given trial, and $*$ the convolution operation. The kernel g can be for instance a Gaussian, a hanning or boxcar window.

While it is true that estimating coherence in this fashion can lead to spurious high values, the intrinsic bias of this metric can be estimated analytically (LACHAUX et al. 2002). Here, to control for spurious coherence values we computed coherence of the trial-shuffled data. We further assumed that the significance threshold estimated from the surrogates is the same for all trials. This is equivalent to generating one surrogate and taking its 95% percentile over the trial's axis. This leads to a significance level per channel, time and frequency.

When computing the single-trial coherence, we applied a decimation of 20 to the single-trials spectra of 20.

2.2.4. Gaussian-Copula mutual information and stimuli encoding

The mutual information (MI) is a general metric of correlation between two random variables x, and y. It is general because it does not assume an a priori statistical distribution for the relation between the variables as the Pearson's correlation. Nonetheless, for data that follows certain distributions the MI can be estimated analytically. For instance, for normally distributed data, the mutual information assumes the form given by :

$$\mathrm{MI}(x,y) = \frac{1}{2}[(2\pi e)^2|\Sigma|],$$

where Σ is the covariance matrix between x and y

In most cases, data does not follow a normal distribution, which makes the direct application of the equation above unsuitable. However, a recent estimator for the MI allows transforming the marginal distributions of high-dimensional data-sets into normal distributions by using a copula function, hence the name Gauss-Copula estimator (INCE et al. 2017). In the present work we made use of this estimator in order to compute the mutual information between power and stimulus. It is worth noting that this approach was already adopted in recent works in neuroscience (ZBILI et al. 2021 ; ASHRAFI et al. 2022 ; COMBRISSON et al. 2022a).

To assess the statistical significance of the MI values measured, we computed MI with the stimulus labels shuffled 200 times. We then compared the original and the shuffled using a t-test. The p-values were corrected with FDR, and the threshold for significance used was 0.01.

We define the encoding of stimuli as the t-values obtained by computing the mutual information between the stimuli identity and the average power per epoch, frequency band and cortical area.

2.2.5. Detecting crackles

Crackles can be detected by binarizing a region's power time-series using a relative threshold (Figure 2C). This is done by first computing the quantile of the power distribution for each channel and frequency across trials.

To obtain the binary crackle train (in analogy to spike-trains) for a given channel A_C, we simply set $A_C(t) = 1$ for all times t in which power $A_C(t) > Q$, where $Q(\mathrm{power}_C)$ is the quantile used as a threshold. The crackle train has the same dimensionality as the power multidimensional matrices. Hence, there is one per region, trial, and frequency.

2.2.6. Flattened spacetime graph representation and crackle assemblies

To detect the crackle assemblies ("CrAs"), we start from the already thresholded power-time series. We consider that a set of regions are co-crackling if all of them crackle at a

given instant t. A crackle assembly would be any co-crackling activity starting at time t in which a spatio-temporal path can be drawn until a time t+δ.

Since each column in the crackle raster plots is a network, the raster plot contains a collection of ordered networks. By adding directed edges from nodes in time t to nodes in time $t+1$, one can devise a representation of the sequence of co-activations of channels in which the detection of CrAs becomes trivial (BADIE-MODIRI et al. 2020). Here, we do so by assuming that two areas that co-crackle at time t are also connected to themselves and between them at time $t+1$ we could build a directed and binary static representation of the temporal graph, that we named "flattened spatiotemporal graph", for which all the network theory tools for static graphs could then be applied.

More specifically, if **A**, is the rank 2 matrix, with one row for each cortical area, and each column corresponding to a sampled time t. If N areas were sampled T times, then $\mathbf{A} \in \mathscr{R}^{NxT}$. Additionally, $\mathbf{A}_{it} = 1$ whenever channel i crackles at time t. The corresponding flattened spacetime graph (FST), is a NxT by NxT matrix, and can be written its element representing the connection between channels i, and j from time t to $t+1$ is given by :

$$FST_{\tilde{i};\hat{j}} = A_{it}A_{jt},$$

where $\tilde{i} = i + Nt$, and $\hat{j} = i + N(t+1)$.

Additionally, since at a given time step all areas that co-crackle are considered to form a clique, we have :

$$FST_{\tilde{i};\tilde{j}} = A_{it}A_{jt}.$$

However, in this case the network has no self-loops, i.e., $FST_{\tilde{i};\tilde{i}} = 0$.

By using the FST representation, the dynamics of collective crackling and the information on activity propagation are effectively "crystallized" into a static network. Consequently, detecting Crackling Assemblies (CrAs) is simplified to identifying their strongly connected components. Each connected component consists of a list of areas that participated in the corresponding CrA and the timings when they crackled. By using this information, one can construct two graphlets : (i) An undirected graphlet where areas participating together in a CrA are connected; (ii) and a directed graphlet in which any area that was not crackling in time t, and crackles at time $t+1$, a directed edge from the areas active at time t. We define (i) as the CrAs' crackling scaffold, and (ii) as their propagation scaffold (sequence). The crackling scaffold can be interpreted as the spatial structure of a given CrA, the propagation scaffold contains information about the ordering in which areas "entered" a given CrA event.

The global scaffolds are obtained by averaging over all the graphlets obtained (per each task period and frequency band), resulting in the global crackling scaffold (GCS), and the global propagation scaffold (GPS). While the edges in the GCS can be interpreted as being proportional to the probability of a given pair of areas participating together in CrAs. The GPS yields the number of times a source node i in the active state ($A_i = 1$), was followed by a node target j in the active state ($A_j = 1$), when j was not active in the previous step. Since A_i and A_j are just logical time-series, this gives a

naive estimate of $P(A_{j,t+1}|A_{i,t} \wedge \neg A_{j,t})$, hence the GPS for elements i and j, are :

$$\mathrm{GPS}_{ij} \propto P(A_{j,t+1}|A_{i,t} \wedge \neg A_{j,t}).$$

2.3. Results

Working memory is mediated by a widespread system involving the large-scale coordination among cortical areas. Here, we investigated whether transient power comodulations serve as the substrate for integrating mnemonic representations across subsystems mediating the working memory process. To test this hypothesis, we recorded local field potentials (LFP) from 56 separate cortical areas in two monkeys. The monkeys performed a delayed-match-to-sample task, where they memorized a visual cue during a delay period and later chose between this cue and a distractor image during the match phase. Using a single-trial power time series derived from the LFPs, we identified frequency-dependent events of excitability, which we named "crackles". Crackles are events that are locally strong, i.e., they correspond to power fluctuations going above a given quantile of the power activity (e.g., the 90 percentile) recorded in a given channel. In this sense, they might be strong relative to this channel average power activity, but globally weak. As a consequence, these events can only be detected through single-trial analysis, as averaging tends to eliminate fluctuations that are not locked to task events. We found evidence supporting our hypothesis by demonstrating that : (1) The probability of crackle occurrence is modulated by the task (2) crackle properties vary with the sample stimulus held in short-term memory (3) the network properties of crackles' spatiotemporal dynamics predict stimulus identity and reveal cortical circuits related to feature-based visual short-term memory (4) A large-scale computational model showed that broadband crackle activity emerges in a regime on the verge of synchrony, where transient fluctuations in the beta to low gamma frequency are present.

2.3.1. Power time-series are stochastic and emits burst-like events

Understanding how working memory is mediated by brain dynamics both spatially and across frequency bands can shed light on the canonical computations supporting this cognitive function. More specifically, the coordination of transient oscillatory events may be a general mechanism by which areas can momentarily exchange information (i.e., integrate), as it creates windows where both phase- and amplitude locking can be established. To motivate this idea, we decomposed the recorded LFPs into their single-trial spectrograms and verified that across the entire task, power modulations were characterized by brief events where power is transiently strong. In particular, uncovering the extent to which these events occur across cortical areas and frequency bands would reveal if these events could potentially be used to mediate the interactions among cortical areas. Therefore, in this section, we investigate whe-

ther these events happen across all task epochs, frequency bands, and their spatial dependence.

To disentangle effects related to different brain rhythms, we decomposed the recorded LFPs into the time-frequency domain using the Morlet transform for 10 discrete bands ranging from 3 to 80 Hz, unless stated otherwise (see Methods). In Figure 2.1A, we show an example of the z-scored single-trial spectrograms for a V1 channel. Inspection reveals that power fluctuates stochastically and sporadically increases to several standard deviations above its average value, appearing as reddish "blobs". Most importantly, these stronger fluctuations, which we will generally refer to as "power activations", tend to occur quite irregularly. Consequently, averaging these maps across trials would suppress these periods of increased excitability.

The moments of stronger power fluctuations can be better appreciated by selecting a band of interest and inspecting the single-trial power time series for this band. In Figure 2.1B, we show the time series of z-scored power for eight selected trials in the 27 Hz band (high-beta band for monkey L) of the same V1 channel. Notice that, since only a few power activations are locked across trials (e.g., the power activations at cue onset for this V1 channel), the evoked-related potential averages out most of them (Figure 2.1B; black curve at the bottom).

Additionally, the spatial distribution of power across the cortex follows a gradient that depends on task conditions and the individual animal (HOFFMAN et al. 2024). In Figure 2.1C (left), we show an example of the power map for the high-beta band during the D1 task period. Some regions exhibit comparatively low oscillatory power. This discrepancy hinders the detection of power activations in these areas, as setting a detection threshold based on overall activity would exclude regions with lower average power amplitudes. Nonetheless, these areas can have transiently strong power, evidenced by the long-tailed power distributions (Figure 2.1C, right). This effect is present across all analyzed bands and for monkey E, as detailed in the supplementary materials (Figure 2.10).

To detect these events, setting a threshold based on global power, which we refer to as absolute threshold, would suppress power activations in regions with lower power. Conversely, setting a threshold relative to the region's own activity at the single-trial level, a relative relative threshold, allows for their detection (Figure 2.1D). This results in two types of power activations : (i) globally strong power increases, corresponding to increased oscillatory activity (which we will define rather generally as bursts), and (ii) locally strong power increases that are not necessarily oscillatory, since they might be globally weak, in the power time series, which we call "crackles". Evidently, by using a relative threshold to detect these events bursts and crackles are confounded in the analysis, as a consequence there is an overlap between the burst and crackle emission rates, which also follows a spatial gradient (Figure 2.11).

In practice, the first step requires the detection of crackles, whether and when they are present in the neural time series and their duration. This can be achieved using a relative threshold analysis, which involves estimating a given quantile of the power distribution for each recording channel and frequency band across trials, for each session separately, and then a binarization. In Figure 2.1E, to provide a visual

representation of crackle events, we show selected power time series in the 27 Hz band and the correspondence between detected crackle events (for three different threshold levels) and the LFP filtered in the corresponding band.

To avoid inserting a dependence on a specific threshold value, in the subsequent analysis we use the z-scored power time-series rather than its binary version. In this case, moments where the power have increases of a few standard deviations will be refereed to as power activations, and are the continuous version of crackles. Conversely, when we inspect crackling coordination we use the binarized power time-series.

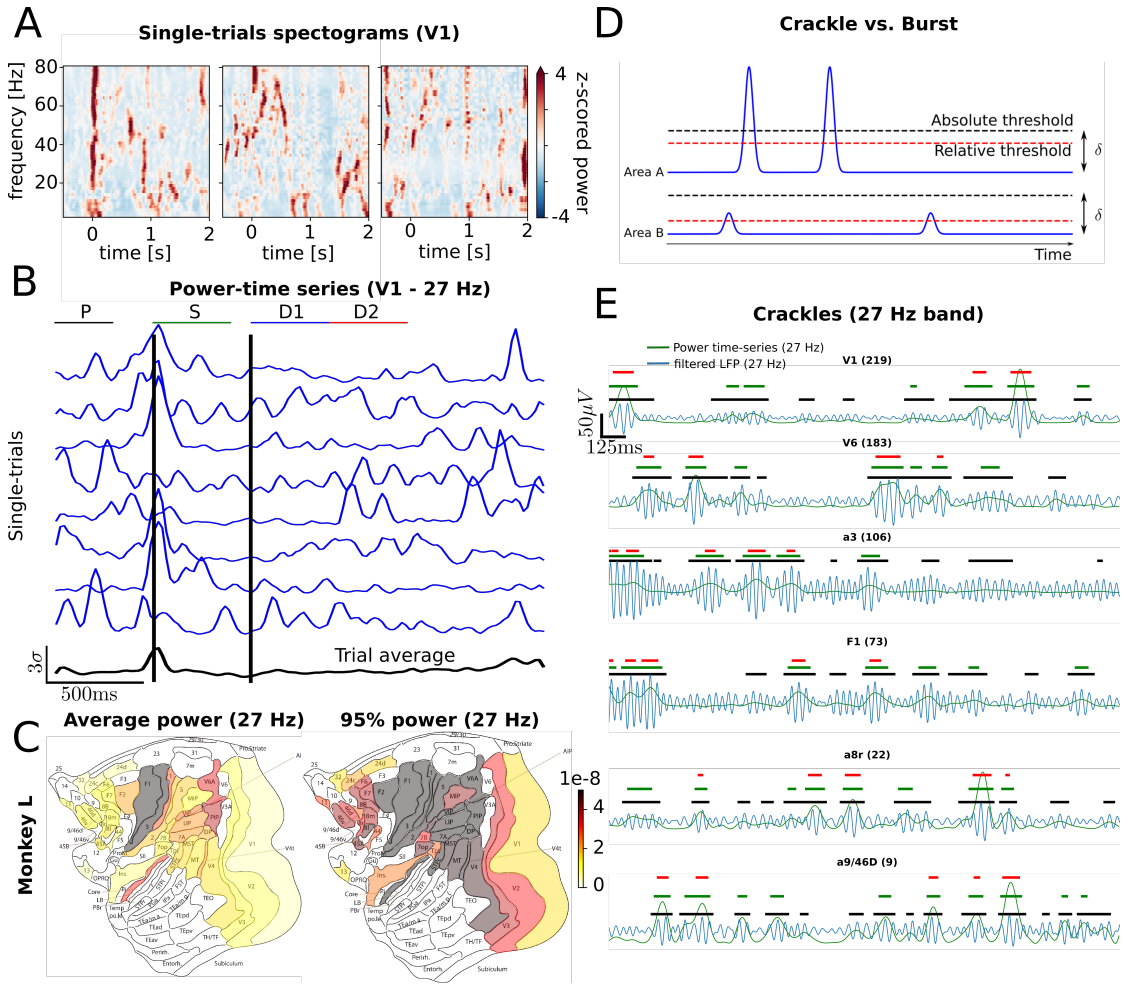

FIGURE 2.1. : Power time series trial-by-trial variability. (A) Three single-trial z-scored spectrograms for a channel located at V1 in Monkey L. (B) Ten single-trial power time-series (in blue; z-scored) for the same V1 channel shown in A, but for the 27 Hz band only, the black curve in the bottom represents the evoked-response potential obtained by averaging the aligned power time-series over trials. (C) The spatial distribution of average power (left), the 95 percentile power (right). (D) A cartoon representing the distinction between absolute and a relative threshold, events that are globally strong may be detected with an absolute or relative threshold and are referred to as bursts. Otherwise, a local threshold is needed in order to detect them, in which case, we refer to those events as crackles. (E) The power time-series in the 27 Hz band, for a few selected channels in different cortical areas (blue), alongside their filtered LFP (green). For each of those time-series we show the crackle detected for three threshold quantile levels 50% (black), 80% (green), and 90% (red).

2.3.2. Power crackles dynamics are task modulated

In order to crackling activity to play a role supporting WM, at least two conditions should be met to support their role in long-range communication : (i) they should display some kind of task modulation, reflecting internal processes that might occur

during working memory (ii) if they truly mediate integration of information distributed across cortical areas, meaning they are the means by which sensory information travels back and forth through the cortical hierarchy to achieve a distributed representation of the cue, they should be informative about its identity. In this section and the next, we aim to probe points (i) and (ii). Here, we start by showing that the probability of occurrence of crackle events is, on average, modulated by the task. In the next section, we demonstrate that they contain stimulus-specific information (i.e., encoding cue identity) by estimating the mutual information across trials between the stimulus identity and the average power in each trial epoch.

To visualize the spatial and temporal dynamics of crackling events more effectively, we employed a raster-like representation, similar to what is done with single and multi-unit recordings. Firstly, we z-scored power time series at the single-trial level to enhance crackle events (Figure 2.2A,B). Next, we defined two quantities based on the resulting z-scored power time series : the **crackling rate**, which, similar to units' spiking frequency, measures how many crackles a given channel emitted during a specific task epoch; and the **crackling event sizes**, which measure the number of crackles emitted across all recording channels at a given instant.

We investigated whether crackling rates significantly differed during the task compared to fixation trials. To answer this question, we conducted a two-sample t-test between the crackling rates from each period of the visual task and fixation trials. These analyses were performed at each frequency and at the single-channel level, and we reported the average T-values within each cortical area of significant channels (Figure 2.2C).

During the presample period, we observed sparse crackling rate modulation. We identified higher rates of crackling events compared to fixation, particularly in early visual areas (shown in green) in the low and high-gamma bands (>27Hz), especially during D2. Conversely, we found lower rates of crackling events compared to fixation in the low and high beta bands of frontal areas (F1, F2 in red) and parietal areas (e.g., MIP and LIP in light blue). In general, all cortical areas displayed some modulation in their crackling rates during the task.

To illustrate how the dynamics of crackling events' sizes are modulated by the task, we averaged it over all channels of V1 in the frequency range from X-Y Hz (high-beta band, see Table 2.2; Figure 2.2B) and generalized over all channels of each area at each time point (Figure 2.2D). These time series represent the probability of observing crackles at a given instant in each recorded area.

We find that the probability of observing crackles is modulated by the task with a clear spatial dependence. For instance, motor areas display higher crackle probabilities during the presample period, while visual areas have a high crackling probability during cue onset. Most of the recorded areas show bouts of increased crackling probability during the delay period.

We acknowledge that this analysis suffers from artifacts due to the across-trials "counting" used to estimate probabilities. For example, the probabilities for motor areas during the presample period are affected by a "blurred" effect. It is likely that probabilities measured during the delay period come from crackles that survive the

averaging. Nonetheless, the analysis helps to identify task modulations in the time courses of crackling.

To obtain a decomposition of the modulation of the crackle time series (Figure 2.2D), we utilized the Non-negative Matrix Factorization technique (NMF) on crackling event sizes (Figure 2.2D) averaged over the high-beta band (Table 2.2). This helped us identify the first four components revealing the cortical areas associated with each pattern (Figure 2.2E), along with the instantaneous time series describing periods when patterns were active (Figure 2.2F).

The first component encapsulates the decay in activity observed in motor areas, while the second shows stable activity during the delay period mainly in parietal and prefrontal areas. The third component captures ramping activity primarily in visuo-parietal areas and a few prefrontal areas, while the fourth is related to the sharp transient response of visual areas at cue onset. The components were obtained from data pooled for all sessions for each monkey separately. The results obtained for Monkey E were qualitatively similar to those obtained from Monkey L. (Figure 2.12).

Additionally, we found that NMF factors were widely correlated across frequency bands, indicating that crackle synchronization is a phenomenon widespread at multiple scales (Figure 2.13). Altogether, this suggests a coherent organization of task-modulated crackling activity across spatial, temporal and spectral scales.

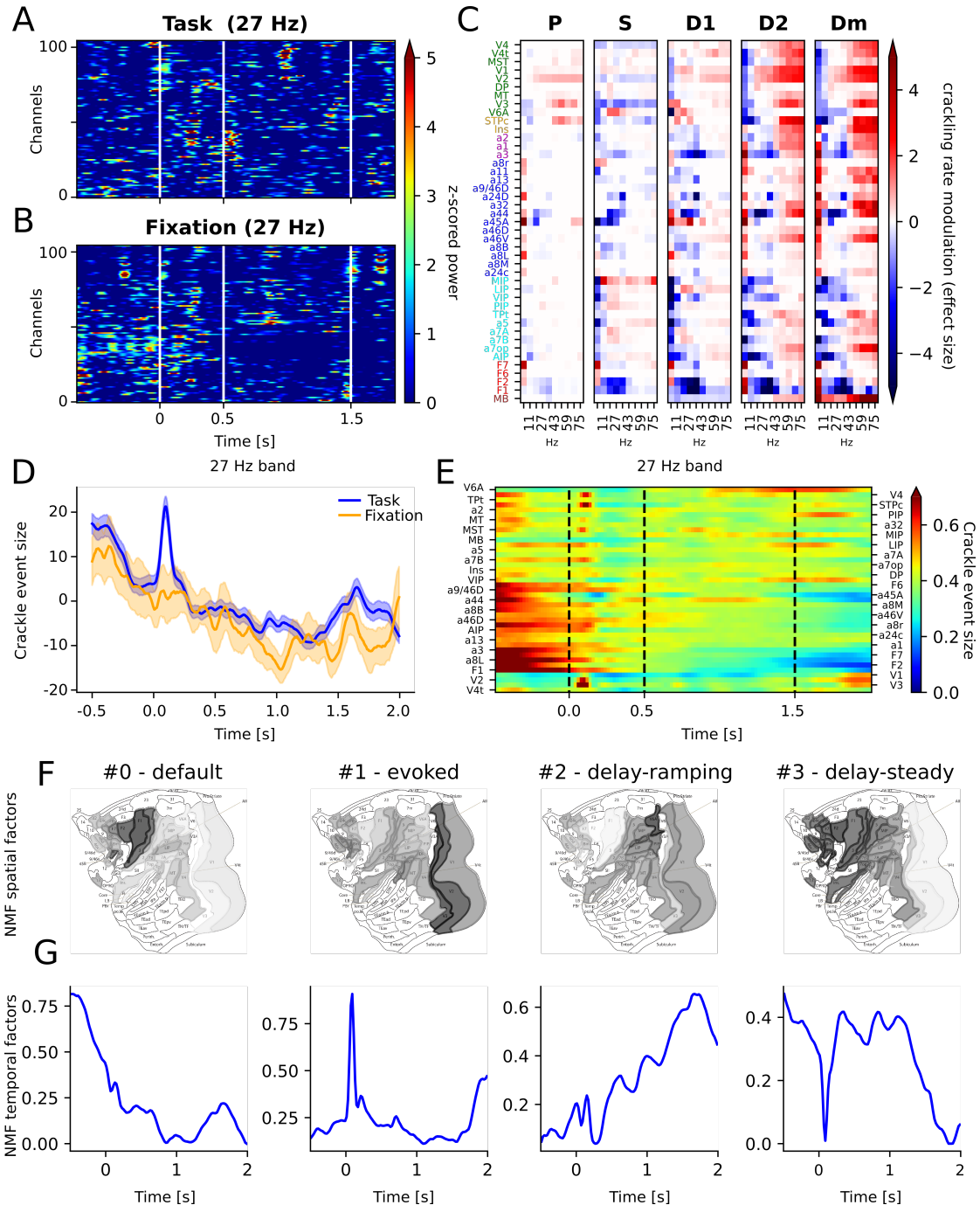

FIGURE 2.2. : Temporal and spatial task modulation of crackling. (A,B) Single trial z-scored power time-series for each channel (y-axis), for task (A) and fixation (B). Warmer colors encode higher z-scored power (e.g, events above a certain activation level as 3 STDs could be considered crackles). (C) Task modulation on the crackling rates (two-sample t-test between task and fixation, $p < 0.01$ FDR corrected across areas and frequencies). Visual, temporal, auditory, insular, parietal and frontal areas are respectively color coded in green, yellow, purple, dark and light blue, and red. (D) Crackle event size for channels in the V1 regions, for task (blue) and fixation (orange); horizontal black bars represent significant modulations ($p < 0.01$; FDR corrected) (E) Time-resolved crackle probability; same as in D, but computed for all recordings in a given session. Warmer colors indicate higher probabilities of observing crackling events (continue on next page).

FIGURE 2.2. : (F) Cortical areas representing the first four NMF components and (G) The instantaneous time series describing instants at which the NMF components appear, for the high-beta band in Monkey L.

2.3.3. Power time-series contains stimulus related information

If crackling rates, as defined above, are task-modulated, they could also carry stimulus specific information, similar to the rate codes observed in neuronal activity. We tested this hypothesis by estimating the mutual information (MI) between single-trial crackling rates and stimulus identity across task epochs and frequency bands. Notice that this approach also avoids the problem that might arise for computing MI across aligned to event onset due to the stochasticity of the emission times of single crackle events. In what follows, we define the *encoding* of stimuli as the effect-size of the measure mutual-information (see Methods).

We determined the spatial and spectral dependence of mutual information (MI) and displayed the total stimulus-related information by summing the MI effect sizes across cortical areas (Figure 2.3A). We found information encoded across all bands during task epochs in both animals, with peak encoding for the S and D1 epochs in bands up to 35 Hz.

To explore the anatomical dependency of encoding, we show the effect sizes from the group level statistics (Can you be more specific as to what "group level statistics" is?) for D1 and D2 epochs (Figure 2.3B; other task epochs in the supplementary material). Specifically, during D1, encoding in prefrontal (areas 11, 46D/V, 24D, 9/46D, 8M), premotor (F1, F2, F6, F7), and parietal (areas 5, PIP, LIP,, etc.) (I see 1 colored value at 3 Hz in VIP in Monkey L. Hardly a big effect.) areas increased in the range of 3-43 Hz (delta to high beta).

The stimulus encoding dependency on task epoch is shown for a few selected areas where the encoding effect is particularly strong (Figure 2.3C). In both animals, visual areas V1/V2 hold stimulus information during the S and D1 periods. For monkey L, there is also significant encoding in motor areas such as F1 and F2 (which are strongly sub-sampled in animal E).

Altogether, the presence of significant stimulus encoding provides evidence that the single-trial power time series are not only task-modulated but also support memory maintenance. But is average power a good predictor of stimulus encoding? A preliminary check can be made by comparing the regions with strong encoding in Figure 2.3B with the regions whose power is stronger in Figure 2.10. Remarkably, this comparison reveals that the few areas encoding the stimulus are not the areas with strong oscillatory power. This leaves the question : which features extracted from the single-trial power time series could be better predictors of encoding?

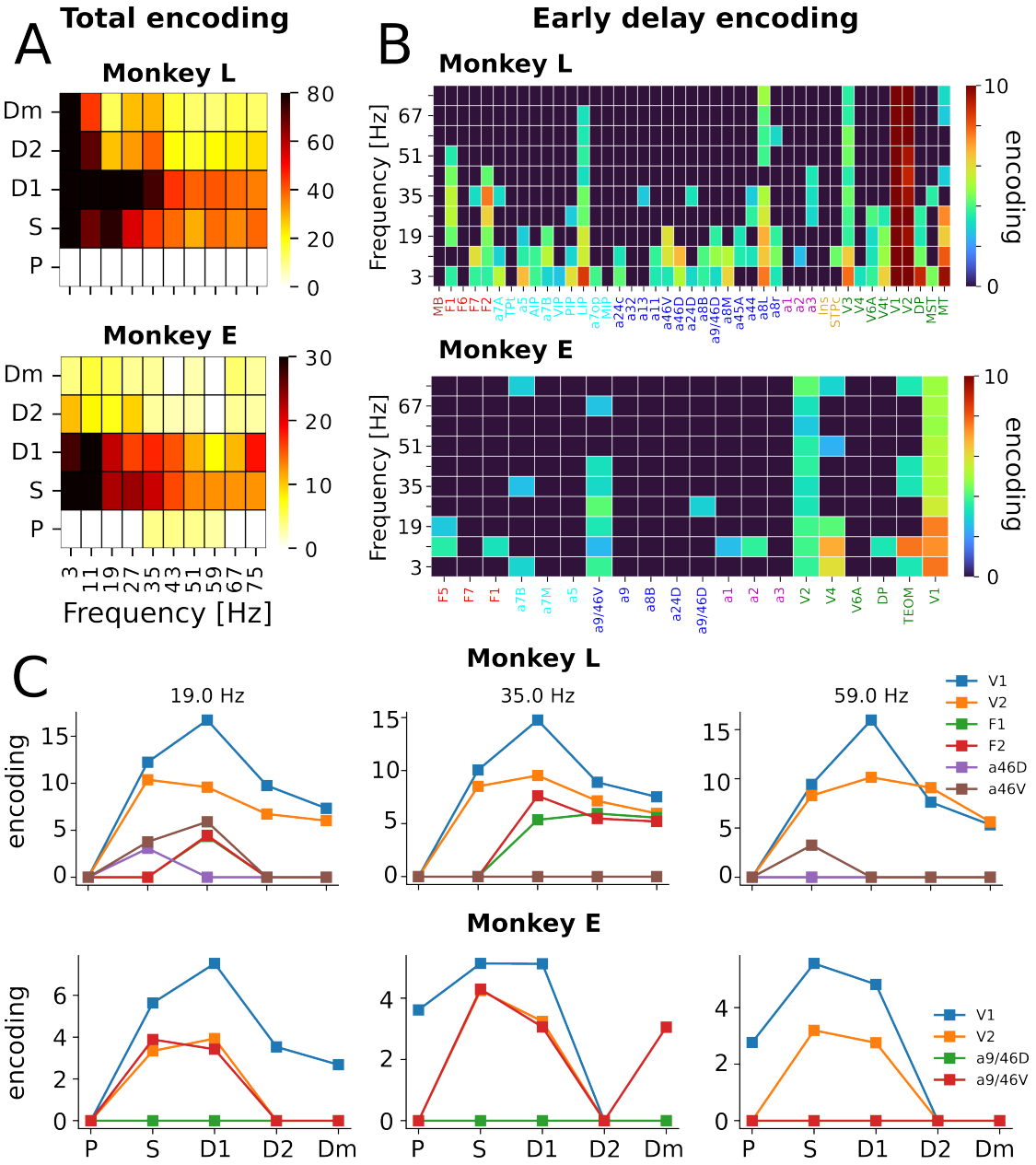

FIGURE 2.3. : Power time-series' stimulus encoding. (A) Total stimulus related information contained in the power time-series, obtained by summing the effect sizes of MI across regions of interest, for monkey L (top) and monkey E, bottom. (B) Spatial and spectral distribution of stimulus encoding during D1 for monkey L (top) and monkey E, bottom. (C) The encoding dependency for each task epoch (x-axis), for three selected bands : 19 Hz (left), 35 Hz (middle), and 59 Hz (right). For monkey L (top) we show the areas V1, V2, F1, F2, a46D, a46V. For monkey E (bottom), areas V1, V2, a9/46D, and a9/46V.

2.3.4. Crackles' assemblies predicts stimulus encoding

Crackling activity was shown to reflect both the task and working memory maintenance by encoding the stimulus identity. But how could it favor long-range integration and a distributed representation of the stimulus present? We hypothesize that this is achieved through the coordination of crackling activity across cortical areas. More specifically, the states formed by crackling coordination could be general fingerprints of canonical computations taking place in the brain during working memory, as suggested in past studies (SIEGEL et al. 2012).

To test this hypothesis, we detected crackle assemblies across task epochs and frequency bands and used features extracted from them (see below) to infer stimulus encoding across brain areas. We found that the extent to which areas coordinate among themselves is a better predictor of which areas encode the stimulus identity. We frame our findings within the hypothesis we call communication-through-coordination. Note that we do not restrict crackles to be the result of phase-only or amplitude-only coupling they might contain both (and other) effects.

To determine whether coordinated crackling dynamics predict stimulus encoding, we detected cascades of activity consisting of areas with coordinated crackling. Specifically, we searched for moments where areas crackle together, forming a transient uninterrupted pattern of activity, which we termed crackle assemblies (CrAs). This transient collective activity defines an event where all involved areas are simultaneously active (i.e., above threshold) and they are considered to interact (participate). In particular, it captures beyond zero-lag pairwise co-activations, since within a CrA, interactions are considered to happen from delay zero up to the duration of the CrA. The CrAs can be extracted directly from the raster representation of the thresholded power-time series (Figure 2.4A) by adding directed links from areas at time t to areas at time $t+1$, creating a temporal graph. This allows for a representation of the sequence of co-activations of channels in which the detection of CrAs becomes straightforward and consists of finding connected components of the resulting temporal graph ((BADIE-MODIRI et al. 2020) ; see Methods).

More specifically, we estimate the crackling scaffold, which is a network where all areas participating in a specific CrA are connected, reflecting the structure of the CrA. And the propagation scaffold encodes the order in which areas activate during a given CrA. The crackling and propagation scaffolds averaged over all CrAs, yield the global crackling scaffold (GCS ; Figure 2.4B)and the global propagation scaffold (GPS ; Figure 2.5C,D). We computed the GCS and GPS for each animal, task epoch and frequency band.

While the GCS between a pair of areas is a measurement of how much they participated together in CrAs, the areal strength measured on the GCS quantifies how much a given area engages in coordinated activity with all others. We used the GCS strength as the main feature representing the spatiotemporal dynamics of CrAs, we computed the bootstrap correlation between the GCS strength versus encoding across regions (Figure 2.4C, magenta curves), as well as the correlation between average oscillatory power and encoding, the distribution of the correlation (Figure 2.4C, green curves). In

Figure 2.4C, the left hemisphere of the circular plot shows the correlations obtained for monkey L and the right hemisphere those obtained for monkey E, the angular axis show the correlations as a function of the center frequency analysis. Overall, an improvement of stimulus encoding is obtained from the GCS strength. For the S task epoch, monkey L has increased correlations for bands greater than 19 Hz, while the same effect occurs for bands greater than 27 Hz for monkey E. A similar effect is observed for the other task epochs for monkey L. For monkey E, it is weaker for the D1 and Dm epoch, but stronger for the D2 epoch (in all bands).

Next, we investigated how the threshold used to obtain the crackle time-series (Figure 2.4D,E) impacted the correlations obtained, by calculating the correlations for a few selected bands (19, 35, and 59 Hz), task epochs S and D1, and as thresholds 85, 90, and 95 percentiles of the power distributions for monkey L and E. We observed an overall increase in the measured correlations with an increasing threshold, except for a few discrepancies (e.g., 59 Hz for monkey L during D1, and 19 Hz for monkey E during S).

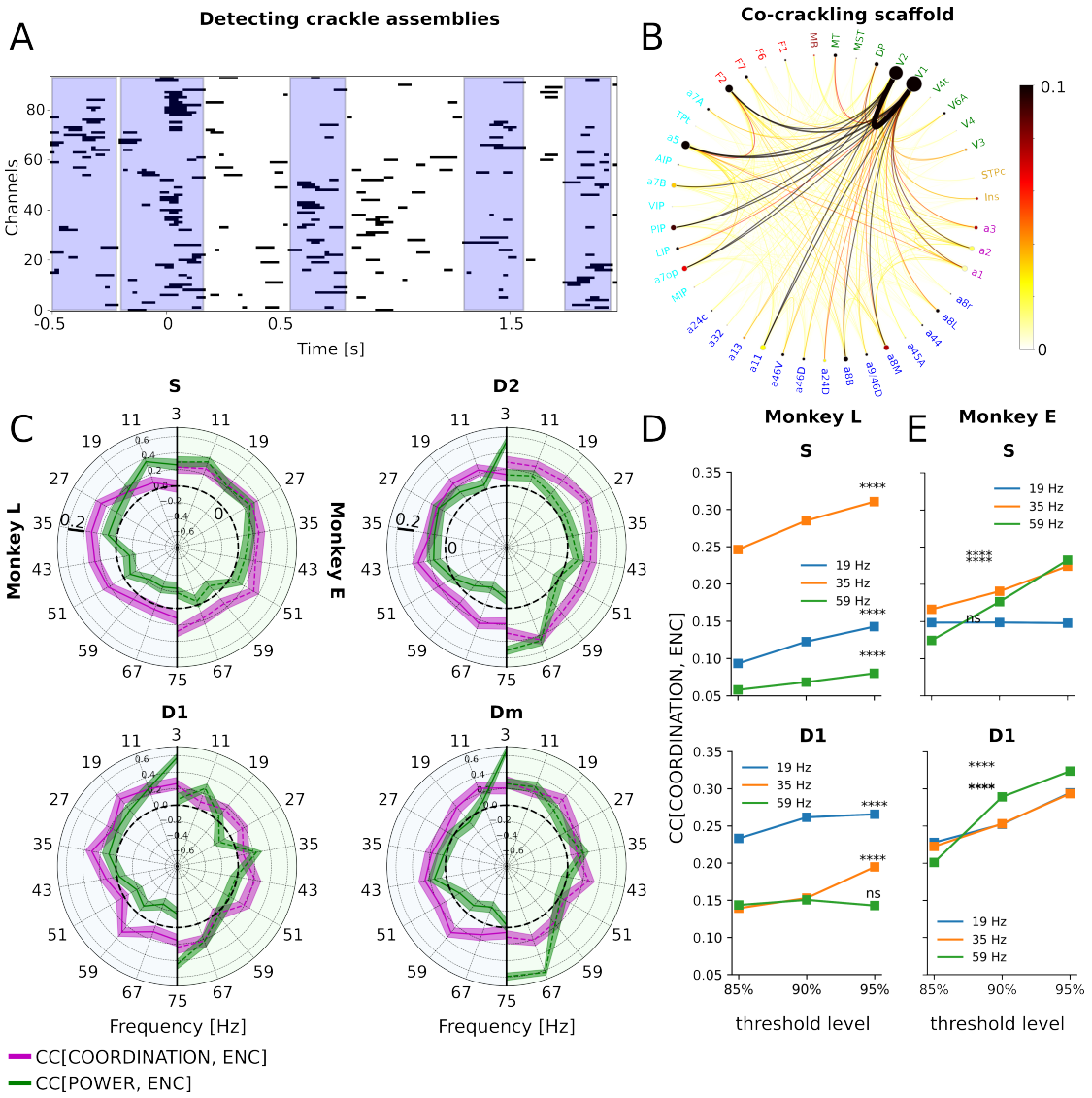

FIGURE 2.4. : Global crackling scaffold strength and encoding predictability. (A) Example raster plot displaying the crackle activity. The crackle assemblies detected (in this example with at least 10 areas involved), are highlighted with the blue transparent windows. (B) Global co-crackling scaffold obtained for Monkey L, for the 27 Hz band and D1 task epoch. (C) Correlations (radial axis) between average power and encoding (green), and co-crackling strength and encoding (magenta) for all frequencies (angular axis), and monkey L (left hemisphere, light blue), and monkey E (right hemisphere, light green) for the S, D1, D2, and Dm task epochs. The dotted line represents the circumference of correlation zero (D) Dependence on the threshold used to detect the crackle in the correlations, for monkey L (left), and E (right) and S (top), and D1 (bottom) task epochs, and three different bands : 19 Hz (blue), 35 Hz (orange), and 59 Hz (green).

2.3.5. Crackles' assemblies unveils how information is transferred across cortical areas

The crackle assemblies detected had different sequences of activations. For instance, some start in visual areas and propagate forward, while others have the opposite directionality. For example, in Figure 2.5A, we show an example of a feedforward CrA starting at V1 and propagating to V2 and parietal areas such as area 7A and 1, and ending up in the motor areas (F1, F2, and others) and frontal areas (area 8M, 8l, 8r, 7B). In Figure 2.5B, we show a CrA with feedback propagation sense, starting at frontal and motor cortices (area 46D, and F6) then extending to the motor cortex (F2), and finishing with a set of frontal, motor and visual areas active (areas 46d, 7B, F2, F7, V1). The propagation of crackling activity through the cortex can be better characterized by a set of regions that (i) ignite CrAs (sources), (ii) where CrAs tend to finish (sinks), and (iii) bridge information between sources and sinks (relays).

To identify the roles of different regions as being either sources, sinks, or relays, during crackle assemblies (CrAs) events, we computed the net tendency of a region to be a source or sink by taking the difference between its in-strength and out-strength (Figure 2.5E, right). We also measured how much regions relay information by computing their betweenness (Figure 2.5E, left) on the GPS. The betweenness quantifies the ratio of shortest paths passing through a given edge of the network, indicating its relative importance for relaying information in the network. During the presample period, most areas act primarily as sinks, except for V1, a3, F1, F2, 45A, and 8l, which include visual, motor, parietal, and prefrontal areas. These areas also primarily relay information, along with a5.

As the task progresses, a few areas have their roles as sources and sinks inverted. For instance, prefrontal areas such as 46v and 46d slowly transition to a balanced (slightly source) state during the delays. While V1 acts mainly as a source, it becomes a sink during the D2 epoch, interestingly, just before the moment of choice. The role of relays is quite stable; however, during the task, we see the emergence of numerous parietal areas and a few prefrontal areas acting as relays, while the motor area F1 stops relaying during the D2 epoch. Results were generally similar for monkey E (Figures S2.15-2.18), though they do not necessarily occur in the same epochs (e.g., the inversion of V1 from sender to receiver happens at D1 for monkey E), and the areas involved may change given the differences in sampled areas.

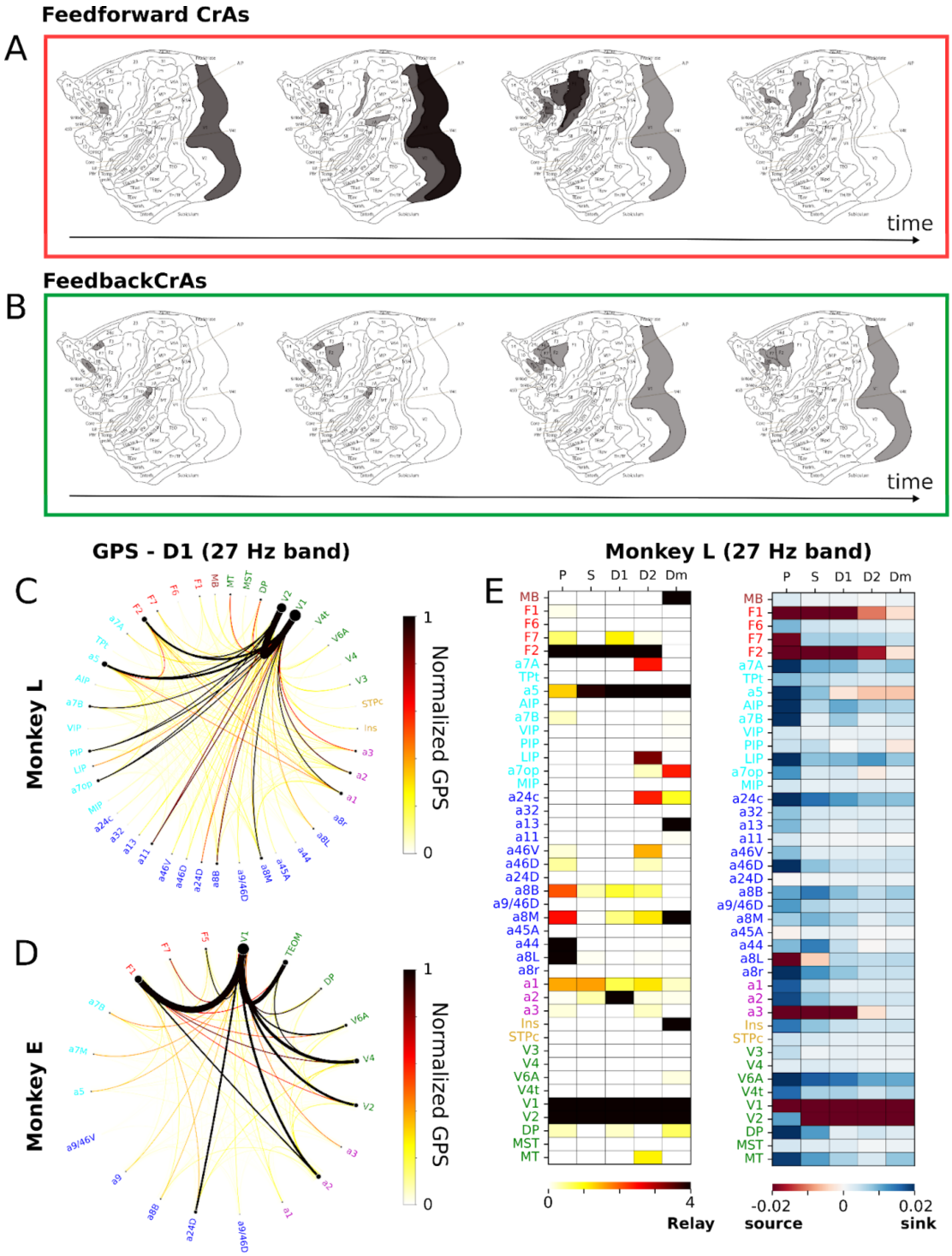

FIGURE 2.5. : Net sink/source and betweenness of each region. (A) A selected feedforward CrA, starting in V1 and propagating to motor and frontal areas, and (B) feedback CrA. (C) Symmetrized global propagation scaffold (GPS) for Monkey L, and (D) Monkey E, both for the 27 Hz band and D1 task epoch. (E) The betweenness centrality (left), and source/sink balance (right) derived from the GPS for each region of interest in Monkey L, 27 Hz band and D1 task epoch.

2.3.6. Crackles' assemblies are mainly from functional origin and predict pairwise coherence

The fact that we observe co-crackling across widespread cortical areas raise the question of how the underlying structural connections of the macaque cortex is exploited by co-crackling activity. Here we investigate this relation by estimating the correlation between co-crackling and structure (Figure 2.6B). To do this, we used anatomical connectivity data estimated using retrograde tracing from MARKOV et al. (2014). This dataset contains 29 areas (Table 2.3). We depicted the anatomical connectivity, an example GCS, and a GPS for the 27 Hz band during the D1 epoch (Figure 2.6, left to right).

From these examples, it is noticeable that the anatomical connectivity networks are sparser than both the GCS and GPS. Some edges that are strong in the anatomical connectivity (e.g., a8B to a2; V2 to a8M) are not necessarily present or strong in the GCS or GPS. This suggests that the scaffolds are not strictly anatomically constrained.

To verify this effect, we computed the bootstrapped correlation between edge weights from GCS/GPS and the anatomical connection weights for the data pooled across all sessions (Figure 2.6B). The correlations for both scaffolds suggest that the CrAs have little correspondence to the anatomical pathways, and sometimes are even anti-correlated with structure. This trend is consistent across bands and task epochs (Figure 2.19).

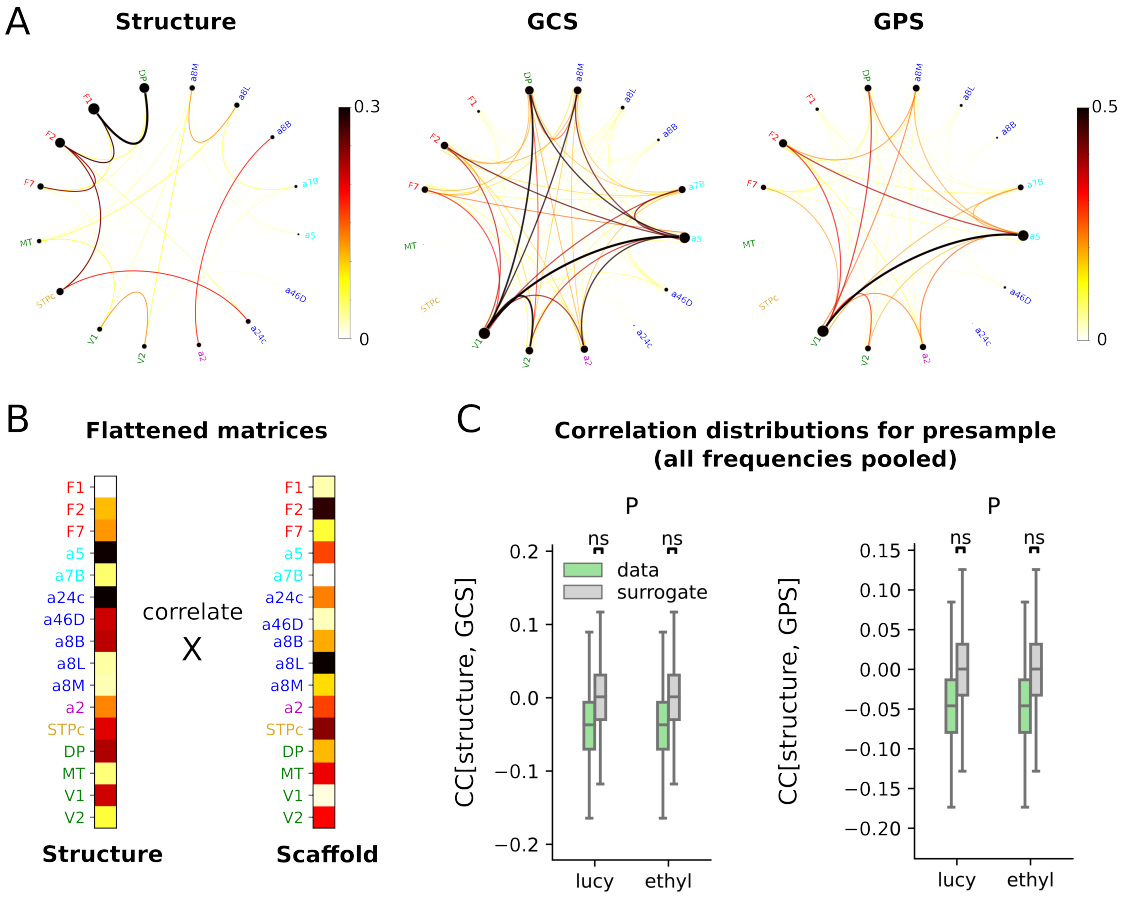

FIGURE 2.6. : The functional origin of CrAs. (A) The network representation of the anatomical data from Markov et. al., the edges between pairs of regions represent the fraction of labeled neurons between those regions. (B) We correlate the upper triangle entries of the GCS/GPS matrix with the upper triangle of the FLN matrix (with the GPS and FLN symmetrized). The surrogate distribution is obtained by shuffling those vectors. (C) Distribution of correlations structure-GCS (left), and structure-GPS (right), for monkey L during the P task epoch and all frequency bands pooled.

Since pairwise interaction within a CrA consists of strong power co-fluctuations, in theory they could correspond to moments of enhanced pairwise coherence. Conversely, the average power of an area is not necessarily indicative of pairwise coherence, given that the time-resolved power fluctuations of two time-series may be uncorrelated, i.e., have asynchronous crackling. Consequently, CrA events should hold a relation with coherence networks. To test this hypothesis, we computed single-trial coherence (COH) for all pairs of channels across the entire dataset. We illustrate the fact that single-trial coherence bouts sometimes come followed by strong power co-fluctuations by plotting the single trial coherence for a pair of channels, and their power-to-power instantaneous correlations in the alpha band (Figure 2.20).

Next, we computed the average coherence networks across frequency bands, and task epochs for each animal (Figure 2.7A,B). First, we examined the relationship

between the average power of each region and its coherence strength (Figure 2.7C). We found that power was generally not predictive of coherence strength (in Figure 2.7A, this can be seen by the fact that most nodes have a small size even when a coherence edge is present). Except for monkey E for the band around 20Hz, the correlation between power and coherence strength typically hovered around zero with no task dependency.

Finally, we repeated this procedure and computed the correlations between GCS strength and coherence strength (Figure 2.7D). The correlations obtained were generally high for both monkeys in bands above 10 Hz. Like the correlations from power, no strong task modulations were observed as well.

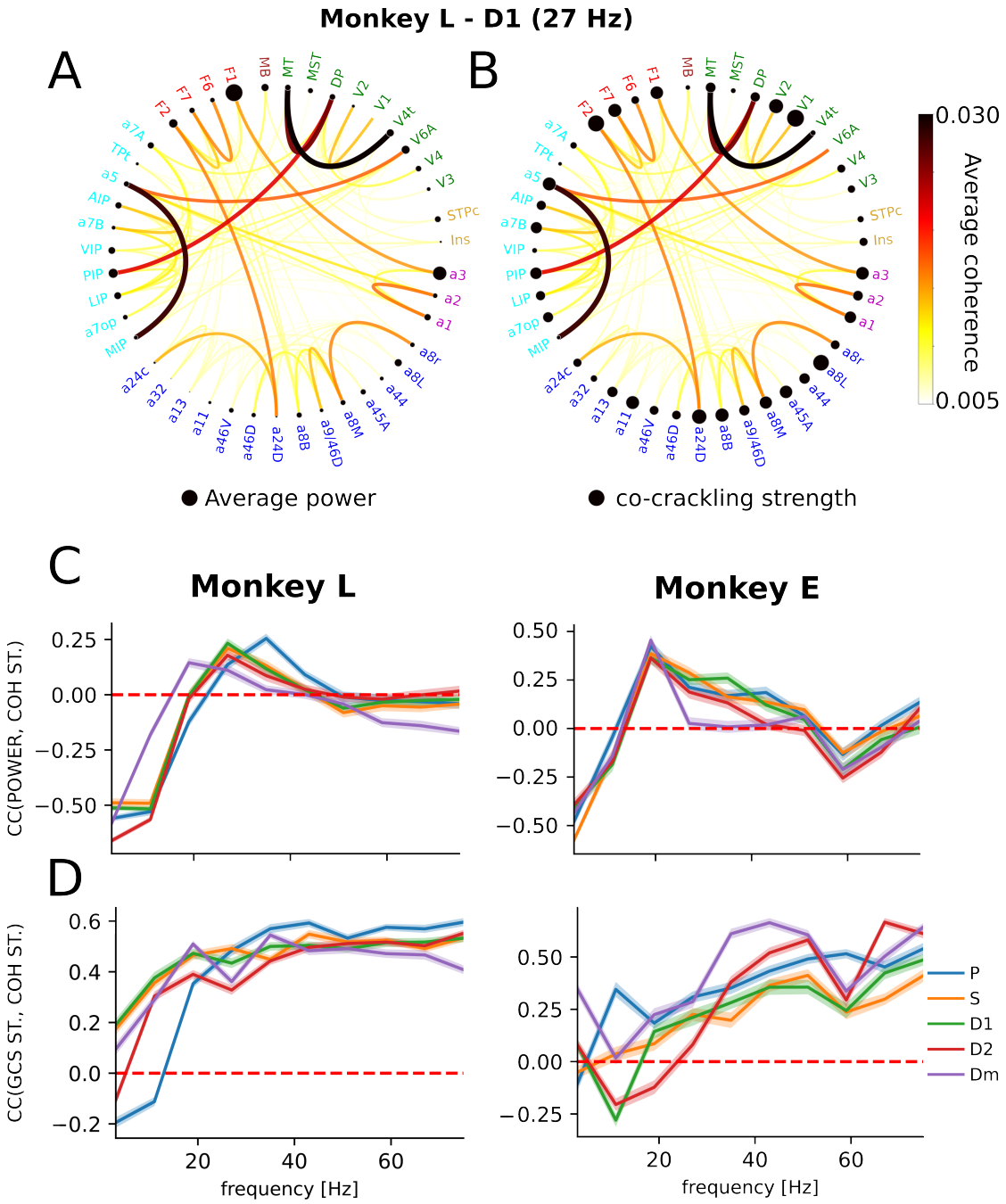

FIGURE 2.7. : The relation between communication through-coordination and coherence. (A) Example network plot depicting the average coherence between each pair of regions (edges). The size of each node representing a region is proportional to its average power (normalized as $5(x/\max(x))^3$), for the D1 period and 27 Hz band. (B) The same as A, but the size of each node is proportional to its GCS strength. (C) Correlation between and coherence strength for each frequency (x-axis), and task epochs (see plot legends), for monkey L (left) and monkey E (right). The dashed horizontal line indicates the zero correlation line. (D) The same as in C but correlating GCS strength with coherence strength.

2.3.7. Interplay between local recurrent connections and connection delays gives rise to co-crackling activity

Under which conditions (or regime) does co-crackling activity emerge? Could co-crackling patterns present in resting state be exploited when required by a cognitive function? To address this question, we reimplemented a large-scale rate-based model based on macaque brain studies (JOGLEKAR et al. 2018; VOGES et al. 2024). We then determined the dynamical regimes where the model's activity is characterized by transient oscillations (or crackling activity). These regimes arise from the interplay of local delays (d) and local recursive inhibition strength (ω_{EI}; (WILSON et al. 1972; WANG 2010)).

We simulated the model for each combination of these parameters and computed the correlation between empirical and simulated GCS strength. The local delays were scaled according to the cortical hierarchy, with integration times increasing as we moved to frontal areas. The correlation was computed between the GCS strength extracted from the broadband simulated signals and the GCS strength for each task epoch and frequency band in the empirical data.

The model state space was characterized using the average variance of the simulated signals (Figure 2.8A, left) and their average peak frequency (Figure 2.8A, right). The variability of the simulated signals tended to decrease with the effect of ω_{EI}, but this effect diminished with increasing delays. The interplay between ω_{EI} and local delay created a region in the state space corresponding to a transition from low to high variability signals. This region featured activity that was, on average, concentrated in the $10-50$ Hz band. Therefore, the activity did not correspond to persistent oscillations due to its intermediate variability, but it was still capable of producing fluctuations that transiently resembled beta and low gamma activity.

Next, for each combination of ω_{EI} and d, we computed the correlation between empirical and simulated GCS strength (Figure 2.8B; 27 Hz data for S on the left and D1 on the right; see also Figure 2.21). Interestingly, there was a particularly large region of high correlations within the transition region of the state space. These correlations decreased if delays were not scaled with the cortical hierarchy (Figure 2.21).

We selected a point in this high-correlation region (marked with a white star; d = 2.5 ms, and ω_{EI} = 55), and the time-series of the model for this point is shown in Figure 2.8C. The model's activity is characterized by short amplitude oscillations that sporadically "crackle". Additionally, the introduction of hierarchy-scaled delays not only improves data-simulation correlations but also allows the reproduction of the empirically observed spectral spatial gradient (Figure 2.8D) and the burst/crackling rate (Figure 2.8E).

To verify how the correlations between data and simulation vary with task epoch and frequency band, we estimated the simulated co-crackling scaffold from the model's crackling raster plot and correlated its GCS strength with the empirical data for each task epoch, frequency band, and monkey (Figure 2.8F). We found overall good correlations for all frequency bands and periods, significantly above chance level, for both animals.

In Figures 2.8G, we show the empirical (D1 - 27 Hz) and simulated GCS, along with the scatter plot of empirical vs. simulated GCS strength as an example, where the correlation is around $r = 0.4$ ($p < 6x10^{12}$). Notably, even areas that are structurally weakly connected (e.g., F1-V1, F2-V2) show increased co-crackling strength, consistent with the empirical data.

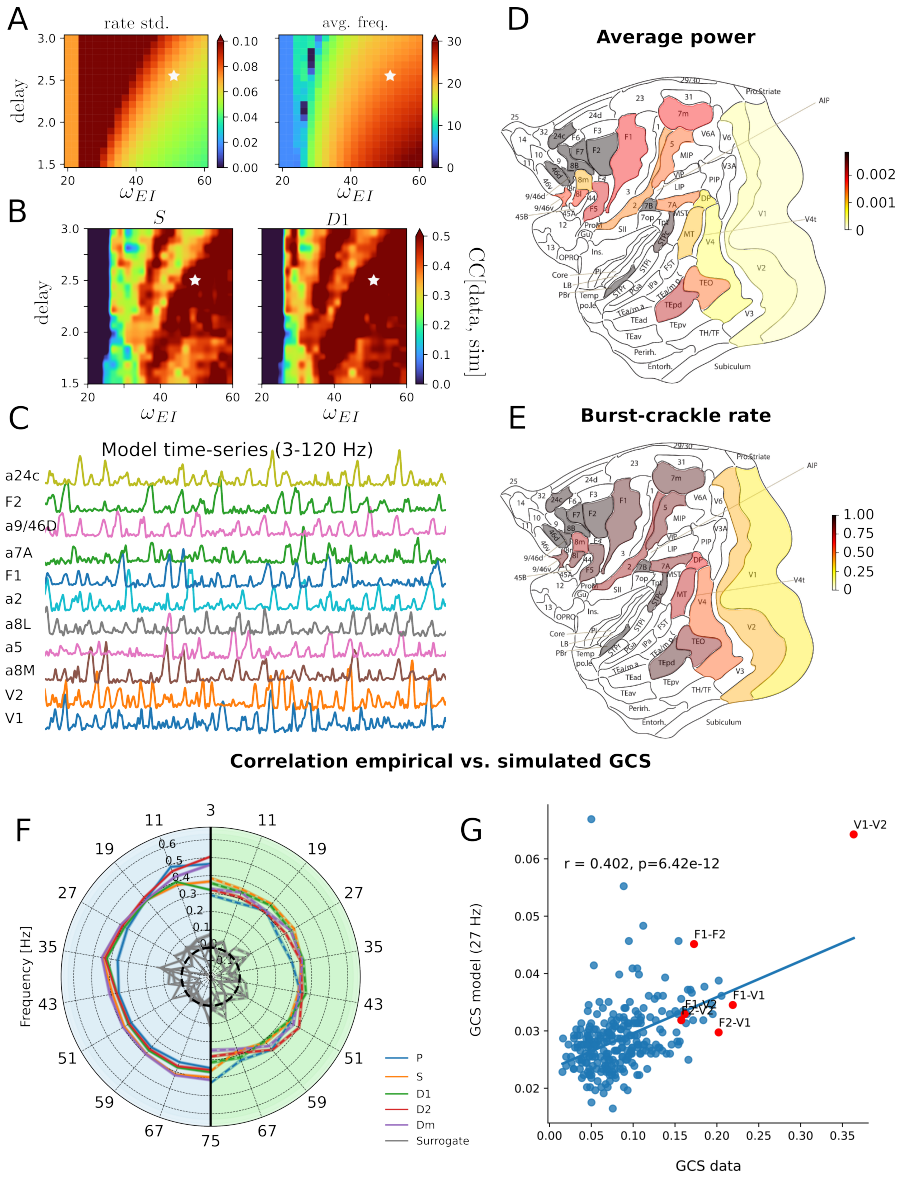

FIGURE 2.8. : Modeling crackles. (A) Model state-space as a function of local delays (y-axis), and recursive inhibitory weights (ω_{EI}). The model's dynamics is characterized by its average standard variation (left) and peak frequency (right). (B) The correlations between the empirical and simulated GCS strength for monkey L, S (left) and D1 (right), and the 27 Hz band. (C) The activity of a few selected areas in the model for local delay =2.5 ms, and $\omega_{EI} = 55$, the point in the state space corresponding to those parameters is indicated with a white star in (A-B). (D) The average power for each brain region in the model, corresponding mostly to frequencies between 10-50 Hz (supplementary). (E) The spatial dependence of the bursts-crackle rate (how many crackles are bursts). (F) The correlation between empirical and simulated GCS strength as a function of frequency (angular axis), for each task epoch (P to Dm), and each monkey L (left hemisphere), E (right hemisphere) (G) Scatter plot with empirical vs. simulated GCS strength for the example GCS for the 27 Hz bands and all epochs.

2.4. Discussion

In this study, we evaluated large-scale LFP recordings from two non-human primates performing a visual delayed match-to-sample task (DOTSON et al. 2017; DOTSON et al. 2018; HOFFMAN et al. 2024). The recordings covered multiple cortical areas, spanning almost an entire brain hemisphere. This extensive dataset allowed us to investigate how coordination among cortical areas supports memory maintenance during a visual working memory (WM) task. Specifically, we found that stimuli encoding in cortical areas during the WM task is maintained in network activity by means of coalitions of areas. Those coalitions were formed by the coordination of non-linear events detected in the regions' power time-series, which we termed "crackles." This finding suggests a general principle of integration in the brain that we refer to as "communication-through-coordination" (Comm-t-Coord).

Importantly, Comm-t-Coord is not incompatible with CTC (GRAY et al. 1989; WOMELSDORF et al. 2007a; FRIES 2005; FRIES 2015), as power co-modulations may reflect transient coherence modulations (PALMIGIANO et al. 2017). At the same time, Comm-t-Coord is also compatible with coherence-through-communication (Coh-t-Comm), where coherence emerges as a consequence rather than the cause of communication (SCHNEIDER et al. 2021; DOWDALL et al. 2023). Consequently, Comm-t-Coord offers a general principle of long-range integration, and co-crackling assemblies could be a "spectral fingertip" of canonical computations taking place during WM (SIEGEL et al. 2012). More specifically, our results suggests a prominent role of beta oscillation in supporting WM, in line with previous works that reported long-range interaction in the beta band during tasks in humans (AOKI et al. 2001; DONNER et al. 2007; PESARAN et al. 2008; DONNER et al. 2009; SIEGEL et al. 2011; SIEGEL et al. 2009) and non-human primates (MURTHY et al. 1992; BROVELLI et al. 2004; HAEGENS et al. 2011; LUNDQVIST et al. 2016; LUNDQVIST et al. 2018; LUNDQVIST et al. 2024).

Additionally, we found that coordinated crackling is predicted by a large-scale model built on top of the macaque connectome (MARKOV et al. 2014; JOGLEKAR et al. 2018; LIMA et al. 2023), in which activity is tuned to the edge of synchrony. Here's a revised version of your text with corrections for grammar and concordance errors :

For this regime, the model is capable of displaying transient activity that resembles the crackling observed in the data, with a characteristic frequency lying within the beta frequency range. Additionally, the co-crackle patterns generated by the model occur in the absence of external stimuli, suggesting that these activity patterns may be available for the system to recruit "on demand" for information processing in the context of a task. In this sense, co-crackling patterns could constitute an alphabet of system states that are exploited for information processing during working memory (WM) (BUZSÁKI et al. 2022; BUZSÁKI et al. 2023), representing attractor states (HOPFIELD 1982; SANDBERG et al. 2003; LUNDQVIST et al. 2016; BARBOSA 2017; MONGILLO et al. 2018; BARBOSA et al. 2020).

Previous studies have shown that power dynamics, appearing as transient bursts of activity (LUNDQVIST et al. 2024), are intrinsically related to the control and maintenance aspects of WM (MILLER et al. 2018; MILLER et al. 2024). Here, we found that

the power time-series are characterized by a significant variability of bursting activity. These bursts are rarely trial locked, except in a few instances, such as the visual response evoked by stimulus presentation. The power fluctuations that exceed a relative threshold based on a quantile of the power distribution (typically the 90th percentile) were considered crackle events (borrowing the term from statistical physics SETHNA et al. 2001), and these events were the main focus of our analysis. Specifically, we investigated whether these events are : (i) task-modulated, (ii) capable of implementing long-range integration through their coordination, and (iii) whether this integration can support WM maintenance.

Crackle events were modulation across cortical areas, in line with multi-unit activity findings using the same dataset (DOTSON et al. 2018), and studies suggesting the widely distributed nature of WM (SALAZAR et al. 2012; BOUCHACOURT et al. 2019; CHRISTOPHEL et al. 2017; BUSCHMAN 2021; MEJIAS et al. 2022; FENG et al. 2023). In particular, we identified four stereotypical modulation factors in the beta band of both monkeys : (i) one corresponding to motor activity present during the task, (ii) a factor representing sustained activity during the delay, involving mostly frontal and parietal areas, (iii) a delay-ramping factor, involving visual, parietal, motor, and frontal areas, and (iv) a visual-evoked response during cue presentation. Additionally, crackling rates contained widespread stimulus encoding across all task epochs (except for the presample epoch, as one would expect) and frequencies.

Given the rich repertoire of task-modulated activity offered by the crackling dynamics, by which means can they support integration, and a distributed representation of memory? We proposed the hypothesis that distributed encoding is derived from collective dynamics characterized by the coordination of crackling activity. Here, we detected crackle assemblies (CrAs), and defined the degree of coordination of a region as being proportional to the number of times it participates in CrAs with other regions. By measuring coordination in this way, the obtained quantity differs from correlation for at least three reasons : (i) by thresholding the time series, only the nonlinear part of the signal is retained; (ii) while correlation is measured with lag one, inside a CrA, interactions are allowed from lag one up to the length of the CrA event; (iii) in order to have high coordination, an area must engage in CrAs with multiple areas, while correlation is purely pairwise. Similar metrics have been used in the literature. For instance, in the work by Sorrentino and colleagues (SORRENTINO et al. 2023), they showed that interactions measured in this fashion are more effective for differentiating subjects. Also, in a recent review by Vinck and others (VINCK et al. 2023), they propose that this kind of activity can provide short windows in which information integration can take place.

We found that coordination is a better predictor of which areas will carry stimulus encoding for a broad range of frequency bands analyzed, in both monkeys. In some instances, the correlations were at a comparable level (e.g., in monkey L, epoch D1 for bands less than or equal to 19 Hz), but even this result is surprising in the sense that if one ignores the absolute power level, encoding predictability can be retrieved based only on the basis of brain areas' interactions. Additionally, we observed a tendency of obtaining bigger correlations for higher threshold levels (from 80 to 95 percentile).

This indicates that while local (sub-threshold) power can sub-serve local processing, large-scale integration would rely on extreme (but coordinated) events. In fact, such coordinated extreme events can be typically captured by the co-kurtosis between two time-series, which has been shown not only to capture "co-bursting" in neural time-series but also to better reflect resting-state networks in MEG studies (HINDRIKS et al. 2023). These results add to the body of studies showing that collective interactions are relevant in a range of cognitive functions (LUPPI et al. 2022; COMBRISSON et al. 2023; VARLEY et al. 2023a; VARLEY et al. 2023b).

The link between co-crackling and encoding suggests that CrAs should somehow mediate information transfer among areas. Specifically, during a CrA, we found that some areas acted as source areas (igniting CrAs), sinks (ending CrAs), and relays (passing information from sources to sinks). This was evident from the clear directionality CrAs exhibited, where some of them propagated feedforward from visual to frontal areas, and others in the opposite direction. This suggests that CrAs may be used to establish pathways through which information travels across cortical areas.

By analyzing the crackle assemblies' propagation scaffolds, we found that areas usually related to WM in the prefrontal, parietal, and somatosensory cortices act as relays at different moments of the task. Additionally, areas such as F2, V1, and V2 are quite stable relays. We also found that initially, most areas act as sinks. However, a more complex dynamic unfolds as the task progresses, with prefrontal areas slowly acting as a source. Interestingly, V1, which is mainly a source, transitions to a sink in the moments preceding the match period. This observation could be related to information from the frontal cortex being sent back to visual areas, as proposed by the prediction error hypothesis (GABHART et al. 2023). However, interpretations regarding the directions of propagation of information transfer should be made with caution, as more investigations using transfer entropy or Granger causality should be performed to correctly address this issue.

One interesting observation, is that correlations between the crackling scaffolds and anatomic connection were overall poor (MARKOV et al. 2013), indicating that the form of non-linear interaction implemented by co-crackling explores a wide range of interactions that are not necessarily hardwired (i.e., co-fluctuations between areas that are not directly coupled but may be linked by undirected paths in the connectome, or driven by common inputs). Interestingly, in (VEZOLI et al. 2021), the authors reported a good correspondence between functional and structural connectivity. However, in their work, they compute correlation, coherence, and Granger causality (GC), which are all linear and pairwise metrics; hence, they are fundamentally distinct from our interaction metric. Furthermore, it was shown that correlation captures both phase-coherence and co-kurtosis (HINDRIKS et al. 2023). Since coherence is the equivalent of correlation in the frequency domain, and total GC reduces to the logarithm of one minus coherence, these three metrics carry a degree of redundancy and none captures co-bursting (co-kurtosis). Finally, this analysis suggests that, although brain structure constrains the pathways through which information can flow, it does not determine them in a fully hardwired manner. This finding aligns with theoretical works suggesting that the brain's natural evolution may have maximized the number

of possible functional motifs while maintaining a constrained number of structural ones.(SPORNS et al. 2004 ; SANTANA et al. 2011).

Finally, we propose three different scenarios for interpreting our findings : (1) during limited times crackles can be as strong as bursts, hence communication can be established as posed by the CTC hypothesis ; (2) oscillations cannot mediate excitability modulations, but their coordination indicates selection of a specific collective dynamics mode ; and (3) there are no real oscillations but the statistics of the measured fluctuations are driven by inputs or brain state. As already mentioned, moments where power strongly co-fluctuates can reflect in significant coherence, hence this can either fit on the CTC (scenario 1) or Coh-t-Comm hypothesis (scenario 3). Even if oscillatory activity can not implement coherence, Scenario 2 proposes a scenario where the system self-organizes into a state where widespread coordination of oscillation can still mediate communication. But where does Comm-t-Coord stands ? We observed both globally strong crackles (i.e., bursts) and, due to the cortical gradient of average power, crackles originating from power modulations that are relatively weak. It is arguable if these weaker events can be termed oscillations. Consequently Comm-t-Coord would allow for states of coordination involving both of oscillatory activity and non-linear fluctuations, offering a way of reconciliations between CTC and Coh-t-Comm. In this sense, crackling activity, despite corresponding to an oscillation or not, re still useful as “neuromarkers“, and their coordination indicates selection of a specific collective dynamics mode.

TABLEAU 2.1. : Number of recordings per region used for each animal. Number of recorded sessions and the total number of task and fixation trials are shown.

	Monkey L	**Monkey E**
# sessions	62	25
# task trials	31257	13534
# fixation trials	5552	1853
AIP	66	0
Core	5	0
DP	128	30
F1	248	90
F2	340	2
F3	0	3
F5	0	15
F6	12	0
F7	116	24
FST	2	0
Ins	50	0
LIP	109	0
MB	14	0
MIP	13	1
MST	15	3

MT	116	9
OPRO	8	0
PBr	2	0
PIP	75	1
SII	2	0
STPc	13	8
TEO	0	1
TEOM	0	13
TEpd	1	0
TPt	17	4
V1	681	196
V2	439	57
V3	27	6
V3A	1	0
V4	14	54
V4t	37	0
V6A	86	44
VIP	13	0
a1	63	17
a11	13	0
a12	8	0
a13	26	0
a14	6	0
a2	53	43
a23	2	0
a24D	15	10
a24c	72	4
a3	142	17
a32	19	0
a44	63	0
a45A	15	0
a45B	8	5
a46D	66	4
a46V	48	0
a5	236	14
a7A	88	7
a7B	98	23
a7M	1	12
a7op	79	1
a8B	140	10
a8L	149	9
a8M	129	6

a8r	60	0
a9	0	21
a9/46D	49	15
a9/46V	4	14
Total recordings	4302	793

TABLEAU 2.2. : Frequency bands determined empirically for each animal.

band	**Monkey L**	**Monkey E**
theta (θ)	0 - 6 Hz	0 - 8 Hz
alpha (α)	6 - 14 Hz	8 - 21 Hz
beta (β)	14 - 26 Hz	21 - 32 Hz
high-beta(β^+)	26 - 42 Hz	—
gamma (γ)	42 - 80 Hz	32 - 80 Hz

TABLEAU 2.3. : List with the 29 available areas in the anatomical data for the macaque connectivity database from Markov et. al., 2014.

Areas available on the Markov dataset
V1, V2, V4, DP, MT, 8m, 5, 8l, TEO, 2, F1, STPc, 7A, 46d, 10, 9/46v, 9/46d
F5, TEpd, PBr, 7m, 7B, F2, STPi, PROm, F7, 8B, STPr, 24c

TABLEAU 2.4. : List of abbreviations used in the manuscript

Abbreviation	**Long-name**	**Description**
DMTS	Delayed match-to-sample task	Visual task used in empirical studies of working memory.
P, S, D1, D2, Dm	Presample, Sample, early delay, late delay, match/delay	Epochs or periods of the visual task.
WM	Working Memory	Short-term memory associated with goal directed behavior.
MI	Mutual information	Statistical relation between two random variables.
CrAs	Crackle assembly	Coordinated crackling activity of a group of brain areas/channels/etc, that is cohese during a given period.
CS / CP	Crackling scaffold / Propagation Scaffold	Networks describing the spatio-temporal structure of individual CrAs.
GCS / GCP	Global Crackling scaffold / Global Propagation Scaffold	The summary CS and CP obtained by averaging/summing/aggregating over the CS/CP of all CrAs.
ROI	Region of interest	A given cortical region in which the analysis is focused on.

CTC	Communication through coherence	Hypothesis that states that brain areas phase-lock their oscillatory activity in order to bridge communication (Fries, 2015).
COH	Coherence	The squared magnitude of coherence. Which is a metric of correlation in the time-frequency domain.
Coh-t-Comm	Coherence through communication	Hypothesis that state that communication could occur even through means of weak or non-oscillatory transient activity, given that the brain is found in a state in which those weak transients could coordinate (Schneider et. al., 2021).
Comm-t-Coord	Communication through coordination	Hypothesis that state that communication could occur even through means of weak or non-oscillatory transient activity, given that the brain is found in a state in which those weak transients could coordinate.

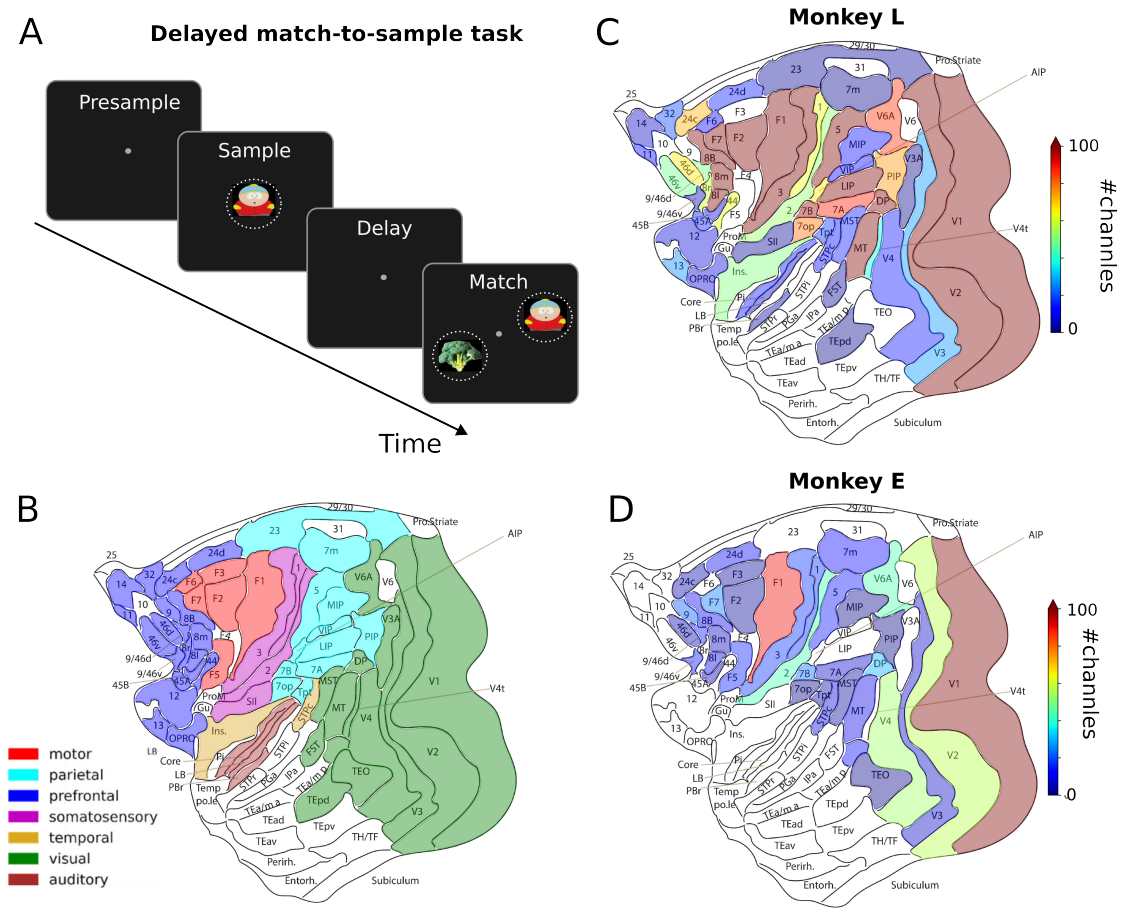

FIGURE 2.9. : Visual task structure and area recorders for each monkey. (A) Time course of events in the delayed match-to-sample task. The upper frames illustrate the sequence of images viewed by the monkeys during the task. The dashed circles represent the windows for monitoring eye position. These were not visible to the animal. The sample and match stimuli are symbolized by the letters A-E.The white dashed circle in the right plot indicates a correct match. The lower plot illustrates the timeline of task events. The presample duration was 500 ms for monkey E and 800 ms for monkey L. The duration of the delay period was 800-1200 ms for monkey E and 1000-1500 ms for monkey L. Match stimuli were randomly presented on opposite sides of the horizontal for monkey E and on opposite sides of axes lying at 0, 45 and 90 degrees for monkey L. The colored horizontal bars at the bottom indicate the time and duration (400 ms) of the Presample (P), Sample (S), Delay1 (D1), Delay2 (D2) and DelayM (Dm) epochs, respectively. (B) Flatmap showing all the recorded areas. (C-D) The number of recordings per recorded area for monkey E, and L.

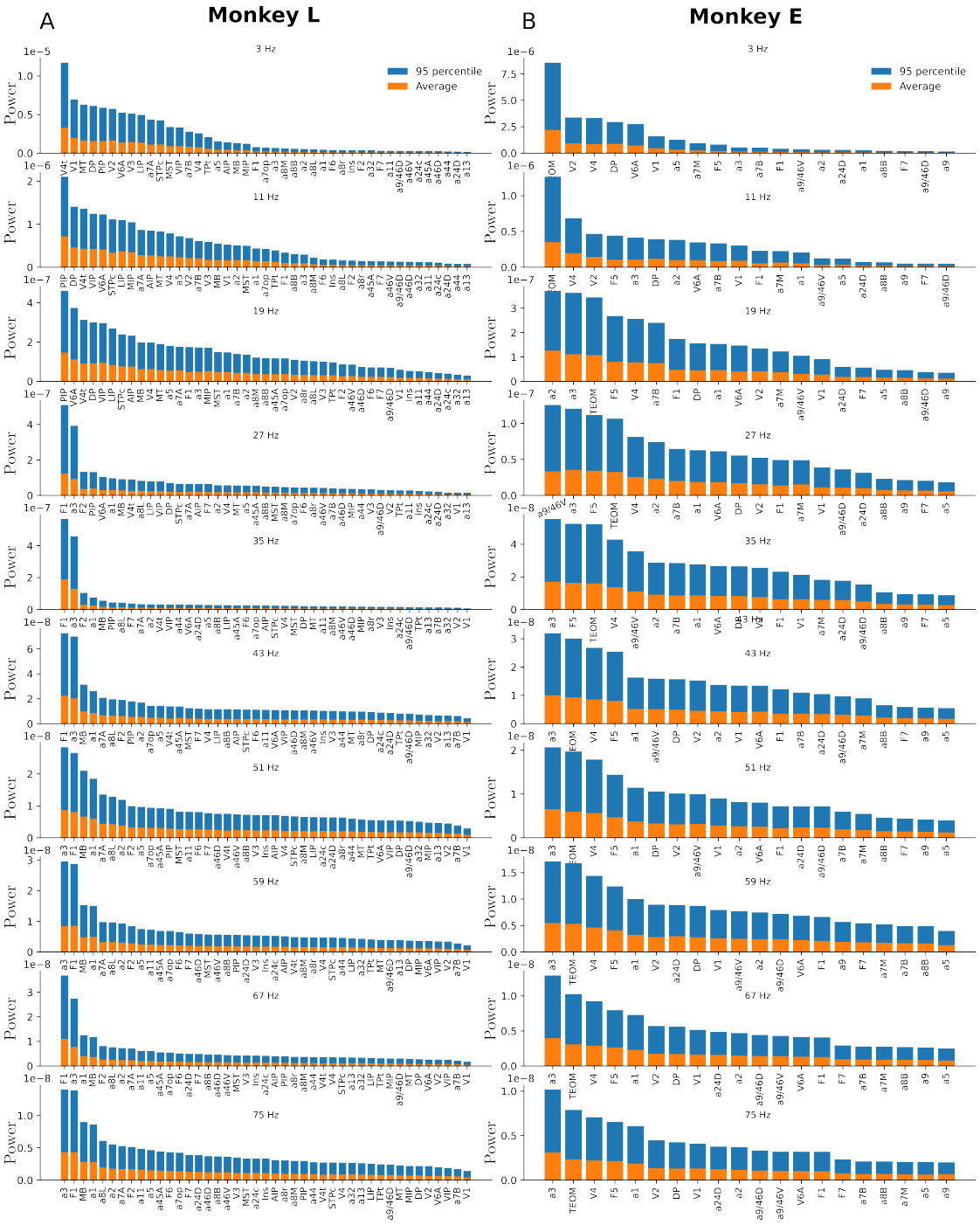

FIGURE 2.10. : Average and 95 percentile power spatial distribution. The distribution of average power (orange) and 95 percentile power (blue) during the D1 period, for (A) monkey L, and (B) monkey E.

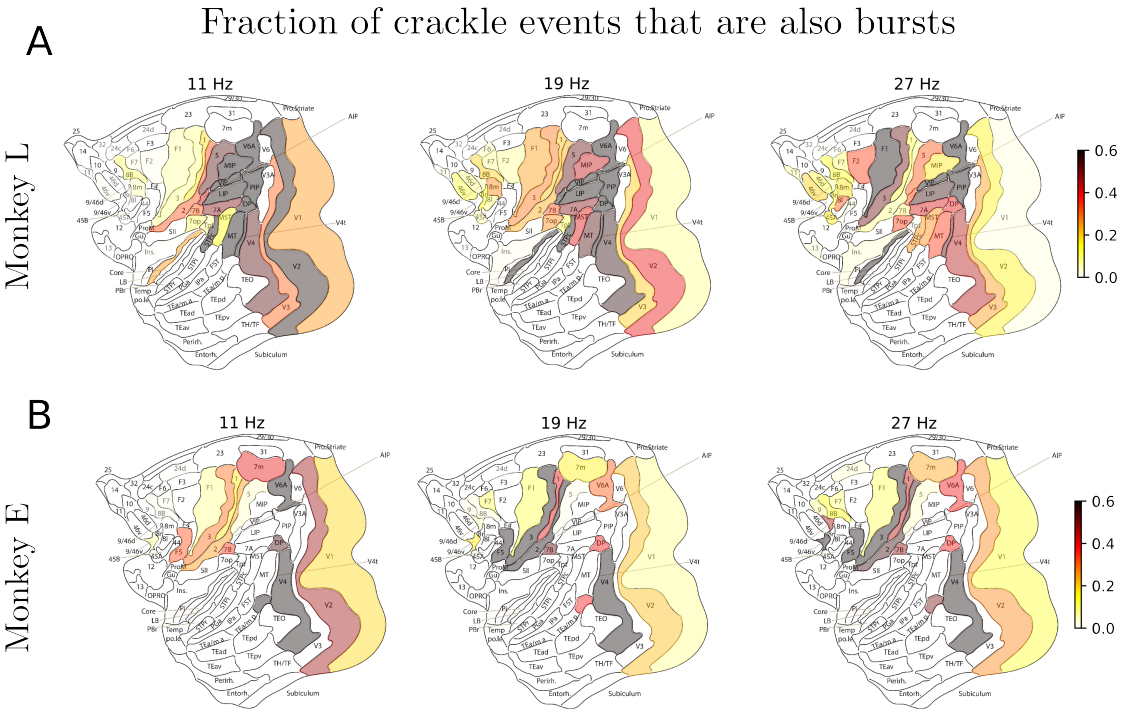

FIGURE 2.11. : Fraction of crackle events that are globally strong (bursts). The spatial distribution is shown on the flatmaps for (A) monkey L, and (B) monkey E. For the bands 11 Hz, 19 Hz, and 27 Hz (from left to right).

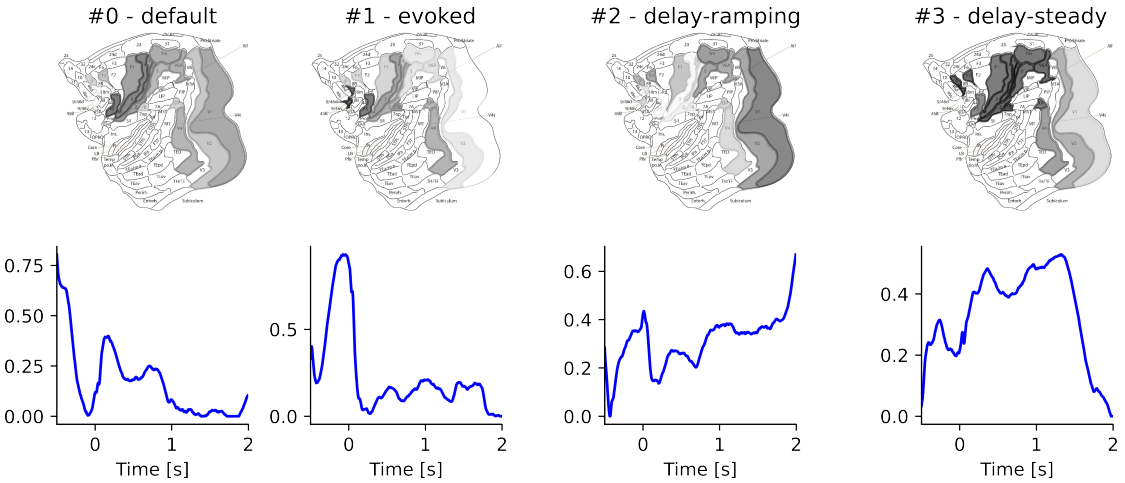

FIGURE 2.12. : Temporal and spatial task modulation of crackling. (A) cortical areas representing the first four NMF components and (B) the instantaneous time series describing instants at which the NMF components appear, for the high-beta band in Monkey E.

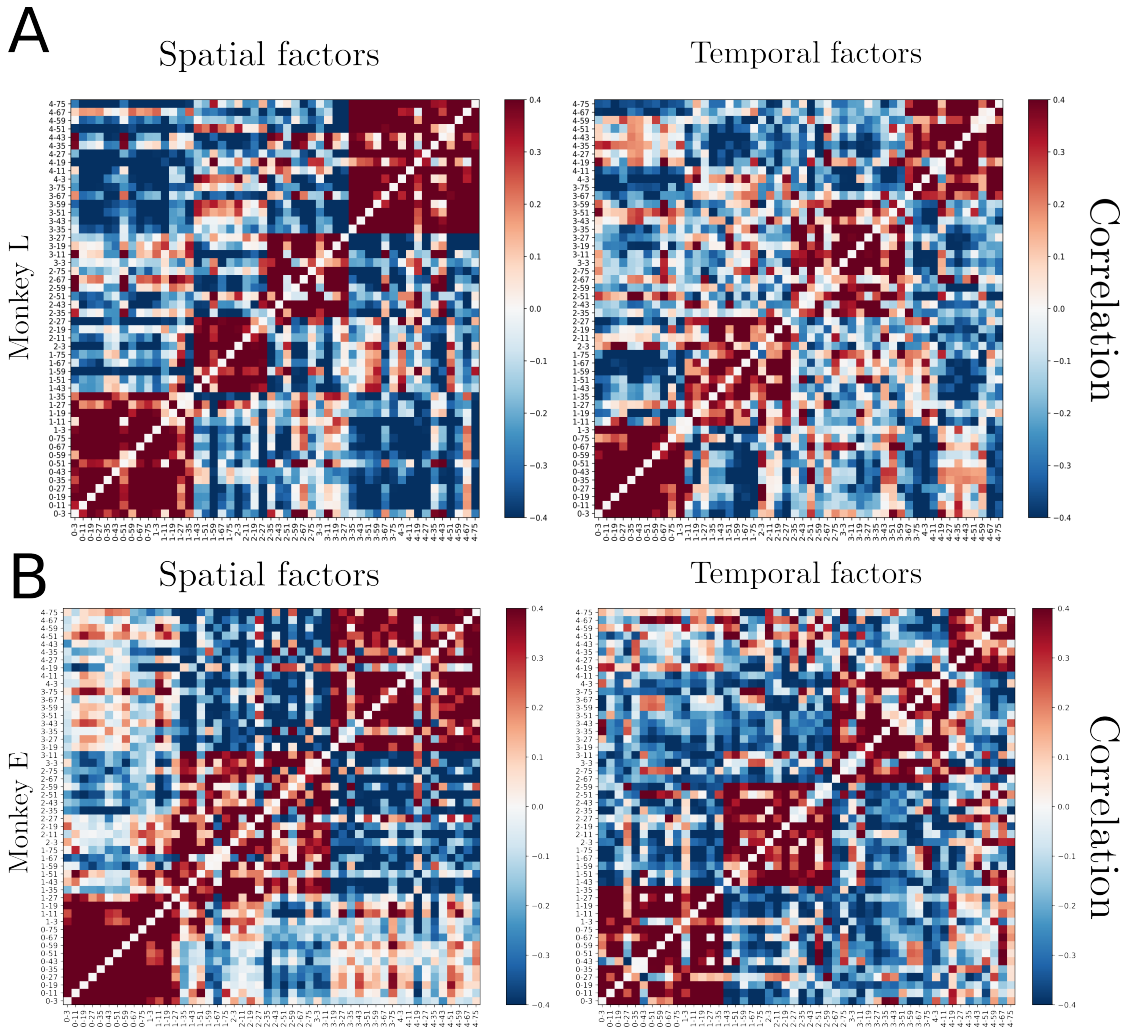

FIGURE 2.13. : Cross-frequency correlation between NMF factor. In (A) for monkey L, and in (B) for monkey E. The matrices on the left show the correlation between the spatial factors of the NMF, and in the right between the temporal factor. The numbers in the row/columns in the matrix are formatted as "factor-band". Notice how factor tend to group in clusters detected using the Louvain algorithm. Those matrices were computed for a single session of each animal.

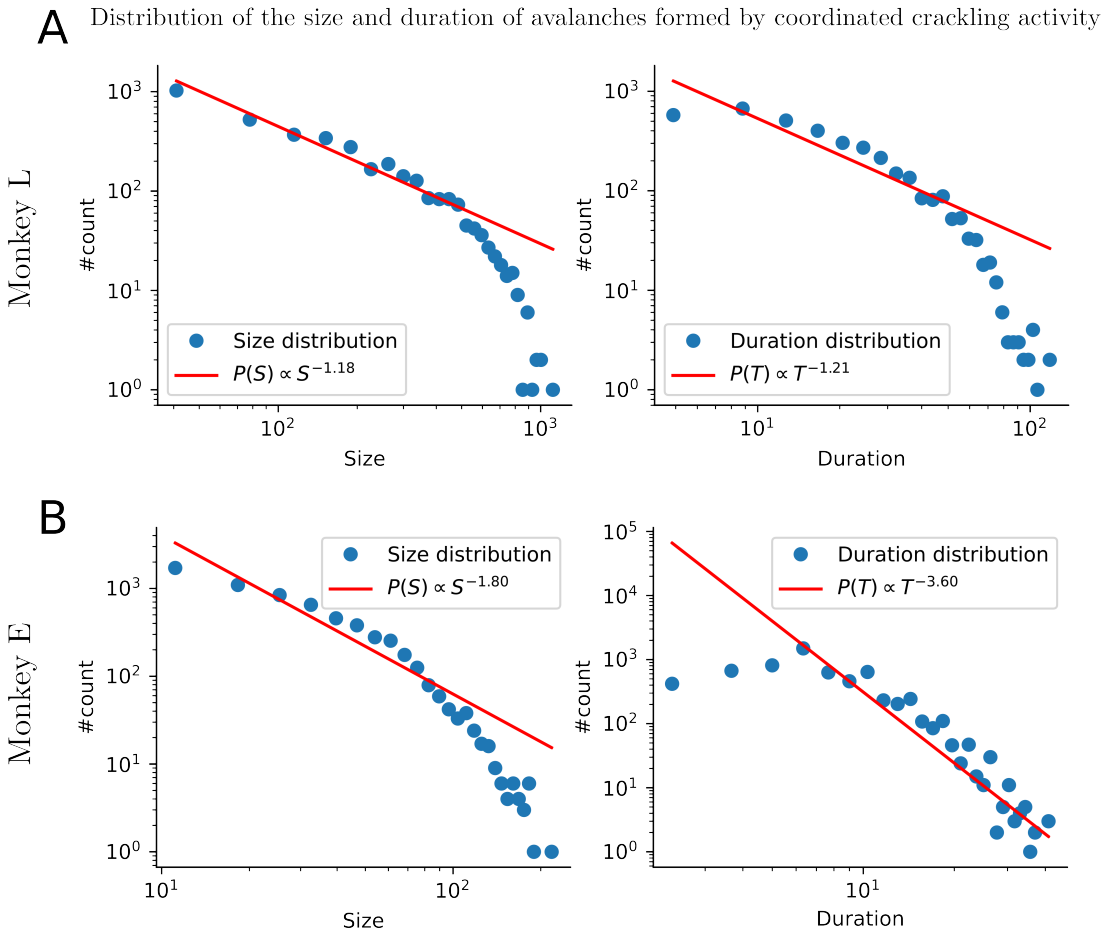

FIGURE 2.14. : Distribution of the size and duration of avalanches formed by coordinated crackling activity. In (A) for monkey L, and in (B) for monkey E. The plots on the left show the distribution of the event size (how many areas participated on the event), and on the right the distribution of event durations on log-log scale, for the 27 Hz band. In blue the distribution is shown, while in red we show the respective power-law fit.

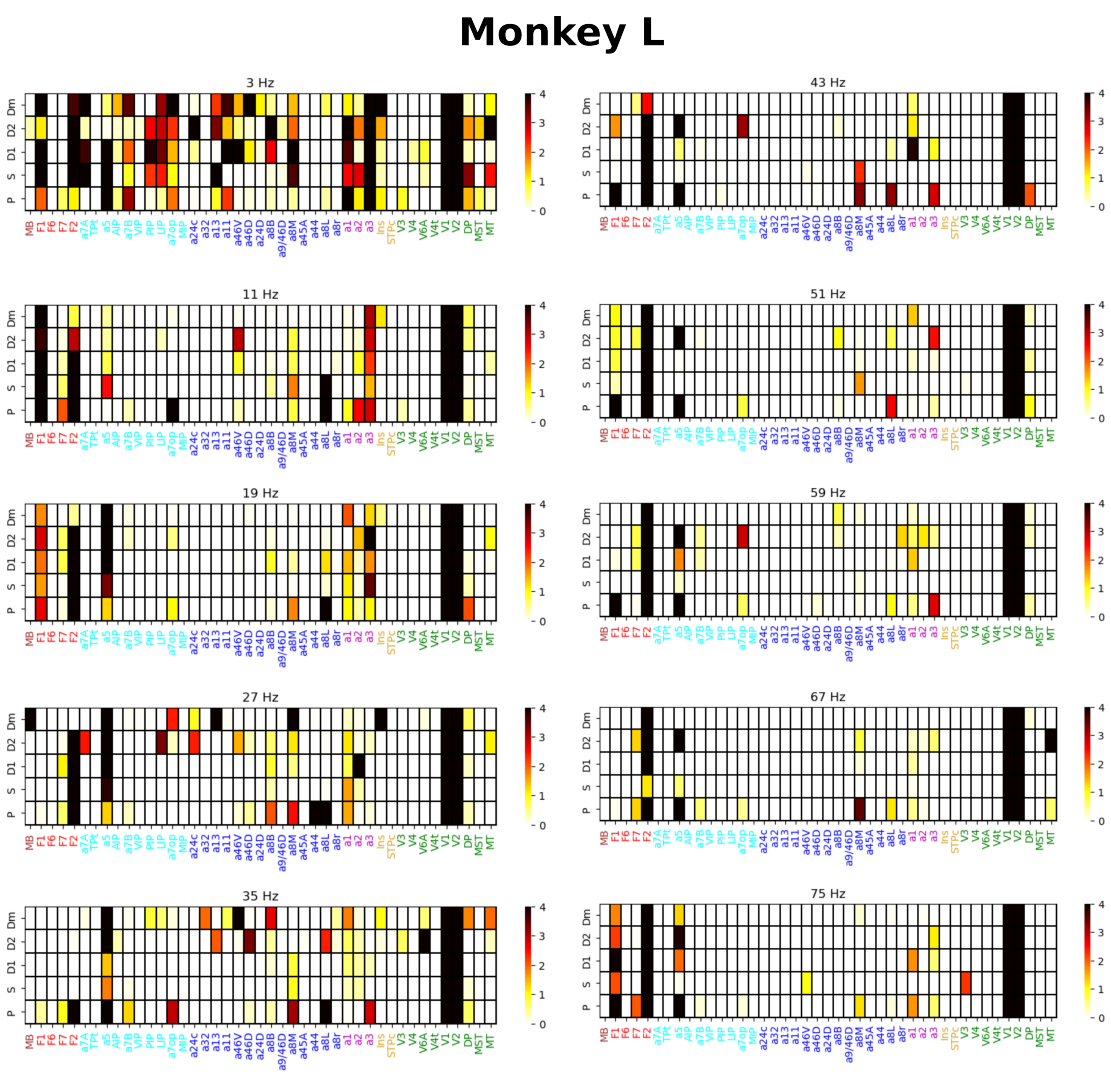

FIGURE 2.15. : Betweenness centrality on the GPS for monkey L. Each subplot corresponds to a frequency band (see subplot title). The vertical axis indicates the task period while the x-axis indicates the respective cortical region.

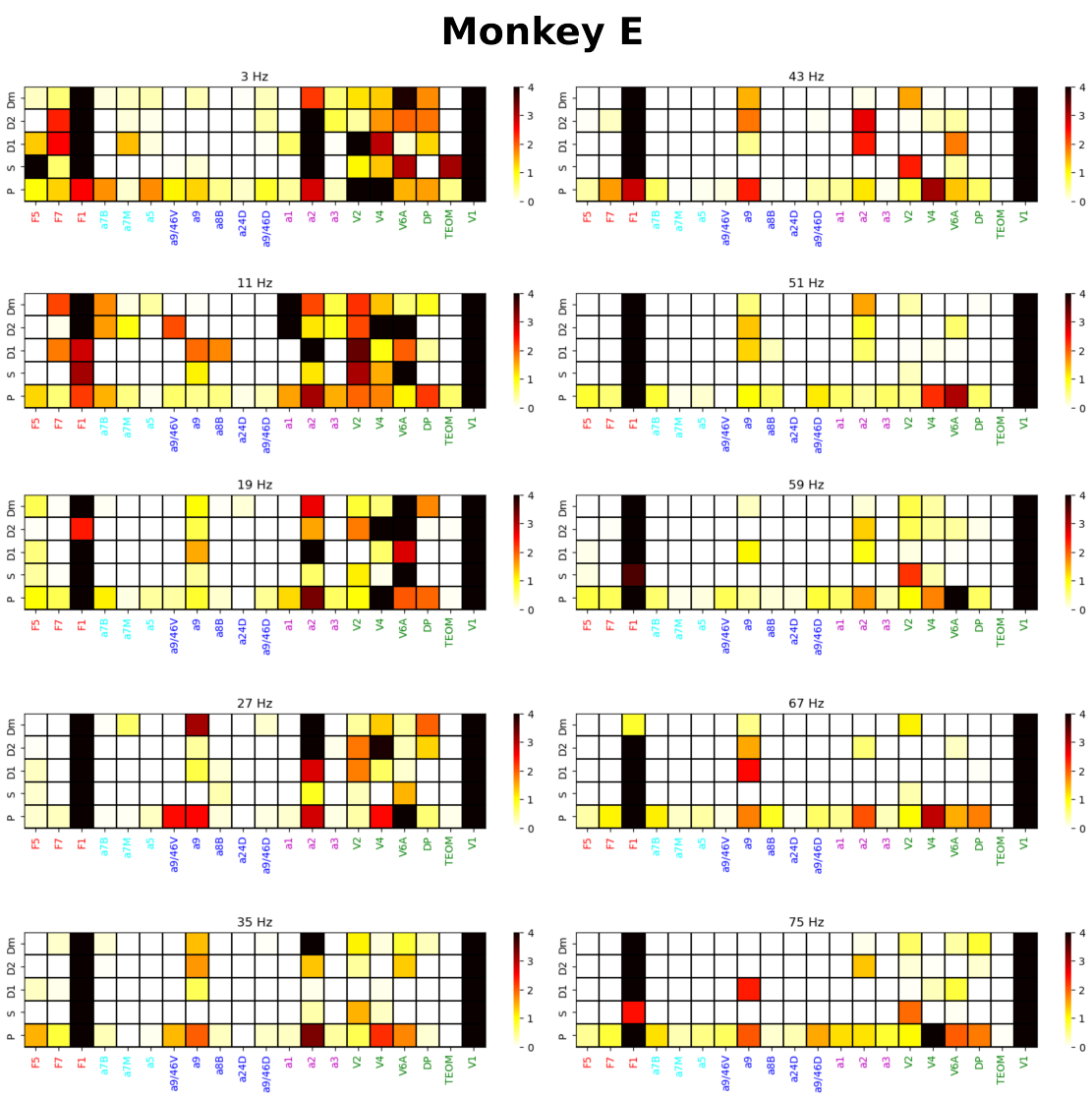

FIGURE 2.16. : Betweenness centrality on the GPS for monkey E. Each subplot corresponds to a frequency band (see subplot title). The vertical axis indicates the task period while the horizontal indicates the respective cortical region.

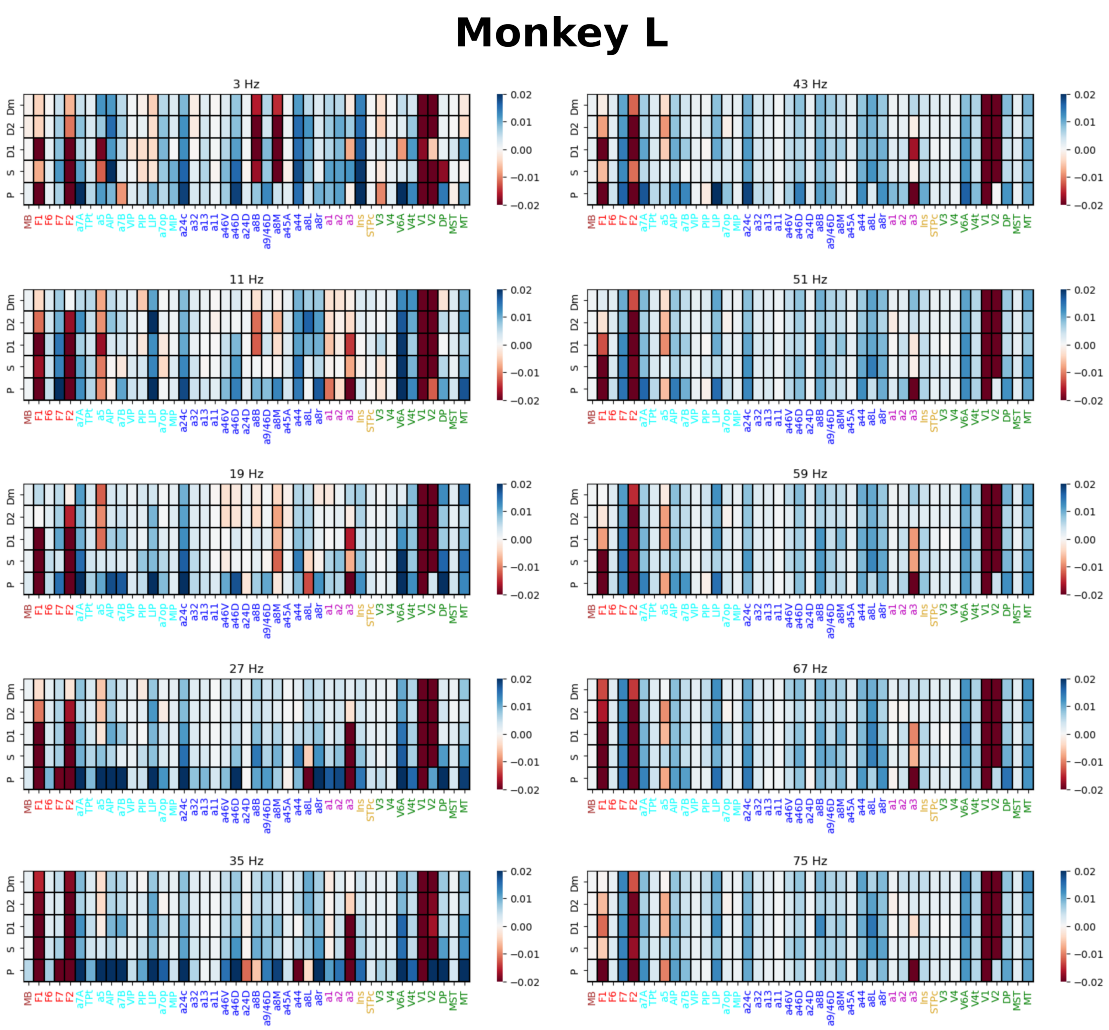

FIGURE 2.17. : Tendency of regions to be sinks or sources in the GPS for monkey L. Each subplot corresponds to a frequency band (see subplot title). The vertical axis indicates the task period while the horizontal indicates the respective cortical region.

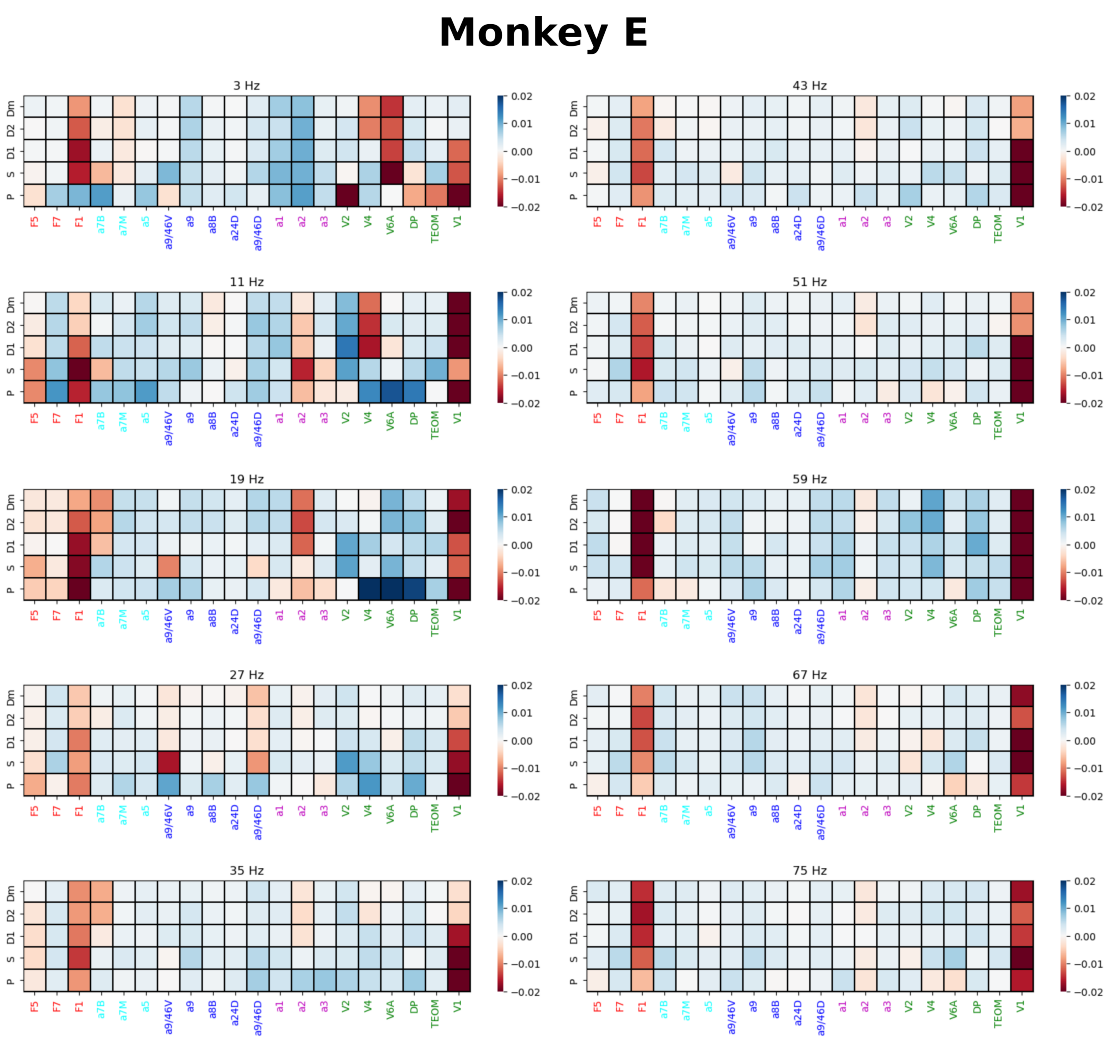

FIGURE 2.18. : Tendency of regions to be sinks or sources in the GPS for monkey E. Each subplot corresponds to a frequency band (see subplot title). The vertical axis indicates the task period while the horizontal indicates the respective cortical region.

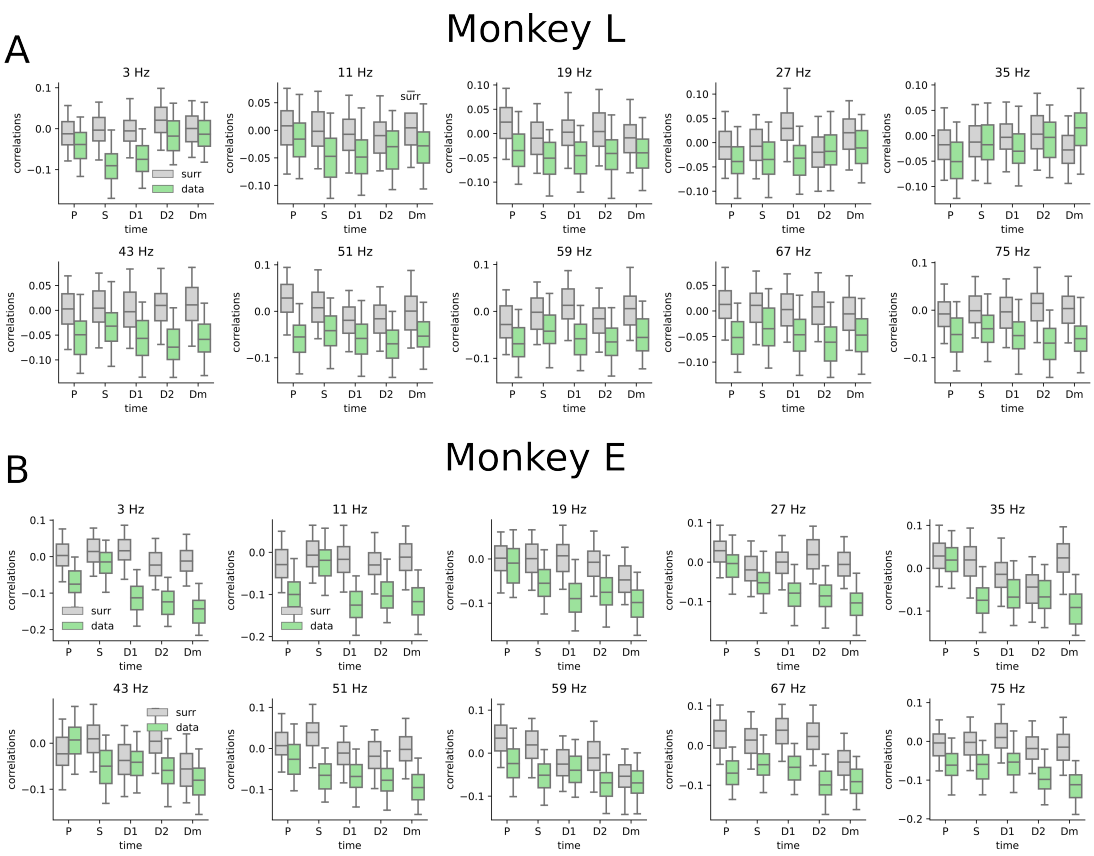

FIGURE 2.19. : Structure-function relation based on the GCS We show the correlations between anatomy and GCS In (A) for monkey L, and in (B) for monkey E. Each subplot corresponds to a frequency band (see subplot title). The vertical axis show the correlation values for each period in the horizontal axis.

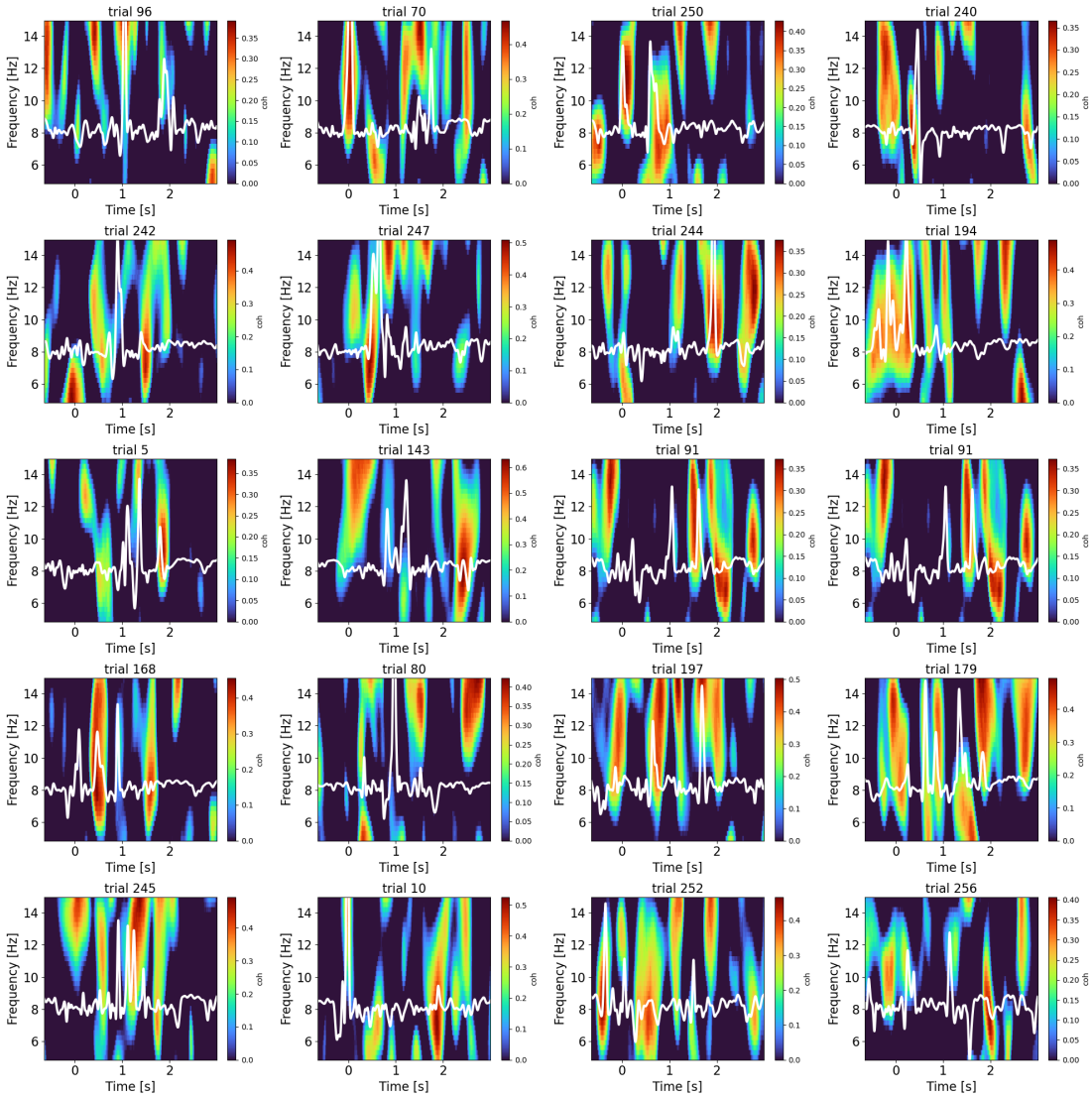

FIGURE 2.20. : Single-trial coherence Example of the single-trial coherence between two channels in area 7A and 8M in the 5 – 15 Hz range, for monkey L. Each subplot corresponds to a single trial. The colormap indicates the coherence values for each frequency (vertical axis) and time (horizontal axis), the white time-series superposed to the map is the instances correlations between the power-times series (in the same frequency range as the coherence). Notice that most coherence "blobs" corresponds to moments of high power co-fluctuations.

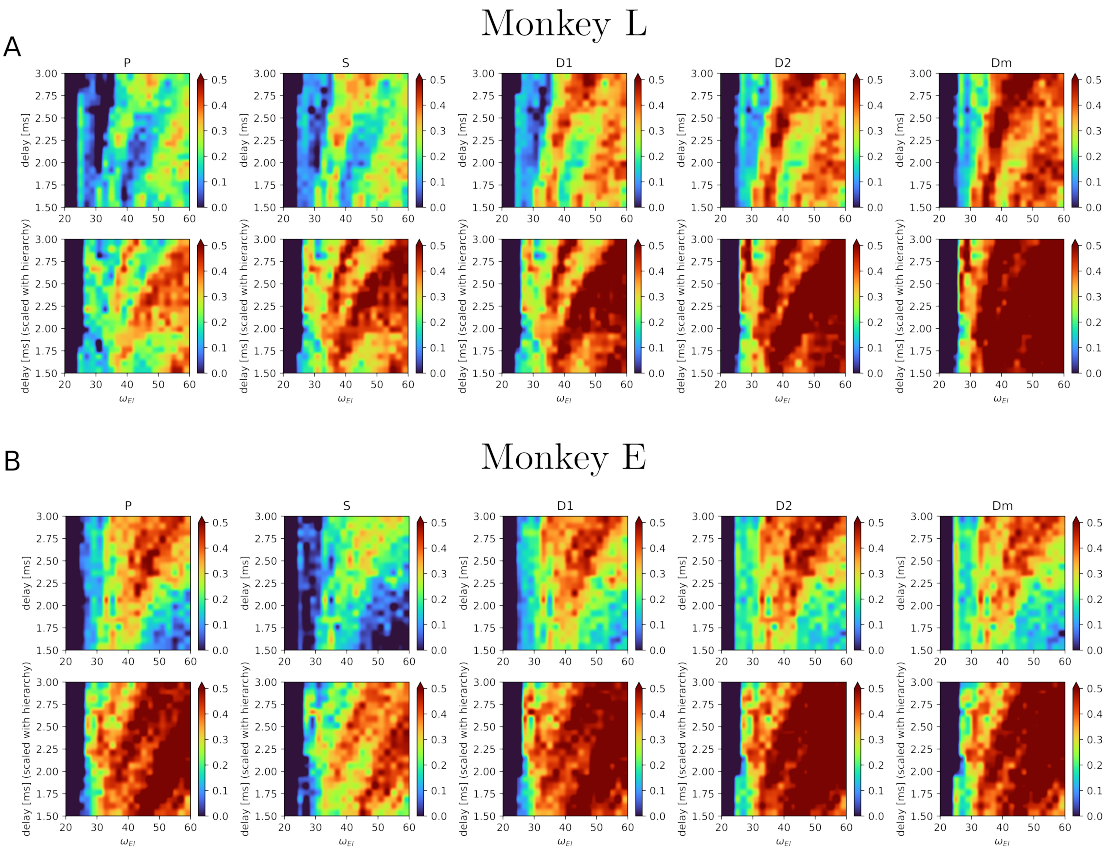

FIGURE 2.21. : Correlation between the simulated and empirical GCS We show the between the simulated and empirical GCS (in the 27 Hz band) correlations as a function of delay (vertical axis), and local inhibitory to excitatory coupling. In (A) for monkey L, and in (B) for monkey E. For each monkey we show the correlations obtained when all regions in the model had the same local delay (top-row) and when the delays were scaled with hierarchy (bottom-row). Each column corresponds to a task period (see titles).

While in the previous chapter we identified that the collective activity of brain areas, in the form of crackle assemblies, offers a set of states in which information can be processed to support working memory processes, we did not formally quantify the exact types of computations carried out by the elements within these crackle assemblies. In this chapter, by using tools from information theory and partial information decomposition, which allow for decomposing dynamics into the "primitives of computation" of storage, transfer, and modification, we aim to show a general framework for achieving this. We used two computational models : one consisting of coupled ring networks in which nodes responded to specific stimulus orientations and stimulus maintenance could be achieved by tuning the networks into a stationary bump regime ; the second model was constructed on top of the macaque connectome, where each node consisted of two mean-field populations : one excitatory and one inhibitory. In this model, an attentive state could be achieved by regulating a mechanism of global balanced amplification, enabling stimuli applied to V1 to propagate better through the cortical hierarchy. Using this model, we were not only able to show that the tools from information theory correctly capture the algorithmic operations reflected in the dynamics but also reveal emergent properties of the studied systems. This work suggests that the neuronal dynamics of single areas and the networks they form implement complex computational operations, and possibly different motifs in this network may carry different coexisting information processing functions. Consequently, it had theoretical consequences that might be important for the first study in this dissertation.

3. DECOMPOSING NEURAL CIRCUIT FUNCTION INTO INFORMATION PROCESSING PRIMITIVES

Authors

Nicole Voges[1,4,*], Vinicius Lima[1,2,*], Johannes Hausmann[5], Andrea Brovelli[1,4], Demian Battaglia[3],

[1]Institut de Neurosciences de La Timone, UMR 7289, CNRS, Université Aix-Marseille, Marseille 13005, France
[2]Aix-Marseille Université, Institut de Neurosciences des Systèmes (INS), UMR 1106, Marseille, France
[3]Institute for Advanced Studies (USIAS), Strasbourg, France
[4]Institute for Language, Communication and the Brain (ILCB), Aix-Marseille Université, Marseille 13005, France
[5]RD Department, Hyland Switzerland Sarl, Corcelles NE 2035, Switzerland [*]shared first authorship.

abstract : It is challenging to measure how specific aspects of coordinated neural dynamics translate into operations of information processing and, ultimately, cognitive functions. An obstacle is that simple circuit mechanisms - such as self-sustained or propagating activity and nonlinear summation of inputs- do not directly give rise to high-level functions. Nevertheless, they already implement the information carried by neural activity. Here, we propose that distinct functions, such as stimulus representation, working memory, or selective attention, stem from different combinations and types of low-level manipulations of information or information processing primitives. To test this hypothesis, we combine approaches from information theory with simulations of multi-scale neural circuits involving interacting brain regions that emulate well-defined cognitive functions. Specifically, we track the information dynamics emergent from patterns of neural dynamics, using quantitative metrics to detect

where and when information is actively buffered, transferred or non linearly merged, as possible modes of low-level processing (storage, transfer and modification). We find that neuronal subsets maintaining representations in working memory or performing attentional gain modulation are signaled by their boosted involvement in operations of information storage or modification, respectively. Thus, information dynamic metrics,beyond detecting which network units participate in cognitive processing, also promise to specify how and when they do it, that is,through which type of primitive computation, a capability that may be exploited for the analysis of experimental recordings.

3.1. Introduction

In a seminal proposal, David Marr observed that a neural system can be described at three different levels. First, the functional level "at which the nature of a computation is expressed". Second, the algorithmic level "at which the algorithms implementing a computation are characterized". Third, the structural level "at which the mechanisms are realized in hardware" (MARR et al. 1976b; see Figure 3.1A for graphical cartoons of these levels). The third level is directly accessible to experimental investigation : the structure of neural circuits (HELMSTAEDTER 2013; MARKOV et al. 2014) and their activity has been measured across different scales with a variety of techniques. Likewise, one can identify the resulting function such as sensory representation, working memory, or selective attention, and measure the associated cognitive and behavioral performance. However, the quantitative definition of the algorithmic level still poses challenges. The assumption is that it comprises information processing operations which are intermediate steps to produce meaningful functional computations.

Various attempts have been made to identify such canonic computations. Some remain closely inspired by the structural level, emphasizing the role of connectivity motifs (CARANDINI et al. 2012; MILLER 2016). Others propose to decompose cognitive processes into simpler constituents shared across multiple functions (TAATGEN 2013; SABAN et al. 2021). Here, we propose to directly track the way in which patterns of neural activity give rise to emergent transformations of information. Information theory provides the tools to quantify the amount of information in a set of observed signals (SHANNON 1948). Beyond that, recent developments in the frameworks of Information Dynamics (LIZIER et al. 2013) and Partial Information Decomposition (PID, WILLIAMS et al. 2010; WIBRAL et al. 2017) permit to assess how such information is propagated and transformed. We define a (non-exhaustive) list of low-level operations –'buffering', 'transferring', 'integrating' – which highlights different ways to handle raw information, defined here as Information Processing Primitives (IPPs; see Figure 3.1B for cartoons of a proposed set of primitive operations). We then present a rich toolset of information-theoretical metrics to quantify the enactment of specific IPPs (see Figure 3.1C for a list of these metrics, matching the IPPs of Figure 3.1B) : we evaluate these metrics on simulated time-series produced during the execution

of tasks probing certain functions, and measure which IPPs are required for their implementation, i.e., an algorithmic decomposition of the task.

The advantage of data simulated with computational models are arbitrarily many trials in fully controlled dynamical conditions without fluctuating brain states (SHINE et al. 2016; GROSSMAN et al. 2019), and a controllable noise level. Our models of choice are neural circuits composed of coupled ring networks. Multi-ring circuits with a known architecture (third Marr's level) can be tailored to implement specific goal function (first Marr's level), so that we can study the IPPs enabled by their dynamics (second Marr's level). Although stylized, they retain important features of cortical connectivity, such as spatial modulation of excitatory-inhibitory recurrent interactions. Ring networks were introduced to study feature-selective representations (BEN-YISHAI et al. 1995) and produce a rich spatiotemporal variety of dynamic patterns (ROXIN et al. 2005; ROXIN et al. 2006). Multiple rings can be coupled to account for interactions between multiple cortical layers, columns (STETTER et al. 2000; BATTAGLIA et al. 2011) or even brain regions. Ardid and collaborators (ARDID et al. 2007; ARDID et al. 2010 a network composed of two coupled rings, representing sensory and frontal cortical modules, to model the attentional modulation of responses to oriented visual stimuli. We capitalize on these studies to perform simulated functions : i) the generation of sensory responses and their maintenance in working memory; ii) the propagation of sensory responses across cortical regions; iii) the selective attentional modulation of these responses as an effect of top-down influences.

To validate our IPP approach beyond generic and ad hoc constrained ring-models, we additionally analyze stimulus-evoked activity in a large-scale, realistic connectome-based model (JOGLEKAR et al. 2018) reproducing some of the circuit mechanisms seen in the ring models (and the associated algorithmic effects). We provide a proof-of-concept demonstrating algorithmic decompositions on controllable dynamics with well-identified functions. We demonstrate that data-driven information-theoretical metrics are suitable to capture IPPs involved in different functions, and to identify which circuit units are participating in specific types of information processing at different spatial positions or times. The proposed framework may thus be suitable for probing the inner workings of actual cognitive processes in electrophysiological or neuroimaging recordings.

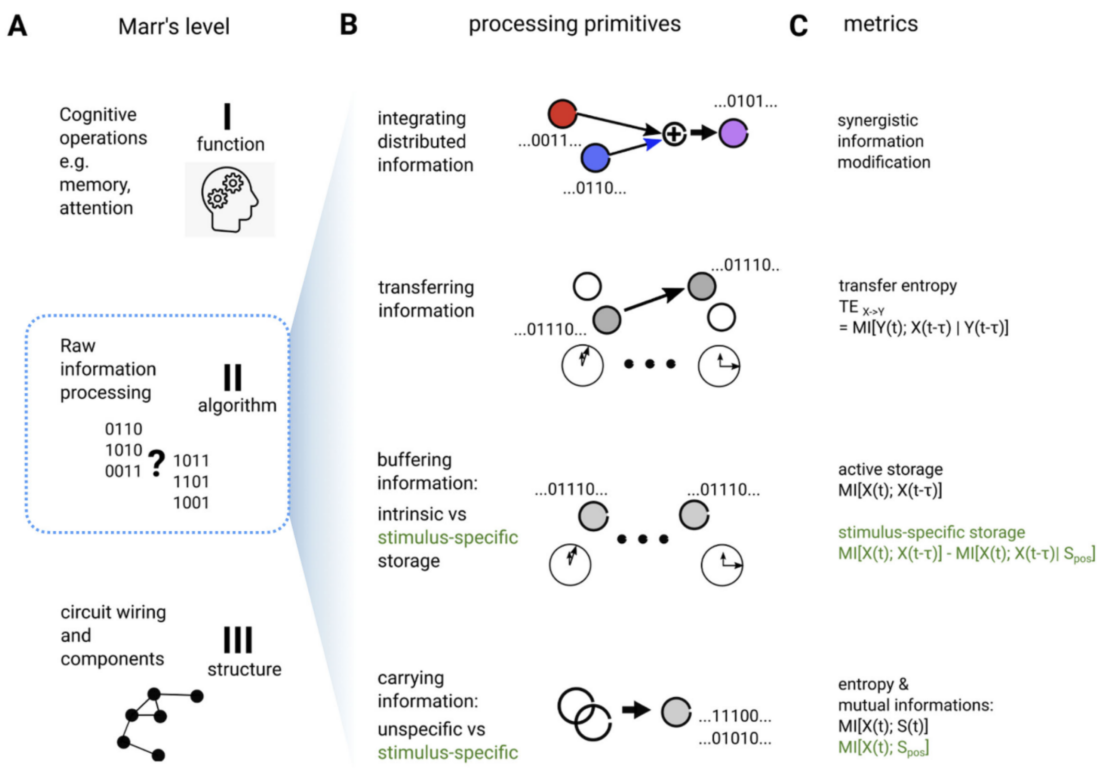

FIGURE 3.1. : Notions of algorithmic level and information processing primitive operations. (A), Neural circuits can be analyzed at three different levels (MARR et al. 1976b), here presented from top to bottom : the high-level function performed by the circuit (i.e., the final cognitive operation, first functional level, top) ; the nature of the circuit components (neuronal types, etc.) and the anatomical wiring between them (third structural level, bottom) ; and the second algorithmic level of the raw information processing, bridging between circuit structure and function (middle). (B), IPPs are elementary algorithmic-level operations performed on streams of information conveyed by neuronal activity, which are involved in building up different functions. IPP's complexity increases from bottom to top. (C), The occurrence of such IPPs can be directly tracked and quantified from neural activity data with the corresponding suitable information-theoretical functionals,the metrics used in this paper.

3.2. Model and methods

We begin with a description of the basic computational model used in this study to reproduce tuned sensory responses, working memory, signal propagation through a hierarchy of areas, and the modulatory effects of selective attention on sensory responses. Then, we specify three setups demonstrating different types of low-level information processing underlying emulated functional computations. Finally, we detail the IPPs (low-level information processing primitives) that characterize different types of basic information transformations. A graphical summary of the IPPs at the functional level and the corresponding metrics is given in Figure 3.1, panels B and C.

All abbreviations are summarized in Table 3.1 and all model parameters for the circuit module presented in Figure 3.2 and the different numerical experiments performed in Figures 3.3-3.5 are specified in Table 3.2. Table 3.3 gives the list of regions included in the large-scale model and Table 3.4 the parameters of the connectome-based simulations.

3.2.1. Computational model of one region : ring network model

The building block of all ring networks studied here is the rate-model version of the one-dimensional ring network with delayed interactions analyzed by Roxin and collaborators (ROXIN et al. 2005; ROXIN et al. 2006), see Figure 3.2A. The one-ring network provides a canonical model for a feature-selective cortical module (e.g., a visual cortex hypercolumn). In ring rate models, the activity of N coupled nodes (also called units) is characterized by their firing rates $R_k(t)$, $k = 0 \dots N-1$. The total input to each node k is a linear combination of the activity of all presynaptic nodes, an external stimulus, and the average value of the external drive I_{ext}, indicated In Table 3.2 is set to have a baseline stationary rate equal to $R_k(t) \approx 0.1$. In addition each node k also receives a noisy component $\eta_k(t)$ drawn independently at every time and for every node from the uniform distribution over the interval $[-0.5, 0.5]$.

Each node may receive additional external input I_{stim} at certain times, associated with the presentation of an external stimulus. Such stimulus current is spatially localized to model the nodes' stimulus selectivity. We choose a Gaussian kernel (cf. Figure 3.2B) of prescribed maximum amplitude A_{stim} and width σ_{stim} , centered at a position $S_{pos} = \theta_{stim}$, which varies across different simulated trials. The stimulus time-course is given by a function $S(t)$, equal to one during stimulus presentation and zero otherwise.

The time evolution of the activity of each node is governed by a first-order delay differential equation with time delay D involving a threshold-linear input-output transfer function $\Phi(x) = x$ if $x > 0$ and $\Phi(x) = 0$ otherwise :

$$\frac{dR_k}{dt} = R_k(t) + \Phi\left(I_{ext} + \eta_k(t) + I_{stim}(k,t) + \sum_{l \neq k} J_{kl} R_l(t-D) \right) \tag{3.1}$$

We consider rings of $N = 100$ nodes, where each node k is labeled by its angular position on the ring $\theta_k = 2\pi k/N$, $k = 0, 1 \dots N-1$, coupled to all other nodes $l \neq k$ through a distance-dependent coupling kernel J_{kl}, depending on the angular distance between nodes,

$$J_{kl} = J_0 + J_1 \cos(\Delta\theta_{kl}), \tag{3.2}$$

with $\Delta\theta_{kl} = 2\pi(k-l)/N$.

for the link between nodes k and l. The coefficients J_0 and J_1 control the spatial modulation and the net sign of interactions (excitatory or inhibitory) between nodes. Figure 3.2C shows an example of a coupling kernel for the parameters $J_0 = 0$ and

$J_1 = 1$, resulting in excitatory short-range interactions with nodes within a range $-\pi/2 \leq \Delta\theta_{kl} \leq \pi/2$, and inhibitory long-range interactions with nodes farther away, i.e. $|\Delta\theta_{kl}| > \pi/2$ ("Mexican hat" profile).

3.2.2. Dynamical regimes of the ring model and properties of stimulus response

The ring network exhibits a rich spectrum of dynamical states, depending on J_0 and J_1. Figure 3.2D (top) shows a schematic phase diagram The model exhibits a stationary fixed-point solution for small coupling values J_0 and J_1, corresponding to an asynchronous regime in which the average firing rate is constant in time and spatially homogeneous in absence of external stimuli (Stationary Uniform regime, SU). When modifying J_0 and J_1, the SU regime loses stability. For large J_0 or J_1 the firing rate of every node explodes toward infinitely large values, as the chosen threshold-linear transfer function does not saturate. When $J_0 < 0$, i.e. on average negative collective interactions, there is a finite range of positive J_1 Mexican-hat modulation, for which the system's activity spontaneously gives rise to localized bumps of activity. These are centered at some stochastically selected angular position (spontaneous symmetry breaking or "Turing instability") and surrounded by silent nodes (Stationary Bump regime, SB). When the average interaction level becomes strongly inhibitory for $J_0 << 0$, the SU regime undergoes a transition ("Hopf instability") to a regime in which the firing rates oscillate homogeneously and in-phase. This Oscillatory Uniform regime, and other possible regimes (such as traveling waves, etc.), are not further explored in this study.

We focus on SU and SB regimes, notably on their responses to externally presented stimuli (Figure 3.2D, bottom). In absence of a stimulus, the activation in the SU regime is uniform throughout the network. Upon stimulus presentation at an angle θ_{stim}, a bump of stronger activity centered on θ_{stim} develops due to the locally increased excitatory drive. This silences the surrounding nodes outside of the bump via lateral inhibition. Such a bump can be seen as a representation of the presented stimulus, as its position along the ring follows the stimulus' angle. Once the stimulus ends, i.e. the additional I_{stim} input goes back to zero, the bumps dissolve and activity relaxes back to uniform (fading encoding, Figure 3.2D bottom left).

The situation is different in the SB regime where a spontaneously generated bump is already present before the stimulus occurs. In SB, the effect of presenting an external oriented stimulus is the displacement of the previously existing bump, moving it to the location corresponding to the stimulus angle θ_{stim}. Once the stimulus is removed, the evoked bump continues to exist, because it is self-sustained by local recurrent excitation. It persists for a certain time (persistent encoding, Figure 3.2D bottom right), before noise may cause it to drift. In the following, we perform simulations at selected working points within the SU and the SB regimes (see Table 3.2 for our parameters). Note that the parameters A_{stim} and σ_{stim} of the stimulus are chosen and tuned in a way that the bump evoked by a stimulus in said SU working-point has similar width and amplitude to the bump arising in the SB working-point, such that the results

obtained from simulations in the two regimes are comparable.

3.2.3. Multi-regional architectures : coupled ring networks

To model circuits involving more cortical modules, we use networks composed of multiple coupled rings. Each ring is modeled as the previously described single-ring architecture with the possibility to tune different rings to different dynamical regimes and working-points. However, an additional current term I_{lr} must be fed to the transfer function Φ of each unit R_k to account for an additional drive provided by the long-range (lr) coupling to nodes in remote rings :

$$I_{lr}(k,t) = \sum_{q \in \text{ remote ring}} W_{qk} R_q(t - D_{lr}) \tag{3.3}$$

where the long-range connectivity kernel is W_{qk} is a Gaussian with amplitude A_{lr} and width σ_{lr} centered on k, thus ensuring a strict spatiotopy of inter-regional excitatory projections. Inter-ring interactions are also delayed and can have an independently tuned, longer delay D_{lr}. We consider two types of multi-ring architectures.

Three-rings network with feed-forward coupling. We study the propagation of a stimulus representation through a hierarchy of different ring modules (Figure 3.4). To emulate the transfer of information from one area to another, we couple three rings as a feed-forward chain (Figure 3.4A), called "3FF rings" setup (cf. Tables 1 and 2). The bottom ring (R1) represents a sensory cortical area which receives subcortical stimulus-related input. The middle ring R2 receives long-range feed-forward input from R1, and the top ring R3 from R2. The couplings from R1 to R2 and R2 to R3 have identical strengths and widths. There is no feedback coupling in order to study the capacity of information-theoretical metrics to capture the processing operation of propagation and transfer through a directed hierarchy.

Reciprocally coupled two-rings network. In a second circuit configuration two regions simultaneously interact via both feed-forward and feed-back connections. The goal is to study the capacity of information-theoretical metrics to track effects of interacting bottom-up and top-down inputs as occurring, e.g., in selective attention (Figure 3.5). In this setup, called 2RC rings (cf. Tables 1 and 2) two rings are reciprocally coupled, similar to the model in ARDID et al. (2007). The bottom ring R1 again constitutes a sensory cortical area, while the top ring R2 represents a prefrontal cortical area. The latter implements working memory, later acting as a source of top-down influences. Parameters of feed-forward and feed-back connections are fine-tuned (see Table 3.2) to obtain attention-like enhancements of stimulus-response.

3.2.4. Task simulations with the ring models

For the one ring configuration of Figure 3.3 , and for the 3FF rings setup of Figure 3.4 , we generate 1000 trials with different noise realizations per each of four possible orientations S_{pos} of the stimulus, thus 4000 trials in total, for both the SU and SB working-points. The stimulus injection center positions S_{pos} are equally spaced along

the ring (at angles 0, $\pi/2$, π and $3\pi/2$), alternating randomly from trial to trial. Time is measured in arbitrary units δt (10 numeric integration steps per δt, fourth-order Runge-Kutta integration scheme, augmented with delay). For all analyses, we drop an initial period of $400\delta t$ to discard early transients. In each simulated trial, we first record $100\delta t$ of baseline dynamics, before injecting a stimulus, which is then maintained for $150\delta t$, i.e. $S(t) = 1$ for $t_{ON} = 100\delta t < t < t_{OFF} = 250\delta^t$, and $S(t) = 0$ otherwise.

For the analyses shown in Figure 3.5 (probing attentional modulation), the task organization is more complex with two stimulus presentations : the first stimulation at position S_{pos} ("cue") starts at $t_{ON} = 110\delta t$ and stops at $t_{OFF} = 310\delta t$; the second stimulation at positions S_{pos2} ("match") starts at $t_{ON2} = 460\delta t$ and stops at $t_{OFF2} = 610\delta t$. The cue position is fixed in all trials at $S_{pos} = \pi$, while S_{pos2} alternates randomly between 0 and 2π, in steps of $2\pi/10$. These stimulus combinations are generated for two different conditions. The first condition is called "attention-OFF" (att-OFF), mimicking empirical experiments in which no attentional modulations are expected (as the receptive field of recorded neurons is not attended to, i.e., the "unattended" condition described by TREUE (2001)). In att-OFF, both the bottom ring R1 and the top ring R2 of the 2RC setup are in SU state, thus bump representations of cue and match stimuli are formed during stimulus presentation and decay thereafter. The second condition is called "attention-ON" (att-ON), mimicking experiments in which attentional modulations of responses are expected (as attention is directed to the receptive-field of the recorded neurons, i.e., the "attended" condition described by TREUE (ibid.) and MAUNSELL et al. (2006). The information that attention must be engaged toward the cue is provided shortly before cue presentation : at time $t_{switch} = 100\delta t$, the top ring R2 is moved from the SU to a SB regime (parameters are detailed in Table 3.2). As a result of attention being "switched on", the top ring R2 maintains a persistent representation of the cue through the entire delay period between the offset of cue at t_{OFF} and the onset of the match stimulus at t_{ON2}. This working memory representation interacts non-linearly with the representation evoked by match in R1. To generate Figure 3.5, we run 5000 trials for each S_{pos} and S_{pos2} combination, in both att-ON and att-OFF condition.

3.2.5. Estimating information-theoretical quantities

We track effects of neural function at the algorithmic level by quantifying how simulated dynamic patterns translate into elementary information transformations. All information-theoretical metrics we introduce to detect the enactment of different Information Processing Primitives (IPPs) can be seen as elaborations of a few basic quantities (COVER et al. 2006). The amount of information carried on average by observations of a random variable X is quantified by Shannon Entropy :

$$H(X) = -\sum_{x \in X} P(x) \log_2 P(X) \tag{3.4}$$

which is a functional of the empirical probabilities $P(X)$ of observing different possible values of the variable X. Conditional entropy quantifies the amount of infor-

mation needed to describe the outcome of a random variable X given that the value of another random variable Y is known, it is defined as

$$H(X|Y) = -\sum_{x\in X, y\in Y} P(x,y)\log_2 P(X|Y) \tag{3.5}$$

The mutual information (MI) between X and Y quantifies the statistical dependence between the two variables and it is defined as the difference between marginal and conditional entropies :

$$MI(X;Y) = H(X) - H(X|Y) = \sum_{x\in X, y\in Y} P(x,y)\log_2 \frac{P(x,y)}{P(x)P(y)} \tag{3.6}$$

It describes the fraction of information, which is shared, i.e., redundantly encoded by both X and Y. The Conditional Mutual Information between X and Y conditioned on a third variable Z is defined as :

$$MI(X;Y|Z) = \sum_{x\in X, y\in Y, z\in Z} P(x,y,z)\log_2 \frac{P(x,y|z)}{P(x|z)P(y|z)} \tag{3.7}$$

providing the average amount of information redundantly carried by X and Y which is not already carried by Z.

A crucial step to evaluate any information-theoretical quantity is the proper estimation of the empirical probability distributions of one or more observables jointly. For most analyses of the results obtained with the (coupled) ring models, we use "plug-in" or "direct" estimators, biased for the small amounts of data typically available in neurophysiological experiments, but converging to stable values for large datasets. We estimate histograms of firing rate variables using 24 equally spaced bins (qualitatively analogous results are obtained using 18 and 32 bins).

For some other analyses (Figure 3.6 and Figure 3.4-1C), estimates are computed using a semi-parametric Gaussian-Copula approach (INCE et al. 2017). The Gaussian-Copula Mutual Information (GCMI) approach exploits the fact that MI is invariant under monotonic transformations of the marginals. This can be exploited to render the joint distribution of variables Gaussian by means of local transformations on the marginals, using the so-called Gaussian copula. It involves calculating the inverse standard normal cumulative density function (CDF) of the empirical CDF of each sample, separately for each input dimension. Then, entropy values can be estimated using a standard covariance-based formula for Gaussian variables. It includes a parametric bias-correction for estimates, an analytic correction to compensate for the bias due to the estimation of the covariance matrix from limited data. GCMI is a robust rank-based approach allowing to detect any type of relation as long as this relation is monotone. GCMI is computed using functions implemented in the Frites Python toolbox (COMBRISSON et al. 2022a; COMBRISSON et al. 2022b). Finally, information-theoretical quantities are normalized by the largest of the entropies of the involved variables (e.g. normalizing $MI(X;Y)$ to $MI(X;Y)/\max(H(X),H(Y))$), so that they are bounded in the unit interval and express relative fractions of information rather than

absolute amounts.

We now present in detail the specific information-theoretical quantities that we use to define and track Information Processing Primitives (IPPs).

3.2.6. Tracking Information Processing Primitives (IPPs)

We focus on a simple set of elementary processes of information manipulation stemming from neural activity. To detect their presence and quantify the degree to which different circuit nodes are engaged at different times along the simulated tasks, we use the above information-theoretical functionals. The simplest possible operation one can perform with information is to carry it. Once a network node carries some information it can keep carrying it actively for an extended time, i.e. it can buffer it; or it can push it to another network node, i.e. transfer it. The most complicated primitive operation we consider is integrating multiple streams of information, i.e. combining information from multiple sources to reveal the existence of information that was inaccessible prior to their combination. Figure 3.1B shows cartoons illustrating these basic IPPs (in ascending order of complexity from bottom to top) and Figure 3.1C lists the associated information-theoretical functionals.

Note that the metrics we use to quantify IPPs have some limitations. For instance, the functional to quantify transfer conflates into the estimated quantity of "transferred" information (in quotes) a part of information conveyed by nonlinear and nonlocal synergies. We comment on several of these limitations and drawbacks later in the Discussion. For now, be aware that through the entire manuscript, terms such as "buffering", "transfer" or "integration" refer to nothing more than the operative definitions provided in the following and may thus not perfectly correspond to other formulations from more elaborate theories.

The IPP of carrying information or local encoding of information : Entropy and Mutual Information

The average information carried by a network node at time t is given by the functional $H(R(t))$, where the across-trials firing rate $R(t)$ (sampled at time t) is used to estimate the probability distribution $P(R(t))$. One can also evaluate the fraction of the information carried relative to the presented stimulus, either by considering stimulus presence or absence $MI(R(t);S(t))$, where $S(t)$ is the spatially inhomogeneous stimulus time-course, or the feature carried by the stimulus, $MI(R(t);S_{pos})$, where S_{pos} is the stimulus' orientation angle. Both mutual information terms are then normalized by $H(R(t))$ to be expressed in relative form.

The IPP of buffering information : Active Information Storage

A circuit node buffering information continues carrying some information which was already present. This primitive processing operation can be quantified by Active Information Storage (LIZIER 2012; WIBRAL et al. 2014). In its simplest manifestation, it corresponds to the mutual information between past and present activity,

$MI(R(t);R(t-\tau))$, where τ is an adjustable latency, set to $\tau = 40\delta t$, unless otherwise specified.

Additionally, one may evaluate the fraction of information about the orientation of the stimulus presented in a trial actively buffered by a node. The resulting stimulus-specific active storage is given by : $MI(R(t);R(t-\tau)) - MI(R(t);R(t-\tau)|S_{pos})$, i.e., the totally stored information minus the part of this stored information which does not depend on the stimulus orientation. This corresponds to the so-called co-information, or negative Interaction Information, between three variables $R(t)$, $R(t-\tau)$ and S_{pos} (McGill 1954; Ince et al. 2017). Note that co- and interaction information may be negative when there are synergistic interactions involved (see Discussion). However, in our simulations, we always obtain positive values - indicating that the correlation between rates $R(t)$ and $R(t-\tau)$ is indeed mostly accounted for by redundant information about S_{pos}.

Finally, in all cases, storage measures are also normalized by $H(R(t-\tau))$ to make them relative.

The IPP of transferring information : Transfer Entropy

Information transfer between neural populations can be estimated from the statistical dependencies between neural signals (Bressler et al. 2011; Brovelli et al. 2004; Seth et al. 2015) using model-free methods relying on the Wiener-Granger principle (Wiener 1956; Granger 1969). It identifies information transfer between time series when future values of a given signal can be predicted from the past values of another signal, above and beyond what can be achieved from its autocorrelation. A general information-theoretic measure to detect directed information transfer according to the Wiener-Granger principle is Transfer Entropy (Schreiber 2000), it captures any (linear and nonlinear) time-lagged conditional dependence between neural signals (Besserve et al. 2015; Vicente et al. 2011). We note again that the "transfer" captured by Transfer Entropy conflates synergistic information atoms and is thus not the most exclusive definition of transfer that may be possible (see Discussion). We nevertheless favor it here for its simplicity and clarity. Transfer Entropy from X to Y is defined as the conditional mutual information between the past of the X and the present of Y, conditioned on the past of Y

$$TE_{X\to Y} = MI(Y(t);X(t-\tau)|Y(t-\tau)) \tag{3.8}$$

Note that Transfer Entropy is asymmetric, i.e., $TE_{X\to Y} \neq TE_{Y\to X}$, thus a suitable measure for directed functional connectivity (Battaglia et al. 2012; Palmigiano et al. 2017). We compute two types of transfer entropy. First, active transfer from stimulus time-course to response rate $TE_{S\imath R}(t) = MI(R(t);S(t-\tau)|R(t-\tau))$ in the one ring configuration. Second, active transfer between the activities $R1_k$ of node k in ring 1 and $R2_k$ of another homologous node (with identical angular coordinate) located in a second ring $TE_{R1,k\to R2,k}(t) = MI(R2_k(t);R1_k(t-\tau)|R2k(t-\tau))$ in the 3FF rings setup (Figure 3.4). For comparison (and assessment of numerical estimation artifacts), we also compute the backward terms $TE_{R\imath S}(t)$ and $TE_{R2\imath R1,k}(t)$ that should be zero by

construction since there are no feedback couplings. Again, TE is normalized by the entropy of the source variable. For the 3FF rings setup in SB state, we additionally calculate $TE_{RN,k\imath RN+1,k}(t)$ and $TE_{RN+1,k\imath RN,k}(t)$, with $N = 1,2$ the ring number, using multiple delays ($dt = 5,10,15,...40\delta t$) simultaneously without entropy normalization. For this analysis, we use the GCMI approach implemented in the Frites Python toolbox (see the Methods subsection on downloadable codes).

The IPP of integrating information : Synergistic Modification

A third type of primitive processing operation can arise when two input sources X_1 and X_2 interact and communicate with a common target Y. Synergy may emerge, where extra information is conveyed by the interaction between the sources. This implies that the combined inputs X_1 and X_2 provide surplus information with respect to the inputs considered separately (BRENNER et al. 2000; LATHAM et al. 2005). The process of extracting this surplus information –performed by the output node Y– has been called synergistic modification (LIZIER et al. 2013; LIZIER et al. 2018).

Our two source variables are the firing rate of a node in one ring and a stimulus position (X_1 and X_2), while the target variable is the firing rate of a node in a second ring (Y). We suggest that a primitive processing operation is the extraction of synergistic information by the target node. To do so, we exploit a formalism that allows the decomposition of multivariate mutual information between a system of predictors and a target variable. It quantifies the information that several predictors provide uniquely, redundantly or synergistically about a target variable, the so-called Partial Information Decomposition (PID, WILLIAMS et al. 2010). The PID formalism can be outlined using the information Venn diagram (Figure 3.5E). The total information that the output Y carries about the pair of inputs (X_1, X_2) consists of unique, redundant, and synergistic parts. The information Y shares with X_1, but not with X_2 is denoted as $MI(Y;X_1\ X_2)$, and, conversely, the other unique information term as $MI(Y;X_2\ X_1)$. The redundant part is the information shared by both X_1 and X_2 , denoted $MI(Y;X_1 \cap X_2)$. The remaining part is thus synergy whose amount can be determined by subtracting the non-synergistic fractions from the total amount of information $MI(Y;(X_1,X_2))$ that Y carries about the pair of inputs. However, these quantities cannot be estimated directly. We operate under the so-called minimum mutual information (MMI) ansatz, which has been shown to provide correct estimations for Gaussian systems (BARRETT 2015; LUPPI et al. 2022). According to MMI, redundant information can be computed as the minimum of the information provided by each individual source to the target (i.e., an upper bound estimation : one input is supposed not to carry any unique information)

$$Red := \min\{MI(X_1;Y), MI(X_2;Y)\} \tag{3.9}$$

Then, the synergistic information can be computed by subtracting the mutual information of the single source variables from the total information. Each of the individual $MI(X_1;Y)$ and $MI(X_2;Y)$ terms is the sum of unique contributions from the considered variable and the redundant fraction. Thus, when subtracting these

terms from the total $MI(X_1, X_2; Y)$ we subtract redundancy twice, so we have to "add back" one Red term (in order to subtract it only once, as we should). Therefore, with some simple algebra (see the Venn diagram of Figure 3.5E), we can write :

$$Syn = MI(X_1, X_2; Y) - MI(X_1; Y) - MI(X_2; Y) + Red \tag{3.10}$$

The two equations represent the redundant and synergistic information carried by the co-modulations in firing rate X_1 and input-related variable X_2 about the target node Y, respectively. Once again, this metric is normalized by an entropy term, here the one of the target output Y, to evaluate the synergistic fraction of the total output information flow.

3.2.7. Large-scale connectome-based model

Model implementation

To go beyond generic models of interacting areas, we also re-implemented a large-scale model of cortical activity previously published by JOGLEKAR et al. (2018). It consists of 29 cortical areas (see list in Table 3.3) whose local activity is modeled with simple neural mass equations, i.e., population dynamics are represented as firing rates. Each local circuit is composed of an excitatory (E) and an inhibitory (I) population with the corresponding EI, IE, EE and II couplings (Figure 3.6B, top row). Every region is driven by a baseline current term (representing ongoing background activity). In addition, transient sensory stimulation can be implemented via additional local activity injection (see later).

All areas are reciprocally coupled to each other according to a connectivity matrix derived from systematic tracer experiments in non-human primates (MARKOV et al. 2014; see Figure 3.6A, left). Such a directed and weighted connectome defines the strength of the input each region receives from all other cortical areas and is given by the fraction of neurons labeled by the tracer (FLN) in a given source area, normalized by the total number of labeled neurons over cortical regions. The inter-areal long-range connections are purely excitatory. Different from the original model (Joglekar et al. 2018), we add transmission delays between areas in the model, which have also been estimated empirically (ibid.). They rely on the (physical) distance between areas (Figure 3.6A, right), which is converted to propagation delays by assuming a propagation speed of 3.5 m/s. Cortical areas are ordered according to their hierarchical level (ibid.). Following JOGLEKAR et al. (2018), the local circuits in higher-order regions are endowed with stronger excitability and correspondingly longer time-constants.

The "bow-tie" architecture of the connectome (MARKOV et al. 2013; MARKOV et al. 2014) introduces a barrier to the free propagation of externally injected stimuli. Mimicking a visual stimulus presentation, Figure 3.6B (bottom row) shows the rate dynamics for a brief transient input injection to area V1, which leads to a very limited propagation along the visual stream. To enable a dynamical regime with enhanced signal propagation, JOGLEKAR et al. (2018) introduces a Global Balanced Amplification (GBA) mechanism in which long-range excitatory connectivity is strengthened,

while simultaneously strengthening the local inhibition (IE connections) within each region, see Figure 3.6B (top row). In the weak GBA regime (left), the stimulus-related activity volley remains local while it reaches higher order regions due to the facilitated propagation in the strong GBA regime (right). The increased amount of excitation is controlled by a modified inhibitory-to-excitatory balance. In this manuscript, we use these weak and strong GBA regimes as equivalent, respectively, to the "attend OFF" and "ON" scenarios defined for the coupled ring models.

All parameters for model simulations are listed in Table 3.4. Full detail about our JOGLEKAR et al. (2018) model reimplementation can be found at the address : github.com/ViniciusLima94/ReScience-Joglekar. Our published reproduction of the model is inserted annexed to this dissertation in Appendix A.

Stimulus presentation and IPP analyses

To investigate the information processing in the large-scale model, we apply a brief stimulus injection of 0.5 ms to the excitatory population in area V1, in the weak and strong GBA regime. Note that for the large-scale model, in contrast to the ring model simulations, there is no stimulus orientation. The stimulation tag S (S_{pos} for the ring models) merely represents the presence or absence of the stimulus. Here, we analyze the IPPs of "buffering", information transfer, synergistic integration and stimulus-specific storage using the metrics described above. Note that all analyses are based on the GCMI approach as implemented in the Frites Python toolbox (COMBRISSON et al. 2022b; see Appendix B of this dissertation for the reference publication of the toolbox). In the Frites implementation latency-dependent functionals as AIS and TE are computed for all latencies τ until a maximum latency and then averaged over this range of τ's (as we did already in supporting analyses of the 3FF ring configuration).

Active Information Storage (AIS) is computed as $MI(R_n(t); R_n(t-\tau))$ with a maximum latency τ of 40 ms where R_n represents the firing rates of the cortical areas $n = 1 \dots N$. In addition, the stimulus-specific AIS is calculated as $MI(R_n(t); R_n(t-\tau)) - MI(R_n(t); R_n(t-\tau)|S)$, with S indicating stimulus presence or absence. Transfer Entropy from V1 to all other areas is computed as $TE_{V1 \to N} = MI(R_n(t); R_{V1}(t-\tau)|R_n(t-\tau))$ with R_{V1} representing the rate in V1 and $n = 1 \dots N-1$ indexing all other areas. Likewise, we calculate the backward transfer $TE_{N \to V1} = MI(R_{V1}(t); R_n(t-\tau)|R_{V1}(t-\tau))$ from all other areas to V1. Finally, we compute the synergistic information encoded by V1 ($R_{V1}(t)$), emerging from the integration of stimulus-related (bottom-up) input S and the feedback (top-down) signals $R_n(t)$ from other cortical areas as $Syn = MI(R_n(t), S; R_{V1}(t)) - MI(R_n(t); R_{V1}(t)) - MI(S; R_{V1}(t)) + Red$. To additionally investigate the relation between timing and distance, we calculate the peak latency (time of the synergy peak - time of the rate $R_n(t)$ peaks) and correlate it to the distance of all areas to V1. Using this model, we simulated 1000 trials with stimulation and 1000 without stimulation, each in the weak and strong GBA regimes, respectively, amounting to a total of 4000 trials. The total simulation time is seven seconds, the initial four seconds are discarded. Stimulus onset occurs at $t = 4.5$ seconds with a duration of 500 ms. The strength of the stimulus applied to V1 is 42 pA and 22 pA

for weak and strong GBA, respectively. The model is implemented using the NEST simulator toolbox for Python (EPPLER et al. 2009).

3.3. Results

3.3.1. Two dynamic regimes of response to stimulus

As presented in detail in the Models and Methods section, we model a stimulus-selective cortical region as a ring network with a "Mexican-hat" connectivity profile (Figure 3.2C), i.e., more excitatory interactions with units (also called nodes) at nearby positions along the ring and more inhibitory with nodes farther away. In our ring model, the activity of coupled network units is characterized by their noisy firing rates. The corresponding phase diagram, i.e., its parameter-dependent dynamical regimes, is shown in Figure 3.2D. We measure simulated responses to stimulus presentations (emulating specific tasks) in two different regimes : a stationary uniform (SU) and a stationary bump (SB) dynamic working-point (Figure 3.2D, bottom).

The simplest possible task entails (correctly) responding to the presentation of stimuli with different orientations/angles S_{pos} in different trials. Each stimulus is spatially localized, yielding a stimulus selectivity of different units, and can be transiently presented at any chosen time. We show simulated recordings of the activity of units in a single receiving region in Figure 3.3A. The firing rates measured in six exemplary trials are shown in Figure 3.3B, three operating in the SU regime (top) and three in the SB regime (bottom). For each of the trials, we show spatial maps of activity, where the horizontal axis represents time, the vertical axis different units along the ring-network, and the firing rate is color coded. The curves below the spatial maps show the corresponding firing rates for all units over time. We highlight in color the time-series of units located at specific positions (indicated by matching-color lines on the corresponding spatial maps). As anticipated, we observe a clear distinction between responses in the SU and SB dynamic working-points. In the SU regime, a localized stimulus injection generates a bump-like pattern of increased activity around the injection center (red lines and curves) which disappears soon after the stimulus is switched off. The firing rates of units outside a neighborhood of the injection are either unaffected (blue trace in SU trial $\#n$ & trial $\#j$) or, at larger distances from the injection site, decrease due to the increased lateral inhibition exerted by active units inside the bump (blue trace in trial $\#k$). In contrast, in the SB regime, bumps of increased activity develop spontaneously, at random positions along the ring, even without any stimulation. Upon stimulation, the bump's position shifts towards the injection site, its amplitude increases, and it remains stable until the end of the stimulus. After stimulus removal, the bump amplitude relaxes back to its initial value, but position remains stable around the injection site.

These two configurations correspond to distinct functional behaviors : in SU, stimuli are only transiently represented. In contrast, in SB, a sustained activation is observed, supporting the maintenance in working memory of the presented stimulus after its removal. The two IPPs associated with these two simple functional behaviors are

"carrying" and "buffering" information, respectively (cf. Figure 3.1B, top two cartoons). They can be tracked by different information-theoretical metrics. We focus first on the "carrying" IPP and address the "buffering" IPP in the next section.

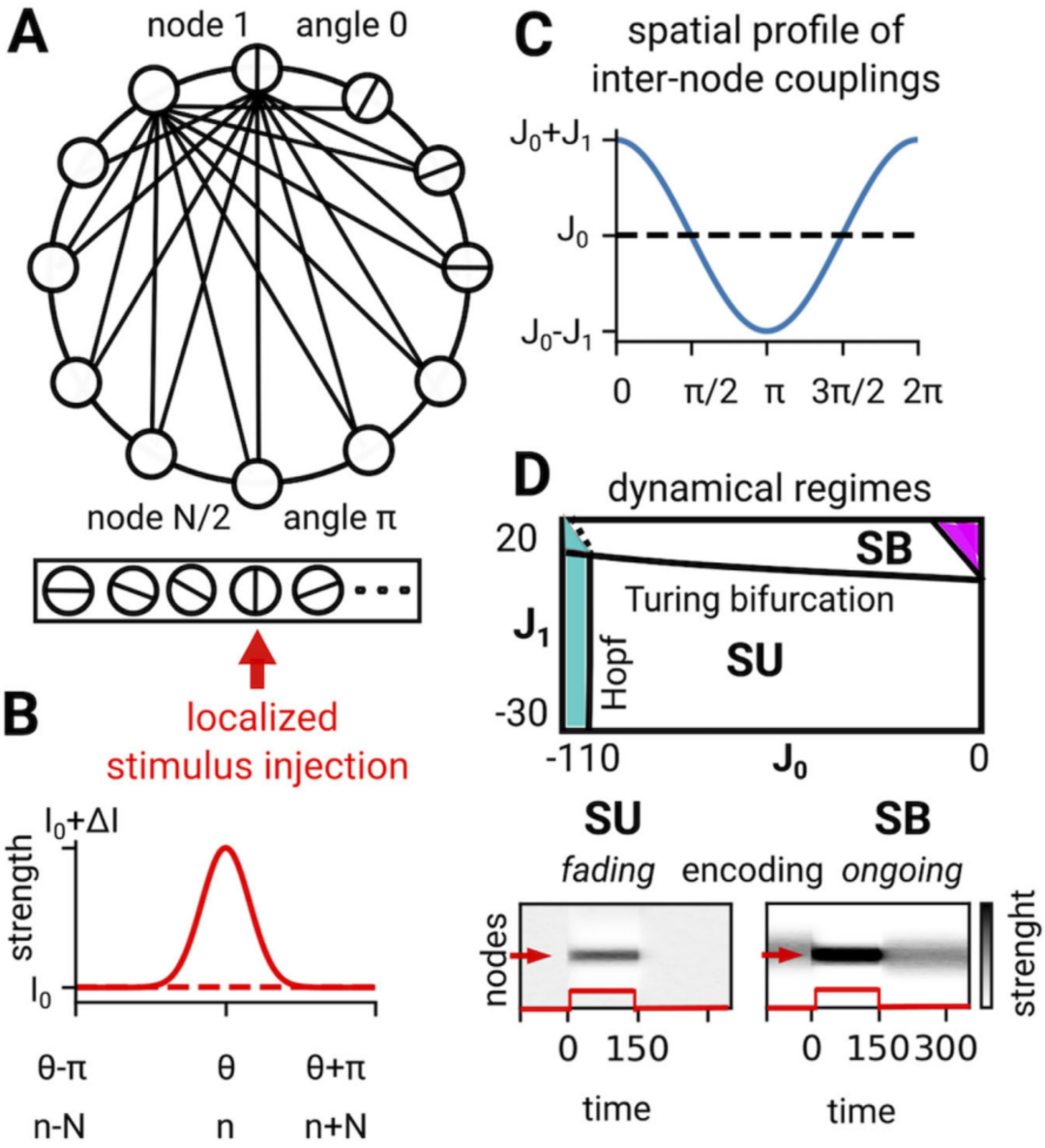

FIGURE 3.2. : Dynamical states of the ring model of one cortical region. (A), Ring model to emulate information encoding and storage : circles represent feature-specific neuronal nodes,parametrized by an angle coordinate θ along the ring, indicating the preferred stimulus direction (denoted by differently oriented lines within the circles) ; connecting edges indicate internal all-to-all structural couplings, whose weights depend on the distance between the coupled network nodes (compare (C)). The rectangle below the ring indicates that stimulus-related inputs are injected in a localized fashion to network nodes with a specific stimulus direction preference (indicated by a red arrow), following (C), a narrowly tuned Gaussian spatial profile. (C), Example profile of spatial modulation for internal ring couplings, here with a "Mexican hat" shape for parameters $J_0 = 0$ and $J_1 = 1$ (see Methods). (D), Top : phase diagram reporting different dynamical regimes obtained for different coupling parameter values.Bottom : spatial maps (nodes vs time) for the two dynamical regimes explored in this study : SU activity with transient, stimulus-induced bumps of activity and SB activity with an ongoing, self-sustained bump, persisting after stimulus offset.

3.3.2. IPP analysis can track the representation of a stimulus

In Figure 3.3C (top), we show the amount of total information that a ring unit carries as a function of time, averaged across all units and trials, provided by the entropy $H(R(t))$ of the activity rates $R(t)$ as they change in response to stimulus presentation. Average entropy of activity differs between the SU and SB regimes. In SU, entropy is rather low in the absence of stimulus, due to the temporal and spatial homogeneity of baseline firing rates, fluctuating only due to a weak background noise. Entropy increases during stimulus presentation, as stimulus-evoked bumps emerge and produce differences in response rates for different stimulus positions, increasing inter-trial variance. In contrast, in SB, entropy is higher before stimulation, because of the stochasticity of the spontaneously emergent bump positions. In our simulated experiments, stimuli are presented at four discrete possible positions (a configuration often met in empirical experiments). Therefore, upon stimulation, the bump positions are quenched to only four pronounced maxima (cf. spatial maps in Figure 3.7A), resulting in a strong entropy reduction with respect to baseline. Entropy rises again after stimulus removal, as firing rates are reduced and noisy fluctuations more evident. For both the SU and SB regimes, we furthermore observe tiny peaks and kinks of the entropy time-courses in correspondence with stimulus onset and offset at times t_{ON} and t_{OFF}. These variations can be explained by the non-instantaneous response of the system to instantaneous inputs, causing fast transient dynamics (like impulse responses) to occur shortly after stimulus onset and offset (so that inter-trial variance is temporarily increased during these transients).

This simple analysis illustrates how strongly the values of information-theoretical quantities depend on aspects of the neural recordings, such as signal-to-noise ratio and actual task design, which have little to do with algorithmic-level operations. Entropy is an upper-bound to other metrics, e.g., Mutual Information (MI) which quantifies the statistical dependence between two or more variables. Entropy variations could result in absolute MI variations, which simply reflect changes of the available informational bandwidth. For the study of primitive processing operations, we thus focus on relative metrics which are normalized by entropy. We therefore do not have to account for the additional complexity of total entropy fluctuations unrelated to the processing probed.

We show the relative amount of information that a unit's activity carries about the stimulus, disentangling two of its aspects : the stimulus time-course $S(t)$, i.e. its presence/absence at specific times t and the orientation S_{pos} of the stimulus, which is a trial-specific property (changed every trial, see Models and Methods). This fraction of information is captured by the entropy-normalized mutual information between firing rate $R(t)$ and stimulus time-course $S(t)$ ($MI(R(t);S(t))$ in Figure 3.3C, middle; or stimulus orientation label S_{pos} ($MI(R(t);S_{pos})$ in Figure 3.3C, bottom; and Figure 3.7B-C for the corresponding spatially resolved maps). Before stimulus presentation no information about the stimulus can be extracted from the neural activity, since the baseline noise entropy is unrelated to the stimulus. In contrast, during stimulus presentation, activity is modulated in dependence of stimulus position (i.e., the distance between

S_{pos} and the angle of the recorded unit).

The information about the stimulus-related time-course $S(t)$ becomes positive during stimulus presentation, in both the SU and SB regimes, saturating to a higher value in SU (Figure 3.3C, middle), as the evoked bump activity configuration differs strongly from the homogeneous baseline. During stimulus presentation, some units develop much lower or higher firing rates than in spontaneous conditions, thus, signatures of stimulus presence. No $S(t)$-related information exists before or after stimulus presentation. Similarly, mutual information with stimulus position S_{pos} (Figure 3.3C, bottom) is absent before stimulus presentations and saturates to a plateau shortly after stimulus onset. It is higher for the SB than the SU regime, as SB provides a larger dynamic range of responses and sharpened bumps. Stimulus encoding is slightly delayed in SB, since the re-arrangement of the bump positions is not as fast as the sudden, stimulus-evoked bump in SU. In the SU regime, all stimulus-related information vanishes shortly after stimulus offset. In contrast to SU, information about stimulus position remains present after stimulus offset in the SB regime, as the stimulus-evoked bump self-sustains itself in its (new) position. It may slowly drift away under the influence of background noise over timescales longer than the observation window considered here.

Figure 3.7B-C show that spatial maps of Mutual Information not only depend on time, but also on spatial location. Stripes are clearly visible in these "Infogram surfaces", because our design comprises only a discrete number of possible stimulus orientations (Figure 3.7A). Encoding of stimulus features is in general stronger in the bump centers as these locations have a larger dynamic range.

In summary, the normalized MI of firing rate with stimulus provides an interpretable marker of the IPP of "carrying" stimulus (un-)specific information.

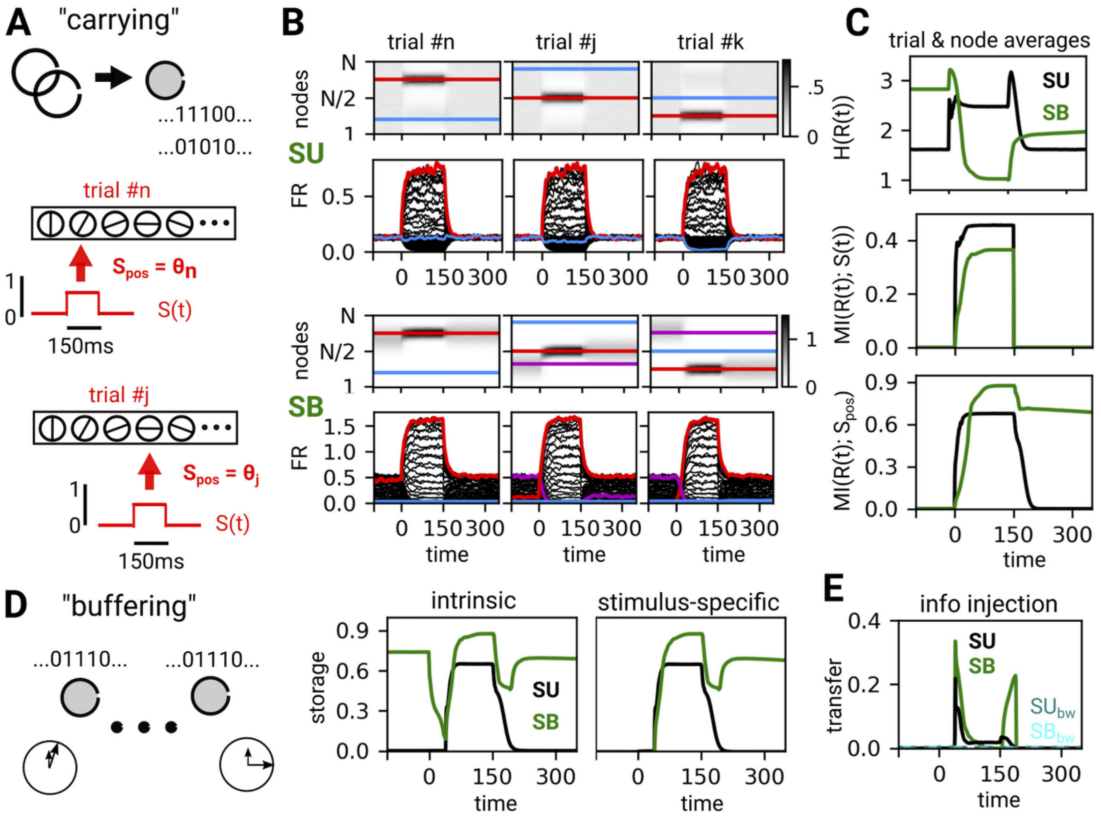

FIGURE 3.3. : Information encoding and storage in a single-region circuit. (A), To track the simplest possible IPP of information "carrying", we simulate different trials in which stimuli with different directions θ are presented for a short, fixed time of 150 ms (as indicated by the stimulus-related input time course $S(t)$). The direction S_{pos} of the presented stimulus is denoted by a red arrow as in Figure 3.1A. (B), Spatial maps (top row, units vs time) and single-trial firing rate traces (bottom row) of neuronal activity in a one-ring network, in the SU and SB dynamical regimes. Red lines indicate traces for nodes located at the stimulus center, blue lines nodes far from it, and magenta lines indicate the initial bump position for the SB regime (SB trial $\#n$: red covers magenta line). (C), Time courses of entropy (top row) and stimulus-related MI averaged over nodes and trials (normalized by entropy), for SU (black) and SB (green lines) regimes. Middle and bottom rows : stimulus presence and orientation (stimulus-specific) are transiently encoded by activity in both SU and SB regimes, as revealed by the MI between rates and, respectively, $S(t)$ and S_{pos}. (D), Moving to the IPP of "buffering", we quantify and show time courses of AIS (intrinsic and stimulus-specific) in both the SU and SB regimes averaged over nodes and trials. Stimulus-specific storage persists after stimulus offset in SB, denoting working memory implementation. (E), Time courses of information transfer from injected stimulus to rates, quantified by TE. Light and dark cyan lines indicate (negligible) backward transfer from rate to stimulus. See also Figure 3.7

3.3.3. IPP analysis can track the loading and maintenance of a representation in working memory

We are able to detect that the post-stimulus activity in the SB regime still "carries" stimulus position information. Through which primitive processing operations can this representation be held in working memory? Answering this question requires turning to Information Dynamics metrics, such as Active Information Storage (AIS, see Methods), which quantifies the fraction of the information carried by a node's activity at a time t that was already carried at an earlier time t–τ, i.e., $MI(R(t);R(t-\tau))$, with delay $\tau = 40\delta t$. Plain AIS tracks the time-lagged maintenance of information by neural activity, irrespective of the origin of this information (stimulus-related or intrinsically given). The process through which this fraction of information is maintained corresponds to the IPP of "buffering" (cf. second cartoon from top in Figure 3.1B and Figure 3.3D, left). Note that we focus on buffering by one node only (as we did with "carrying"). Strictly speaking, however, information about stimulus may be carried (redundantly and/or cooperatively) by more than one node simultaneously. Accounting for these more complex scenarios would require using more advanced metrics of storage that discriminate storage of redundant vs synergistic information (see Discussion), which we do not consider here, for the sake of simplicity.

Figure 3.3D shows averaged time-traces of Active Information Storage computed with the ring model in Figs. 3A–C. In the SU regime, AIS is positive only during stimulus presentation. It relaxes back to zero after stimulus offset as the stimulus-evoked bumps dissolve back to homogeneous baseline activation. In the baseline pre- and post-stimulus presence, all entropy is due to spatially and temporally uncorrelated noise, which is by construction memory-less, thus resulting in null Active Storage.

The situation is different in the SB regime, in which (spontaneous) bump formation is associated with Active Storage and thus positive at baseline and after stimulus offset. However, AIS drops at stimulus onset and offset. These events induce changes of activity that cannot be predicted based on prior intrinsic activity and hence convey information which is not the outcome of "buffering" but must come from outside the system. This information injection is captured by another information-theoretical metric, Transfer Entropy $TE_{S\to R}(t)$ from stimulus to rate (see Methods), tracking the complementary IPP of "transferring". In general, Transfer Entropy TE identifies the information flow between time series when a given signal Y is influenced by another signal X. It is defined as the conditional mutual information between the present of Y and the past of X, conditioned on (i.e., factoring out) the past of Y. As shown in Figure 3.3E, the TE peaks match the drops in AIS visible in the middle of Figure 3.3D. At stimulus onset, network nodes modify their algorithmic role, reducing their implication in the IPP of "buffering" and becoming the recipients of information conveyed by the IPP of "transferring". Transfer of information from stimulus to activity occurs also at stimulus offset, when a new information injection indicated by a second peak in TE encodes a release command to either produce bump dispersion (in SU), or a decrease in firing rate together with re-adjustments of the bump shapes (in SB). See also Figure 3.7D for detailed spatial maps showing the nodes that are most strongly

affected by externally injected information at different times.

The information buffered at baseline in the SB regime cannot yet be stimulus specific as the stimulus has not yet been presented (the positions of spontaneously generated bumps in SB are random). To formalize this intuition, we quantify the fraction of information about the stimulus stored by the network nodes, i.e., the stimulus-specific active storage. It is the totally stored information minus the part which does not depend on the presented stimulus orientation. (see Methods). The averaged time course of stimulus-specific active storage is shown in the rightmost subpanel of Figure 3.3D. Its trace correctly captures that there is no stimulus-specific information buffering prior to stimulus presentation, while it displays a transient increase after stimulus presentation, for SB also during the post-stimulus period. Stimulus-specific Active Storage thus provides a valid metric to track the active maintenance of information relative to a presented stimulus.

In this single-ring example, the dynamics of "carrying" and "buffering" stimulus-related information are very similar, because all information "carried" by a node exists as a form of "buffering" well after stimulus onset and offset. However, they are not completely identical. In SB, the rebound after stimulus offset in the curve for buffering is the most obvious difference to the carrying curve. It reflects the fact that some of the transient variations in "carrying" are due to "transfer" (cf. Figure 3.3E). In general, compared to the IPP of carrying, buffering is always delayed, since only information already carried by the system can be buffered.

At the functional level, such stimulus-specific maintenance marks the implementation of working memory. At the algorithmic level, our IPP analyses allow a decomposition of working memory : it arises via the loading of stimulus-specific information –through the IPP of "transferring"– into the system's units. By virtue of their collective dynamics, these units are intrinsically devoted to the IPP of "buffering". This algorithmic decomposition provides not only a narrative of how a system's dynamics translates into a function, but also yields a quantitative characterization : suitable information-theoretical metrics –AIS for "buffering" and TE for "transferring"– provide a precise evaluation of when, where, and how distinct IPPs are performed.

3.3.4. IPP analysis can track the propagation of representations through a multi-regional hierarchy

We now tackle the algorithmic decomposition of the function of activity propagation. As detailed in Models and Methods, we simulated a feed-forward chain of three ring modules, representing three hierarchically ordered regions (e.g. V1, V2 and above, see Figure 3.4A, bottom). The bottom ring R1 represents a sensory cortical area. It receives an input stimulus, which is sent to hierarchically higher cortical areas (R2 and R3). Each unit in the bottom and middle rings (R1 and R2) is coupled to the corresponding unit (and its local neighbors) in the subsequent rings (R2 and R3), respectively.

Figure 3.4B shows a representative example of single-trial firing rate traces (together with the associated spatial maps of activity) for all three rings, for both the SU (top) and SB regimes (bottom). Red lines and curves indicate units at the position of

stimulus injection, blue units far from it, and magenta the initial bump position in SB simulations. All panels show the propagation of activity bumps through the hierarchy of rings. Again, bumps are purely stimulus-evoked in the SU regime, while they emerge spontaneously (and are persistent) in the SB regime. The bump maximum amplitude decreases, and its peak latency is delayed when propagating from bottom to top ring. This effect is more pronounced in the SU regime than in the SB regime, where self-amplification via local recurrent excitation acts as a facilitator for propagation. In SB, the effect of forward coupling is already observable without any stimulation : the intrinsic bump positions (magenta lines and curves before stimulus onset) are very similar in the three rings, whereas they would be completely decorrelated if rings were uncoupled.

As for the one ring model, we study whether bump activity performs the basic IPP of "carrying" information about the stimulus. The encoding dynamics revealed by the MI analyses in Figure 3.4C closely mirror the dynamics of firing rates in Figure 3.4B. The peak amount of information carried about stimulus position is larger in the bottom ring (black curve) and weaker in the top ring (dotted curve). Furthermore, the rise of encoded information is slower and delayed in rings R2 and R3, particularly in the SB regime where the re-alignment of bump positions is slow and continues in higher order rings even after stimulus offset. Our model thus successfully captures the propagation of sensory representations.

The obvious IPP algorithmically mediating this propagation is that of "transferring" (cf. Figure 3.3E). In Figure 3.4D, we show the time series of inter-regional information transfer evaluated via Transfer Entropy TE (again, see Discussion for some limitations of this metric). TE quickly rises after stimulus presentation, reaching a peak when MI with the stimulus saturates at its maximum plateau value (cf. Figure 3.4C). Transfer is stronger and faster from R1 to R2 than from R2 to R3, again in agreement with the firing rate dynamics in Figure 3.4B. After the peak, transfer drops to a plateau level, which slowly decays after stimulus offset. The profile of transfer is more complex for the SB than for the SU regime. Firstly, in SB, there is inter-ring transfer of information prior to stimulus onset, since the bump positions in R1 and R2 influence those in R2 and R3, respectively (cf. Figure 3.4B). Secondly, SB curves are broader with marked secondary peaks, associated with the rearrangement of bump positions. Their rearrangement takes longer than their mere creation. The spatial maps of Transfer Entropy in Figure 3.8A show that substantial transfer occurs even to units far from the stimulus centers as the generation or drift of bumps at locations misaligned with the stimulus must be actively controlled (another inter-regional functional interaction that TE is able to track).

Since the wiring of the multi-regional circuit is purely feed-forward, there should not be any significant feed-back information transfer. In the SU regime, the backward TE from higher-order toward lower-order rings is close to zero. However, in the SB regime, a finite backward TE is detected. It is clearly smaller than the forward TE, allowing it to correctly capture the dominant direction of transfer. This spurious backward transfer is due to misestimation of joint probability density given the finite amount of data, as well as to systematic biases of our simple "plug-in" estimators. It can be reduced by

using a longer delay in estimating TE (Figure 3.8B), and it vanishes almost completely when using multivariate delay coordinate embeddings as originally prescribed for TE (SCHREIBER 2000), see Figure 3.8C. Both approaches allow limiting the impact of fast transients not properly captured by our quantized estimation of joint activity distributions (see Methods). The spurious backward transfer occurs primarily in the particular case of three coupled rings in SB state : here, the changes in the internal dynamics (bump displacement) are very slow compared to the fast change in the external input (stimulus onset), because the reformation of bumps inside each ring takes a certain amount of time and is even more delayed in ring two and three. In this case, a multi-delay estimator of TE can be used to substantially reduce the bias. In all presented cases, the conclusions reached by more sophisticated (and computationally costly) estimators are qualitatively equivalent to the ones of simpler single-delay TE.

In summary, all estimators were able to correctly detect the existence of dominantly feed-forward information transfer. The “transfer” IPP is always the main component in the algorithmic decomposition of the propagation of a sensory representation.

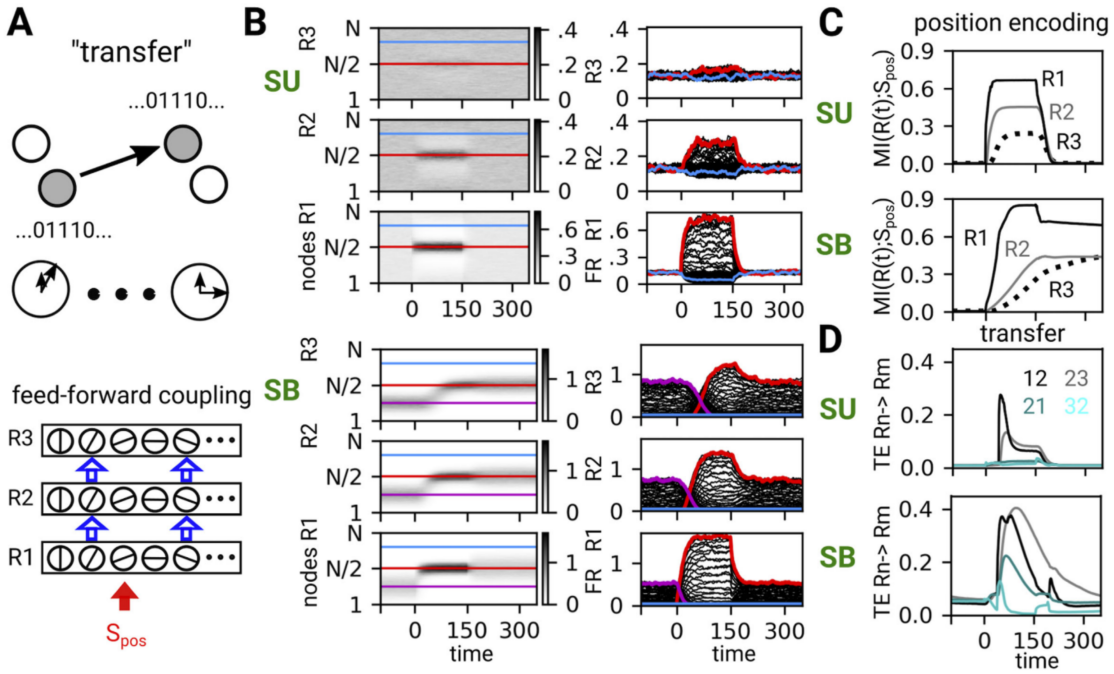

FIGURE 3.4. : Information transfer in multi-regional feed-forward circuits. (A), We study the IPP of "transferring" as it gives rise to stimulus propagation across a chain of three feed-forwarded connected regions, each modeled by a different ring network. Only the bottom ring (R1) directly receives stimulus-related inputs (red arrow). (B), Spatial maps (left) of single-trial firing rates and corresponding rate time series (right) in R1, R2, and R3 (top, SU regime; bottom, SB regime). Red lines indicate nodes located at the stimulus center, blue lines nodes far from it, and magenta lines indicate the initial bump position for SB, as in Figure 3.3B. (C), Time courses of relative MI between rates and stimulus feature (trial and node averages, entropy normalized) reveal stimulus position encoding, transient in SU (top) and persistent in SB (bottom), progressively weaker and more delayed ascending from R1 (black line) to R2 (gray line) and R3 (dotted line). (D), Time courses of information transfer, quantified by TE (trial and node averages, entropy normalized) from R1 to R2 (black), R2 to R3 (gray), R2 to R1 (dark cyan), and R3 to R2 (cyan; SU on the top, SB on the bottom). See also Figure 3.8, notably for an analysis of the dependency of TE on lag and a comparison with time-lagged MI.

3.3.5. IPP analysis can track the integration of bottom-up and top-down information flows

Our last model configuration is specifically designed to reproduce another important cognitive function : selective attention and the involvement of working memory into its implementation. An attentional effect is depicted as boosting responses to stimuli with attended features and suppressing responses to stimuli with features far from the attended ones (feature-gain-similarity principle, MAUNSELL et al. 2006). Seminal modeling work by ARDID et al. (2007) has first shown that the attentional effects on sensory responses can be explained as a byproduct of the nonlinear integration

of sensory bottom-up inputs and top-down inputs from a higher-order region with working memory. This is in line with earlier hypotheses that working memory could be a fundamental component of mechanisms mediating attentional modulation (DESIMONE et al. 1995). In the following, we will show that this merging of bottom-up and top-down influences can be tracked by the IPP of "integrating", quantified by synergistic information modification (Figure 3.5A). In the model proposed by Ardid & co-workers, two ring networks are reciprocally coupled (2RC architecture, see Methods). The lower-order ring R1 represents a sensory area tuned in SU, thus generating stimulus-driven bumps upon stimulus injection. The higher-order ring R2, represents the prefrontal cortex, conditionally set to be in SU or SB regime, respectively, depending on attention state "off" (att-OFF) or "on" (att-ON). With att-ON, the second ring is enabled to sustain an induced representation of a presented stimulus, even after the stimulus is removed (i.e. it can act as working memory).

Following ARDID et al. (2007) in the main aspects, we simulate a classic delayed match-to-sample task (Figure 3.5B). This virtual task mimics actual experiments probing the response of cells recorded in MT cortex to drifting dot patterns. Cells in MT show a strongly selective response to stimuli drifting in their preferred angular direction (Albright, 1984), resulting typically in bell-shaped tuning curves with a marked unique peak. In our computational model, this selectivity is captured by the heterogeneous responses of units along the sensory ring, resulting in the response profile given by the black curve in the top panel of Figure 3.5C. In the virtual task design of Figure 3.5B, two types of trials exist. The "att-OFF" trials correspond to an empirical condition in which the subject actively attends to a stimulus presented outside the receptive field of the recorded cells (called "unattended" in TREUE (2001)). The "att-ON" trials conversely correspond to the empirical "attended" condition where the attentional spotlight is in the receptive field of the recorded cells. In both conditions, a first cue stimulus is shown and then removed (red stage in Figure 3.5B), followed by a delay period of a certain length (black stage in Figure 3.5B) with no stimulus. Then, a second stimulus is presented, whose direction can be close to or far from the direction of the initially cued stimulus (match stage, magenta in Figure 3.5B). Individual simulated trials for different cue and match stimulus configurations are shown in Figure 3.5D, in both the att-ON (top) and att-OFF (bottom) condition.

When simulating neural responses in the att-OFF condition (prefrontal area ring R2 tuned to SU), the response profile of the sensory ring to the match stimulus is unchanged with respect to the one during cue stage. The presentation of match stimuli with different directions simply produces rotated response profiles (black and dashed gray lines in Figure 3.5C). Inspecting the responses in individual trials, we see that all match stage activity bumps in the sensory ring look similar, and that the activity in the prefrontal ring R2 has a smaller rate and a worse signal-to-noise ratio compared to R1 (Figure 3.5D, bottom).

In contrast, in the att-ON condition (a copy of cue has been held through the delay period by R2 switched to SB), the response profile at match stimulus is differently modulated depending on the relative difference of orientation between cue and match stimuli ($\Delta\theta$ in Figure 3.5C). If cue and match stimulus have identical orientations ($\Delta\theta =$

0), the response of the direction selective units in R1 is boosted, while the response of units selective to stimuli far from the attended one is reduced. This can be seen in single trial responses (Figure 3.5D, top), where the match bump is slightly darker for identical cue and match configuration (trial #n). It is clearer in the red activation profile in Figure 3.5C whose peak at $\Delta\theta = 0$ is higher than the black one obtained for att-OFF. If cue and match stimulus have different directions, the difference in $\Delta\theta$ modulates the corresponding response profile (purple curves in Figure 3.5C) in the att-ON condition. The net amount of (simulated) attention-induced modulation can be quantified by computing the percent difference ratio between the response profiles to a stimulus in att-OFF and ON conditions as shown in the bottom panel of Figure 3.5C. In our virtual task, the positive modulation can be as large as +15% for responses to identical cue and match stimuli and down to between −10% and even −45% for stimuli which are $\approx 45^\circ$ displaced. We now study the algorithmic effects of these nonlinear dynamics.

We focus specifically on the IPP of "integrating", occurring here at match stage when the sensory response (R1 in Figure 3.5D) is the byproduct of nonlinearly merged bottom-up stimulus-related input (S_{pos2}) and top-down attention-related input (R2). The information-theoretical quantity we use to track this IPP is synergistic information modification (TREUE 2001; LIZIER et al. 2014). As graphically depicted in the information Venn diagram of Figure 3.5E, the two bottom-up S_{pos2} and top-down R2 inputs carry together (when considered jointly) a certain amount of information $MI_{tot} = MI((R2, S_{pos2}); R1)$ about what is going to be the output sensory response R1. A fraction of this total information is contributed uniquely by each of the two considered inputs. At match stimulus onset, only the bottom-up input S_{pos2} can convey information about the direction of the newly shown match stimulus, while only the top-down input R2 can carry information about the previously presented cue stimulus. Both inputs contribute to determine the final output response, they comprise two unique information fractions conveyed exclusively by each of the two inputs (green and blue areas in Figure 3.5E). Some additional information may be shared between the two inputs –including noise entropy– as captured by the redundant information fraction (cyan intersection in Figure 3.5E). Yet, the sum of unique and redundant contributions could be smaller than the total information MI_{tot}. Some information necessary to determine the response could be conveyed by the two inputs in combination, but by neither of them in isolation. This surplus contribution – "more than the sum of the parts" (Anderson, 1972) – is the synergistic fraction of the total information (white area in Figure 3.5E), and its extraction by the output nodes is termed the synergistic modification operation. We estimate these unique, redundant, and synergistic contributions, quantifying when and where along the virtual task (Figure 3.5B), the activity of the interacting rings implements the IPP of "integrating".

This extraction of the synergistic information is tracked and quantified by the information modification surfaces shown in Figure 3.5F, for both att-ON (left) and att-OFF (right) conditions (cf. Figure 3.9 for details on the individual terms contributing to its computation). In addition, Figure 3.5G shows the profile of a section of the modification surface at the beginning of the match stage (averaging range delimited by the

dotted black rectangle in Figure 3.5F). Clearly, sensory ring units perform information modification at specific task-related locations and times in the att-ON condition while there is nearly no synergistic modification for att-OFF.

The most prominent involvement in information modification occurs in the match stage, particularly at the immediate onset of the match. This is precisely when attentional modulations of stimulus response occur. As visible when comparing the profiles of attentional modulation (Figure 3.5C bottom) and of information modification (Figure 3.5G), the participation of a node in information modification is stronger for the prominent bump in attentional modulations. Specifically, modification is enhanced at the bump flanks, where the most attentional depression is observed. Modification at the bump center position is weaker, because here, the strong net drive helps the recurrent excitatory connectivity within the sensory ring to sustain the boosted activity.

For att-ON, information modification can be seen to occur during different virtual task stages. Modification stripes preceding the match-stage occur during the delay stage with a much weaker intensity. They are related to the fact that some small-intensity activity is top-down transferred from the bump in R2 (cf. Figure 3.5F). These nonlinear interactions between the working memory bump during delay and its "sensory shadow" effectively reduce the variability of the sensory ring activity in att-ON versus att-OFF.. This is another type of nonlinear phenomenon beyond rate modulations that can result in modification (see Discussion). Other modification events occur during the cue stage, probably due to the transient reshaping dynamics of activity bumps caused by the parameter changes for R2 to switch from SU to SB regime.

In the att-OFF state, information modification is close to zero and possibly estimated to small positive values, because of numeric estimation artifacts. As detailed in Figure 3.9, the surfaces shown in Figure 3.5C are the sum of several other surfaces corresponding to the different terms in the expression for the synergistic information part (see Methods). Numerical errors could thus be more important, as more steps are involved.

In conclusion, the function of selective attention admits an algorithmic decomposition involving the IPP of "integrating", a much more complex function than the IPPs of "carrying", "buffering" or "transferring" described in previous sections.

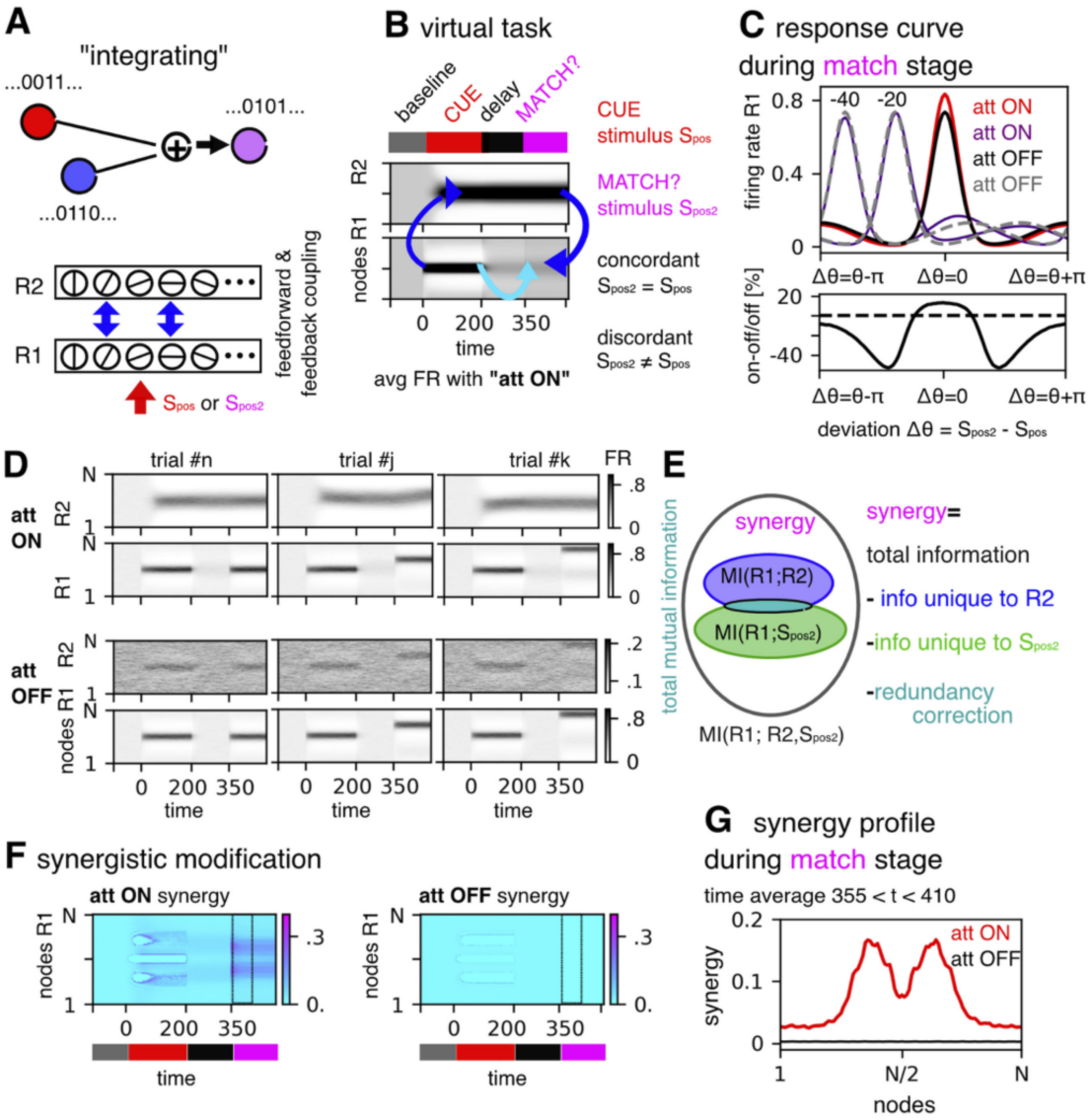

FIGURE 3.5. : Information integration and synergy in the presence of top-down attentional modulation. (A), We study the IPP of "integrating" as it mediates the emergence of top-down attention-like modulation of stimulus response in a bi-regional circuit, composed of two reciprocally coupled ring networks, representing respectively a low hierarchical order sensory region and a higher-order frontal region. (B), In the virtual task we simulate, after a baseline period, two stimulus presentations, during a cue and match stage, respectively, with positions S_{pos} and S_{pos2} (red arrow),separated by a delay period without stimulation. Such a configuration mimics a selective attention experiment in which a copy of the presented stimulus is uploaded to a frontal working memory module (upward blue arrow), which stores it actively through the extent of the delay period (light blue arrow). At the moment of the match, this working memory copy interacts (downward blue arrow) with the sensory representation evoked by the newly presented stimulus, matching or not the previously cued direction. The circuit can be set into an "attention-ON" (upper ring in SB regime) or an "attention-OFF" (upper ring in SU mode) condition. Panel B shows trial-averaged spatial maps in the att-ON condition for matching stimuli directions ($S_{pos} = S_{pos2}$). (Continue on next page).

FIGURE 3.5. : **C**, Response curves of firing rates averaged over trials and time during S_{pos2} presentation (match stage). The red curve for match trials ($S_{pos} = S_{pos2}$), purple curves for no-match, and both for att-ON. In att-OFF, the black curve corresponds to a match, otherwise dotted gray curves. Bottom : attentional modulation index showing the percent enhancement (or depression) of firing rate during match stage in att-ON versus att-OFF conditions. **D**, Firing rate spatial maps for three single trials with different configurations of S_{pos} and S_{pos2}), in bottom (R1) and top ring (R2 ; top, att-ON ;bottom, att-OFF conditions). **E**, Venn diagram indicating the PID of the total MI between the sensory response in R1 and the pair of bottom-up sensory and top-down frontal inputs : synergy equates the fraction of this total which is neither uniquely carried by R2 and S_{pos2}, nor redundant between them. For details on individual terms of the PID, see Figure 3.9. This synergistic information is extracted by nodes in R1 through the process of information modification. **F**, Spatial map of the synergistic modification (normalized) in ring R1 in attention-ON (left)and OFF (right) conditions. Synergy is much stronger in att-ON condition, particularly in the match stage. G, Section of the synergy surface during the early match stage (section averaged over the time window indicated in **F**, by the dotted black rectangle).

3.3.6. Information dynamics in a large-scale model of cerebral cortex

The ring models we have studied so far represent generic coupled brain regions with only stylized notions of hierarchical connectivity (feed-forward propagation in Figure 3.4 and top-down integration in Figure 3.5). Detailed information about inter-regional cortical connectivity is, however, available and large-scale models of cortical activity have been constructed, embedding empirically derived multi-regional connectomes (DECO et al. 2011). In these models, the local activity of individual regions is modeled with simple neural mass equations. Each region receives inputs from other regions, scaled by the relative strength of connections within a connectome matrix. In addition, the distinct fiber tract lengths of the connections can be represented by different propagation delays. To validate our IPP approach beyond generic and ad hoc constrained ring-model architectures, we now consider the case of stimulus-evoked activity in a large-scale model of macaque monkey cortex with realistic connectivity (Figure 3.6).

Specifically, we re-implemented a model previously published by JOGLEKAR et al. (2018), embedding a directed and weighted connectome derived from systematic tracer experiments (MARKOV et al. 2014 ; see Figure 3.6A). The "bow-tie" architecture of such a connectome introduces a barrier to the free propagation of externally injected stimuli. As shown in Figure 3.6B, the application of a brief transient input to region V1, mimicking the presentation of an external visual stimulus, leads to a very limited propagation of activity along the visual stream. However, a Global Balanced Amplification (GBA) mechanism can be introduced, in which long-range excitatory connectivity is enhanced, while simultaneously strengthening local inhibition (to excitatory populations within each region, see Figure 3.6B, top right). In this way, propagation is facilitated by stronger connections, while the increased amount of

excitation is controlled by a modified inhibitory-to-excitatory balance. Figure 3.6B compares a scenario of weak (left) versus strong GBA (right), revealing that stimulus-related activity volleys can reach higher order regions only in the latter case. Following JOGLEKAR et al. (2018), higher order regions are endowed with stronger excitability and correspondingly longer time-constants. Thus, once a stimulus-related volley has reached a higher-order region (e.g., region 46d), the stimulus-evoked activity will last well beyond the offset of the applied stimulus. Adoption of a strong GBA regime and hierarchy-scaled excitabilities allows thus to implement in the large-scale model a scenario reminiscent of the att-ON condition in Figure 3.5, where the top ring, after being cued to attend a stimulus direction, is switched in the SB regime, sustaining bumps in absence of stimulus.

We performed simulations of stimulus propagation in this large-scale cortical model and extracted its algorithmic decomposition, revealing "buffering", "transferring" and "integrating" IPPs. Figure 3.6C shows raster plots of IPP metrics, computed in the strong GBA regime, whereas Figure 3.6D shows an alternative representation of these IPPs, time-averaged radar charts, where blue lines indicate strong and red lines weak GBA regimes. The results of analyzing (stimulus unspecific) Active Information Storage (AIS) are reported in the first column on the left. We observe that sensory regions (e.g., V1, V4) and (pre-) frontal regions (e.g., 46d, 8) have very different storage dynamics. The raster plot (Figure 3.6C) shows that in sensory regions, AIS drops relatively quickly after stimulus offset, while in higher-order regions it persists for a longer time span, an effect of the longer intrinsic time-constants. Areas 46d and 8 display positive AIS before stimulus presentation, reminiscent of ring networks in the SB regime (cf. Figure 3.3B). However, when additionally computing stimulus-specific storage (for area 46d, see Figure 3.4E), we see that the fraction of storage imputable to stimulus is zero before stimulus onset and increases thereafter. In the low GBA condition, only a limited set of regions displays noticeable AIS (Figure 3.4D).

Finally, we consider V1 as a target node integrating the bottom-up stimulus-related input and top-down inputs from other regions in the large-scale cortical circuit and compute the amount of synergistic modification performed by V1 (rightmost columns in Figure 3.6C and 6D). Strong stimulus-related synergies exist with a variety of regions through the entire cortical hierarchy, particularly strong with frontal and prefrontal regions (areas 8 and 46s). Similar to the IPPs of "buffering" and "transferring", the strong GBA regime is needed to establish substantial synergistic modification. In Figure 3.6F, we study in detail the latencies with which synergistic integration arises. Figure 3.6F (left) shows the synergistic information in the stimulus-induced V1 response due to the integration of top-down inputs from region 46d. As expected, the V1 response peak precedes the peak in the 46d response which lasts longer than the V1 response. Synergy starts growing in parallel with the increase of activity in area 46d region, and the synergy peak occurs very close to the area 46d response peak, indicating a fast integration of top-down signals by V1. Remarkably, as shown by the scatter plot in Figure 3.6G, synergistic integration is achieved first with top-down inputs from regions hierarchically distant from V1. Indeed, a significant anti-correlation ($R = -0.66$, $p = 0.0002$) exists between distances in the matrix of Figure 3.6A (right)

and the peak of the synergy time-course. This finding is non-trivial and reveals how the bow-tie topology of the cortico-cortical connectome supports a fast “forward” transfer of stimulus-related information followed by a “backward” integration of top-down influences, initiated by the top-most regions (see Discussion).

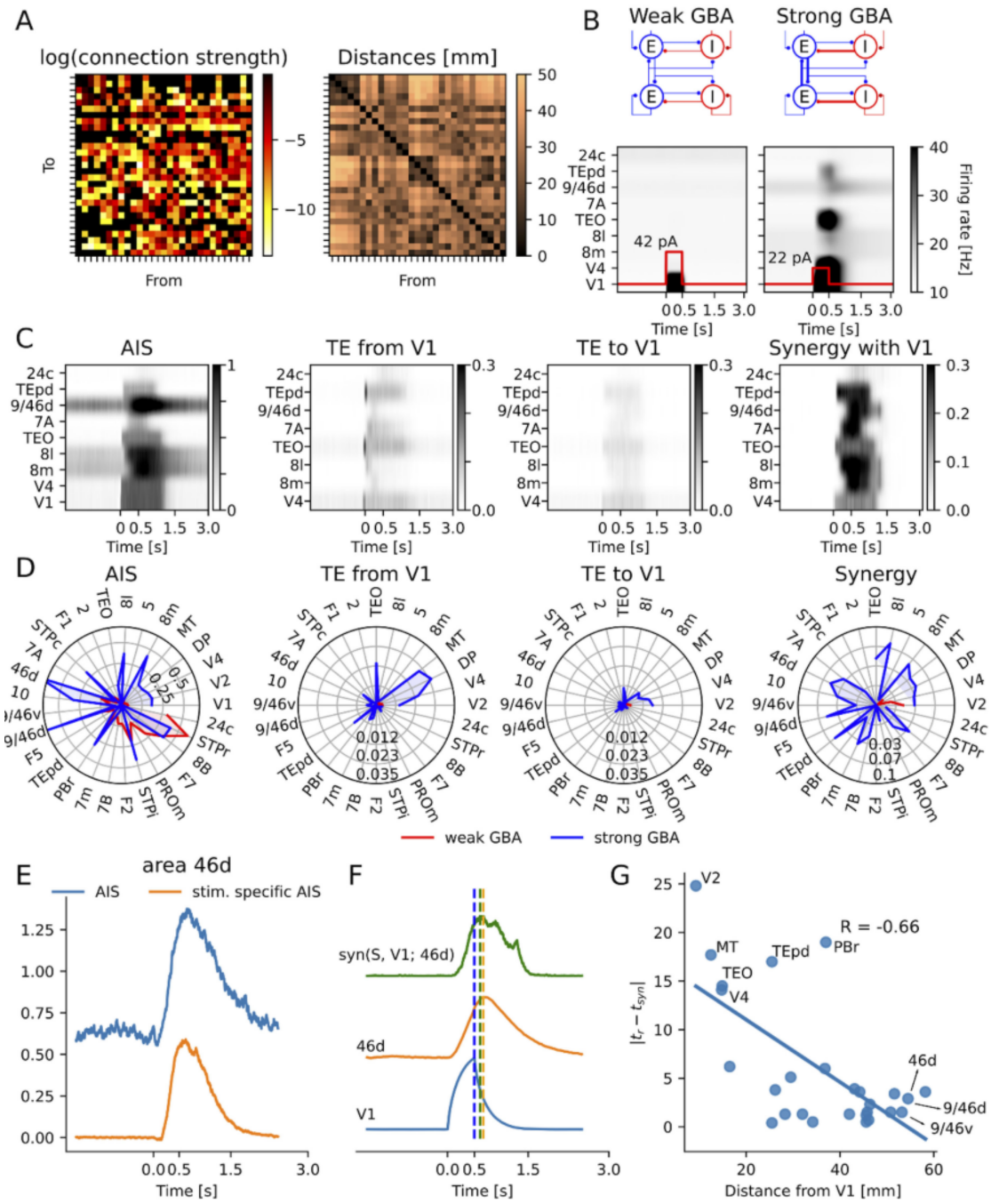

FIGURE 3.6. : Information dynamics in a large-scale model of the cerebral cortex. Large-scale connectome-based mean-field model of nonhuman primate cerebral cortex. (A), Inter-regional connectivity is described by empirically derived matrices of connection strength (left) and connection length (right), determining efficacy and delay of inputs from remote regions. (B), We consider two regimes of the model, a weak and a strong GBA mode. To favor signal propagation, in strong GBA, long-range excitation is strengthened together with an increase of local inhibition to excitation,to avoid rate explosion. Shown at the bottom are rasters of the rate response of different regions of interest in response to a stimulus pulse presented to region V1, in the weak and strong GBA modes. (C), Rasters of IPP metrics dynamics associated with the presentation of a stimulus in the strong GBA regime (as in panel B, right). (Continue on next page).

FIGURE 3.6. : D, Alternative representation of IPP metrics in the form of radar plots (blue, strong GBA; red, weak GBA). From left to right : AIS (stimulus-unspecific, see panel E for an example of stimulus-specific, in orange, vs stimulus-unspecific, in blue, storage) ; TE from and to region V1 ; synergistic integration by region V1 of stimulus-related and top-down inputs from different regions. F, From bottom to top : time series of rate responses of a sensory and a frontal region, together with the synergistic integration by V1 of the bottom-up stimulus and top-down frontal inputs. Peak positions are highlighted by dashed lines. G, Scatter plot of synergistic modification peak latency versus distance of top-down input source from V1 reveals an anti-correlation (significant Pearson's R, 95% confidence intervals −0.658 and −0.643).

3.4. Discussion

Information processing in cognitive sciences is commonly viewed in terms of box-arrow models linking perception to behavior, not necessarily with explicit reference to neural mechanisms (FODOR 1968; MCCLELLAND et al. 1987), but increasingly so (SCHAPIRO et al. 2013), also due to the rise of neuroimaging (Price, 2018). Hypotheses about processing architectures are validated through experimental tasks designed to disentangle the relative contributions of different boxes in such models. It is difficult, however, to interpret the results without implicit reference to concepts of the postulated theory (COOPER 2007). If this theory deviates strongly from the (unknown) underlying neuronal computations, the resulting analyses may be inherently biased. There is thus a need for data-driven, agnostic approaches to get access to the algorithmic level.

We propose a set of metrics to detect and measure elementary processing operations when applied to the analysis of neural activity. The rigor in the definition of these information processing primitives (IPPs : buffering, transferring, and integrating) necessitates that they must be abstract and act in plain, identifiable ways on information conveyed by neural activity. Although these operations are far from evident cognitive functions (e.g., attentional modulation), they constitute their necessary low-level ingredients, a sort of "neural assembly language". Varying combinations of IPPs build up into a variety of functions, like the instruction set of a conventional digital computer (WILKES et al. 1958) : despite their deceptive simplicity, low-level instructions are sufficient to generate a variety of software outputs, from the word-processors we used to write this article to the media players that have distracted us during its preparation.

Low-level information processing naturally emerges from the collective dynamics of complex non-linear systems. For instance, in cellular automata, like Conway's "Game of Life", dynamical patterns known as "gliders" act as agents of information transfer and their collisions as information modification events (LIZIER et al. 2013). In our study, the IPP of "transferring" is materialized by volleys of propagating activity in coupled ring networks (Figure 3.4) –like gliders in the Game of Life–, and the IPP of "integrating" by activity volleys colliding within the sensory ring (Figure 3.5). In contrast to abstract toy systems, coupled ring models correspond to actual neural circuits mimicking cognitive functions. Within this framework, we can thus make

a first step towards bridging the gap between Marr's first and third level, i.e., from the structure of the neural circuit to its function. The missing link (Marr's second level) is provided by the algorithmic decomposition of the simulated activity which precisely quantifies how (through which primitive operations), when (in which epochs during the task), and where (by which network nodes) information is processed. In this respect, our study is based on a ground-truth model : knowing both the circuit wiring and the emulated cognitive function with precision and certainty allows us to determine the cocktail of IPPs associated with a certain function. The measured spatiotemporal patterns of IPP recruitment are compatible with reasonable, a priori expectations, confirming that the output results of our analyses are trustworthy.

Next, we apply our metrics to the non-human primate connectome model (Figure 3.6), which represents many cortical regions with realistic connectivity. The structural connectivity for this model is characterized by a double-hierarchical organization despite its heterogeneous and irregular structure. Those characteristics allow one to formulate hypotheses on how computations are performed only up to some extent since they are not prescribed by an imposed custom architecture.

As shown by JOGLEKAR et al. (2018), the forward hierarchy can serve as a substrate for forward propagation of stimulus-related information to high-order regions which is here tracked by Transfer Entropy. After reaching the frontal subnetworks, their longer time-constants allow the reverberation of this information in working memory, as tracked by Active Information Storage. Our IPP analyses also allow identifying another algorithmic effect of the bow-tie connectome, now serving as substrate for the synergistic integration of top-down inputs. Similar to the two reciprocally coupled rings, top-down modulations of V1 activity are an automated consequence of reverberant stimulus-related activity in high order regions. Thus, analyzing IPPs provides a picture of the algorithmic effects of stimulus propagation in a realistic connectome model. It even allows disentangling the detailed timing of three distinct primitive computations of "transferring", "buffering" and "integrating", in relation to the ascending and descending hierarchy within the connectome.

The anticorrelation between hierarchical distance and synergy maximum revealed by Figure 3.6F is an intriguing prediction, supporting the role of frontal and prefrontal regions as leading top-down controllers (PANERI et al. 2017). Although these regions are "far away" from V1, they are the first to exert a measurable information modification effect in V1. Additional information modification in V1 then occurs via the integration of inputs from other "closer" cortical regions, however, only with greater latency, as the activity of these regions must also be first modified as an influence of top-down influences from the top of the hierarchy. Such anticorrelation is thus interpretable and reasonable. It was, however, unanticipated and makes us optimistic about the heuristic potential that IPP analyses may have when applied agnostically to large-scale activity recordings.

Our proposal to seek IPPs underlying cognitive computations is not completely novel (e.g., INCE et al. 2015; LUNGARELLA et al. 2006. Training in specific tasks has been shown to automatically confer superior performance in apparently unrelated tasks (SINGLEY et al. 1989). This finding led to the speculation that cognitive algorithms may

involve shared processing subroutines so that training of low-level processes explains the transfer of cognitive skills across tasks. Such a notion of "primitive elements" of cognitive processing (TAATGEN 2013) is naturally algorithmic, since it refers to "pre-functional" information manipulations, participating in the implementation of the final function. Analogously, other cognitive theories postulate the existence of intermediate representations (WICKELGREN 1999; MEL et al. 2000) between the encoding of isolated parts of objects (e.g., contour segments) and the fully-integrated encoding of whole objects (e.g. shapes). Such intermediate representations could be reinterpreted as primitive algorithmic steps towards object recognition. Our notion of IPPs lies at an even lower hierarchical level, since such pre-functional cognitive operations could themselves be further decomposed into IPPs.

Another asset of our IPP analysis is that it goes beyond the conventional study of functional connectivity. The latter just detects which units process information together, while IPPs additionally reveal the qualitative type of processing. For instance, very similar functional connectivity motifs (activity bumps in the sensory ring) are generated in attend-ON and OFF conditions during match in the simulated experiment of Figure 3.5. Functional connectivity primarily captures information transfer for both conditions, while IPPs additionally detect substantial information modification for attend-ON, revealing two qualitatively distinct modes of processing. The IPP framework thus enables stronger constraints on hypotheses about cognitive processing implementations. The capacity to simultaneously track different types of processing across different locations will facilitate the identification of putative cognitive architectures combining parallel and sequential aspects (ZYLBERBERG et al. 2011). Information decomposition techniques can also be used to reveal distinct information-processing roles in different cognitive domains (LUPPI et al. 2022).

The rate models considered here are extremely simplified with respect to biological neural circuits. They simply serve to generate activity time-series from generic neural systems mimicking cognitive functions, without bothering too much about realism. Despite their simplicity, ring models can generate a huge variety of dynamics. We focus on asynchronous activity regimes, however, enhancing inhibition or varying delays gives rise to alternative regimes characterized by oscillatory activity, including traveling waves or even chaotic oscillations (ROXIN et al. 2005; ROXIN et al. 2006; ARDID et al. 2010; BATTAGLIA et al. 2011). In perspective, oscillatory regimes could be used to quantify whether their presence affects primitive computations (e.g. boosting modification and/or transfer), to elucidate the effects of cortical traveling waves (MULLER et al. 2018; GONG et al. 2009; CHEMLA et al. 2019) on information processing (colliding wavefronts might act as information modification events), or to benchmark tools for spectrally-resolved information-theoretical analyses (PINZUTI et al. 2020).

Like previous studies of state-dependent information transfer (BATTAGLIA et al. 2012; PALMIGIANO et al. 2017), we capitalize on the possibility to simulate arbitrarily large quantities of data in perfectly controlled conditions to enable a straightforward (binning) estimation of information-theoretical functionals. Still, estimation is error-prone, as revealed by the spurious inference of information transfer from higher- to lower-order rings in the feed-forward configuration of Figure 3.4. The correct qualita-

tive conclusion is achieved (i.e., the dominant direction of transfer), but these results give a warning about the use of estimators. Binning strongly depends on the number of samples, is biased and suffers from the curse of dimensionality PALMIGIANO et al. 2017; PANZERI et al. 2007. For the analyses shown in Figure 3.8B-C, we used an alternative based on semi-parametric estimation techniques, namely the Gaussian Copula Mutual Information (GCMI, INCE et al. 2017).

Note that we use a mixture of classical metrics and the modern PID approach. Both can have certain deficiencies, especially with respect to their interpretation. For example, our "classic" definitions of Active Storage and Transfer Entropy may conflate synergetic and unique information (e.g., see BARRETT 2015 for the case of Gaussian systems; cf. also GUTKNECHT et al. 2021). Transfer Entropy may, under certain circumstances, overestimate the information flow (JAMES et al. 2016). Another concern could be caused by the pairwise analysis, rather than multivariate, to calculate transfer. However, in a system of many components, transfer may occur groupwise ("polyadic interactions" in ibid.). Yet, the network approach provides a useful first approximation to track dynamics (BULLMORE et al. 2009; KIRST et al. 2016), as long as we are aware that higher-order interactions may be present (e.g., DAVISON et al. 2015). Yet another limitation of our approach is the use of the MMI implementation of PID that may overestimate the amount of redundancy or synergy, given that it just provides upper bounds for them. For instance, the redundancy between two Gaussian inputs both carrying some information on a third univariate output can be proved to be positive in the MMI ansatz, even if the two input variables are completely uncorrelated (BARRETT 2015), and this redundancy misestimation necessarily leads to synergy misestimation. Superior metrics have been proposed, see, e.g.BERTSCHINGER et al. (2014) for alternatives to the MMI ansatz in special cases ,as well as JAMES et al. (2016)) and KAY et al. (2018) for formulations of PID in terms of dependency constraints decomposition (available for both discrete and Gaussian variables). Eventually, even superior evaluation of unique information beyond MMI and explicit accounting of synergies never fully protect against the possibility that paradoxical cases arise. It is likely, however, that the extreme scenarios introduced in the theoretical literature to probe the limits of different paradigms occur only rarely in actual neural activity recordings (and simulations from realistic models). Nevertheless, in both "legacy" and "modern" approaches, the interpretations of information flow, transfer, synergy, redundant and unique information, etc. should always be taken with due caution.

Here, we do not address open questions regarding the most adequate estimators to compute IPPs, which is beyond the scope of this study. We propose instead a pragmatic set of measures that helps extracting information about neural computing from data. Nevertheless, for the specific case of our results, constructed from real mechanistic circuit simulations rather than abstract statistical models (conceived to test metric limits), the estimated synergistic modification maps are perfectly interpretable, making us more confident that we are tracking genuinely non-trivial computations. Our methodological choices have at least the advantage of being widely used (cf. the use of the MMI ansatz by LUPPI et al. (2022)) and simple to implement.

The set of IPPs we propose is far from exhaustive. PID exists for more than three va-

riables, yielding a combinatorially exploding number of information "atoms" (WILLIAMS et al. 2010). Multivariate frameworks to quantify informational effects of emergent collective behavior have been proposed for arbitrarily large systems (ROSAS et al. 2020). Any additional IPP would still capture informational effects of coordinated dynamics. The name of "dynome" has been proposed for the collection of possible dynamical modes that a neural circuit with a given connectome can support (KOPELL et al. 2014). In our algorithmic-centered view, every dynamical mode within the "dynome" could map to an element within the "infome", a repertoire of operators on information conveyed by the corresponding dynamics. Possible examples are transiently coherent oscillatory bursts, serving as information routing enablers (PALMIGIANO et al. 2017), or the recruitment of distinct subsystems with identical neurons processing information differently at different times (CLAWSON et al. 2019; PEDRESCHI et al. 2020). In general, the number of considered IPPs should be tailored to match the variety of intrinsic activity patterns that the considered neural circuit engenders.

Until now, most attempts to identify canonical computations, e.g., inhibition-driven rerouting or normalization (POUILLE et al. 2004; CARANDINI et al. 2012; MILLER 2016; HANGYA et al. 2014), were committed to specific connectivity motifs being responsible for specific processing types. Such structure-centric views may be limited by the fact that a connectivity motif can behave differently in different contexts (AERTSEN et al. 1989; NADIM et al. 2008; DAHMEN et al. 2022; KIRST et al. 2016), so that a single motif could perform multiple computations. Alternatively, it is possible that different connectivities implement similar dynamics (MARDER et al. 2006; YGER et al. 2011; VOGES et al. 2012), resulting in similar computations. The quantification of IPPs allows to study information processing directly at the algorithmic level, in a way commensurable with, but "disembodied" from the specific circuit mechanisms producing it. This may allow the detection of specific cognitive processes (e.g., attentional modulation) through the identification of their informational signatures (e.g., boosted information modification). IPP analyses may, also in absence of (apparent) damage in the underlying circuits, allow the detection of disruptions in the information processing itself, thus providing a fundamental "software" explanation for cognitive impairments in pathologies (CLAWSON et al. 2021).

TABLEAU 3.2. : List of parameters for ring model simulations.

parameter	**description**	**values**	**remark**
$\delta_{t_i nt}$	integration time step	0.01	arbitrary units
δ_t	time step for the analysis	10 $\delta_{t_i nt}$	
D	delay between ring units	1 δ_t	
$D_l r$	external delay between rings	2 δ_t	
dt	time delay for MI analysis	40 δ_t	for binning
		5,10,...40 δ_t	for multiple delays
N	number of units	100	0 to 99

ν	noise	50 %	relative to the external drive
J_0 *for SU state*	internal coupling	-30	stationary uniform activity
J_1 *for SU state*	internal coupling	-8	stationary uniform activity
J_0 *for SB state*	internal coupling	-25	stationary bump activity
J_1 *for SB state*	internal coupling	11	stationary bump activity
A_{lr}	external forward coupling strength	35	for 3FF rings
σ_{lr}	external forward coupling width	3 nodes	for 3FF rings
A_{lr}	external forward coupling strength	15	for 2RC rings
σ_{lr}	external forward coupling width	3 nodes	for 2RC rings
A_{lr}	external backward coupling strength	23	for 2RC rings
σ_{lr}	external backward coupling width	6 nodes	for 2RC rings
A_{stim}	constant stimulus amplitude	2.0	rate S(t) units
σ_{stim}	stimulus width	8 nodes	
S_{pos} *(4 features)*	stimulus injection position	0, 25, 50, 75	for one ring and 3FF rings
S_{pos} *(1 feature)*	1st stimulus position	50	for 2RC rings
S_{pos2} (10 features)	2nd stimulus position	0, 10... 90	for 2RC rings
t_{ON}	stimulus onset	100 δ_t	for one ring and 3FF rings
t_{OFF}	stimulus offset	250 δ_t	for one ring and 3FF rings
t_{end}	end of simulation	450 δ_t	for one ring and 3FF rings
t_{ON}	1st stimulus onset	110 δ_t	for 2RC rings
t_{OFF}	1st stimulus offset	310 δ_t	for 2RC rings
t_{ON2}	2nd stimulus onset	460 δ_t	for 2RC rings
t_{end2}	end of simulation	610 δ_t	for 2RC rings

abbreviation	**full name**	**explanation**
SU	stationary uniform	dynamical state with spatially homogeneous activity
SB	stationary bump	dynamical state with spatially inhomogeneous activity
3FF	three feed-forward coupled rings	setup to demonstrate information transfer
2RC	two reciprocally coupled rings	setup to demonstrate information integration
FR	firing rates	ring model output
MI	mutual information	information-theoretic measure
TE	transfer entropy	information-theoretic measure
H	entropy	information-theoretic measure
GCMI	Gaussian copula mutual information	alternate method to calculate MI, TE, and H
att-ON	attention-ON state	configuration of the 2RC setup
att-OFF	attention-OFF state	configuration of the 2RC setup
GBA	Global Balanced Amplification	Increase in long-range excitation and local inhibition
FLN	Fraction of labeled neurons	Fraction of neurons labeled by the tracer between a given source and target area.

TABLEAU 3.1. : List of abbreviations.

	Weak GBA	**Strong GBA**
ω_{EI} [pA/Hz]	12.5	
ω_{II} [pA/Hz]	12.5	
ω_{EE} [pA/Hz]	24.3	
μ_{EI} [pA/Hz]	24.3	
β_E/β_I	0.066/0.351	
rBG_E/rBG_I	10/35	
$r(0)_E/r(0)_I$	10/35	
τ_E/τ_I	20/10	
η	0.68	
τ_i/τ_f[ms]	200/225	
ω_{IE} [pA/Hz]	19.7	25.2
μ_{EI} [pA/Hz]	33.7	51.5
$I(V1)_E$ [pA/Hz]	41.90	21.93

TABLEAU 3.3. : List of parameters for ring model simulations.

Included regions
V1, V2, V4, DP, MT, 8m, 5, 8l, TEO, 2, F1, STPc, 7A, 46d, 10, 9/46v, 9/46d, F5, TEpd, PBr, 7m, 7B, F2, STPi, PROm, F7, 8B, STPr, 24c

TABLEAU 3.4. : List of regions included in connectome-based model simulations.

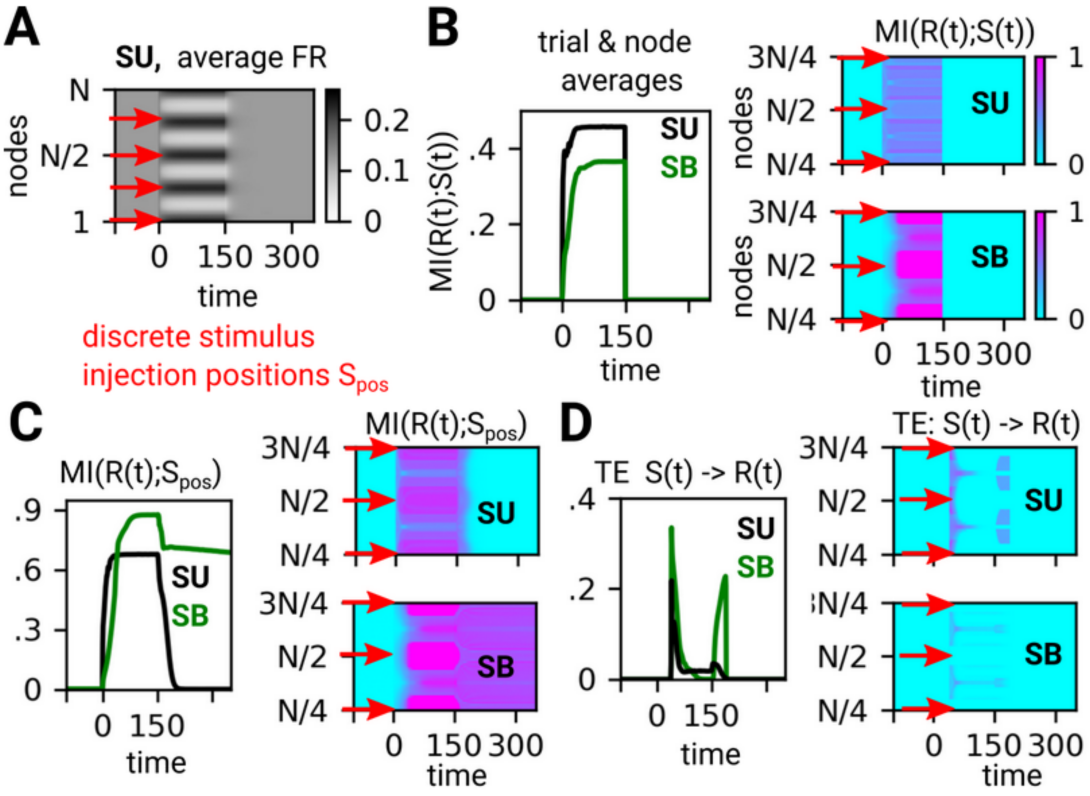

FIGURE 3.7. : Details about information encoding in the single-region circuit (A) Spatial map (all units vs time) of the trial-averaged firing rates in SU in the single-region model composed of one ring network, red arrows indicate stimulus positions S_{pos} in all trials. This and other spatial maps have a striped appearance due to the use of a finite, discrete number of possible stimulus orientations in our numerical experiment setup, as it is often the case in empirical experiments. (B-D) Analogous spatial maps for : mutual information between rates and (B) stimulus time-course S(t) (cf. also Figure 3.3C middle) or (C) stimulus position S_{pos} (cf. Figure 3.3 bottom) ; and (D) Transfer Entropy from stimulus time-course to firing rate responses. We note that the stronger transfer from stimulus to rate occurs at the response bump flanks which are the positions experiencing the stronger response modulation (a suppression in this case) as an effect of stimulus presentation.

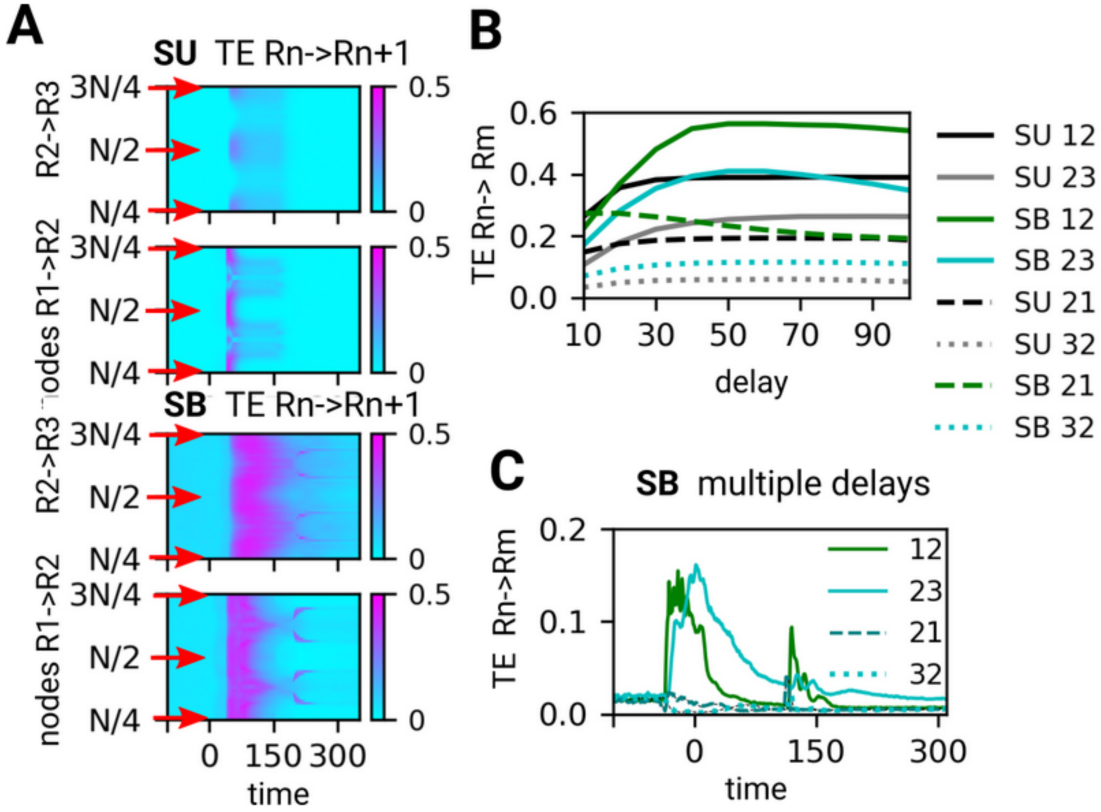

FIGURE 3.8. : Details on the information transfer in the multi-regional feed-forward circuit. (A) Spatial maps (for a subset of units) of the trial-averaged information transfer from ring 1 (R1) to R2 (lower map) and R2 to R3 (upper map). Results from SU state on the top, from SB on the bottom, red arrows indicate stimulus positions S_{pos}. (B) Dependence of peak transfer entropy TE on the delay used for their calculation (no entropy normalization). Backward transfer is indicated by dotted lines and is reduced for longer delays in the case of R2 to R1 transfer (C) Transfer entropy in SB state (trial & node averages) between R1 and R2 and R2 and R3, here calculated through a multivariate scheme using multiple delays (dt = 5,10,15,...40 δt) simultaneously (no entropy normalization). See Methods for details.

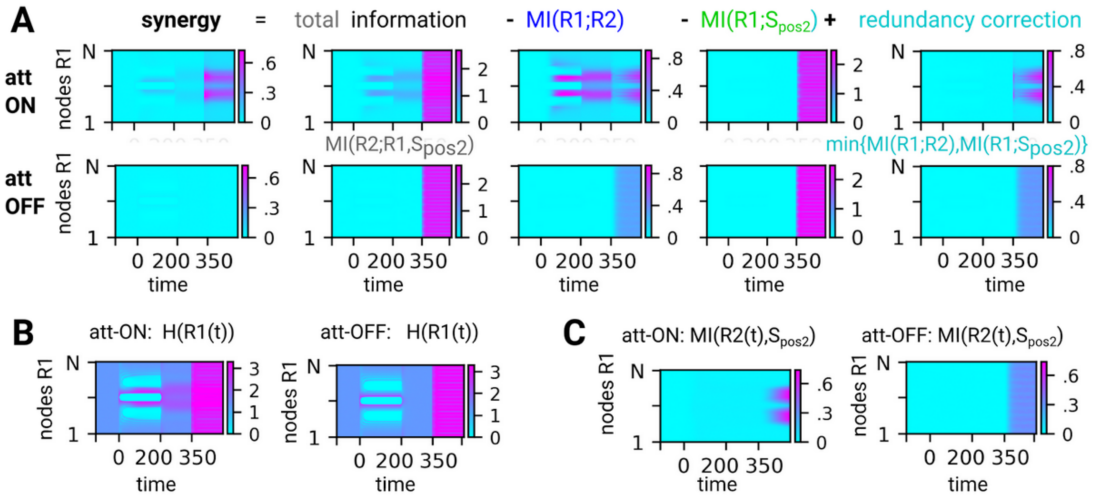

FIGURE 3.9. : Individual terms of the PID for computing synergistic modification in the biregional selective attention model. (A) Composition of synergy, all the "infograms" for the shown terms are raw and without entropy normalization. Top row, attend ON; bottom row, attend OFF conditions. (B) Spatial maps of the entropy of the firing rates in the first sensory ring R1 used for entropy normalizations of the other quantities (left for att-ON, right for att-OFF conditions). (C) Spatial maps of the mutual information between the rates in R1 and the stimulus angle shown during match S_{pos2} (left for att-ON, right for att-OFF). We remark that, to prove that there are no modification effects in the attend OFF condition, the redundancy correction is necessary, as it brings about an exact cancellation of doubly counted Mutual Information to the stimulus, redundant between the rings.

Throughout this dissertation, one central topic was the role of transient activity (or bursts) in a range of cognitive functions. In particular, in the first study we showed their role in supporting working memory by serving as the scaffold of co-crackle assemblies. In the following project, our aim is to better characterize the computational role of bursts, this time by analyzing hippocampal recordings from two monkeys during a task and sleep conditions. In a first stage, we developed a methods for the detection and characterization of bursts defined in the time-frequency domain across recording channels implanted in the hippocampus (i.e., a dependency on depth can also be studied). While the next chapter is focused on this method I also provide information for the next steps of this research project to elucidate how it fits on the general context of this dissertation, i.e., characterize the computational role of neuronal dynamics.

4. HIPPOCAMPAL BURST VARIETY IN A FREELY EXPLORING NON-HUMAN PRIMATE

Authors

Vinicius Lima[1,2], Saman Abbaspoor[4], Kari Hoffman[4,5], Andrea Brovelli[2], Demian Battaglia[3],

[1]Aix-Marseille Université, Institut de Neurosciences des Systèmes (INS), UMR 1106, Marseille, France
[2]Institut de Neurosciences de La Timone, UMR 7289, CNRS, Université Aix-Marseille, Marseille 13005, France
[3]Institute for Advanced Studies (USIAS), Strasbourg, France
[4]Department of Psychology, Vanderbilt Vision Research Center, Vanderbilt Brain Institute, Vanderbilt University, Nashville, Tennessee
[5]Department of Biomedical Engineering, Vanderbilt University,7 Nashville, Tennessee

abstract : Transient oscillatory activity has been implicated in a range of cognitive functions, such as working memory, and has also been found to code for rats' positions during an exploration task. Given the relevance of this type of neuronal activity, methods allowing for its proper characterization are essential for unveiling its role in these functions. Here, I present a preliminary analysis of data recorded from the hippocampus of two freely-behaving monkeys. In particular, I present a method developed as an extension of what was done in Douchamps (2024), which allows the extraction of bursts resolved in both the space and time domains for each recording channel (i.e., space in this case refers to recording depth). In the following, I delineate the details about the method, and how it can be used to extract burst features. I finish by presenting the future plans and perspectives for this project.

4.1. Introduction

When performing a task, behavior requires rapid information processing by widespread neuronal populations, and their dynamics reflect the computations supporting

behavior on timescales compatible with those required by the task. Consequently, evaluating the neuronal correlates of a specific brain function using trial averaging or statistical measures that perform computations across trials can provide insightful descriptions but may obscure finer details of those computations. For example, it is known that trial averaging can either overestimate oscillatory power or average out events that are not consistent across trials (JONES 2016; COLE et al. 2017). Therefore, it is desirable to develop methods that characterize neuronal dynamics at the level of single trials and relate them to external events as a task unfolds.

As discussed in Section 1.4.4, the development of techniques for exploring neuronal dynamics at a single trial by characterizing burst activity has unveiled new aspects of information processing in the brain (FEINGOLD et al. 2015; FRANSEN et al. 2015; LUNDQVIST et al. 2016; SHIN et al. 2017; LITTLE et al. 2019; RAYSON et al. 2022; SCHMIDT et al. 2023; LUNDQVIST et al. 2024). In this chapter, I present a preliminary analysis that has as final aim to deepen the understanding of the computational role of bursting activity in the hippocampus by replicating many of the steps in DOUCHAMPS et al. (2024), and improving over some of the limitations of this study. Notably, here we generalize their analysis for multiple frequency components, and hippocampal layers in a different animal model, i.e., the monkey. To do so, we use a large dataset, consisting of local-field potentials, recorded from two non-human primates during freely-exploring behavior (SAMAN et al. 2023; ABBASPOOR et al. 2023a). But first, given its relevance for the conceptualization of the project I will present in this chapter, next I will provide a brief review of the results reported in DOUCHAMPS et al. (2024).

In the CA1 region of the hippocampus, the interplay between theta and gamma rhythms serves as a general marker of information processing associated with several cognitive processes. More specifically, the phase relationship between gamma activity at distinct frequencies and the ongoing theta cycle is thought to route information from different structures. The prominent model describing theta-gamma interactions suggests that lower gamma (30-80 Hz) is prevalent in the CA1 stratum radiatum (rad) during the descending phase of CA1 pyramidal layer theta. Conversely, medium gamma (60-120 Hz) is mostly located in the CA1 stratum lacunosum moleculare (lm) during the peak of CA1 pyramidal layer theta. While rad receives inputs from CA3, lm receives its inputs mostly from the entorhinal cortex. Consequently, this model allows for the segregation of processes within CA1 (e.g., memory encoding or retrieval) that originate from the dynamics of distinct sources into two discrete gamma sub-bands. However, hippocampal gamma activity is extremely rich, and a model comprising only two rigid sub-bands may not only miss this variability but also overlook its computational role, as shown by Douchamps and colleagues.

To investigate the multiple states (and their computational role) offered by the combination of gamma frequencies, theta phase, and anatomical location, Douchamps and colleagues recorded and analyzed LFP data from the CA1 area of five mice. In their analysis, they did not assume any *a priori* model of theta-gamma interactions and showed : (i) that the model based on gamma sub-bands captures stronger gamma bursts across CA1 layers; however, gamma frequencies and phase relationships to

theta are varied, with significant overlaps across layers; and (ii) that even though these gamma bursts (including the weaker ones) had varied frequencies and behaved rather stochastically, they could self-organize to process information and were informative about the ongoing behavior of the mice.

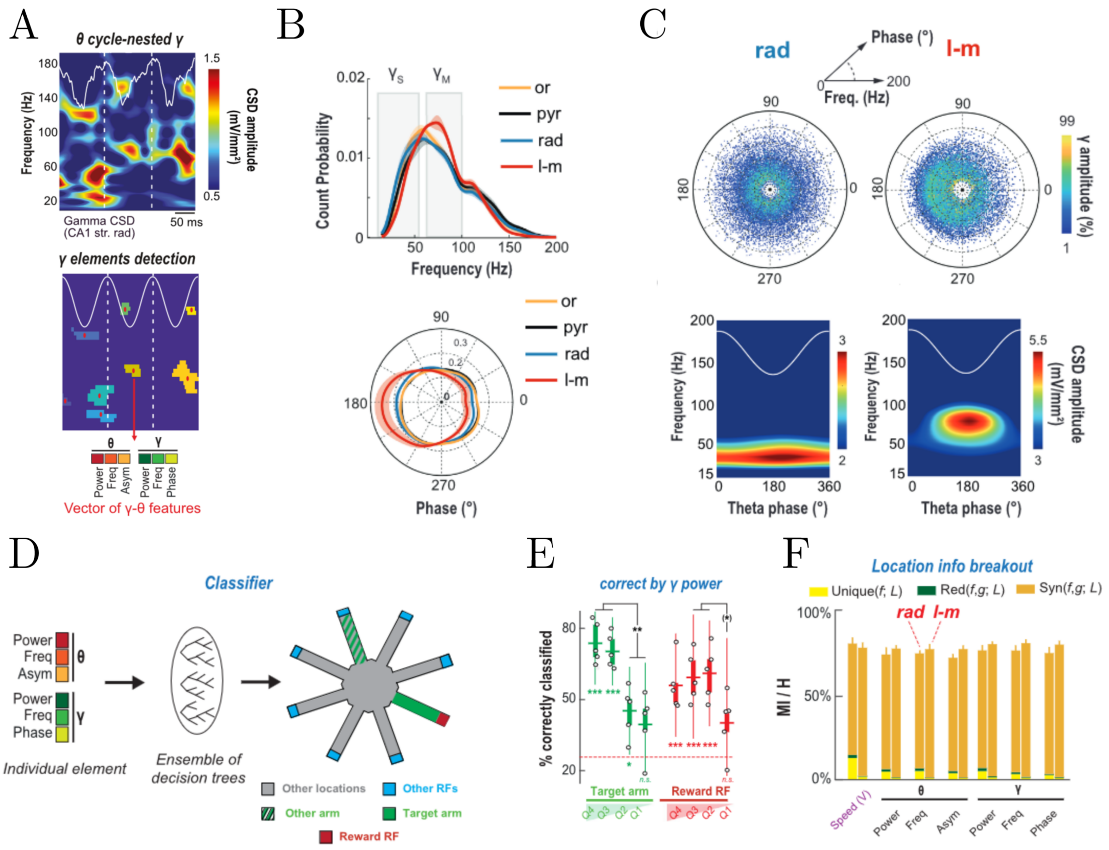

FIGURE 4.1. : Main results from DOUCHAMPS et al. (2024). In (A) we show the time-frequency decomposition of the CSD computed from the gamma filtered signal (30-250 Hz) for a given theta cycle (white time-series superposed over the spectrogram), on the bottom we show the gamma bursts detected on and a cartoon representing the 6 features extracted from each of them (three theta and three gamma features, see text). In (B), we show the probability of bursts with a given average frequency for each of the CA1 layers recorded on top (gray shaded areas indicated the slow gamma (γ_S) and medium gamma (γ_M) sub-bands), and the distribution of theta phase in which those bursts tend to occur in the bottom. In (C), we show the joint distribution of theta phase and gamma frequency, each dot corresponds to a gamma bursts and the color of the dots indicate the power associated to each of them. In the bottom we show the spectograms obtained by averaging over the high power events, notice how in this case they correspond to the classical γ_S and γ_M. In (D), we show the classifier pipeline used to decode either the target arm (green) or the reward RF (red), based on the set of features of each burst, using random forest classifiers. In (E), we show the decoding accuracy (vertical axis) obtained for bursts belonging for each power quantile (horizontal axis) for target equals "Target Arm" (left), and "Reward RF" (right). In (F), we show the partial information decomposition analysis results, the height of the bars in the plot corresponds to the mutual information a given feature f carries about the position in the maze L, different colors represent how much of this total mutual information corresponds to unique (light yellow), redundant (green), and synergistic (dark yellow) information. These panels were adapted from DOUCHAMPS et al. (2024).

More specifically, they decomposed the recorded LFPs into their rhythmic compo-

nents using the ensemble empirical mode decomposition method (EEMD), which I will also widely utilize and explain in the next sections. Since the components of the signal extracted with EEMD are often broadband, they can be summed to result in signals containing a range of frequencies of interest. In their case, they obtained a theta (4-12 Hz) and a gamma band (30-250 Hz) component. The filtered LFPs were used to compute the current source-density (CSD), which was subsequently decomposed in the time-frequency domain and segmented into short epochs with durations equivalent to individual theta cycles (Figure 4.1A top). For each of those epochs, they detected the respective gamma bouts and represented each as a multi-dimensional feature vector with three gamma features (amplitude, frequency, and theta phase of the gamma element) and three theta features (amplitude, frequency, and asymmetry of the coincident theta cycle) (Figure 4.1A bottom).

Interestingly, unlike the aforementioned model, which posits a layer-dependent specificity of theta phase and gamma frequency, DOUCHAMPS et al. (2024) observed highly overlapping probability distributions for these two features across each of the recording CA1 layers (Figure 4.1B). Which raises the question, if gamma bursts are so varied across CA1 layers, how could a model based on rigid layer-specific gamma sub-types be proposed? To address this, Douchamps and colleagues computed the joint distribution of gamma frequency and theta phase (Figure 4.1C top) for both rad and lm. These distributions were highly scattered, although lm exhibited a slightly asymmetrical concentration of samples towards high frequency and a theta phase around 180 degrees, revealing a high diversity of gamma burst types. The gamma sub-bands can be recovered by considering the average spectrogram corresponding to the strongest gamma events (Figure 4.1C bottom). These results highlight a dichotomy between two approaches : one based on averages (classical) and one based on counting (adopted by Douchamps), suggesting that the classical approach may be biased by a subset of high-power transient gamma bursts.

Now, if gamma oscillations are better described by ensembles of bursts constituted of scattered frequencies and phases rather than strict narrow-band oscillations, is this diversity exploited to support behavior or merely noise? To address this question, Douchamps and colleagues, trained mice in a task, where they had to search for a target within an 8-arm radial maze and learned a consistent goal location over a period of 10 days with 4 daily trials. Subsequently, the authors attempted decoding the mouse's current position within the maze during navigation using the features extracted from simultaneously recorded gamma elements. In particular, they used random forest classifiers to predict the mouse's approximate location within the maze, dividing it into four non-overlapping sections : target arm approach, target arm reward field (Reward RF), reward fields of other arms (other RF, no reward), and the remainder of the maze (Figure 4.1D).

The performance for classifying either the target arm or reward RF was overall well above chance level (Figure 4.1E). Interestingly, even though the classifier's performance improves with stronger gamma events, as indicated by the division of the classifier by quartiles of power, the weaker power gamma events also decode the position with accuracies well above chance level. This trend was consistent even when

decoding was corrected by speed, which is known to modulate theta activity in the hippocampus, and when the structure of the decoder was modified to decode randomly selected arms rather than the departure and reward arms (I do not reproduce these results here). In summary, decoding was possible across a wide category of gamma elements with varied features, indicating that even events that are weaker or outside the rigid structure imposed by the classical slow and medium gamma model are modulated by behavior.

If behavior modulates the gamma elements and these complex modulations can be captured by a machine-learning algorithm, which features most contribute to the obtained decoding? Are they derived from theta, gamma, or the joint theta-gamma features? To test this hypothesis, Douchamps and colleagues trained another set of random forest classifiers using either theta or gamma features separately and observed a considerable drop in classifying accuracy compared to when both features were considered together. But how does the interplay between these features yield information about behavior? To disentangle the possible combination effects, the authors used the framework of partial information decomposition (see Section 1.5.2 and Chapter 3), which allows for decomposing the mutual information between maze location (L) and theta/gamma features into : (1) unique information, carried only by a particular feature or set of features; (2) redundant information, carried by two distinct features; and (3) synergistic information, retrievable only by considering the interaction between two or more features. Through this analysis, the authors found that over 75% of the information needed to accurately specify maze location during the task (Figure 4.1F) came from the features. Interestingly, the synergistic fraction corresponded to 70% of the measured mutual information, indicating that the interaction of gamma and theta oscillations is complexly modulated by the task, which explains the small amount of unique information contained in each feature.

In conclusion, the set of results from DOUCHAMPS et al. (2024) highlights the richness of gamma activity that is often overlooked by classical models of gamma subtypes. Additionally, many gamma events typically disregarded as noise are actually modulated by behavior, suggesting a potential computational role for the interactions of theta-gamma oscillations. This is further supported by the synergistic nature of the relationship between these oscillations. Instead of relying on "hardcoded" relations between gamma frequency and theta phase, these results suggest that the system exploits the rich variety of gamma activity during theta cycles in self-organized regimes, balancing between noise and the coordination of weak oscillations, to implement function.

Here, we have devised a plan for the scientific investigation of hippocampal bursts using the same "counting" strategy adopted by Douchamps and colleagues. In particular, we have generalized their analysis to encompass multiple frequency bands in recordings across hippocampal layers of non-human primates. This generalization of the counting procedure is valuable given that recent research by ABBASPOOR et al. (2023b) demonstrated that the theta-gamma relationship in non-human primates is more fleeting, and is a issue where further investigation is needed. Specifically, while theta-gamma coupling in rodents occurs during exploration and sharp-wave

ripples (SWR) during rest in CA1, ABBASPOOR et al. (2023b) showed that these oscillations are divided between behavioral regimes in non-human primates. Moreover, beta2/gamma oscillations (15-70 Hz) were predominant during visual search, while theta (3-10 Hz) oscillations were prevalent during rest and sleep.

In summary, by adopting a data-driven approach, Abbaspoor and colleagues demonstrated that theta band (7-10 Hz) power increases were more prominent during rest, whereas higher frequency power peaking in the 20-30 Hz range was stronger during an active search task (Figure 4.2A). Additionally, power at slower bands (3-8 Hz) was uncorrelated with beta2/gamma power (20-35 Hz) but correlated with faster gamma (80-150 Hz) (Figure 4.2B). This observation makes it difficult to fit hippocampal gamma into two distinct classes as in the classical model of hippocampal theta-gamma coupling in rodents. In this case, slow gamma not only decorrelated with theta, but the latter oscillation was also not present during the task, unlike what is observed in rodents.

Additionally, by characterizing the rhythmicity of spikes in each frequency band using pairwise phase consistency, the authors showed that in non-human primates, rhythmic spiking related to slower oscillations is spuriously evoked by SWR, unlike what is observed in faster oscillations (Figure 4.2C). Moreover, by measuring the spike-field autocorrelograms, the authors verified the lack of spike rhythmicity during theta events when compared to data collected from rats. This lack of rhythmicity was also evident from the theta modulation index, which was mostly zero for the recorded monkeys and positive for rats (Figure 4.2D,E).

Overall, these observations provides a challenging set of questions that we aim to address in the future of developments of the project I describe in this chapter. In particular, we aim not only to investigate the intricate relation between rhythms in the monkey hippocampus during sleep and task conditions but to unveil their computational role in supporting behavior. In the remaining of this chapter, I will describe in details the method we developed for extracting the single-trial bursts, and the future perspectives for this project.

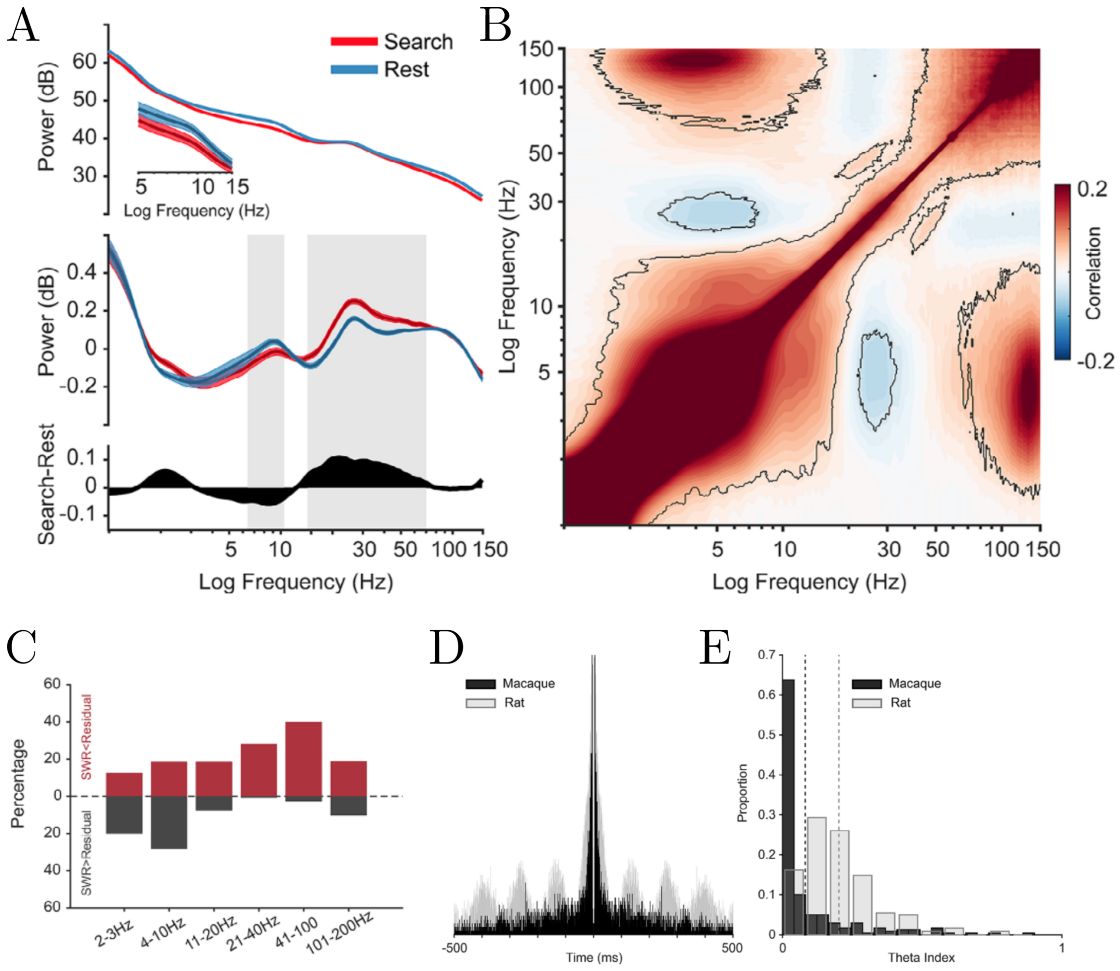

FIGURE 4.2. : Main results from ABBASPOOR et al. (2023b). In (A), we show the power-spectra for the active search (red) and rest conditions (blue), gray shaded areas represents significant modulations of power between conditions. In (B), we show the cross-frequency correlation between for rhythms in the hippocampus, dark contours indicate regions with significant correlations for at least 80% of the recording sessions. In (C), we the percentage (vertical axis) of pairwise phase consistency driven by SWR events for each frequency band considered (horizontal axis). In (D), e show the spike-field autocorrelogram for an example theta unity for the macaque (black) and the rat (gray). In (E), we show the proportion of units (vertical axis) with a given theta modulations index (horizontal axis) for the macaque (black) and the rat (gray). These panels were adapted from ABBASPOOR et al. (2023b).

4.2. Methods

4.2.1. Empirical Mode Decomposition

To decompose the time series into its oscillatory components without imposing any narrow band filtering in imposed frequency bands, we used the ensemble empirical mode decomposition (EEMD) method (HUANG et al. 1998; WU et al. 2009; HUANG

2014). EEMD is a data-driven approach that differs from Fourier decomposition, which decomposes signals into a series of sines and cosines. Instead, EEMD extracts oscillatory modes directly from the data, ranging from the fastest to the slowest components, by iteratively identifying and extracting the envelopes formed by the signal's extrema.

More specifically, EEMD extracts a series of intrinsic mode functions (IMFs) from the signal by performing three steps : (1) detect all peaks and troughs in the time series; (2) compute the upper and lower envelopes by applying a cubic spline to the detected extrema and calculate their average; (3) subtract this average from the original time series to obtain the first IMF. These three steps are repeated until there are no extrema left to detect, or until other criteria are met, such as a maximum number of IMFs or a minimal residual is reached. The EEMD algorithm differs from classical EMD in that it estimates the IMFs for E versions of the time series, each with a different noise realization added. This procedure is intended to reduce mode-mixing in the obtained IMFs. For further details on the algorithm, see the detailed description in WU et al. 2009.

Here we extract the IMFs for a given channel's time-series, that is initially subdivided in B blocks containing N samples. For each block, we extract all possible M_B IMFs, the subscript is used to indicate the number of IMFs per block may vary.

For the analysis carried here we used $E = 5$, and $B = 200$. We used the EEMD implementation available in python in the EMD toolbox (QUINN et al. 2021).

4.2.2. Estimation of the composite time-series

To obtain the components of the time series corresponding to different rhythms, we first estimate the power spectrum for all the IMFs found for a given channel (for all B blocks pooled) using the multitaper technique, setting its bandwidth to 4 (corresponding to 3 Slepian tapers; BABADI et al. 2014). We normalize the spectra obtained by their area and then cluster them using DBSCAN (SCHUBERT et al. 2017). We set the minimal number of neighbors (#neighbors) required for a pair of points to be considered part of the same cluster to #neighbors = 20. The maximal distance (ϵ) is estimated for each channel by computing the maximal Euclidean distance from these channels to their nearest neighbors. The DBSCAN clustering yields labels indicating to which cluster each IMF belongs. Note that the number of clusters is not fixed and may vary from channel to channel.

To get the composite signals, we sum the IMFs belonging to the same cluster, in each block B. After clustering, we get a composite signal ranging from slow to faster rhythms. This approach allows the extraction of the rhythmic components of the recorded signals in an unsupervised and data-driven fashion.

We used the multitaper implementation from MNE-python (GRAMFORT et al. 2013), and the DBSCAN implementation present in the sci-kit learn toolbox (PEDREGOSA et al. 2011).

4.2.3. Burst-detection and feature extraction

The burst detection was done by applying the watershed algorithm. This algorithm is typically used in computer vision for patch detection and segmentation (ROMERO-ZALIZ et al. 2018), and operates according to the following steps :

1. Apply an initial threshold thr_0 to an image.
2. Detect patches of connected components in the thresholded image, and assign a label to each of them.
3. Decrease the threshold by a factor γ and threshold the original image.
4. Check if any patches detected in the previous step were merged with the new ones.
5. If yes, keep their old labels (avoid merging).
6. Check for patches that have grown in size.
7. Repeat from Step 3 until a desired minimum threshold thr_{min} is reached.

For burst detection, the input image corresponds to the spectrograms computed for the composite signals of each channel. Here, we detected bursts for each channel separately, resulting in bursts spanning the time-frequency domain. To do so, we first compute the Multitaper decomposition for each composite signal ($n_{\text{cycles}} = 6$) with a bandwidth of 4 for each channel, animal, and session, using 100 linearly spaced frequencies from 4 to 150 Hz. We normalize the spectrograms of channel c and block b (W_c^b) by extracting its average and normalizing it by its standard deviation (over time and frequency). For each channel and block, we use the 95th percentile of the power distribution (for W_c^b) as the initial threshold (thr_0), and its 75th percentile as the final threshold (thr_{min}), with the thresholds decreasing by a factor $\gamma = 0.1$.

4.3. Results

In this section, we present the method for extracting bursts from LFPs' single-trial time-frequency maps using an example channel in monkey F during the task period. The presentation of the method is divided into three steps :

1. Decomposition of the LFPs into Intrinsic Mode Functions (IMFs) using EEMD ;
2. Estimation of composite signals from the IMFs, representing different oscillatory modes of the LFPs ;
3. Extraction of bursts' features from the spectrograms of the composite signals.

4.3.1. Decomposing the LFPs into oscillatory modes

Applying the EEMD decomposition required reshaping the recorded LFPs into a series of blocks, primarily for computational reasons. The recordings for the analyzed session and channel had a duration of approximately 80 minutes, resulting in 200 blocks, each comprising a 24-second period. Notice that the lack of a pacemaker rhythm as the rodents' theta it is difficult to segment the data according to distinct theta cycles as it was done in DOUCHAMPS et al. (2024), for example.

In Figure 4.3, we show the decomposition of a 20-second signal snippet (Figure 4.3A) into intrinsic mode functions (IMFs). We extract all possible IMFs and display the sixth to the tenth IMFs (Figure 4.3B), as the lower-order IMFs do not exhibit any oscillatory peaks in their power spectrum (Figure 4.3C).

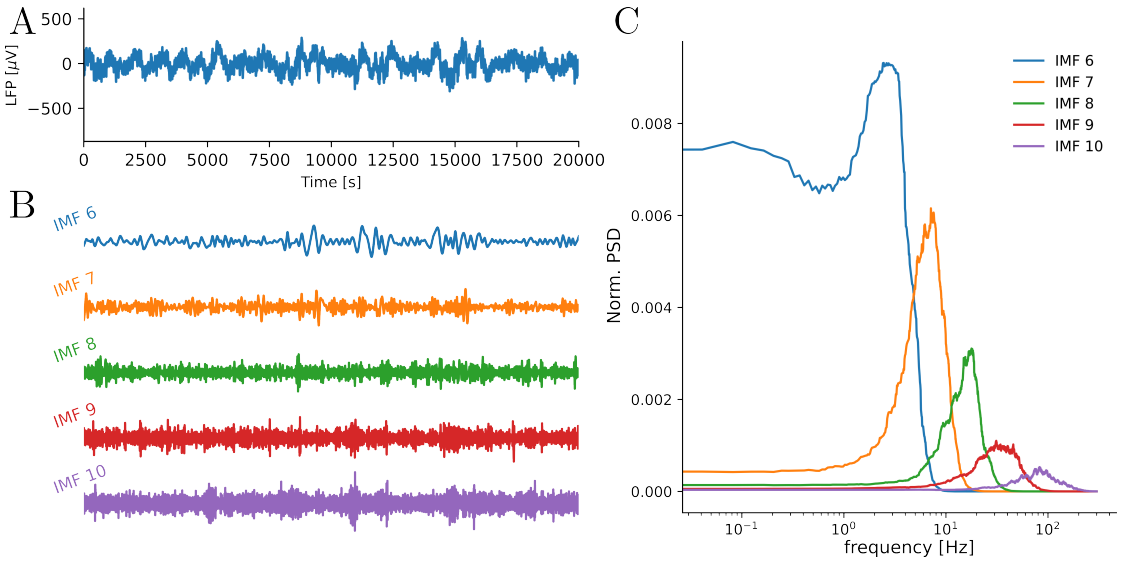

FIGURE 4.3. : Decomposition of the LFP into intrinsic mode functions. In (A), we show a 20-second snippet from the LFP recorded by channel 33 in monkey F. In (B), we display its last five IMFs (6 to 10), and in (C), their respective power spectra.

4.3.2. Estimating the composite signals

Since we extract all possible IMFs for each channel block, the number of IMFs extract across blocks are not necessarily the same. In order to standardize the number of IMFs across blocks, we clustered them based on their spectral profile, i.e., their power-spectrum, and create composite signals for each corresponding cluster. In particular, the clustering algorithm can exploit the fact that most of the IMFs obtained are broadband and overlapping to attempt to merge some of them, yielding distinct (and less-overlapping) sub-bands.

In Figure 4.4A, we plot the power spectra for all IMFs detected across all blocks for channel 33 in monkey F. Even by visual inspection, it is evident that although the blocks contain either 10 or 11 IMFs for this channel, they can be grouped into 7 categories by collapsing the low-frequency IMFs. In Figure 4.4B, we project the power

spectra from Figure 4.4A using UMAP and color the dots in the projection based on the cluster labels obtained by clustering the spectra using DBSCAN. As anticipated from visual inspection, we identified 7 distinct clusters (the spectra for each obtained cluster are shown separately in Figure 4.4C).

Next, we checked whether the obtained composites corresponded to the same frequency band across blocks. In Figure 4.4D, we show the peak frequency of each composite for each data block. The composites corresponded to three slow components (< 5 Hz), two alpha and beta-like components around 10 and 20 Hz, and two fast components around 40 and 80 Hz, respectively.

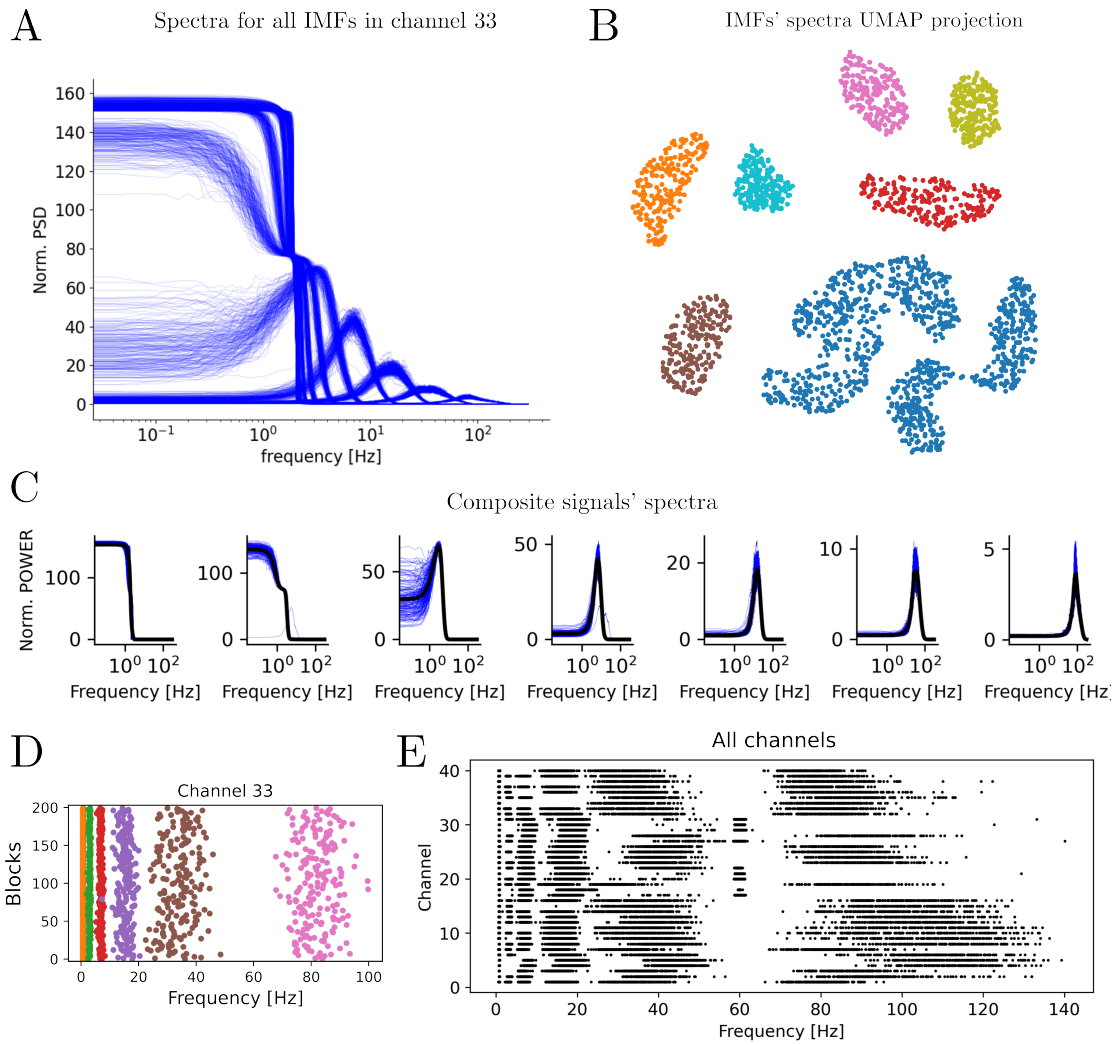

FIGURE 4.4. : Computing the composite signals from the IMFs. In (A), we show the power spectra obtained for all the IMFs detected in channel 33. In (B), we display their UMAP projection, with each color representing a label obtained by clustering the spectra using DBSCAN. In (C), we show the spectra from (A), but separated for each obtained cluster, with increasing average frequency from left to right. The black line in each subplot represents the average spectrum for that cluster. In (D), we show the peak frequency (horizontal axis) for each composite signal across each block (vertical axis). In (E), we show the peak frequency for each composite signal across blocks in each channel (vertical axis).

We also examined the distribution of spectral peaks in the composite signals for all channels in this session (Figure 4.4E). Although there was some variation in peak frequency values, most channels possessed the same components. In Figure 4.6, we show the plot for each channel separately. This analysis helped to identify the channels that possess all frequencies of interest and to discard those that do not or that possess strong artifacts, such as the 60 Hz line noise present in some channels. Additionally, we found that the method yields good agreement across animals as well.

4.3.3. Bursts' features extraction

Once the composite signals are extracted, they were decomposed in the time-frequency (Figure 4.5A,C) domain and single-trial bursts detected using the watershed algorithm (Figure 4.5B,D). In practice, each burst detected is represented by a feature vector, exactly as it was done in DOUCHAMPS et al. (2024). So for one channel, each composite signal has a set of feature vectors per burst (Figure 4.5E).

Here, we extract four features to use as an example : bursts' average power, duration, average frequency, and frequency spread (i.e., how long the burst is in the frequency axis; Δfrequency). In Figure 4.5, we show the distribution of those features for the composite signals 5, 6, and 7.

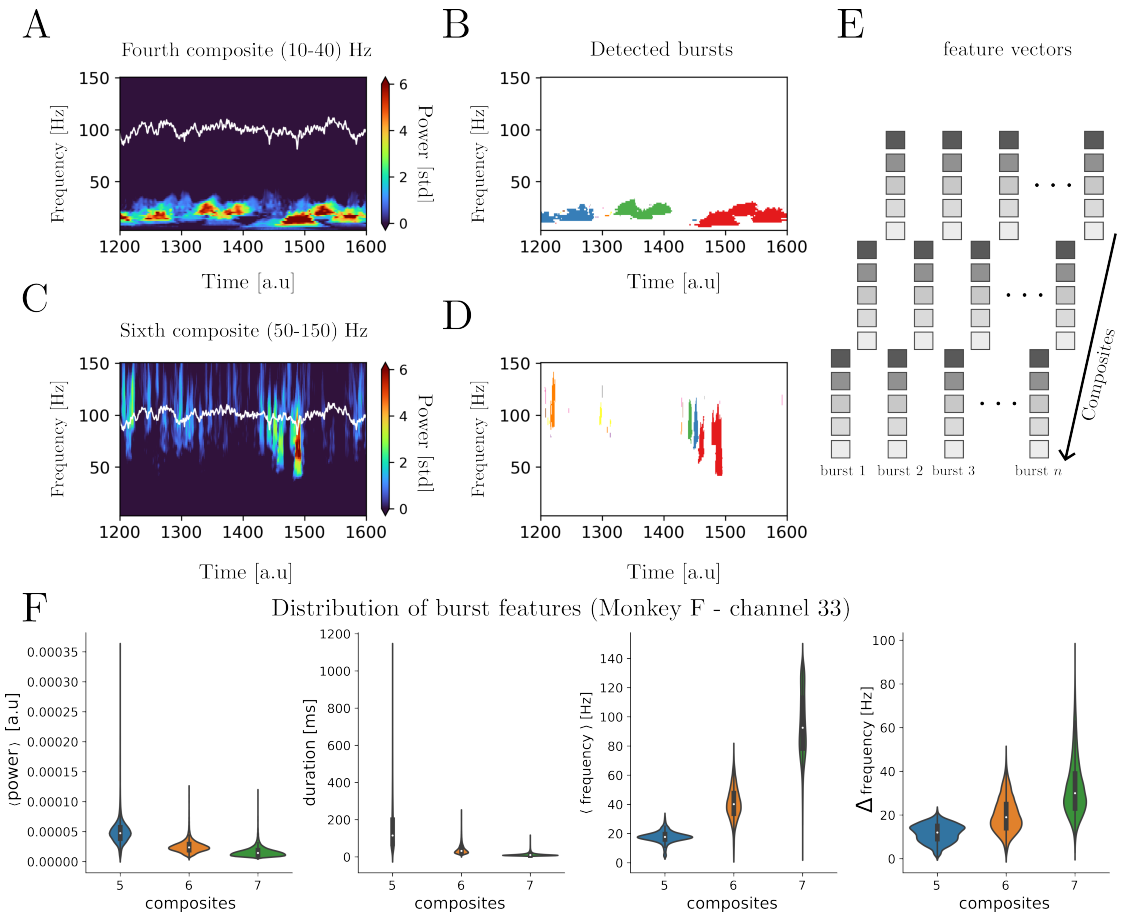

FIGURE 4.5. : Extracting burst features from the composite signals. In (A), we show the spectrogram for the fourth composite signal for channel 33 of monkey F. In (B), we highlight several bursts detected by the watershed algorithm. In (C-D), we show the same analysis but for the sixth composite signal. In (E), we illustrate the data structure obtained when each burst is "converted" into a feature vector for each composite signal. In (F), we show the distributions of four example features (average power, duration, average frequency, and frequency spread; from left to right). In each subplot, the horizontal axis corresponds to the distribution originating from a composite signal : the fifth composite is shown in blue, the sixth in orange, and the seventh in green. Only the top 20 strongest bursts in each block of data were considered when extracting the features to make these distributions.

4.4. Future steps and directions

The long-term goal of this project, is not only to map single-trial neuronal dynamics to behavior, but also to understand the neuronal basis of different categories of bursts (e.g., how burst generate by different cell population differ). During this chapter, we presented the algorithm developed to detect single-trial bursts, which serves as the foundation for achieving our goals. Even though the method lacks some refinements, its current implementation can already be used to proceed our investigations. Many of the drawbacks of the method can be addressed after the feature extraction step

without significantly increasing computational cost. For example, burst events that are shorter than a cycle of the oscillation analyzed, and can be considered artefactual, can be filtered out *a posteriori* based on a duration criterion.

For the remaining of the analysis, we will follow the steps in DOUCHAMPS et al. (2024). In this study the authors showed that single-trial bursts in rodents hippocampus not only differs drastically from their "average picture", but also that they reflect underlying computations carried during navigation. In particular, they were able to show that the behavior of the rat can be decoded from the features extracted from those bursts.

Here, we proceed by first exploring the results reported in ABBASPOOR et al. (2023b), where the authors demonstrated that theta and gamma oscillations in the CA1 region of the hippocampus in non-human primates are decoupled, contrary to observations in rodents. Our method allows for a more in-depth verification of the theta-gamma relationship by inspecting the phase relationship between single bursts in a slow (theta-like) composite and a fast (gamma-like) composite. Additionally, the phase-relation between bursts belonging to each composite can shed light in the cross-frequency relations in the non-human primates hippocampus.

Another major interest is determining how the features of the bursts are related to different task conditions and behavior, akin to the analysis done in DOUCHAMPS et al. (2024). Here, there are additional layers of complexity since the monkeys are in a 3D cage and are free to perform a task at any time to receive a reward. One possible approach is to understand how the bursting statistics change when the monkey is, for example, idling, exploring, or performing the task. These behaviors correspond to variables of interest that can be decoded from the burst features using machine learning or information theory analysis.

Additionally, during the moments when the monkey performs the task, one could try to decode the stimuli identity from the burst features as well. In practice, this can be done by pooling burst events related to a given behavioral condition or stimulus for the moments the animals perform the task and training a decoder by feeding it the feature vectors. Alternatively, one can compute the mutual information between the feature vector and a discrete variable representing either a stimulus label or a behavior.

While the procedure above is typically done for the bursts extracted from each composite, one can also determine if the interaction between different frequencies is informative about the task. This can be achieved by including features in the feature vectors that correspond to, for example, phase-coupling between bursts from different composites. Alternatively, one could use frameworks like partial information decomposition to determine whether the interaction of bursts from different composites provides mostly redundant or synergistic information about a given task condition.

For example, synergy between burst features from a slow and a fast component and an external condition indicates that information about this condition is non-trivially distributed across these frequencies and can only be fully recovered by inspecting their interactions.

While here I discuss some perspectives related to characterizing computations that may be carried by those bursts. In Chapter 5, I will further discuss the perspectives

of this project in a broader context, i.e., relating it to the other results chapters. In particular, one major aspect we aim to uncover is how the bursts happening across different hippocampus layers organize spatially to support function. In this sense, looking for co-bursting motifs is not so different to what it was done in Chapter 2, and I will discuss it in a broader context in the General Discussion (Chapter 5).

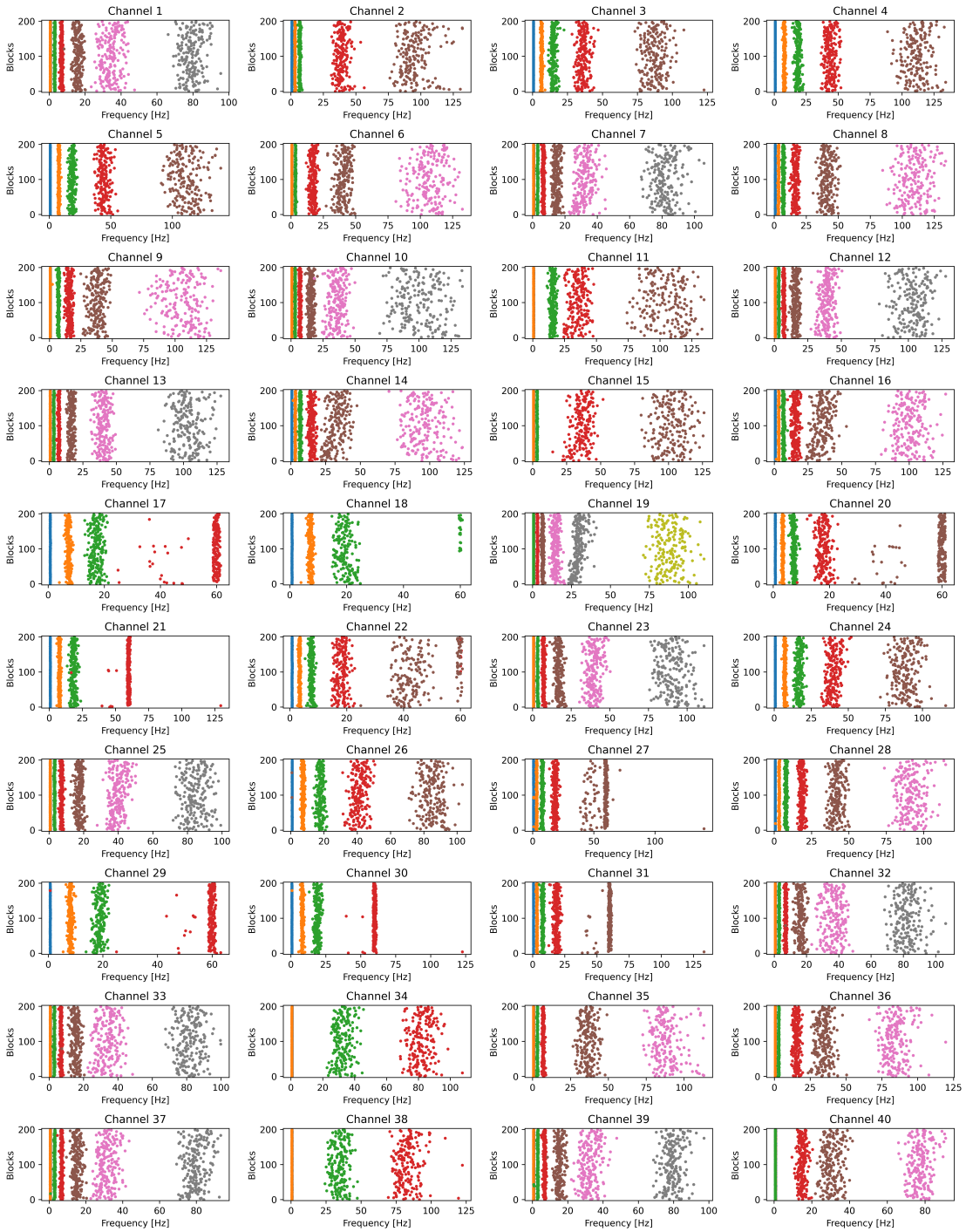

FIGURE 4.6. : Peak frequency for each composite signal detected across blocks for all channels of monkey F. In each subplot we show the peak frequency (horizontal axis) for each composite signal across each block (vertical axis) for a given channel (see subplot titles).

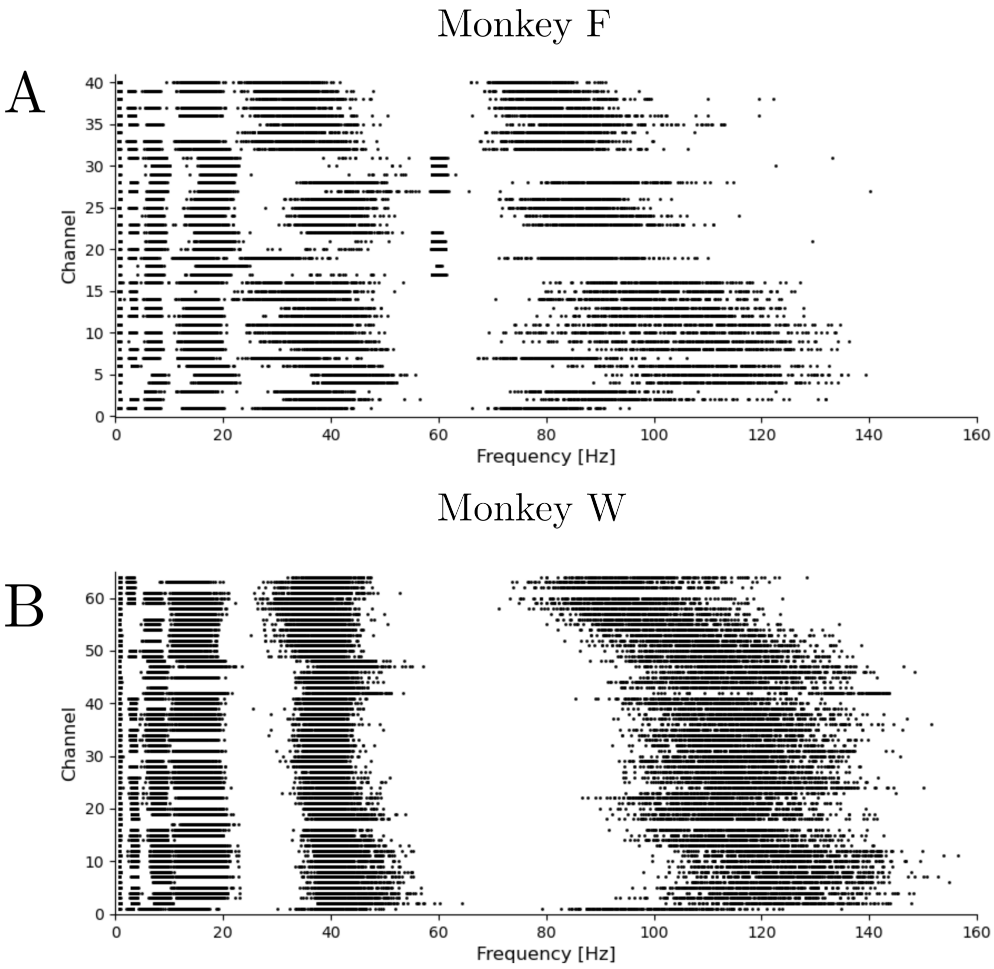

FIGURE 4.7. : Raster plot of frequency peaks. In (A), we show the frequency (horizontal axis) in which the power spectra of the composite signals peaks for each recording channel (vertical axis), for monkey F. In (B) we show the same for monkey W.

5. GENERAL DISCUSSION

Throughout this dissertation, we explored the question of how neuronal dynamics might reflect computations supporting cognitive functions. We sought to understand this relationship by relying on both data analysis and computational modeling of distributed cortical regions. In both cases, we focused on meso-scale dynamics derived from local field potential (LFP) recordings in multiple cortical areas supporting working memory. Specifically, in Chapter 2, we demonstrated the computational role of neuronal dynamics by providing evidence that it does not only contain stimulus-specific information during a working memory task (a proxy for memory maintenance), but it is associated with a set of "internal states" or "collective phenomena", formed by the coordination of transient oscillatory bursts (which we named *crackle* assemblies), to distribute and store this information across cortical areas during a visual working memory task. The methods for multi-frequency burst (or crackle) detection and characterization we develop in chapter 4 also aim at better assessing the relations existing between behavior and transient oscillatory activity, on the line of DOUCHAMPS et al. (2024).

Since in Chapter 2, we used an *ad-hoc* method for extracting transient packets of coordinated activity, we could not track the types of computations the interactions within crackle assemblies were performing or how they differed from correlations. Consequently, in Chapter 2, we used two types of models to better study the mechanistic role of crackle assemblies : feedforward connected ring models and a mean-field model built on the macaque connectome, both capable of implementing mechanisms of memory maintenance. In this study, we used tools from partial information decomposition (WILLIAMS et al. 2010; WIBRAL et al. 2017; LIZIER et al. 2018) to decompose the neuronal interactions among units in the ring and cortical areas in the large-scale model into a series of "information processing primitive" (IPP) metrics, corresponding to information storage, transfer, and modification (VOGES et al. 2024).

Interestingly, tracking these IPPs not only allowed us to quantify the algorithmic operations carried out by neuronal dynamics but also revealed emergent properties of the analyzed systems. Additionally, this theoretical work suggests that crackle assemblies may implement a rich set of coexisting computations. For example, in a given crackle assembly, some regions may be responsible for transferring information to another region that will then modify the input information, while others will store it.

Finally, in the last chapter, we analyzed hippocampal local field potential data recorded from two non-human primates, during sleep and task conditions. While I presented this project in its preliminary phase, where we first attempted to correctly detect and characterize transient oscillatory activity, its future development follows

the same path as the projects described above. Specifically, by categorizing a family of single-trial bursts, we seek to map behavior to their "real-time" dynamical substrates. Furthermore, we can delve into the level of multi-unit activity to understand how the spiking dynamics of different cell groups generate different categories of bursts,thereby helping to elucidate the connection between field and spiking activity.

In the remainder of this chapter, I will discuss in more detail the projects I presented from Chapters 2 to 4 . In particular, I will elaborate on why the activity we measure can be considered to reflect genuine computations used internally by the system to implement a given function, as well as the drawbacks and caveats of such an interpretation. Next, I will discuss how these projects contribute to the debate on transient versus sustained oscillation, which I first introduced in Section 1.4.4. Finally, I will conclude by discussing future perspectives for these projects and the ones that may derive from them.

5.1. Computation... but why ?

The idea of a "neural code" arises from considering the brain as an information-processing organ that transforms inputs by means of an unknown coding function, and it might be the first concept that comes to mind when discussing neuronal computation (BARLOW et al. 1961; BIALEK et al. 1989; EGGERMONT 1998; RIEKE et al. 1999; DAYAN et al. 2005; PANZERI et al. 2010; PANZERI et al. 2022). However, whether the information carried by this "code" is truly exploited by the nervous system remains unclear. More specifically, how can we claim that the computations we measure are internally exploited by the system and not merely useful for researchers to differentiate experimental conditions, thereby moving closer to the "inside-out" approach?

As I have previously discussed (see Section 1.2), one way to address this issue is by identifying features of the neural code in a given source population that impact the dynamics of a downstream target population. This paradigm is referred to as the reader-centric approach (BRITTEN et al. 1996; NEWSOME et al. 1989; BUZSÁKI 2010) and has stimulated ideas on how to properly identify such features. For instance, in PANZERI et al. (2017), the authors propose identifying the neural code by finding the intersection between features of neuronal activity that are informative about the stimulus and those informative about the behavioral choice of the animal, i.e., the readout. This procedure allows researchers to develop a better understanding of the neural code through behavioral tasks (KRAKAUER et al. 2017) and infer how certain features of neuronal activity causally impact behavior through single-trial stimulation (TEHOVNIK et al. 2006; PENG et al. 2015; O'CONNOR et al. 2013).

Here, instead of focusing on a specific neural code, we quantify neuronal computation that arises from the interaction among different brain areas. To achieve this, it is essential to distinguish between statistics that inform the experimenter about task-modulated dynamics and those that reflect operations resulting from neuronal populations acting on each other (Figure 5.1). If the information processing metrics of storage, transfer and modification quantify the computations emerging from the

direct action of neuronal population A on population B, then information theory can correctly capture computations that are internally implemented by the system [1].

Even though the neural code behind a specific computation is inaccessible by means of information theory alone, it can be accessed by further investigation of the system in question or via computational modeling (BUONOMANO et al. 2009; HARVEY et al. 2013; SHAMIR 2014; PANZERI et al. 2022). For example, in Chapter 3, we estimated information primitives using ring models. In these models, stimulus representation could be maintained in specific neurons, depending on the angular position of a given population. This stimulus could then be transferred via feedforward excitatory connections to other regions, emulating sensory information being sent from sensory to frontal areas. Later, the information could be modified when projected back and conflicted with new incoming input, as it happens in the match period of delayed match-to-sample tasks.

The same happens in the large-scale model that uses the macaque connectome as its structure. In this model, we found that information modification is implemented backwards; that is, frontal areas drive synergistic modification, consistent with the expected role of the PFC in top-down control, as discussed in Section 1.3.2. Most importantly, this was a property emerging from the interaction between dynamics and structure. Analogously, we have shown in Chapter 2 that collective self-organization is sufficient to account for the observed co-crackling dynamics, without need of additional ingredients to achieve distributed brain-wide coordination then the ones needed to generate oscillatory crackles and bursts locally within each region independently. Our results in large-scale connectome models thus generalize earlier predictions previously made for toy systems made of fewer interacting areas (PALMIGIANO et al. 2017).

[1] For instance, in a scenario where specific neuronal motifs can implement logical operations as described in VOGELS et al. (2005), the XOR gate configuration would be correctly captured by the primitive of modification.

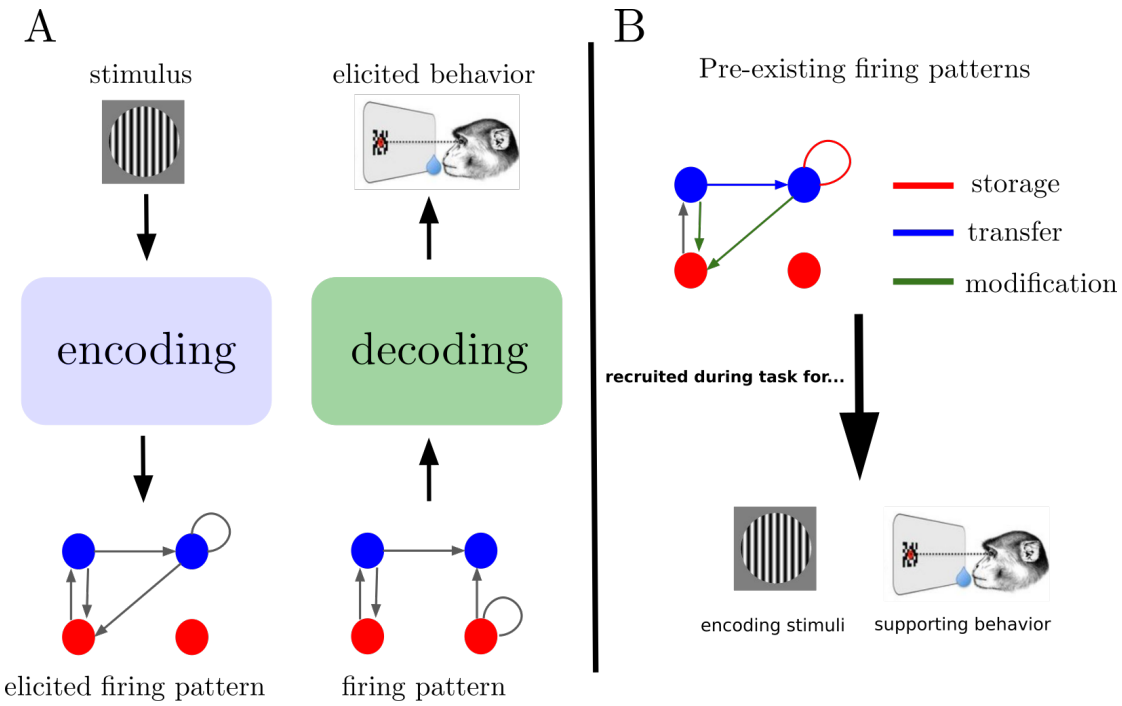

FIGURE 5.1. : Task-related statistics vs. metrics reflecting neuronal computation. In (A), we illustrate an approach where the conversion between stimulus and activity (left) or from activity to behavior (right) is carried out by an unknown coding function. In this scenario, statistics such as correlation and mutual information can be used to test causal relations between a given condition and the dynamics evoked during an experiment. However, they do not inform us about the specific computations these neuronal populations perform to support function. In (B), it is assumed that distinct neuronal populations have the intrinsic capability of implementing the computational primitives of storage, transfer, and modification (e.g., by means of lateral and recurrent excitation). These populations, characterized by different firing patterns, are then recruited during a task so their computational capabilities can be exploited to support function. The cartoon with the monkey doing a task was adapted from (SCHWEDHELM et al. 2017).

In both ring and connectome-based models, recurrent excitation plays a crucial role in creating stimulus storage within different populations, while long-range excitation facilitates information transfer. Most importantly, spatial differentiation—achieved via angular preference and the feedforward structure in the ring model, and through the macaque connectome in the large-scale model—was essential for information modification to occur. These details help to unveil the mechanism by which the measured computations are implemented in neural systems.

Additionally, these results suggest that top-down and bottom-up propagation may correspond to distinct processes in terms of information decomposition. This may also allow us to hypothesize about the computational roles of feedback and feedforward CrAs in the first study. More generally, we hypothesize that bottom-up processes are dominated by redundancy in a feedforward architecture, whereas top-down processes, with convergence from several areas to lower levels, may be more synergy-dominated.

While in the models, the simulated activity represented the firing rate of neuronal populations. In the brain, activity spans multiple temporal and spatial scales, from single neurons to entire brain regions, potentially offering a rich repertoire of dynamics for computation to take place. On one hand, the highly organized structural connectivity of the brain sets the basic blueprint by which neuronal populations can interact. On the other hand, there is flexibility for neurons to create connections during development and throughout life by establishing novel synaptic connections. This flexibility allows the system to self-organize through learning.

Additionally, this organization seems to provide a balance between the brain's capability to integrate and segregate information by exploiting network properties that permit efficient communication while optimizing wiring cost and robustness (see Section 1.4.2; VANDIERENDONCK 2016; CHRISTOPHEL et al. 2017; DOTSON et al. 2017; DOTSON et al. 2018). Some of these properties, such as small-worldness, enable the exchange of information across widespread brain areas via the transient coupling of their local dynamics (WATTS et al. 1998; BASSETT et al. 2006). Consequently, while brain structure constrains the pathways through which information can flow, it is through dynamics and functional interactions that information processing in the brain takes place on timescales compatible with changes in the environment, potentially supporting a range of cognitive functions essential for survival (BATTAGLIA et al. 2020).

In this way, dynamics not only serve as the intermediate level linking structure and function, but it also reflects how neuronal populations internally self-organize to efficiently process information. This self-organization gives rise to the co-crackling assemblies we found to support stimulus encoding during working memory. Therefore, while the measurement of stimulus encoding is a statistic that informs the experimenter on how to map the observed dynamics to a given input, the crackling assemblies reflect internal system states, capturing how cortical areas interact to support working memory[2].

The role of crackles in distributing information is illustrated by the fact that assemblies capture feedforward and feedback patterns of activity across cortical areas. Most interestingly, we have shown evidence that many assemblies are present even under baseline conditions. Specifically, in the large-scale model, the crackle assemblies that correlated with those measured empirically were observed in the resting state without any stimuli applied. This results seems to support the idea of the pre-configured brain model, in which available brain states are assigned to distinct events[3] according to

[2] One can think of the presentation of the stimulus as a perturbation on the complex system, resulting in an internal reorganization of states that is reflected as different computations. In information theoretical terms, one can consider the measurement of a specific computation primitive between a group of neurons during both resting state and a task. The first measurement quantifies the intrinsic capacity of those neurons to create the specific IPP, while the task-related measurement reveals how this capacity is exploited by the task (e.g., as we have done in Chapter 3 when we measured storage and stimulus-specific storage).

[3] Or by thinking of the system as a Liquid State Machine (Figure 5.1B; GRZYB et al. 2009; MAASS 2011) where co-crackle assemblies would correspond to out-of-equilibrium transients (so in this case there not really attractor states) indicating that the liquid computation is over and that a remote

their relevance or frequency via learning (BUZSÁKI et al. 2022; BUZSÁKI et al. 2023). In this setting, those patterns could - for example - correspond to attractor states to which collective dynamics is pushed to in order for stimuli representation to be refreshed (SANDBERG et al. 2003; LUNDQVIST et al. 2016; MONGILLO et al. 2018; BARBOSA et al. 2020).

To finalize, in Section 1.5, I began to explore the equivalence between dynamics and information using examples coming from theoretical work using cellular automata (SHAW 1984; LANGTON 1990). Those studies proposed the insightful idea that computation arises in complex systems that are on the verge of a phase transition from order to chaos. Intuitively, computation emerges in this regime because the system displays dynamics containing patterns of activity with long transients. Specifically, these patterns can either repeat themselves locally or propagate across the spatial extent of the system, thereby implementing the operations of storage and transfer,respectively. Additionally, propagating patterns can interact such that information propagating from position A is transformed when it interacts with information contained at position B, thus implementing modification.

The brain, as a complex system, seems to fulfill the necessary conditions to implement computation. First, cortical dynamics is thought to lie close to a critical point or phase transition, as discussed in Section 1.5.3. In Chapter 2, the crackle assemblies we detected displayed sizes and durations that followed a power-law distribution - a necessary but not sufficient condition of criticality. Notability, lying at the vicinity of a critical point is often associated with optimality in information processing and computation, as I have discussed in Section 1.5 (SHEW et al. 2011). This was also reflected in the high correlation between the temporal and spatial factors representing crackling probability across frequency bands, indicating a phenomenon broadcasted across many spatial, temporal, and spectral scales. Finally, we found that patterns of co-crackling in a large-scale model of the macaque cortex better predict empirical data when the model is near a phase transition.

Second, across scales, the brain exhibits spatial differentiation that allows tracing activity back to specific neuronal populations. At the same time, local dynamics is mostly likely influenced by inputs arriving from remote cortical areas and other brain structures, such as the thalamus and hippocampus. Consequently, in a given cortical region, information storage can be achieved by preserving local dynamics, information transfer can occur through inputs sent between regions, and transformation can happen via the interaction of local and distributed dynamics. Such a state, where those computations can take place are thought to emerge in the brain due to a fine equilibrium between its capability to integrate and segregate information (TONONI et al. 1998).

Consequently, exploring the nervous system from a computational perspective is not only valid, but it can also unveil important aspects of information processing that support diverse cognitive functions. Furthermore, contrary to what is stated in BUZSÁKI et al. (2023), information processing can be well-defined in terms of quanti-

reader can read out its outcome. More generally, the system could be conceptualized as a "reservoir" (SUSSILLO et al. 2009; JAZAYERI et al. 2021).

fiable metrics that operate on dynamics to track algorithmic operations. Additionally, the conceptualization of the nervous system in the three levels — structural, algorithmic, and functional — where dynamics reflects algorithmic operations (as outlined above and discussed in Chapter 3; MARR et al. 1976a), does not necessarily imply an outside-in view of the nervous system. Rather, it represents a general hierarchical organization displayed by self-organized complex systems (ROSAS et al. 2024).

5.2. Bursting activity and computation

Neuronal dynamics exhibit enormous variability from the micro- to the mesoscopic level. As I have discussed throughout this dissertation, a characteristic marker of this variability in the dynamics at the mesoscopic level are bursts of activity. Usually, bursts are strong transient fluctuations that can be detected as bouts in the time-frequency domain, possessing a characteristic frequency and duration. In Section 1.4.4, I highlighted an increasing number of studies reporting the relevance of burst activity in a range of cognitive functions (FEINGOLD et al. 2015; LUNDQVIST et al. 2016; PALMIGIANO et al. 2017; MIRZAEI et al. 2017; MILLER et al. 2018; LUNDQVIST et al. 2018; LUNDQVIST et al. 2024; DOUCHAMPS et al. 2024). Here, we build on those studies and consider bursts as a tentative candidate to implement computation on faster timescales, as required by working memory. We stressed the relevance of mechanisms capable of doing so; after all, whatever processing that happens in the brain allowing us to not only mentally represent the world but also interact with it must occur on relatively fast scales. In this scenario, bursts could be the mean by which representations are "refreshed" via activity replays similar to what is observed in prospective sequences (FERBINTEANU et al. 2003; WANG et al. 2020).

Here, we aimed to understand how this kind of activity could support integration among multiple cortical areas during a working memory task, hence allowing information to be transformed from a local to a distributed (or network) representation. Our main contribution to interpreting bursts as relevant markers of information processing in the brain was to show that cortical areas can form transient coalitions, which we named co-crackling assemblies, allowing for non-linear integration of information (VINCK et al. 2023). These assemblies could predict stimulus encodability and also revealed the sequencing of activity propagation during the working memory task. Interestingly, the basic entities of co-crackling assemblies (i.e., the crackles) were somewhat more general than bursts, as they included relatively weak upward modulations that were nonetheless useful for predicting encoding in visual and motor areas. In this study, although we did not formally calculate the computations performed by crackles and co-crackling using the tools from Chapter 3, we could infer their computational role in supporting memory maintenance by relating it to function. In particular, we conjectured that those assemblies could favor both cortico-wide integration as well as distributed representation by means of their coordinated activity (communication-through-coordination; Coh-T-Coord).

Another important aspect raised by this study is the importance of characterizing

modulations in neuronal activity as behavior goes on. As suggested in Chapter 3, for the quantification of computation, the temporal dimension is essential[4]. In fact, drawing a relation between specific events in neuronal dynamics (without necessarily quantifying computation) requires detecting those events of interest and then relating their properties to a given function, since averaging would most likely suppress those events. For instance, in PALMIGIANO et al. (2017) the authors computed information transfer in an event-based fashion, rather than relying on averaging. Similarly, here, since crackles were rarely trial-locked, we computed statistics based on the aggregation of events (our co-crackling and propagation scaffolds) rather than taking trial averages. Analogously,we intend to first categorize the hippocampal burst events from Chapter 4, following the strategy in DOUCHAMPS et al. (2024), before delving into their functional role.

These strategies can potentially help to disambiguate the role of oscillatory activity in favoring communication in the cortex. To illustrate how the crackling analysis can contribute to comprehending how communication may be mediated by transient activity, I presented a new preliminary result. Already in Chapter 2, we explored the relation between co-crackling activity and communication-through-coherence (CTC). As I have discussed there, we had good reasons to expect that the Coh-T-Coord comprises CTC. Firstly, co-crackling is essentially the coincidence of upward modulation in the power time-series. If phase-locking is achieved during those transient oscillatory events, then mathematically, coherence should be observed. We motivated this intuition by showing that the instantaneous correlations of power envelopes usually coincides with single-trial bouts in the time-frequency coherence spectrogram.

This is better appreciated by plotting the histogram of the power envelope correlation for the values obtained across trials (Figure 5.2D, E left), which reveals that power co-fluctuations for channels 103-17 are considerably above chance level. To investigate whether these co-occurring bursts can mediate communication during transient events, we can inspect the phase relation between these channel pairs during burst events (Figure 5.2D, E right). In fact, channels 103-125 tend to phase-lock their alpha activity during moments of co-bursting, suggesting that, in principle, these events could be exploited to implement communication as proposed in the modeling work by (PALMIGIANO et al. 2017). Notice that the alpha band is not usually thought to mediate CTC, even though the observation in Figure 5.2 holds for the beta band for those channels. However, for faster frequencies, the mechanisms underlying communication may correspond to state selection (the system collectively enters a different state, of which co-bursting is a signature, as observed) when phase synchrony is not observed (e.g., channel pairs that displayed high co-crackling but weak oscillatory power in the beta or gamma bands in Chapter 2).

[4]Even if it is true that in this modeling study, trial averaging was not so problematic since, in the simulations, they were structured roughly in the same way

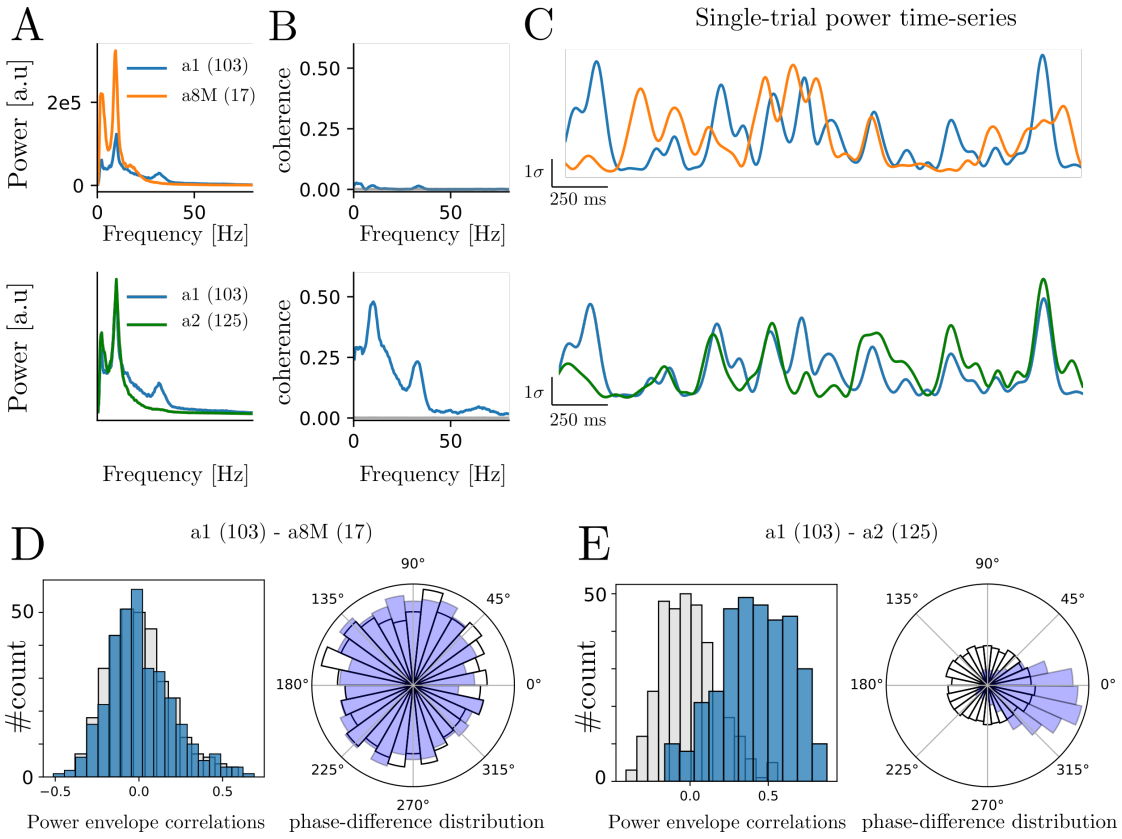

FIGURE 5.2. : CTC from transient co-bursting In (A), we show the trial-averaged power spectrum for channels 103 in a1, 17 in a8M (top), and 103 and 125 in a2 (bottom). In (B), we show the trial-averaged squared coherence between these pairs of channels (gray shaded area indicates the chance level measured with trial-swapping surrogates). In (C), we show the single-trial power time-series in the alpha band (5-15 Hz) for each of those channels. In (D) on the left, we show the distribution of power envelope correlations (chance level in gray), and on the right, the distribution of phase differences for moments where the instantaneous correlations of time-series in (C) surpassed 3 STDs, for the pair of channels 103-17. In (E), we show the same for the pair of channels 103-125.

In the example given in Figure 5.2, the functional role of the bursts found to implement CTC, by for instance detecting the coherence networks related to stimulus encoding or other control aspects related to working memory, as we have done with the co-crackling analysis in Chapter 2[5] .

5.3. Future directions

In our first project, we have gathered substantial evidence indicating that neuronal collective dynamics, facilitated by transient co-bursting across widespread cortical

[5]As a matter of fact, the procedure above may even help to elucidate weirder situations, where coherence emerges between a region with no power in a given band and other with strong power, an issue we have called ghost coherence and was also investigated elsewhere (SCHNEIDER et al. 2021)

areas, can implement complex information processing operations that support critical cognitive functions such as working memory.

The first development direction involves characterizing the actual computational primitives associated with different co-crackling motifs. This includes examining how these primitives change for different crackling phenotypes (e.g., bursts of oscillatory activity versus non-oscillatory weaker upward excitability), brain regions involved, and task conditions (e.g., incorrect versus correct trials). Understanding how specific computations depend on the elements that give rise to them is a significant problem - that interests me greatly - in both neuroscience and the broader context of complex systems (MARINAZZO et al. 2019; MEDIANO et al. 2022; WIBRAL et al. 2017; VARLEY et al. 2024).

The second development builds on the evidence of collective coding during working memory by rigorously characterizing crackle-assemblies within the framework of high-order interactions (HOI). Since the beginning of my thesis, the investigation of HOIs in the brain has gained significant momentum, and numerous tools for their investigation, derived from information theory and network science, have been developed (PETRI et al. 2014; ROSAS et al. 2019; MEDIANO et al. 2019; BATTISTON et al. 2020; CHAZAL et al. 2021; ROSAS et al. 2022; VARLEY et al. 2023a; BETZEL et al. 2023; LUPPI et al. 2022; VARLEY et al. 2024). In the long term, the conjunctions of these two developments could shed light on how high-order mechanisms emerge from their constituent parts and what computations are associated with specific functions of complex systems (LUPPI et al. 2021; ROSAS et al. 2024).

Lastly, the developments of the project presented in Chapter 4 can potentially contribute to understanding the role of bursting activity in the hippocampus. Besides the future plans I discussed in Section 4.3, one way we plan to explore the relation of different burst phenotype (here represented by the bursts' feature vector; Figure 5.3A) to behavior is by inspecting the rate of occurrence of specific functional motifs formed across channels (depth) and frequencies for a given behavioral state (assuming we have a set of discrete behavioral states during the task, such as sleep, exploration, task, etc). In practice, these motifs can be identified by considering each burst detected in a channel as a unit and constructing its "spike-train" based on its onset and offset. For a single channel, these bursts can be sorted by their central frequency The same construction can be extended by combining channels, and motifs can be found using techniques similar to those we applied for detecting crackling assemblies (Figure 5.3C).

In Figure 5.3D, I present a pictorial illustration of three of these motifs. In the cartoon, each column represents a recording channel, and each row represents a center frequency. The size of the nodes indicates how often a channel exhibits a burst at the corresponding center frequency. The color of the edges indicates which channels tend to co-burst at the given frequencies, and the edge colors indicate the behavioral condition in which this co-bursting occurs. Furthermore, the computational role of these motifs can be investigated using the tools presented in Chapter 3, as discussed in Section 4.4. Notice that these motifs correspond to the spectral fingerprints proposed in SIEGEL et al. (2012), where motifs of collaborating areas would be responsible for implementing distinct computations multiplexed across frequency bands. In our case,

co-crackle assemblies show that these motifs are contained within the hippocampus but formed across layers.

Finally, another important aspect of the burst characterization we are pursuing in this study is the potential to link field activity to its neuronal substrate. More specifically, bursts generated by distinct channels may exhibit different phenotypes (LUNDQVIST et al. 2024), and since there is a relationship between cell type and recording depth in the hippocampus (ABBASPOOR et al. 2023a), it might be possible to uncover the connection between cell type and burst phenotype (Figure 5.2B). This, in turn, could reveal the neuronal origins of the burst motifs illustrated in Figure 5.2D.

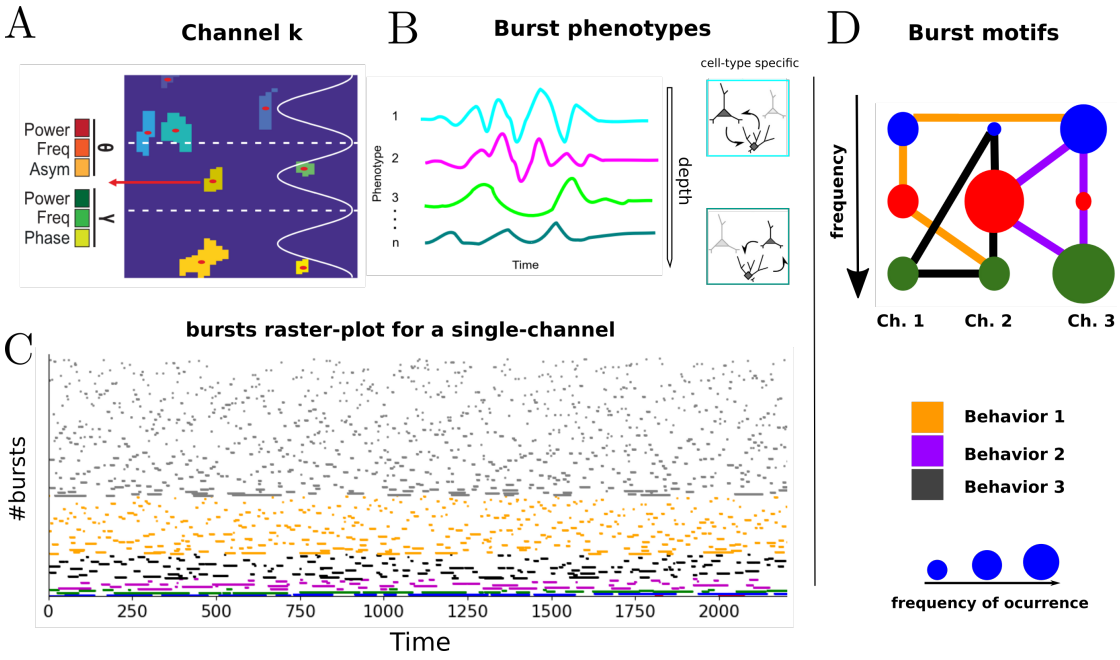

FIGURE 5.3. : From burst motifs to behavior. In (A) we show bursts detected in the time-frequency domain, each color depicts one detected burst. To each burst a vector containing its features is stored (adapted from DOUCHAMPS et al. 2024). In (B) we show that bursts may have different phenotypes, i.e., shapes. Different phenotypes might be due to the underlying spiking activity and cell types that generate a burst (for instance in the cartoon the light blue and dark red phenotypes are generated by different neuronal interactions; adapted from LUNDQVIST et al. 2024). In (C), we show a raster plot containing bursts detected in a single channel the colored bars indicates that a specific burst is active, while colors encode the burst frequency (not their central frequency but the frequency of the composite signal in which they were detected; see Chapter 3), which is increasing from top to bottom. In (D), we show a cartoon representing burst motifs across depth (channels, columns) and frequencies analyzed (rows). In the cartoon, the size of each node represents the frequency of occurrence of bursts in a specific frequency band for a given channel. The edges indicate which types of bursts tend to co-occur and its color indicates in which behavioral condition this happens.

5.4. Conclusion

During the discussion above, we have seen that burst activity is a fundamental signature of local processing across the cortex and hippocampus. Additionally, the local or widespread coordination of bursts may be a fingerprint of distinct computations supporting cognitive functions. But by which mechanisms the coordination of local activity allows integration of information? In Chapter 2, we proposed three alternative scenarios in which co-crackling activity might reflect different integration mechanism :

1. During limited times crackles can be as strong as bursts, hence communication can be established as posed by the CTC hypothesis ;
2. There are no real oscillations but the statistics of the measured fluctuations are driven by inputs or brain state.
3. Oscillations cannot mediate excitability modulations, but their coordination indicates selection of a specific collective dynamics mode ;

Scenario 1 is equivalent to state that crackles are bursts, i.e., transient oscillations, capable of implementing CTC. In which case, the sparsity of crackle events would indicate that CTC happens sporadically but with high efficiency, or some of the crackles are misdetected as not being bursts because of some artifactual (e.g., a problem on the recording apparatus or the relative position of the electrode to the recorded population) reason but would be really able to modulate neuronal excitability if we could measure intracellularly.

Scenario 2 corresponds to the coh-through-comm, in which coherence emerges not from spike entrainment between a pair of areas but from afferent synaptic connections between a sender and receiver area that are structurally connected. In particular, spiking activity in the sender area drives synaptic activity both in itself and in the receiver area. This activity is reflected in the LFPs of both areas and may be captured as coherence.

Scenario 3 corresponds to the compromise scenario we proposed (Coh-T-Coord) and includes two possibilities. In one, co-crackling is epiphenomenal of the global "information processing state" selected, with only the state itself being functional (e.g., alpha state rather than beta state). The other possibility is that co-crackling is collectively functional : a single crackle modulates target excitability very little, but many synchronous crackles together modulate it sufficiently to open a channel for integrative transfer. Here, there is intrinsically a higher-order link (from any coordinated sources to a reader) rather than a sum of individual links.

While there are clear instances where scenario 1 applies, such as in the example in Figure 5.2, I do not like to think of coherence as a mechanism. Coherence is merely a way to quantify the orchestrated activity of widespread local neuronal populations (here measured as bursts). It cannot disentangle which neurons are actually generating the bursting in different conditions (e.g., distinct stimuli), which constitutes the real

mechanisms. It is true that bursts generated by distinct neuronal populations may result in slight modulations in power and coherence, which can be captured by mutual information or machine learning analysis. However, coherence is, in my opinion, a consequence of orchestrated neuronal communication, not a cause. Additionally, the emergence of phase-locking and power correlations, as seen in Figure 5.2, seems to be evident only for pairs of areas with a strong oscillatory component in the frequency band analyzed.

Other examples, such as beta-band coherence between motor and visual areas (which have close to no power in the beta band), seem to be better explained by scenario 2. One possibility is that bursts might be generated in areas with higher spiking activity in the source region, while crackles may be weaker reverberations of this activity detected in the target area. In both cases, some reflection of their intercommunication is being captured; hence, their statistics may be relevant (as shown in Chapter 2) for explaining their functional role. Finally, another possibility is that stronger bursts help drive the system to a given selected state, and other areas with weaker power are driven into the same state as a consequence of synaptic reverberations arriving from those "stronger" areas. Once the collective state is selected, even those weaker areas are capable of causing excitations through crackling coordination, as proposed in scenario 3.

In summary, it seems reasonable to expect a variety of mechanisms to drive brain integration, depending on the task, context, and behavior. The alternative would be to admit that a system as complex as the brain can be explained by a theory of coupled oscillators, which, while possible, is difficult for me to believe. In a general context, the view we presented here proposes a general mechanism for the connectivist perspective in the cognitive sciences. This perspective suggests that low-level processing in the brain is achieved through the self-organized internal coherence of the system, emerging through co-crackling coordination. In contrast, high-level processing might rely on symbolic processing, which, in this case, could be represented by the global system states achieved through the coordinated activity of cortical areas.

Bibliographie

[AH23] Saman ABBASPOOR et Kari L HOFFMAN. « State-dependent circuit dynamics of superficial and deep CA1 pyramidal cells in macaques ». In : *bioRxiv* (2023), p. 2023-12 (cf. p. 160, 189).

[AHH23] Saman ABBASPOOR, Ahmed T HUSSIN et Kari L HOFFMAN. « Theta-and gamma-band oscillatory uncoupling in the macaque hippocampus ». In : *Elife* 12 (2023), e86548 (cf. p. 164-166, 174).

[Adr50] ED ADRIAN. « The electrical activity of the mammalian olfactory bulb ». In : *Electroencephalography and clinical neurophysiology* 2.1-4 (1950), p. 377-388 (cf. p. 39).

[Adr42] Edgar D ADRIAN. « Olfactory reactions in the brain of the hedgehog ». In : *The Journal of physiology* 100.4 (1942), p. 459 (cf. p. 39).

[Adr34] Edgar Douglas ADRIAN. « Electrical activity of the nervous system ». In : *American Journal of EEG Technology* 8.1 (1934), p. 25-36 (cf. p. 28, 38).

[Aer+89] AM AERTSEN, GL GERSTEIN, MK HABIB et al. « Dynamics of neuronal firing correlation : modulation of" effective connectivity" ». In : *Journal of neurophysiology* 61.5 (1989), p. 900-917 (cf. p. 150).

[Ain+12] Matt AINSWORTH, Shane LEE, Mark O CUNNINGHAM et al. « Rates and rhythms : a synergistic view of frequency and temporal coding in neuronal networks ». In : *Neuron* 75.4 (2012), p. 572-583 (cf. p. 55).

[Ale+04] M ALEGRE, IG GURTUBAY, A LABARGA et al. « Frontal and central oscillatory changes related to different aspects of the motor process : a study in go/no-go paradigms ». In : *Experimental brain research* 159 (2004), p. 14-22 (cf. p. 38).

[Alp+06] Kenneth R ALPER, E Roy JOHN, Jonathan BRODIE et al. « Correlation of PET and qEEG in normal subjects ». In : *Psychiatry Research : Neuroimaging* 146.3 (2006), p. 271-282 (cf. p. 37).

[Ami95] Daniel J. AMIT. « The Hebbian paradigm reintegrated : Local reverberations as internal representations ». In : *Behavioral and Brain Sciences* 18.4 (1995), 617–626. DOI : 10.1017/S0140525X00040164 (cf. p. 25).

[AB97] Daniel J AMIT et Nicolas BRUNEL. « Model of global spontaneous activity and local structured activity during delay periods in the cerebral cortex. » In : *Cerebral cortex (New York, NY : 1991)* 7.3 (1997), p. 237-252 (cf. p. 25).

[AKP13] Michael L ANDERSON, Josh KINNISON et Luiz PESSOA. « Describing functional diversity of brain regions and brain networks ». In : *Neuroimage* 73 (2013), p. 50-58 (cf. p. 18).

[Aok+01] F AOKI, EE FETZ, L SHUPE et al. « Changes in power and coherence of brain activity in human sensorimotor cortex during performance of visuomotor tasks ». In : *Biosystems* 63.1-3 (2001), p. 89-99 (cf. p. 91).

[AWC07] Salva ARDID, Xiao-Jing WANG et Albert COMPTE. « An integrated microcircuit model of attentional processing in the neocortex ». In : *Journal of Neuroscience* 27.32 (2007), p. 8486-8495 (cf. p. 26, 115, 119, 137, 138).

[Ard+10] Salva ARDID, Xiao-Jing WANG, David GOMEZ-CABRERO et al. « Reconciling coherent oscillation with modulationof irregular spiking activity in selective attention : gamma-range synchronization between sensoryand executive cortical areas ». In : *Journal of Neuroscience* 30.8 (2010), p. 2856-2870 (cf. p. 34, 115, 148).

[ASZ22] Mahnaz ASHRAFI et Hamid SOLTANIAN-ZADEH. « Multivariate Gaussian Copula Mutual Information to Estimate Functional Connectivity with Less Random Architecture ». In : *Entropy* 24.5 (2022), p. 631 (cf. p. 68).

[AG03] Rony AZOUZ et Charles M GRAY. « Adaptive coincidence detection and dynamic gain control in visual cortical neurons in vivo ». In : *Neuron* 37.3 (2003), p. 513-523 (cf. p. 40).

[BB14] Behtash BABADI et Emery N BROWN. « A review of multitaper spectral analysis ». In : *IEEE Transactions on Biomedical Engineering* 61.5 (2014), p. 1555-1564 (cf. p. 43, 167).

[Bab+06] Claudio BABILONI, Fabrizio VECCHIO, Alessandro BULTRINI et al. « Pre- and poststimulus alpha rhythms are related to conscious visual perception : a high-resolution EEG study ». In : *Cerebral cortex* 16.12 (2006), p. 1690-1700 (cf. p. 38).

[Bad92] Alan BADDELEY. « Working Memory ». In : *Science* 255.5044 (1992), p. 556-559. DOI : 10.1126/science.1736359. eprint : https://www.science.org/doi/pdf/10.1126/science.1736359. URL : https://www.science.org/doi/abs/10.1126/science.1736359 (cf. p. 23, 24).

[Bad96] Alan BADDELEY. « Exploring the central executive ». In : *The Quarterly Journal of Experimental Psychology Section A* 49.1 (1996), p. 5-28 (cf. p. 26).

[Bad00] Alan BADDELEY. « The episodic buffer : a new component of working memory ? » In : *Trends in cognitive sciences* 4.11 (2000), p. 417-423 (cf. p. 23).

[Bad12] Alan BADDELEY. « Working memory : Theories, models, and controversies ». In : *Annual review of psychology* 63.1 (2012), p. 1-29 (cf. p. 22, 23).

[BH01] Alan D BADDELEY et Graham HITCH. *Working memory in perspective*. Psychology Press, 2001 (cf. p. 23).

[BMKK20] Arash BADIE-MODIRI, Márton KARSAI et Mikko KIVELÄ. « Efficient limited-time reachability estimation in temporal networks ». In : *Physical Review E* 101.5 (2020), p. 052303 (cf. p. 69, 79).

[BTW88] Per BAK, Chao TANG et Kurt WIESENFELD. « Self-organized criticality ». In : *Physical review A* 38.1 (1988), p. 364 (cf. p. 45).

[BLK22] Ben BAKER, Benjamin LANSDELL et Konrad P KORDING. « Three aspects of representation in neuroscience ». In : *Trends in cognitive sciences* 26.11 (2022), p. 942-958 (cf. p. 21).

[BT08] David BALDUZZI et Giulio TONONI. « Integrated information in discrete dynamical systems : motivation and theoretical framework ». In : *PLoS computational biology* 4.6 (2008), e1000091 (cf. p. 52).

[BA99] Albert-László BARABÁSI et Réka ALBERT. « Emergence of scaling in random networks ». In : *science* 286.5439 (1999), p. 509-512 (cf. p. 36).

[BRC97] Helen BARBAS et Nancy REMPEL-CLOWER. « Cortical structure predicts the pattern of corticocortical connections. » In : *Cerebral cortex (New York, NY : 1991)* 7.7 (1997), p. 635-646 (cf. p. 39).

[Bar17] Joao BARBOSA. « Working memories are maintained in a stable code ». In : *Journal of Neuroscience* 37.35 (2017), p. 8309-8311 (cf. p. 91).

[Bar+20] Joao BARBOSA, Heike STEIN, Rebecca L MARTINEZ et al. « Interplay between persistent activity and activity-silent dynamics in the prefrontal cortex underlies serial biases in working memory ». In : *Nature neuroscience* 23.8 (2020), p. 1016-1024 (cf. p. 91, 184).

[Bar+61] Horace B BARLOW et al. « Possible principles underlying the transformation of sensory messages ». In : *Sensory communication* 1.01 (1961), p. 217-233 (cf. p. 180).

[BDR16] Jérémie BARRAL et Alex D REYES. « Synaptic scaling rule preserves excitatory–inhibitory balance and salient neuronal network dynamics ». In : *Nature neuroscience* 19.12 (2016), p. 1690-1696 (cf. p. 56).

[Bar15] Adam B BARRETT. « Exploration of synergistic and redundant information sharing in static and dynamical Gaussian systems ». In : *Physical Review E* 91.5 (2015), p. 052802 (cf. p. 124, 149).

[BN31] S Howard BARTLEY et Edwin B NEWMAN. « Studies on the dog's cortex : I. The sensori-motor areas ». In : *American Journal of Physiology-Legacy Content* 99.1 (1931), p. 1-8 (cf. p. 28).

[Bar+02] Marlene BARTOS, Imre VIDA, Michael FROTSCHER et al. « Fast synaptic inhibition promotes synchronized gamma oscillations in hippocampal interneuron networks ». In : *Proceedings of the National Academy of Sciences* 99.20 (2002), p. 13222-13227 (cf. p. 31).

[BVJ07] Marlene BARTOS, Imre VIDA et Peter JONAS. « Synaptic mechanisms of synchronized gamma oscillations in inhibitory interneuron networks ». In : *Nature reviews neuroscience* 8.1 (2007), p. 45-56 (cf. p. 33, 34).

[Baş90] E BAŞAR. « Chaotic dynamics and resonance phenomena in brain function : Progress, perspectives, and thoughts ». In : *Chaos in Brain Function : Containing Original Chapters by E. Başar and TH Bullock and Topical Articles Reprinted from the Springer Series in Brain Dynamics*. Springer, 1990, p. 1-30 (cf. p. 38).

[Baş+97] E BAŞAR, Martin SCHÜRMANN, C BAŞAR-EROGLU et al. « Alpha oscillations in brain functioning : an integrative theory ». In : *International journal of psychophysiology* 26.1-3 (1997), p. 5-29 (cf. p. 38).

[Baş13] Erol BAŞAR. « A review of gamma oscillations in healthy subjects and in cognitive impairment ». In : *International Journal of Psychophysiology* 90.2 (2013), p. 99-117 (cf. p. 28).

[BD16] Erol BAŞAR et Aysel DÜZGÜN. « How is the brain working? : research on brain oscillations and connectivities in a new "take-off" state ». In : *International Journal of Psychophysiology* 103 (2016), p. 3-11 (cf. p. 28).

[BG08] Erol BAŞAR et Bahar GÜNTEKIN. « A review of brain oscillations in cognitive disorders and the role of neurotransmitters ». In : *Brain research* 1235 (2008), p. 172-193 (cf. p. 28).

[Bas+10] Danielle S BASSETT, Daniel L GREENFIELD, Andreas MEYER-LINDENBERG et al. « Efficient physical embedding of topologically complex information processing networks in brains and computer circuits ». In : *PLoS computational biology* 6.4 (2010), e1000748 (cf. p. 36).

[Bas+11] Danielle S BASSETT, Nicholas F WYMBS, Mason A PORTER et al. « Dynamic reconfiguration of human brain networks during learning ». In : *Proceedings of the National Academy of Sciences* 108.18 (2011), p. 7641-7646 (cf. p. 41).

[BB06] Danielle Smith BASSETT et ED BULLMORE. « Small-world brain networks ». In : *The neuroscientist* 12.6 (2006), p. 512-523 (cf. p. 36, 183).

[Bas+15] Andre Moraes BASTOS, Julien VEZOLI, Conrado Arturo BOSMAN et al. « Visual areas exert feedforward and feedback influences through distinct frequency channels ». In : *Neuron* 85.2 (2015), p. 390-401 (cf. p. 39).

[BB20] Demian BATTAGLIA et Andrea BROVELLI. « Functional connectivity and neuronal dynamics : insights from computational methods ». In : *The Cognitive Neurosciences, Sixth Edition* (2020) (cf. p. 65, 183).

[BBH07] Demian BATTAGLIA, Nicolas BRUNEL et David HANSEL. « Temporal Decorrelation of Collective Oscillations in Neural Networks<? format?> with Local Inhibition and Long-Range Excitation ». In : *Physical review letters* 99.23 (2007), p. 238106 (cf. p. 31).

[BH11] Demian BATTAGLIA et David HANSEL. « Synchronous chaos and broad band gamma rhythm in a minimal multi-layer model of primary visual cortex ». In : *PLoS computational biology* 7.10 (2011), e1002176 (cf. p. 31, 115, 148).

[Bat+12] Demian BATTAGLIA, Annette WITT, Fred WOLF et al. « Dynamic effective connectivity of inter-areal brain circuits ». In : *PLoS computational biology* 8.3 (2012), e1002438 (cf. p. 123, 148).

[Bat+20] Federico BATTISTON, Giulia CENCETTI, Iacopo IACOPINI et al. « Networks beyond pairwise interactions : Structure and dynamics ». In : *Physics Reports* 874 (2020), p. 1-92 (cf. p. 19, 59, 60, 188).

[BGR01] Matthew BEAL, Zoubin GHAHRAMANI et Carl RASMUSSEN. « The Infinite Hidden Markov Model ». In : *Advances in Neural Information Processing Systems*. Sous la dir. de T. DIETTERICH, S. BECKER et Z. GHAHRAMANI. T. 14. MIT Press, 2001. URL : https://proceedings.neurips.cc/paper_files/paper/2001/file/e3408432c1a48a52fb6c74d926b38886-Paper.pdf (cf. p. 44).

[BP03] John M BEGGS et Dietmar PLENZ. « Neuronal avalanches in neocortical circuits ». In : *Journal of neuroscience* 23.35 (2003), p. 11167-11177 (cf. p. 55, 56).

[BP04] John M BEGGS et Dietmar PLENZ. « Neuronal avalanches are diverse and precise activity patterns that are stable for many hours in cortical slice cultures ». In : *Journal of neuroscience* 24.22 (2004), p. 5216-5229 (cf. p. 55).

[BYBOS95] Rani BEN-YISHAI, R Lev BAR-OR et Haim SOMPOLINSKY. « Theory of orientation tuning in visual cortex. » In : *Proceedings of the National Academy of Sciences* 92.9 (1995), p. 3844-3848 (cf. p. 115).

[Ber34] Hans BERGER. « Über das elektrenkephalogramm des menschen ». In : *DMW-Deutsche Medizinische Wochenschrift* 60.51 (1934), p. 1947-1949 (cf. p. 28, 38).

[Ber+14] Nils BERTSCHINGER, Johannes RAUH, Eckehard OLBRICH et al. « Quantifying unique information ». In : *Entropy* 16.4 (2014), p. 2161-2183 (cf. p. 149).

[Bes+15] Michel BESSERVE, Scott C LOWE, Nikos K LOGOTHETIS et al. « Shifts of gamma phase across primary visual cortical sites reflect dynamic stimulus-modulated information transfer ». In : *PLoS biology* 13.9 (2015), e1002257 (cf. p. 123).

[BFS23] Richard F BETZEL, Joshua FASKOWITZ et Olaf SPORNS. « Living on the edge : network neuroscience beyond nodes ». In : *Trends in cognitive sciences* (2023) (cf. p. 19, 188).

[Bia+89] William BIALEK, Fred RIEKE, Robert van STEVENINCK et al. « Reading a neural code ». In : *Advances in neural information processing systems* 2 (1989) (cf. p. 19, 57, 180).

[Bia18] Ginestra BIANCONI. *Multilayer networks : structure and function*. Oxford university press, 2018 (cf. p. 57, 60).

[Bia21] Ginestra BIANCONI. *Higher-order networks*. Cambridge University Press, 2021 (cf. p. 19, 59).

[BDM04] Tom BINZEGGER, Rodney J DOUGLAS et Kevan AC MARTIN. « A quantitative map of the circuit of cat primary visual cortex ». In : *Journal of Neuroscience* 24.39 (2004), p. 8441-8453 (cf. p. 35).

[BO36] GH BISHOP et James O'LEARY. « Components of the electrical response of the optic cortex of the rabbit ». In : *American Journal of Physiology-Legacy Content* 117.2 (1936), p. 292-308 (cf. p. 28).

[Blo59] Donald S BLOUGH. « Delayed matching in the pigeon ». In : *Journal of the experimental analysis of behavior* 2.2 (1959), p. 151 (cf. p. 25).

[Bol+11] Anil BOLLIMUNTA, Jue MO, Charles E SCHROEDER et al. « Neuronal mechanisms and attentional modulation of corticothalamic alpha oscillations ». In : *Journal of Neuroscience* 31.13 (2011), p. 4935-4943 (cf. p. 38).

[BJ12] Mathilde BONNEFOND et Ole JENSEN. « Alpha oscillations serve to protect working memory maintenance against anticipated distracters ». In : *Current biology* 22.20 (2012), p. 1969-1974 (cf. p. 38).

[BKJ17] Mathilde BONNEFOND, Sabine KASTNER et Ole JENSEN. « Communication between brain areas based on nested oscillations ». In : *eneuro* 4.2 (2017) (cf. p. 38).

[BK03] Christoph BÖRGERS et Nancy KOPELL. « Synchronization in networks of excitatory and inhibitory neurons with sparse, random connectivity ». In : *Neural computation* 15.3 (2003), p. 509-538 (cf. p. 33).

[Bos+12] Conrado A BOSMAN, Jan-Mathijs SCHOFFELEN, Nicolas BRUNET et al. « Attentional stimulus selection through selective synchronization between monkey visual areas ». In : *Neuron* 75.5 (2012), p. 875-888 (cf. p. 28).

[BB19] Flora BOUCHACOURT et Timothy J BUSCHMAN. « A flexible model of working memory ». In : *Neuron* 103.1 (2019), p. 147-160 (cf. p. 92).

[BMR81] JJ BOUYER, MF MONTARON et A ROUGEUL. « Fast fronto-parietal rhythms during combined focused attentive behaviour and immobility in cat : cortical and thalamic localizations ». In : *Electroencephalography and clinical neurophysiology* 51.3 (1981), p. 244-252 (cf. p. 39).

[Bra+95] Anatol BRAGIN, Gábor JANDÓ, Zoltán NÁDASDY et al. « Gamma (40-100 Hz) oscillation in the hippocampus of the behaving rat ». In : *Journal of neuroscience* 15.1 (1995), p. 47-60 (cf. p. 37).

[Bre+24] Sander van BREE, Daniel LEVENSTEIN, Matthew R KRAUSE et al. « Decoupling measurement and process : on the epiphenomenon debate surrounding brain oscillations and field potentials ». In : *PsyArXiv Preprint* (2024) (cf. p. 29).

[Bre58] Frédéric BREMER. « Cerebral and cerebellar potentials ». In : *Physiological Reviews* 38.3 (1958), p. 357-388 (cf. p. 33).

[Bre+00] Naama BRENNER, Steven P STRONG, Roland KOBERLE et al. « Synergy in a neural code ». In : *Neural computation* 12.7 (2000), p. 1531-1552 (cf. p. 51, 124).

[Bre84] Steven L BRESSLER. « Spatial organization of EEGs from olfactory bulb and cortex ». In : *Electroencephalography and clinical neurophysiology* 57.3 (1984), p. 270-276 (cf. p. 39).

[BF80] Steven L BRESSLER et Walter J FREEMAN. « Frequency analysis of olfactory system EEG in cat, rabbit, and rat ». In : *Electroencephalography and clinical neurophysiology* 50.1-2 (1980), p. 19-24 (cf. p. 39).

[BM10] Steven L BRESSLER et Vinod MENON. « Large-scale brain networks in cognition : emerging methods and principles ». In : *Trends in cognitive sciences* 14.6 (2010), p. 277-290 (cf. p. 18).

[BS11] Steven L BRESSLER et Anil K SETH. « Wiener–Granger causality : a well established methodology ». In : *Neuroimage* 58.2 (2011), p. 323-329 (cf. p. 123).

[Bri+96] Kenneth H BRITTEN, William T NEWSOME, Michael N SHADLEN et al. « A relationship between behavioral choice and the visual responses of neurons in macaque MT ». In : *Visual neuroscience* 13.1 (1996), p. 87-100 (cf. p. 180).

[BJL06] Bede M BROOME, Vivek JAYARAMAN et Gilles LAURENT. « Encoding and decoding of overlapping odor sequences ». In : *Neuron* 51.4 (2006), p. 467-482 (cf. p. 58).

[Bro+15] Andrea BROVELLI, Daniel CHICHARRO, Jean-Michel BADIER et al. « Characterization of cortical networks and corticocortical functional connectivity mediating arbitrary visuomotor mapping ». In : *Journal of Neuroscience* 35.37 (2015), p. 12643-12658 (cf. p. 28).

[Bro+04] Andrea BROVELLI, Mingzhou DING, Anders LEDBERG et al. « Beta oscillations in a large-scale sensorimotor cortical network : directional influences revealed by Granger causality ». In : *Proceedings of the National Academy of Sciences* 101.26 (2004), p. 9849-9854 (cf. p. 39, 91, 123).

[Bro+05] Andrea BROVELLI, Jean-Philippe LACHAUX, Philippe KAHANE et al. « High gamma frequency oscillatory activity dissociates attention from intention in the human premotor cortex ». In : *Neuroimage* 28.1 (2005), p. 154-164 (cf. p. 28).

[Bro+23] Nico BROWN, Carson CHENG, Tanner JACOBI et al. « Conway's Game of Life is Omniperiodic ». In : *arXiv preprint arXiv :2312.02799* (2023) (cf. p. 48).

[Bru00] Nicolas BRUNEL. « Dynamics of sparsely connected networks of excitatory and inhibitory spiking neurons ». In : *Journal of computational neuroscience* 8 (2000), p. 183-208 (cf. p. 20, 31, 34).

[Bru03] Nicolas BRUNEL. « Dynamics and plasticity of stimulus-selective persistent activity in cortical network models ». In : *Cerebral Cortex* 13.11 (2003), p. 1151-1161 (cf. p. 25).

[BH99] Nicolas BRUNEL et Vincent HAKIM. « Fast global oscillations in networks of integrate-and-fire neurons with low firing rates ». In : *Neural computation* 11.7 (1999), p. 1621-1671 (cf. p. 34).

[BH08] Nicolas BRUNEL et Vincent HAKIM. « Sparsely synchronized neuronal oscillations ». In : *Chaos : An Interdisciplinary Journal of Nonlinear Science* 18.1 (2008) (cf. p. 31).

[BW03] Nicolas BRUNEL et Xiao-Jing WANG. « What determines the frequency of fast network oscillations with irregular neural discharges ? I. Synaptic dynamics and excitation-inhibition balance ». In : *Journal of neurophysiology* 90.1 (2003), p. 415-430 (cf. p. 31, 34).

[BMM24] Alessandra BUCCELLA, Uri MAOZ et Liad MUDRIK. « Towards a genuinely interdisciplinary 'science of the mind' ». In : *Authorea Preprints* (2024) (cf. p. 21).

[BD10] Andres BUEHLMANN et Gustavo DECO. « Optimal information transfer in the cortex through synchronization ». In : *PLoS computational biology* 6.9 (2010), e1000934 (cf. p. 65).

[BS09] Ed BULLMORE et Olaf SPORNS. « Complex brain networks : graph theoretical analysis of structural and functional systems ». In : *Nature reviews neuroscience* 10.3 (2009), p. 186-198 (cf. p. 149).

[BS12] Ed BULLMORE et Olaf SPORNS. « The economy of brain network organization ». In : *Nature reviews neuroscience* 13.5 (2012), p. 336-349 (cf. p. 36).

[Bul02] Theodore Holmes BULLOCK. « Biology of Brain waves : natural history and evolution of an information-rich sign of activity. » In : *Advances in Electrophysiolgy in Clinical Practice and Research*. Kjellberg, Inc., 2002 (cf. p. 29, 43).

[BM09] Dean V BUONOMANO et Wolfgang MAASS. « State-dependent computations : spatiotemporal processing in cortical networks ». In : *Nature Reviews Neuroscience* 10.2 (2009), p. 113-125 (cf. p. 58, 181).

[BXS11] Samuel P BURNS, Dajun XING et Robert M SHAPLEY. « Is gamma-band activity in the local field potential of V1 cortex a "clock" or filtered noise ? » In : *Journal of Neuroscience* 31.26 (2011), p. 9658-9664 (cf. p. 41).

[Bus21] Timothy J BUSCHMAN. « Balancing flexibility and interference in working memory ». In : *Annual review of vision science* 7 (2021), p. 367-388 (cf. p. 59, 92).

[Bus+12] Timothy J BUSCHMAN, Eric L DENOVELLIS, Cinira DIOGO et al. « Synchronous oscillatory neural ensembles for rules in the prefrontal cortex ». In : *Neuron* 76.4 (2012), p. 838-846 (cf. p. 39).

[BM07] Timothy J BUSCHMAN et Earl K MILLER. « Top-down versus bottom-up control of attention in the prefrontal and posterior parietal cortices ». In : *science* 315.5820 (2007), p. 1860-1862 (cf. p. 39).

[Buz98] GyÖrgy BUZSÁKI. « Memory consolidation during sleep : a neurophysiological perspective ». In : *Journal of sleep research* 7.S1 (1998), p. 17-23 (cf. p. 29).

[Buz05] György BUZSÁKI. « Theta rhythm of navigation : link between path integration and landmark navigation, episodic and semantic memory ». In : *Hippocampus* 15.7 (2005), p. 827-840 (cf. p. 29).

[Buz06] György BUZSÁKI. *Rhythms of the Brain*. Oxford university press, 2006 (cf. p. 28, 30, 35, 36, 38, 43).

[Buz10] György BUZSÁKI. « Neural syntax : cell assemblies, synapsembles, and readers ». In : *Neuron* 68.3 (2010), p. 362-385 (cf. p. 17, 19, 57, 180).

[BAK12] György BUZSÁKI, Costas A ANASTASSIOU et Christof KOCH. « The origin of extracellular fields and currents—EEG, ECoG, LFP and spikes ». In : *Nature reviews neuroscience* 13.6 (2012), p. 407-420 (cf. p. 30).

[BD04] Gyorgy BUZSAKI et Andreas DRAGUHN. « Neuronal oscillations in cortical networks ». In : *science* 304.5679 (2004), p. 1926-1929 (cf. p. 36, 65).

[Buz+04] György BUZSÁKI, Caroline GEISLER, Darrell A HENZE et al. « Interneuron diversity series : circuit complexity and axon wiring economy of cortical interneurons ». In : *Trends in neurosciences* 27.4 (2004), p. 186-193 (cf. p. 28, 35, 36).

[BMD22] György BUZSÁKI, Sam MCKENZIE et Lila DAVACHI. « Neurophysiology of remembering ». In : *Annual review of psychology* 73 (2022), p. 187-215 (cf. p. 91, 184).

[BTP03] György BUZSÁKI, Roger D TRAUB et Timothy A PEDLEY. « The cellular basis of EEG activity ». In : *Current practice of clinical electroencephalography* 3 (2003), p. 1-11 (cf. p. 30).

[BV23] György BUZSÁKI et Mihály VÖRÖSLAKOS. « Brain rhythms have come of age ». In : *Neuron* 111.7 (2023), p. 922-926 (cf. p. 17, 19, 28, 35, 91, 184).

[BW12] György BUZSÁKI et Xiao-Jing WANG. « Mechanisms of gamma oscillations ». In : *Annual review of neuroscience* 35 (2012), p. 203-225 (cf. p. 34).

[Cal+08] Corrado CALÌ, Thomas K BERGER, Michele PIGNATELLI et al. « Inferring connection proximity in networks of electrically coupled cells by subthreshold frequency response analysis ». In : *Journal of computational neuroscience* 24 (2008), p. 330-345 (cf. p. 32).

[Can+06] Ryan T CANOLTY, Erik EDWARDS, Sarang S DALAL et al. « High gamma power is phase-locked to theta oscillations in human neocortex ». In : *science* 313.5793 (2006), p. 1626-1628 (cf. p. 32, 37).

[CK10] Ryan T CANOLTY et Robert T KNIGHT. « The functional role of cross-frequency coupling ». In : *Trends in cognitive sciences* 14.11 (2010), p. 506-515 (cf. p. 27).

[CH12] Matteo CARANDINI et David J HEEGER. « Normalization as a canonical neural computation ». In : *Nature Reviews Neuroscience* 13.1 (2012), p. 51-62 (cf. p. 114, 150).

[Car+21] Tawan TA CARVALHO, Antonio J FONTENELE, Mauricio GIRARDI-SCHAPPO et al. « Subsampled directed-percolation models explain scaling relations experimentally observed in the brain ». In : *Frontiers in Neural Circuits* 14 (2021), p. 576727 (cf. p. 56).

[Cat70] Richard CATON. *The electric currents of the brain*. 1970 (cf. p. 28).

[Cer71] Gregory W CERMAK. « Short-term recognition memory for complex free-form figures ». In : *Psychonomic Science* 25.4 (1971), p. 209-211 (cf. p. 26).

[Cha+19] Rishidev CHAUDHURI, Berk GERÇEK, Biraj PANDEY et al. « The intrinsic attractor manifold and population dynamics of a canonical cognitive circuit across waking and sleep ». In : *Nature neuroscience* 22.9 (2019), p. 1512-1520 (cf. p. 59).

[CM21] Frédéric CHAZAL et Bertrand MICHEL. « An introduction to topological data analysis : fundamental and practical aspects for data scientists ». In : *Frontiers in artificial intelligence* 4 (2021), p. 667963 (cf. p. 188).

[Che+19] Sandrine CHEMLA, Alexandre REYNAUD, Matteo DI VOLO et al. « Suppressive traveling waves shape representations of illusory motion in primary visual cortex of awake primate ». In : *Journal of Neuroscience* 39.22 (2019), p. 4282-4298 (cf. p. 148).

[Che+16] Yinbo CHEN, Xinping LI, Horacio G ROTSTEIN et al. « Membrane potential resonance frequency directly influences network frequency through electrical coupling ». In : *Journal of Neurophysiology* 116.4 (2016), p. 1554-1563 (cf. p. 32).

[Chr+17] Thomas B CHRISTOPHEL, P Christiaan KLINK, Bernhard SPITZER et al. « The distributed nature of working memory ». In : *Trends in cognitive sciences* 21.2 (2017), p. 111-124 (cf. p. 26, 27, 65, 92, 183).

[CA21] SueYeon CHUNG et Larry F ABBOTT. « Neural population geometry : An approach for understanding biological and artificial neural networks ». In : *Current opinion in neurobiology* 70 (2021), p. 137-144 (cf. p. 59).

[Chu+12] Mark M CHURCHLAND, John P CUNNINGHAM, Matthew T KAUFMAN et al. « Neural population dynamics during reaching ». In : *Nature* 487.7405 (2012), p. 51-56 (cf. p. 58).

[Cla+21] Wesley CLAWSON, Tanguy MADEC, Antoine GHESTEM et al. « Disordered information processing dynamics in experimental epilepsy ». In : *bioRxiv* (2021), p. 2021-02 (cf. p. 150).

[Cla+19] Wesley CLAWSON, Ana F VICENTE, Maëva FERRARIS et al. « Computing hubs in the hippocampus and cortex ». In : *Science advances* 5.6 (2019), eaax4843 (cf. p. 58, 150).

[CD16] Jessica R COHEN et Mark D'ESPOSITO. « The segregation and integration of distinct brain networks and their relationship to cognition ». In : *Journal of Neuroscience* 36.48 (2016), p. 12083-12094 (cf. p. 41, 65).

[CV17] Scott R COLE et Bradley VOYTEK. « Brain oscillations and the importance of waveform shape ». In : *Trends in cognitive sciences* 21.2 (2017), p. 137-149 (cf. p. 66, 160).

[Com+22a] Etienne COMBRISSON, Michele ALLEGRA, Ruggero BASANISI et al. « Group-level inference of information-based measures for the analyses of cognitive brain networks from neurophysiological data ». In : *NeuroImage* 258 (2022), p. 119347 (cf. p. 68, 121).

[Com+22b] Etienne COMBRISSON, Ruggero BASANISI, Vinicius Lima CORDEIRO et al. « Frites : A Python package for functional connectivity analysis and group-level statistics of neurophysiological data ». In : *Journal of Open Source Software* 7.79 (2022), p. 3842 (cf. p. 121, 126).

[Com+23] Etienne COMBRISSON, Ruggero BASANISI, Maëlle CM GUEGUEN et al. « Neural interactions in the human frontal cortex dissociate reward and punishment learning ». In : *bioRxiv* (2023), p. 2023-05 (cf. p. 19, 93).

[Coo+06] Nicholas R COOPER, Adrian P BURGESS, Rodney J CROFT et al. « Investigating evoked and induced electroencephalogram activity in task-related alpha power increases during an internally directed attention task ». In : *Neuroreport* 17.2 (2006), p. 205-208 (cf. p. 38).

[Coo07] Richard P COOPER. « The role of falsification in the development of cognitive architectures : Insights from a Lakatosian analysis ». In : *Cognitive science* 31.3 (2007), p. 509-533 (cf. p. 146).

[Cor+24] Marie-Constance CORSI, Pierpaolo SORRENTINO, Denis SCHWARTZ et al. « Measuring neuronal avalanches to inform brain-computer interfaces ». In : *Iscience* 27.1 (2024) (cf. p. 56).

[Cou+98] Susan M COURTNEY, Laurent PETIT, Jose Ma MAISOG et al. « An area specialized for spatial working memory in human frontal cortex ». In : *Science* 279.5355 (1998), p. 1347-1351 (cf. p. 25).

[Cou09] Iain D COUZIN. « Collective cognition in animal groups ». In : *Trends in cognitive sciences* 13.1 (2009), p. 36-43 (cf. p. 45).

[Cou+02] Iain D COUZIN, Jens KRAUSE, Richard JAMES et al. « Collective memory and spatial sorting in animal groups ». In : *Journal of theoretical biology* 218.1 (2002), p. 1-11 (cf. p. 45).

[CT06] Thomas M COVER et Joy A THOMAS. « Elements of information theory second edition solutions to problems ». In : *Internet Access* (2006), p. 19-20 (cf. p. 120).

[Cow10] Nelson COWAN. « The magical mystery four : How is working memory capacity limited, and why? » In : *Current directions in psychological science* 19.1 (2010), p. 51-57 (cf. p. 23).

[CEB98] Sharon M CROOK, G Bard ERMENTROUT et James M BOWER. « Spike frequency adaptation affects the synchronization properties of networks of cortical oscillators ». In : *Neural Computation* 10.4 (1998), p. 837-854 (cf. p. 32).

[CCB09] Jianxia CUI, Carmen C CANAVIER et Robert J BUTERA. « Functional phase response curves : a method for understanding synchronization of adapting neurons ». In : *Journal of Neurophysiology* 102.1 (2009), p. 387-398 (cf. p. 32).

[CY14] John P CUNNINGHAM et Byron M YU. « Dimensionality reduction for large-scale neural recordings ». In : *Nature neuroscience* 17.11 (2014), p. 1500-1509 (cf. p. 59).

[Cun+04] Mark O CUNNINGHAM, Miles A WHITTINGTON, Andrea BIBBIG et al. « A role for fast rhythmic bursting neurons in cortical gamma oscillations in vitro ». In : *Proceedings of the National Academy of Sciences* 101.18 (2004), p. 7152-7157 (cf. p. 33).

[CD03] Clayton E CURTIS et Mark D'ESPOSITO. « Persistent activity in the prefrontal cortex during working memory ». In : *Trends in cognitive sciences* 7.9 (2003), p. 415-423 (cf. p. 25).

[CD04] Clayton E CURTIS et Mark D'ESPOSITO. « The effects of prefrontal lesions on working memory performance and theory ». In : *Cognitive, Affective, & Behavioral Neuroscience* 4.4 (2004), p. 528-539 (cf. p. 25).

[DS+97] FH Lopes DA SILVA, JP PIJN, D VELIS et al. « Alpha rhythms : noise, dynamics and models ». In : *International Journal of Psychophysiology* 26.1-3 (1997), p. 237-249 (cf. p. 38).

[Dah+22] David DAHMEN, Moritz LAYER, Lukas DEUTZ et al. « Global organization of neuronal activity only requires unstructured local connectivity ». In : *Elife* 11 (2022), e68422 (cf. p. 150).

[DKR16] Thomas A DANIEL, Jeffrey S KATZ et Jennifer L ROBINSON. « Delayed match-to-sample in working memory : A BrainMap meta-analysis ». In : *Biological Psychology* 120 (2016), p. 10-20 (cf. p. 25).

[Dar23] Charles DARWIN. « Origin of the Species ». In : *British Politics and the Environment in the Long Nineteenth Century*. Routledge, 2023, p. 47-55 (cf. p. 45).

[Dav+15] Elizabeth N DAVISON, Kimberly J SCHLESINGER, Danielle S BASSETT et al. « Brain network adaptability across task states ». In : *PLoS computational biology* 11.1 (2015), e1004029 (cf. p. 149).

[DA05] Peter DAYAN et Laurence F ABBOTT. *Theoretical neuroscience : computational and mathematical modeling of neural systems*. MIT press, 2005 (cf. p. 19, 180).

[DG83] JUDITH E DAYHOFF et GEORGE L GERSTEIN. « Favored patterns in spike trains. II. Application ». In : *Journal of Neurophysiology* 49.6 (1983), p. 1349-1363 (cf. p. 55).

[DJM11] Gustavo DECO, Viktor K JIRSA et Anthony R MCINTOSH. « Emerging concepts for the dynamical organization of resting-state activity in the brain ». In : *Nature reviews neuroscience* 12.1 (2011), p. 43-56 (cf. p. 142).

[Dec+21] Gustavo DECO, Yonathan Sanz PERL, Peter VUUST et al. « Rare long-range cortical connections enhance human information processing ». In : *Current Biology* 31.20 (2021), p. 4436-4448 (cf. p. 18).

[Dec+15] Gustavo DECO, Giulio TONONI, Melanie BOLY et al. « Rethinking segregation and integration : contributions of whole-brain modelling ». In : *Nature Reviews Neuroscience* 16.7 (2015), p. 430-439 (cf. p. 65).

[DK84] Bertrand DELGUTTE et Nelson YS KIANG. « Speech coding in the auditory nerve : IV. Sounds with consonant-like dynamic characteristics ». In : *The Journal of the Acoustical Society of America* 75.3 (1984), p. 897-907 (cf. p. 55).

[DD+95] Robert DESIMONE, John DUNCAN et al. « Neural mechanisms of selective visual attention ». In : *Annual review of neuroscience* 18.1 (1995), p. 193-222 (cf. p. 26, 138).

[DP15] Mark D'ESPOSITO et Bradley R POSTLE. « The cognitive neuroscience of working memory ». In : *Annual review of psychology* 66 (2015), p. 115-142 (cf. p. 22).

[DBB90] Shi DI, CHRISTOPH BAUMGARTNER et DANIEL S BARTH. « Laminar analysis of extracellular field potentials in rat vibrissa/barrel cortex ». In : *Journal of neurophysiology* 63.4 (1990), p. 832-840 (cf. p. 31).

[Don+09] Tobias H DONNER, Markus SIEGEL, Pascal FRIES et al. « Buildup of choice-predictive activity in human motor cortex during perceptual decision making ». In : *Current Biology* 19.18 (2009), p. 1581-1585 (cf. p. 91).

[Don+07] Tobias H DONNER, Markus SIEGEL, Robert OOSTENVELD et al. « Population activity in the human dorsal pathway predicts the accuracy of visual motion detection ». In : *Journal of neurophysiology* 98.1 (2007), p. 345-359 (cf. p. 91).

[Dot+17] Nicholas M DOTSON, Steven J HOFFMAN, Baldwin GOODELL et al. « A large-scale semi-chronic microdrive recording system for non-human primates ». In : *Neuron* 96.4 (2017), p. 769-782 (cf. p. 18, 66, 91, 183).

[Dot+18] Nicholas M DOTSON, Steven J HOFFMAN, Baldwin GOODELL et al. « Feature-based visual short-term memory is widely distributed and hierarchically organized ». In : *Neuron* 99.1 (2018), p. 215-226 (cf. p. 18, 26, 27, 41, 65, 66, 91, 92, 183).

[Dou+24] Vincent DOUCHAMPS, Matteo di VOLO, Alessandro TORCINI et al. « Gamma oscillatory complexity conveys behavioral information in hippocampal networks ». In : *Nature Communications* 15.1 (2024), p. 1849 (cf. p. 20, 42-44, 65, 160, 162-164, 169, 172, 174, 179, 185, 186, 189).

[DM04] Rodney J DOUGLAS et Kevan AC MARTIN. « Neuronal circuits of the neocortex ». In : *Annu. Rev. Neurosci.* 27 (2004), p. 419-451 (cf. p. 39).

[DV23] Jarrod Robert DOWDALL et Martin VINCK. « Coherence fails to reliably capture inter-areal interactions in bidirectional neural systems with transmission delays ». In : *NeuroImage* 271 (2023), p. 119998 (cf. p. 41, 91).

[DR19] Agrita DUBEY et Supratim RAY. « Cortical electrocorticogram (ECoG) is a local signal ». In : *Journal of Neuroscience* 39.22 (2019), p. 4299-4311 (cf. p. 31).

[DJ22] Egidio D'ANGELO et Viktor JIRSA. « The quest for multiscale brain modeling ». In : *Trends in neurosciences* 45.10 (2022), p. 777-790 (cf. p. 20).

[Eck+10] Alexander S ECKER, Philipp BERENS, Georgios A KELIRIS et al. « Decorrelated neuronal firing in cortical microcircuits ». In : *science* 327.5965 (2010), p. 584-587 (cf. p. 56).

[Eck+88] Reinhard ECKHORN, Roman BAUER, Wolfgang JORDAN et al. « Coherent oscillations : a mechanism of feature linking in the visual cortex? Multiple electrode and correlation analyses in the cat ». In : *Biological cybernetics* 60 (1988), p. 121-130 (cf. p. 40).

[Ede+18] Freek van EDE, Andrew J QUINN, Mark W WOOLRICH et al. « Neural oscillations : sustained rhythms or transient burst-events? » In : *Trends in neurosciences* 41.7 (2018), p. 415-417 (cf. p. 20, 41).

[Egg98] Jos J EGGERMONT. « Is there a neural code? » In : *Neuroscience & Biobehavioral Reviews* 22.2 (1998), p. 355-370 (cf. p. 19, 55, 180).

[Ein+13] Gaute T EINEVOLL, Christoph KAYSER, Nikos K LOGOTHETIS et al. « Modelling and analysis of local field potentials for studying the function of cortical circuits ». In : *Nature Reviews Neuroscience* 14.11 (2013), p. 770-785 (cf. p. 30, 31).

[Eng+99] Randall W ENGLE, Stephen W TUHOLSKI, James E LAUGHLIN et al. « Working memory, short-term memory, and general fluid intelligence : a latent-variable approach. » In : *Journal of experimental psychology : General* 128.3 (1999), p. 309 (cf. p. 23).

[Epp+09] Jochen M EPPLER, Moritz HELIAS, Eilif MULLER et al. « PyNEST : a convenient interface to the NEST simulator ». In : *Frontiers in neuroinformatics* 2 (2009), p. 363 (cf. p. 127).

[EU07] Nurhan ERBIL et Pekcan UNGAN. « Changes in the alpha and beta amplitudes of the central EEG during the onset, continuation, and offset of long-duration repetitive hand movements ». In : *Brain research* 1169 (2007), p. 44-56 (cf. p. 38).

[ER+60] Paul ERDŐS, Alfréd RÉNYI et al. « On the evolution of random graphs ». In : *Publ. math. inst. hung. acad. sci* 5.1 (1960), p. 17-60 (cf. p. 34).

[EK91] G Bard ERMENTROUT et Nancy KOPELL. « Multiple pulse interactions and averaging in systems of coupled neural oscillators ». In : *Journal of Mathematical Biology* 29.3 (1991), p. 195-217 (cf. p. 32).

[EK98] G Bard ERMENTROUT et Nancy KOPELL. « Fine structure of neural spiking and synchronization in the presence of conduction delays ». In : *Proceedings of the National Academy of Sciences* 95.3 (1998), p. 1259-1264 (cf. p. 33).

[ESS15] Edward F ESTER, Thomas C SPRAGUE et John T SERENCES. « Parietal and frontal cortex encode stimulus-specific mnemonic representations during visual working memory ». In : *Neuron* 87.4 (2015), p. 893-905 (cf. p. 26).

[Fei+15] Joseph FEINGOLD, Daniel J GIBSON, Brian DEPASQUALE et al. « Bursts of beta oscillation differentiate postperformance activity in the striatum and motor cortex of monkeys performing movement tasks ». In : *Proceedings of the National Academy of Sciences* 112.44 (2015), p. 13687-13692 (cf. p. 41-43, 65, 66, 160, 185).

[FVE91] Daniel J FELLEMAN et David C VAN ESSEN. « Distributed hierarchical processing in the primate cerebral cortex. » In : *Cerebral cortex (New York, NY : 1991)* 1.1 (1991), p. 1-47 (cf. p. 35).

[FBM23] Mengli FENG, Abhirup BANDYOPADHYAY et Jorge F MEJIAS. « Emergence of distributed working memory in a human brain network model ». In : *bioRxiv* (2023), p. 2023-01 (cf. p. 92).

[FS03] Janina FERBINTEANU et Matthew L SHAPIRO. « Prospective and retrospective memory coding in the hippocampus ». In : *Neuron* 40.6 (2003), p. 1227-1239 (cf. p. 185).

[Fer+95] Thalía FERNÁNDEZ, Thalía HARMONY, Mario RODRÍGUEZ et al. « EEG activation patterns during the performance of tasks involving different components of mental calculation ». In : *Electroencephalography and clinical neurophysiology* 94.3 (1995), p. 175-182 (cf. p. 37).

[Fin+20] Karolina FINC, Kamil BONNA, Xiaosong HE et al. « Dynamic reconfiguration of functional brain networks during working memory training ». In : *Nature communications* 11.1 (2020), p. 2435 (cf. p. 65).

[Fis+98] Andre FISAHN, Fenella G PIKE, Eberhard H BUHL et al. « Cholinergic induction of network oscillations at 40 Hz in the hippocampus in vitro ». In : *Nature* 394.6689 (1998), p. 186-189 (cf. p. 33).

[Foc+01] Jan W de FOCKERT, Geraint REES, Christopher D FRITH et al. « The role of working memory in visual selective attention ». In : *Science* 291.5509 (2001), p. 1803-1806 (cf. p. 26).

[Fod68] Jerry A FODOR. « The appeal to tacit knowledge in psychological explanation ». In : *The Journal of Philosophy* 65.20 (1968), p. 627-640 (cf. p. 146).

[Fon+24] Antonio J FONTENELE, J Samuel SOOTER, V Kindler NORMAN et al. « Low-dimensional criticality embedded in high-dimensional awake brain dynamics ». In : *Science Advances* 10.17 (2024), eadj9303 (cf. p. 56).

[Fos+21] Leandro J FOSQUE, Rashid V WILLIAMS-GARCÍA, John M BEGGS et al. « Evidence for quasicritical brain dynamics ». In : *Physical Review Letters* 126.9 (2021), p. 098101 (cf. p. 56).

[FEM15] Anne MM FRANSEN, Freek van EDE et Eric MARIS. « Identifying neuronal oscillations using rhythmicity ». In : *Neuroimage* 118 (2015), p. 256-267 (cf. p. 44, 65, 160).

[Fre+01] David J FREEDMAN, Maximilian RIESENHUBER, Tomaso POGGIO et al. « Categorical representation of visual stimuli in the primate prefrontal cortex ». In : *Science* 291.5502 (2001), p. 312-316 (cf. p. 26).

[Fre87] Walter J FREEMAN. « Simulation of chaotic EEG patterns with a dynamic model of the olfactory system ». In : *Biological cybernetics* 56.2 (1987), p. 139-150 (cf. p. 39).

[Fre91] Walter J FREEMAN. « The physiology of perception ». In : *Scientific American* 264.2 (1991), p. 78-87 (cf. p. 39).

[FD87] Walter J FREEMAN et Bob W van DIJK. « Spatial patterns of visual cortical fast EEG during conditioned reflex in a rhesus monkey ». In : *Brain research* 422.2 (1987), p. 267-276 (cf. p. 40).

[Fre+00] Walter J FREEMAN, Linda J ROGERS, Mark D HOLMES et al. « Spatial spectral analysis of human electrocorticograms including the alpha and gamma bands ». In : *Journal of neuroscience methods* 95.2 (2000), p. 111-121 (cf. p. 36).

[FIK10] Walter J FREEMAN III et Robert KOZMA. « Freeman's mass action ». In : *Scholarspedia* 5.1 (2010), p. 8040-8040 (cf. p. 39).

[Fre+16] Julia Natascha FREY, Philipp RUHNAU, Sabine LESKE et al. « The tactile window to consciousness is characterized by frequency-specific integration and segregation of the primary somatosensory cortex ». In : *Scientific reports* 6.1 (2016), p. 20805 (cf. p. 65).

[Fre+09] Frank FREYER, Kevin AQUINO, Peter A ROBINSON et al. « Bistability and non-Gaussian fluctuations in spontaneous cortical activity ». In : *Journal of Neuroscience* 29.26 (2009), p. 8512-8524 (cf. p. 38).

[Fre+11] Frank FREYER, James A ROBERTS, Robert BECKER et al. « Biophysical mechanisms of multistability in resting-state cortical rhythms ». In : *Journal of Neuroscience* 31.17 (2011), p. 6353-6361 (cf. p. 38).

[Fri05] Pascal FRIES. « A mechanism for cognitive dynamics : neuronal communication through neuronal coherence ». In : *Trends in cognitive sciences* 9.10 (2005), p. 474-480 (cf. p. 39, 40, 91).

[Fri09] Pascal FRIES. « Neuronal gamma-band synchronization as a fundamental process in cortical computation ». In : *Annual review of neuroscience* 32 (2009), p. 209-224 (cf. p. 27, 39).

[Fri15] Pascal FRIES. « Rhythms for cognition : communication through coherence ». In : *Neuron* 88.1 (2015), p. 220-235 (cf. p. 29, 39, 40, 91).

[Fri23] Pascal FRIES. « Rhythmic attentional scanning ». In : *Neuron* 111.7 (2023), p. 954-970 (cf. p. 40).

[Fri+01a] Pascal FRIES, Sergio NEUENSCHWANDER, Andreas K ENGEL et al. « Rapid feature selective neuronal synchronization through correlated latency shifting ». In : *Nature neuroscience* 4.2 (2001), p. 194-200 (cf. p. 65).

[Fri+01b] Pascal FRIES, John H REYNOLDS, Alan E RORIE et al. « Modulation of oscillatory neuronal synchronization by selective visual attention ». In : *Science* 291.5508 (2001), p. 1560-1563 (cf. p. 40).

[Fri03] Karl FRISTON. « Learning and inference in the brain ». In : *Neural Networks* 16.9 (2003), p. 1325-1352 (cf. p. 35).

[Fri97] Karl J FRISTON. « Another neural code? » In : *Neuroimage* 5.3 (1997), p. 213-220 (cf. p. 55).

[FCGR93] Shintaro FUNAHASHI, Matthew V CHAFEE et Patricia S GOLDMAN-RAKIC. « Prefrontal neuronal activity in rhesus monkeys performing a delayed anti-saccade task ». In : *Nature* 365.6448 (1993), p. 753-756 (cf. p. 25).

[Fus73] Joaquin M FUSTER. « Unit activity in prefrontal cortex during delayed-response performance : neuronal correlates of transient memory. » In : *Journal of neurophysiology* 36.1 (1973), p. 61-78 (cf. p. 23, 25).

[FA71] Joaquin M FUSTER et Garrett E ALEXANDER. « Neuron activity related to short-term memory ». In : *Science* 173.3997 (1971), p. 652-654 (cf. p. 23, 25).

[GXB23] Kaitlyn GABHART, Yihan Sophy XIONG et Andre BASTOS. « Where are global oddballs? A predictive routing theory ». In : (2023) (cf. p. 93).

[Gal+20] Juan A GALLEGO, Matthew G PERICH, Raeed H CHOWDHURY et al. « Long-term stability of cortical population dynamics underlying consistent behavior ». In : *Nature neuroscience* 23.2 (2020), p. 260-270 (cf. p. 59).

[GL16] Lin GE et Xiao-dong LIU. « Electrical resonance with voltage-gated ion channels : perspectives from biophysical mechanisms and neural electrophysiology ». In : *Acta Pharmacologica Sinica* 37.1 (2016), p. 67-74 (cf. p. 32).

[GBW05] Caroline GEISLER, Nicolas BRUNEL et Xiao-Jing WANG. « Contributions of intrinsic membrane dynamics to fast network oscillations with irregular neuronal discharges ». In : *Journal of neurophysiology* 94.6 (2005), p. 4344-4361 (cf. p. 29, 34).

[GKS88] Apostolos P GEORGOPOULOS, Ronald E KETTNER et Andrew B SCHWARTZ. « Primate motor cortex and free arm movements to visual targets in three-dimensional space. II. Coding of the direction of movement by a neuronal population ». In : *Journal of Neuroscience* 8.8 (1988), p. 2928-2937 (cf. p. 55).

[GP08] Elakkat D GIREESH et Dietmar PLENZ. « Neuronal avalanches organize as nested theta-and beta/gamma-oscillations during development of cortical layer 2/3 ». In : *Proceedings of the National Academy of Sciences* 105.21 (2008), p. 7576-7581 (cf. p. 55).

[GGB16] Chad GIUSTI, Robert GHRIST et Danielle S BASSETT. « Two's company, three (or more) is a simplex : Algebraic-topological tools for understanding higher-order structure in neural data ». In : *Journal of computational neuroscience* 41 (2016), p. 1-14 (cf. p. 19, 60).

[Głk+16] Helena T GŁKABSKA, Eivind NORHEIM, Anna DEVOR et al. « Generalized laminar population analysis (gLPA) for interpretation of multielectrode data from cortex ». In : *Frontiers in neuroinformatics* 10 (2016), p. 1 (cf. p. 31).

[GDW07] Joshua A GOLDBERG, Chris A DEISTER et Charles J WILSON. « Response properties and synchronization of rhythmically firing dendritic neurons ». In : *Journal of neurophysiology* 97.1 (2007), p. 208-219 (cf. p. 32).

[GR87] Patricia S GOLDMAN-RAKIC. « Development of cortical circuitry and cognitive function ». In : *Child development* (1987), p. 601-622 (cf. p. 25).

[GL09] Pulin GONG et Cees van LEEUWEN. « Distributed dynamical computation in neural circuits with propagating coherent activity patterns ». In : *PLoS Computational Biology* 5.12 (2009), e1000611 (cf. p. 148).

[Goo14] David L GOODSTEIN. *States of matter*. Courier Corporation, 2014 (cf. p. 57).

[Gra+13] Alexandre GRAMFORT, Martin LUESSI, Eric LARSON et al. « MEG and EEG data analysis with MNE-Python ». In : *Frontiers in neuroscience* 7 (2013), p. 70133 (cf. p. 167).

[Gra69] Clive WJ GRANGER. « Investigating causal relations by econometric models and cross-spectral methods ». In : *Econometrica : journal of the Econometric Society* (1969), p. 424-438 (cf. p. 123).

[GM96] Charles M GRAY et David A MCCORMICK. « Chattering cells : superficial pyramidal neurons contributing to the generation of synchronous oscillations in the visual cortex ». In : *Science* 274.5284 (1996), p. 109-113 (cf. p. 33).

[GS89] Charles M GRAY et Wolf SINGER. « Stimulus-specific neuronal oscillations in orientation columns of cat visual cortex. » In : *Proceedings of the National Academy of Sciences* 86.5 (1989), p. 1698-1702 (cf. p. 29, 31, 40, 91).

[Gre61] Walter William GREY. *The living brain*. Penguin, 1961 (cf. p. 37).

[Gro+19] Shany GROSSMAN, Erin M YEAGLE, Michal HAREL et al. « The noisy brain : power of resting-state fluctuations predicts individual recognition performance ». In : *Cell reports* 29.12 (2019), p. 3775-3784 (cf. p. 115).

[Grz+09] Beata J GRZYB, Eris CHINELLATO, Grzegorz M WOJCIK et al. « Which model to use for the liquid state machine? » In : *2009 International Joint Conference on Neural Networks*. IEEE. 2009, p. 1018-1024 (cf. p. 183).

[GWM21] Aaron J GUTKNECHT, Michael WIBRAL et Abdullah MAKKEH. « Bits and pieces : Understanding information decomposition from part-whole relationships and formal logic ». In : *Proceedings of the Royal Society A* 477.2251 (2021), p. 20210110 (cf. p. 149).

[Hae+11] Saskia HAEGENS, Verónica NÁCHER, Adrián HERNÁNDEZ et al. « Beta oscillations in the monkey sensorimotor network reflect somatosensory decision making ». In : *Proceedings of the National Academy of Sciences* 108.26 (2011), p. 10708-10713 (cf. p. 91).

[Hah+14] Gerald HAHN, Alejandro F BUJAN, Yves FRÉGNAC et al. « Communication through resonance in spiking neuronal networks ». In : *PLoS computational biology* 10.8 (2014), e1003811 (cf. p. 65).

[Hah+10] Gerald HAHN, Thomas PETERMANN, Martha N HAVENITH et al. « Neuronal avalanches in spontaneous activity in vivo ». In : *Journal of neurophysiology* 104.6 (2010), p. 3312-3322 (cf. p. 55).

[Hah+17] Gerald HAHN, Adrian PONCE-ALVAREZ, Cyril MONIER et al. « Spontaneous cortical activity is transiently poised close to criticality ». In : *PLoS computational biology* 13.5 (2017), e1005543 (cf. p. 55).

[Hal+21] Grace E HALLENBECK, Thomas C SPRAGUE, Masih RAHMATI et al. « Working memory representations in visual cortex mediate distraction effects ». In : *Nature Communications* 12.1 (2021), p. 4714 (cf. p. 25).

[Han+14] Balázs HANGYA, Hyun-Jae PI, Duda KVITSIANI et al. « From circuit motifs to computations : mapping the behavioral repertoire of cortical interneurons ». In : *Current opinion in neurobiology* 26 (2014), p. 117-124 (cf. p. 150).

[HMM95] David HANSEL, Germán MATO et Claude MEUNIER. « Synchrony in excitatory neural networks ». In : *Neural computation* 7.2 (1995), p. 307-337 (cf. p. 33).

[Har13] Thalía HARMONY. « The functional significance of delta oscillations in cognitive processing ». In : *Frontiers in integrative neuroscience* 7 (2013), p. 83 (cf. p. 37).

[Har+96] Thalía HARMONY, Thalía FERNÁNDEZ, Juan SILVA et al. « EEG delta activity : an indicator of attention to internal processing during performance of mental tasks ». In : *International journal of psychophysiology* 24.1-2 (1996), p. 161-171 (cf. p. 37).

[Har+13] Michael A HARVEY, Hannes P SAAL, John F DAMMANN III et al. « Multiplexing stimulus information through rate and temporal codes in primate somatosensory cortex ». In : *PLoS biology* 11.5 (2013), e1001558 (cf. p. 181).

[Has05] Michael E HASSELMO. « What is the function of hippocampal theta rhythm ?—Linking behavioral data to phasic properties of field potential and unit recording data ». In : *Hippocampus* 15.7 (2005), p. 936-949 (cf. p. 37).

[HE05] Michael E HASSELMO et Howard EICHENBAUM. « Hippocampal mechanisms for the context-dependent retrieval of episodes ». In : *Neural networks* 18.9 (2005), p. 1172-1190 (cf. p. 37).

[Has+02] Michael E HASSELMO, Jonathan HAY, Maxim ILYN et al. « Neuromodulation, theta rhythm and rat spatial navigation ». In : *Neural Networks* 15.4-6 (2002), p. 689-707 (cf. p. 29).

[HLE07] Michael HAUCK, Jürgen LORENZ et Andreas K ENGEL. « Attention to painful stimulation enhances γ-band activity and synchronization in human sensorimotor cortex ». In : *Journal of Neuroscience* 27.35 (2007), p. 9270-9277 (cf. p. 40).

[HP17] Drew B HEADLEY et Denis PARÉ. « Common oscillatory mechanisms across multiple memory systems ». In : *npj Science of Learning* 2.1 (2017), p. 1 (cf. p. 37).

[Heb49] Donald O HEBB. « The first stage of perception : growth of the assembly ». In : *The Organization of Behavior* 4.60 (1949), p. 78-60 (cf. p. 57).

[Hel13] Moritz HELMSTAEDTER. « Cellular-resolution connectomics : challenges of dense neural circuit reconstruction ». In : *Nature methods* 10.6 (2013), p. 501-507 (cf. p. 114).

[Her+10] Adrián HERNÁNDEZ, Verónica NÁCHER, Rogelio LUNA et al. « Decoding a perceptual decision process across cortex ». In : *Neuron* 66.2 (2010), p. 300-314 (cf. p. 26).

[HP13] Rikkert HINDRIKS et Michel JAM van PUTTEN. « Thalamo-cortical mechanisms underlying changes in amplitude and frequency of human alpha oscillations ». In : *Neuroimage* 70 (2013), p. 150-163 (cf. p. 38).

[HT23] Rikkert HINDRIKS et Prejaas KB TEWARIE. « Dissociation between phase and power correlation networks in the human brain is driven by co-occurrent bursts ». In : *Communications biology* 6.1 (2023), p. 286 (cf. p. 42, 93).

[HR02] Geoffrey E HINTON et Sam ROWEIS. « Stochastic neighbor embedding ». In : *Advances in neural information processing systems* 15 (2002) (cf. p. 59).

[HES11] Joerg F HIPP, Andreas K ENGEL et Markus SIEGEL. « Oscillatory synchronization in large-scale cortical networks predicts perception ». In : *Neuron* 69.2 (2011), p. 387-396 (cf. p. 65).

[HSB10] Jon P HOBBS, Jodi L SMITH et John M BEGGS. « Aberrant neuronal avalanches in cortical tissue removed from juvenile epilepsy patients ». In : *Journal of Clinical Neurophysiology* 27.6 (2010), p. 380-386 (cf. p. 56).

[Hoe+10] Gregor M HOERZER, Stefanie LIEBE, Alois SCHLOEGL et al. « Directed coupling in local field potentials of macaque v4 during visual short-term memory revealed by multivariate autoregressive models ». In : *Frontiers in computational neuroscience* 4 (2010), p. 1214 (cf. p. 37).

[Hof+24] Steven Joseph HOFFMAN, Nicholas M DOTSON, Vinicius LIMA et al. « The Primate Cortical LFP Exhibits Multiple Spectral and Temporal Gradients and Widespread Task-Dependence During Visual Short-Term Memory ». In : *bioRxiv* (2024), p. 2024-01 (cf. p. 18, 28, 66, 71, 91).

[HS12] Petter HOLME et Jari SARAMÄKI. « Temporal networks ». In : *Physics reports* 519.3 (2012), p. 97-125 (cf. p. 57).

[Hop82] John J HOPFIELD. « Neural networks and physical systems with emergent collective computational abilities. » In : *Proceedings of the national academy of sciences* 79.8 (1982), p. 2554-2558 (cf. p. 91).

[Hua+98] Norden E HUANG, Zheng SHEN, Steven R LONG et al. « The empirical mode decomposition and the Hilbert spectrum for nonlinear and non-stationary time series analysis ». In : *Proceedings of the Royal Society of London. Series A : mathematical, physical and engineering sciences* 454.1971 (1998), p. 903-995 (cf. p. 166).

[Hua14] Norden Eh HUANG. *Hilbert-Huang transform and its applications*. T. 16. World Scientific, 2014 (cf. p. 43, 44, 166).

[HW74] David H HUBEL et Torsten N WIESEL. « Sequence regularity and geometry of orientation columns in the monkey striate cortex ». In : *Journal of Comparative Neurology* 158.3 (1974), p. 267-293 (cf. p. 35).

[HY00] Bruce HUTCHEON et Yosef YAROM. « Resonance, oscillation and the intrinsic frequency preferences of neurons ». In : *Trends in neurosciences* 23.5 (2000), p. 216-222 (cf. p. 28, 30, 32).

[Imp+19] Laura Sophie IMPERATORI, Monica BETTA, Luca CECCHETTI et al. « EEG functional connectivity metrics wPLI and wSMI account for distinct types of brain functional interactions ». In : *Scientific reports* 9.1 (2019), p. 8894 (cf. p. 42).

[Inc+17] Robin AA INCE, Bruno L GIORDANO, Christoph KAYSER et al. « A statistical framework for neuroimaging data analysis based on mutual information estimated via a gaussian copula ». In : *Human brain mapping* 38.3 (2017), p. 1541-1573 (cf. p. 68, 121, 123, 149).

[Inc+15] Robin AA INCE, Nicola J VAN RIJSBERGEN, Gregor THUT et al. « Tracing the flow of perceptual features in an algorithmic brain network ». In : *Scientific reports* 5.1 (2015), p. 17681 (cf. p. 147).

[Izh00] Eugene M IZHIKEVICH. « Neural excitability, spiking and bursting ». In : *International journal of bifurcation and chaos* 10.06 (2000), p. 1171-1266 (cf. p. 28).

[Izh01] Eugene M IZHIKEVICH. « Resonate-and-fire neurons ». In : *Neural networks* 14.6-7 (2001), p. 883-894 (cf. p. 28).

[Izh07] Eugene M IZHIKEVICH. *Dynamical systems in neuroscience*. MIT press, 2007 (cf. p. 28, 32, 34).

[JN14] Simon Nikolas JACOB et Andreas NIEDER. « Complementary roles for primate frontal and parietal cortex in guarding working memory from distractor stimuli ». In : *Neuron* 83.1 (2014), p. 226-237 (cf. p. 27).

[Jac+07] Joshua JACOBS, Michael J KAHANA, Arne D EKSTROM et al. « Brain oscillations control timing of single-neuron activity in humans ». In : *Journal of Neuroscience* 27.14 (2007), p. 3839-3844 (cf. p. 37).

[Jam+13] Gareth JAMES, Daniela WITTEN, Trevor HASTIE et al. *An introduction to statistical learning*. T. 112. Springer, 2013 (cf. p. 59).

[JBC16] Ryan G JAMES, Nix BARNETT et James P CRUTCHFIELD. « Information flows ? A critique of transfer entropies ». In : *Physical review letters* 116.23 (2016), p. 238701 (cf. p. 149).

[JEC11] Ryan G JAMES, Christopher J ELLISON et James P CRUTCHFIELD. « Anatomy of a bit : Information in a time series observation ». In : *Chaos : An Interdisciplinary Journal of Nonlinear Science* 21.3 (2011) (cf. p. 52).

[Jam90] William JAMES. *The Principles Of Psychology Volume II By William James (1890)*. 1890 (cf. p. 17).

[JP49] Herbert JASPER et Wilder PENFIELD. « Electrocorticograms in man : effect of voluntary movement upon the electrical activity of the precentral gyrus ». In : *Archiv für Psychiatrie und Nervenkrankheiten* 183 (1949), p. 163-174 (cf. p. 38).

[JO21] Mehrdad JAZAYERI et Srdjan OSTOJIC. « Interpreting neural computations by examining intrinsic and embedding dimensionality of neural activity ». In : *Current opinion in neurobiology* 70 (2021), p. 113-120 (cf. p. 59, 184).

[JB11] Ned JENKINSON et Peter BROWN. « New insights into the relationship between dopamine, beta oscillations and motor function ». In : *Trends in neurosciences* 34.12 (2011), p. 611-618 (cf. p. 39).

[Jen+02] Ole JENSEN, Jack GELFAND, John KOUNIOS et al. « Oscillations in the alpha band (9–12 Hz) increase with memory load during retention in a short-term memory task ». In : *Cerebral cortex* 12.8 (2002), p. 877-882 (cf. p. 38).

[JM10] Ole JENSEN et Ali MAZAHERI. « Shaping functional architecture by oscillatory alpha activity : gating by inhibition ». In : *Frontiers in human neuroscience* 4 (2010), p. 186 (cf. p. 38).

[Jog+18] Madhura R JOGLEKAR, Jorge F MEJIAS, Guangyu Robert YANG et al. « Inter-areal balanced amplification enhances signal propagation in a large-scale circuit model of the primate cortex ». In : *Neuron* 98.1 (2018), p. 222-234 (cf. p. 20, 34, 88, 91, 115, 125, 126, 142, 143, 147).

[Jon16] Stephanie R JONES. « When brain rhythms aren't 'rhythmic' : implication for their mechanisms and meaning ». In : *Current opinion in neurobiology* 40 (2016), p. 72-80 (cf. p. 43, 66, 160).

[KI18] Jim W KAY et Robin AA INCE. « Exact partial information decompositions for Gaussian systems based on dependency constraints ». In : *Entropy* 20.4 (2018), p. 240 (cf. p. 149).

[KFR17] Stephen KEELEY, André A FENTON et John RINZEL. « Modeling fast and slow gamma oscillations with interneurons of different subtype ». In : *Journal of neurophysiology* 117.3 (2017), p. 950-965 (cf. p. 32).

[Kil+13] Bjørg Elisabeth KILAVIK, Manuel ZAEPFFEL, Andrea BROVELLI et al. « The ups and downs of beta oscillations in sensorimotor cortex ». In : *Experimental neurology* 245 (2013), p. 15-26 (cf. p. 39).

[KC06] Osame KINOUCHI et Mauro COPELLI. « Optimal dynamical range of excitable networks at criticality ». In : *Nature physics* 2.5 (2006), p. 348-351 (cf. p. 20, 46, 56).

[KTB16] Christoph KIRST, Marc TIMME et Demian BATTAGLIA. « Dynamic information routing in complex networks ». In : *Nature communications* 7.1 (2016), p. 11061 (cf. p. 65, 149, 150).

[Kli+96] Wolfgang KLIMESCH, Michael DOPPELMAYR, Hannes SCHIMKE et al. « Alpha frequency, reaction time, and the speed of processing information ». In : *Journal of clinical neurophysiology* 13.6 (1996), p. 511-518 (cf. p. 38).

[KSH07] Wolfgang KLIMESCH, Paul SAUSENG et Simon HANSLMAYR. « EEG alpha oscillations : the inhibition–timing hypothesis ». In : *Brain research reviews* 53.1 (2007), p. 63-88 (cf. p. 38).

[Kny07] Gennady G KNYAZEV. « Motivation, emotion, and their inhibitory control mirrored in brain oscillations ». In : *Neuroscience & Biobehavioral Reviews* 31.3 (2007), p. 377-395 (cf. p. 37).

[KE86] Nancy KOPELL et G Bard ERMENTROUT. « Symmetry and phaselocking in chains of weakly coupled oscillators ». In : *Communications on Pure and Applied Mathematics* 39.5 (1986), p. 623-660 (cf. p. 33).

[KE02] Nancy KOPELL et G Bard ERMENTROUT. « Mechanisms of phase-locking and frequency control in pairs of coupled neural oscillators ». In : *Handbook of dynamical systems* 2 (2002), p. 3-54 (cf. p. 33).

[Kop+14] Nancy J KOPELL, Howard J GRITTON, Miles A WHITTINGTON et al. « Beyond the connectome : the dynome ». In : *Neuron* 83.6 (2014), p. 1319-1328 (cf. p. 150).

[Kos+20] Julian Q KOSCIESSA, Thomas H GRANDY, Douglas D GARRETT et al. « Single-trial characterization of neural rhythms : Potential and challenges ». In : *NeuroImage* 206 (2020), p. 116331 (cf. p. 43).

[Kra+17] John W KRAKAUER, Asif A GHAZANFAR, Alex GOMEZ-MARIN et al. « Neuroscience needs behavior : correcting a reductionist bias ». In : *Neuron* 93.3 (2017), p. 480-490 (cf. p. 21, 180).

[KK84] Yoshiki KURAMOTO et Yoshiki KURAMOTO. *Chemical turbulence*. Springer, 1984 (cf. p. 33).

[Lac+12] Jean-Philippe LACHAUX, Nikolai AXMACHER, Florian MORMANN et al. « High-frequency neural activity and human cognition : past, present and possible future of intracranial EEG research ». In : *Progress in neurobiology* 98.3 (2012), p. 279-301 (cf. p. 28).

[Lac+02] Jean-Philippe LACHAUX, Antoine LUTZ, David RUDRAUF et al. « Estimating the time-course of coherence between single-trial brain signals : an introduction to wavelet coherence ». In : *Neurophysiologie Clinique/Clinical Neurophysiology* 32.3 (2002), p. 157-174 (cf. p. 43, 67).

[Lac+99] Jean-Philippe LACHAUX, Eugenio RODRIGUEZ, Jacques MARTINERIE et al. « Measuring phase synchrony in brain signals ». In : *Human brain mapping* 8.4 (1999), p. 194-208 (cf. p. 67).

[Lal+07] Elodie LALO, Thomas GILBERTSON, Louise DOYLE et al. « Phasic increases in cortical beta activity are associated with alterations in sensory processing in the human ». In : *Experimental brain research* 177 (2007), p. 137-145 (cf. p. 39).

[Lan90] Chris G LANGTON. « Computation at the edge of chaos : Phase transitions and emergent computation ». In : *Physica D : nonlinear phenomena* 42.1-3 (1990), p. 12-37 (cf. p. 46, 48, 50, 52, 65, 184).

[LW14] Antonio H LARA et Jonathan D WALLIS. « Executive control processes underlying multi-item working memory ». In : *Nature neuroscience* 17.6 (2014), p. 876-883 (cf. p. 26, 27).

[LW15] Antonio H LARA et Jonathan D WALLIS. « The role of prefrontal cortex in working memory : a mini review ». In : *Frontiers in systems neuroscience* 9 (2015), p. 173 (cf. p. 25).

[LN05] Peter E LATHAM et Sheila NIRENBERG. « Synergy, redundancy, and independence in population codes, revisited ». In : *Journal of Neuroscience* 25.21 (2005), p. 5195-5206 (cf. p. 51, 124).

[Leb+04] Mikhail A LEBEDEV, Adam MESSINGER, Jerald D KRALIK et al. « Representation of attended versus remembered locations in prefrontal cortex ». In : *PLoS biology* 2.11 (2004), e365 (cf. p. 26).

[Lee+05] Han LEE, Gregory V SIMPSON, Nikos K LOGOTHETIS et al. « Phase locking of single neuron activity to theta oscillations during working memory in monkey extrastriate visual cortex ». In : *Neuron* 45.1 (2005), p. 147-156 (cf. p. 27, 37).

[Leo+97] L LEOCANI, C TORO, Paolo MANGANOTTI et al. « Event-related coherence and event-related desynchronization/synchronization in the 10 Hz and 20 Hz EEG during self-paced movements ». In : *Electroencephalography and Clinical Neurophysiology/Evoked Potentials Section* 104.3 (1997), p. 199-206 (cf. p. 39).

[Lie+12] Stefanie LIEBE, Gregor M HOERZER, Nikos K LOGOTHETIS et al. « Theta coupling between V4 and prefrontal cortex predicts visual short-term memory performance ». In : *Nature neuroscience* 15.3 (2012), p. 456-462 (cf. p. 27, 31, 37).

[Lim+23] Vinicius LIMA, Renan O SHIMOURA, Nilton L KAMIJI et al. « Propagation in a Large-Scale Circuit Model of the Primate Cortex ». In : *ReScience* (2023) (cf. p. 91).

[Lin+11] Henrik LINDÉN, Tom TETZLAFF, Tobias C POTJANS et al. « Modeling the spatial reach of the LFP ». In : *Neuron* 72.5 (2011), p. 859-872 (cf. p. 31).

[Lit+19] Simon LITTLE, James BONAIUTO, Gareth BARNES et al. « Human motor cortical beta bursts relate to movement planning and response errors ». In : *PLoS biology* 17.10 (2019), e3000479 (cf. p. 44, 160).

[LN06] Jing LIU et William T NEWSOME. « Local field potential in cortical area MT : stimulus tuning and behavioral correlations ». In : *Journal of Neuroscience* 26.30 (2006), p. 7779-7790 (cf. p. 31).

[Liz12] Joseph T LIZIER. *The local information dynamics of distributed computation in complex systems*. Springer Science & Business Media, 2012 (cf. p. 53, 65, 122).

[Liz+18] Joseph T LIZIER, Nils BERTSCHINGER, Jürgen JOST et al. *Information decomposition of target effects from multi-source interactions : Perspectives on previous, current and future work*. 2018 (cf. p. 19, 52, 124, 179).

[LFW13] Joseph T LIZIER, Benjamin FLECKER et Paul L WILLIAMS. « Towards a synergy-based approach to measuring information modification ». In : *2013 IEEE Symposium on Artificial Life (ALIFE)*. IEEE. 2013, p. 43-51 (cf. p. 51, 53, 65, 114, 124, 146).

[LPZ07] Joseph T LIZIER, Mikhail PROKOPENKO et Albert Y ZOMAYA. « Information transfer by particles in cellular automata ». In : *Australian Conference on Artificial Life*. Springer. 2007, p. 49-60 (cf. p. 53, 65).

[LPZ10] Joseph T LIZIER, Mikhail PROKOPENKO et Albert Y ZOMAYA. « Information modification and particle collisions in distributed computation ». In : *Chaos : An Interdisciplinary Journal of Nonlinear Science* 20.3 (2010) (cf. p. 53, 65).

[LPZ14] Joseph T LIZIER, Mikhail PROKOPENKO et Albert Y ZOMAYA. « A framework for the local information dynamics of distributed computation in complex systems ». In : *Guided self-organization : inception*. Springer, 2014, p. 115-158 (cf. p. 139).

[Lli88] Rodolfo R LLINÁS. « The intrinsic electrophysiological properties of mammalian neurons : insights into central nervous system function ». In : *Science* 242.4886 (1988), p. 1654-1664 (cf. p. 30).

[LBC15] Fabien LOTTE, Laurent BOUGRAIN et Maureen CLERC. « Electroencephalography (EEG)-based brain-computer interfaces ». In : *Wiley encyclopedia of electrical and electronics engineering* (2015), p. 44 (cf. p. 29).

[LS09] Evgueniy V LUBENOV et Athanassios G SIAPAS. « Hippocampal theta oscillations are travelling waves ». In : *Nature* 459.7246 (2009), p. 534-539 (cf. p. 37).

[Luc+23] Maxime LUCAS, Iacopo IACOPINI, Thomas ROBIGLIO et al. « Simplicially driven simple contagion ». In : *Physical Review Research* 5.1 (2023), p. 013201 (cf. p. 19).

[Lun+18] Mikael LUNDQVIST, Pawel HERMAN, Melissa R WARDEN et al. « Gamma and beta bursts during working memory readout suggest roles in its volitional control ». In : *Nature communications* 9.1 (2018), p. 394 (cf. p. 20, 65, 91, 185).

[Lun+24] Mikael LUNDQVIST, Earl K MILLER, Jonatan NORDMARK et al. « Beta : bursts of cognition ». In : *Trends in Cognitive Sciences* (2024) (cf. p. 20, 42, 65, 91, 160, 185, 189).

[Lun+16] Mikael LUNDQVIST, Jonas ROSE, Pawel HERMAN et al. « Gamma and beta bursts underlie working memory ». In : *Neuron* 90.1 (2016), p. 152-164 (cf. p. 20, 41, 42, 65, 91, 160, 184, 185).

[LS06] Max LUNGARELLA et Olaf SPORNS. « Mapping information flow in sensorimotor networks ». In : *PLoS computational biology* 2.10 (2006), e144 (cf. p. 147).

[Lup+21] Andrea I LUPPI, Pedro AM MEDIANO, Fernando E ROSAS et al. « What it is like to be a bit : an integrated information decomposition account of emergent mental phenomena ». In : *Neuroscience of consciousness* 2021.2 (2021), niab027 (cf. p. 188).

[Lup+22] Andrea I LUPPI, Pedro AM MEDIANO, Fernando E ROSAS et al. « A synergistic core for human brain evolution and cognition ». In : *Nature Neuroscience* 25.6 (2022), p. 771-782 (cf. p. 19, 54, 93, 124, 148, 149, 188).

[Lup+24a] Andrea I LUPPI, Fernando E ROSAS, Pedro AM MEDIANO et al. « Information decomposition and the informational architecture of the brain ». In : *Trends in Cognitive Sciences* (2024) (cf. p. 19).

[Lup+24b] Andrea I LUPPI, Fernando E ROSAS, Pedro AM MEDIANO et al. « Unravelling consciousness and brain function through the lens of time, space, and information ». In : *Trends in Neurosciences* (2024) (cf. p. 19).

[Maa11] Wolfgang MAASS. « Liquid state machines : motivation, theory, and applications ». In : *Computability in context : computation and logic in the real world* (2011), p. 275-296 (cf. p. 183).

[Mac03] David JC MACKAY. *Information theory, inference and learning algorithms*. Cambridge university press, 2003 (cf. p. 50).

[Mah+06] Séverine MAHON, Nicolas VAUTRELLE, Laurent PEZARD et al. « Distinct patterns of striatal medium spiny neuron activity during the natural sleep–wake cycle ». In : *Journal of Neuroscience* 26.48 (2006), p. 12587-12595 (cf. p. 37).

[MWP24] Gabriel MAKDAH, Sidney I WIENER et Marco N POMPILI. « Detection of cell assemblies in high-density extracellular electrophysiological recordings ». In : *bioRxiv* (2024), p. 2024-01 (cf. p. 19).

[MG06] Eve MARDER et Jean-Marc GOAILLARD. « Variability, compensation and homeostasis in neuron and network function ». In : *Nature Reviews Neuroscience* 7.7 (2006), p. 563-574 (cf. p. 150).

[Mar+19] Daniele MARINAZZO, Leonardo ANGELINI, Mario PELLICORO et al. « Synergy as a warning sign of transitions : The case of the two-dimensional Ising model ». In : *Physical Review E* 99.4 (2019), p. 040101 (cf. p. 54, 188).

[Mar+14a] Daniele MARINAZZO, Mario PELLICORO, Guorong WU et al. « Information transfer and criticality in the Ising model on the human connectome ». In : *PloS one* 9.4 (2014), e93616 (cf. p. 54).

[Mar+13] Nikola T MARKOV, Mária ERCSEY-RAVASZ, David C VAN ESSEN et al. « Cortical high-density counterstream architectures ». In : *Science* 342.6158 (2013), p. 1238406 (cf. p. 35, 93, 125).

[Mar+14b] Nikola T MARKOV, Maria M ERCSEY-RAVASZ, AR RIBEIRO GOMES et al. « A weighted and directed interareal connectivity matrix for macaque cerebral cortex ». In : *Cerebral cortex* 24.1 (2014), p. 17-36 (cf. p. 84, 91, 114, 125, 142).

[Mar12] Henry MARKRAM. « The human brain project ». In : *Scientific American* 306.6 (2012), p. 50-55 (cf. p. 20).

[Mar+15] Henry MARKRAM, Eilif MULLER, Srikanth RAMASWAMY et al. « Reconstruction and simulation of neocortical microcircuitry ». In : *Cell* 163.2 (2015), p. 456-492 (cf. p. 20).

[MP76a] David MARR et Tomaso POGGIO. « Cooperative Computation of Stereo Disparity : A cooperative algorithm is derived for extracting disparity information from stereo image pairs. » In : *Science* 194.4262 (1976), p. 283-287 (cf. p. 185).

[MP76b] David MARR et Tomaso POGGIO. « From understanding computation to understanding neural circuitry ». In : (1976) (cf. p. 54, 60, 114, 116).

[MSTMZ13] Genaro J MARTÍNEZ, Juan C SECK-TUOH-MORA et Hector ZENIL. « Wolfram's classification and computation in cellular automata Classes III and IV ». In : *Irreducibility and Computational Equivalence : 10 Years After Wolfram's A New Kind of Science* (2013), p. 237-259 (cf. p. 48, 49).

[MT06] John HR MAUNSELL et Stefan TREUE. « Feature-based attention in visual cortex ». In : *Trends in neurosciences* 29.6 (2006), p. 317-322 (cf. p. 120, 137).

[Maz+07] Alberto MAZZONI, Frédéric D BROCCARD, Elizabeth GARCIA-PEREZ et al. « On the dynamics of the spontaneous activity in neuronal networks ». In : *PloS one* 2.5 (2007), e439 (cf. p. 55, 56).

[Maz+11] Alberto MAZZONI, Nicolas BRUNEL, Stefano CAVALLARI et al. « Cortical dynamics during naturalistic sensory stimulations : experiments and models ». In : *Journal of Physiology-Paris* 105.1-3 (2011), p. 2-15 (cf. p. 31).

[MRG+87] James L MCCLELLAND, David E RUMELHART, PDP Research GROUP et al. *Parallel distributed processing, volume 2 : Explorations in the microstructure of cognition : Psychological and biological models*. T. 2. MIT press, 1987 (cf. p. 146).

[MP43] Warren S MCCULLOCH et Walter PITTS. « A logical calculus of the ideas immanent in nervous activity ». In : *The bulletin of mathematical biophysics* 5 (1943), p. 115-133 (cf. p. 19).

[McG54] William MCGILL. « Multivariate information transmission ». In : *Transactions of the IRE Professional Group on Information Theory* 4.4 (1954), p. 93-111 (cf. p. 123).

[MHM18] Leland MCINNES, John HEALY et James MELVILLE. « Umap : Uniform manifold approximation and projection for dimension reduction ». In : *arXiv preprint arXiv :1802.03426* (2018) (cf. p. 59).

[Med+19] Pedro AM MEDIANO, Fernando ROSAS, Robin L CARHART-HARRIS et al. « Beyond integrated information : A taxonomy of information dynamics phenomena ». In : *arXiv preprint arXiv :1909.02297* (2019) (cf. p. 52, 188).

[Med+22] Pedro AM MEDIANO, Fernando E ROSAS, Juan Carlos FARAH et al. « Integrated information as a common signature of dynamical and information-processing complexity ». In : *Chaos : An Interdisciplinary Journal of Nonlinear Science* 32.1 (2022) (cf. p. 52, 53, 65, 188).

[MW22] Jorge F MEJIAS et Xiao-Jing WANG. « Mechanisms of distributed working memory in a large-scale network of macaque neocortex ». In : *Elife* 11 (2022), e72136 (cf. p. 34, 92).

[MF00] Bartlett W MEL et József FISER. « Minimizing binding errors using learned conjunctive features ». In : *Neural Computation* 12.4 (2000), p. 731-762 (cf. p. 148).

[Mel+08] Jed A MELTZER, Hitten P ZAVERI, Irina I GONCHAROVA et al. « Effects of working memory load on oscillatory power in human intracranial EEG ». In : *Cerebral Cortex* 18.8 (2008), p. 1843-1855 (cf. p. 37).

[MH+24] Diego MENDOZA-HALLIDAY, Alex James MAJOR, Noah LEE et al. « A ubiquitous spectrolaminar motif of local field potential power across the primate cortex ». In : *Nature Neuroscience* 27.3 (2024), p. 547-560 (cf. p. 29).

[MLB10] David MEUNIER, Renaud LAMBIOTTE et Edward T BULLMORE. « Modular and hierarchically modular organization of brain networks ». In : *Frontiers in neuroscience* 4 (2010), p. 7572 (cf. p. 35).

[MBR24] Earl K MILLER, Scott L BRINCAT et Jefferson E ROY. « Cognition is an emergent property ». In : *Current Opinion in Behavioral Sciences* 57 (2024), p. 101388 (cf. p. 45, 91).

[MED96] Earl K MILLER, Cynthia A ERICKSON et Robert DESIMONE. « Neural mechanisms of visual working memory in prefrontal cortex of the macaque ». In : *Journal of neuroscience* 16.16 (1996), p. 5154-5167 (cf. p. 25).

[MLB18] Earl K MILLER, Mikael LUNDQVIST et André M BASTOS. « Working Memory 2.0 ». In : *Neuron* 100.2 (2018), p. 463-475 (cf. p. 25, 42, 91, 185).

[Mil56] George A MILLER. « The magical number seven, plus or minus two : Some limits on our capacity for processing information. » In : *Psychological review* 63.2 (1956), p. 81 (cf. p. 23).

[Mil16] Kenneth D MILLER. « Canonical computations of cerebral cortex ». In : *Current opinion in neurobiology* 37 (2016), p. 75-84 (cf. p. 114, 150).

[Mir+17] Amin MIRZAEI, Arvind KUMAR, Daniel LEVENTHAL et al. « Sensorimotor processing in the basal ganglia leads to transient beta oscillations during behavior ». In : *Journal of Neuroscience* 37.46 (2017), p. 11220-11232 (cf. p. 41, 42, 185).

[Mit09] Melanie MITCHELL. *Complexity : A guided tour*. Oxford university press, 2009 (cf. p. 45).

[MH+23] Rufus MITCHELL-HEGGS, Seigfred PRADO, Giuseppe P GAVA et al. « Neural manifold analysis of brain circuit dynamics in health and disease ». In : *Journal of computational neuroscience* 51.1 (2023), p. 1-21 (cf. p. 59).

[MBT08] Gianluigi MONGILLO, Omri BARAK et Misha TSODYKS. « Synaptic theory of working memory ». In : *Science* 319.5869 (2008), p. 1543-1546 (cf. p. 25).

[MRL18] Gianluigi MONGILLO, Simon RUMPEL et Yonatan LOEWENSTEIN. « Inhibitory connectivity defines the realm of excitatory plasticity ». In : *Nature neuroscience* 21.10 (2018), p. 1463-1470 (cf. p. 91, 184).

[MG+23] Aitor MORALES-GREGORIO, Anno C KURTH, Junji ITO et al. « Neural manifolds in V1 change with top-down signals from V4 targeting the foveal region ». In : *bioRxiv* (2023), p. 2023-06 (cf. p. 60).

[MNS24] Mia C MORRELL, Ilya NEMENMAN et Audrey SEDERBERG. « Neural criticality from effective latent variables ». In : *Elife* 12 (2024), RP89337 (cf. p. 56).

[Mou78] Vernon B MOUNTCASTLE. « Brain mechanisms for directed attention ». In : *Journal of the Royal Society of Medicine* 71.1 (1978), p. 14-28 (cf. p. 19).

[Mou97] Vernon B MOUNTCASTLE. « The columnar organization of the neocortex. » In : *Brain : a journal of neurology* 120.4 (1997), p. 701-722 (cf. p. 35).

[Mul+18] Lyle MULLER, Frédéric CHAVANE, John REYNOLDS et al. « Cortical travelling waves : mechanisms and computational principles ». In : *Nature Reviews Neuroscience* 19.5 (2018), p. 255-268 (cf. p. 148).

[Mun18] Miguel A MUNOZ. « Colloquium : Criticality and dynamical scaling in living systems ». In : *Reviews of Modern Physics* 90.3 (2018), p. 031001 (cf. p. 46).

[MF92] Venkatesh N MURTHY et Eberhard E FETZ. « Coherent 25-to 35-Hz oscillations in the sensorimotor cortex of awake behaving monkeys. » In : *Proceedings of the National Academy of Sciences* 89.12 (1992), p. 5670-5674 (cf. p. 91).

[Nad+08] Farzan NADIM, Vladimir BREZINA, Alain DESTEXHE et al. « State dependence of network output : modeling and experiments ». In : *Journal of Neuroscience* 28.46 (2008), p. 11806-11813 (cf. p. 150).

[NSM96] Yuji NAYA, Kuniyoshi SAKAI et Yasushi MIYASHITA. « Activity of primate inferotemporal neurons related to a sought target in pair-association task. » In : *Proceedings of the National Academy of Sciences* 93.7 (1996), p. 2664-2669 (cf. p. 25).

[Nes16] Garrett T NESKE. « The slow oscillation in cortical and thalamic networks : mechanisms and functions ». In : *Frontiers in neural circuits* 9 (2016), p. 88 (cf. p. 37).

[NBM89] William T NEWSOME, Kenneth H BRITTEN et J Anthony MOVSHON. « Neuronal correlates of a perceptual decision ». In : *Nature* 341.6237 (1989), p. 52-54 (cf. p. 180).

[Nie+21] Edward H NIEH, Manuel SCHOTTDORF, Nicolas W FREEMAN et al. « Geometry of abstract learned knowledge in the hippocampus ». In : *Nature* 595.7865 (2021), p. 80-84 (cf. p. 59).

[Nie94] Rudolf NIEUWENHUYS. « The neocortex : an overview of its evolutionary development, structural organization and synaptology ». In : *Anatomy and embryology* 190 (1994), p. 307-337 (cf. p. 35).

[NA96] Jacob NORDFALK et Preben ALSTRØM. « Phase transitions near the" game of Life" ». In : *Physical Review E* 54.2 (1996), R1025 (cf. p. 48).

[Obe+22] Virginie J OBERTO, Céline J BOUCLY, HongYing GAO et al. « Distributed cell assemblies spanning prefrontal cortex and striatum ». In : *Current Biology* 32.1 (2022), p. 1-13 (cf. p. 57).

[O'c+13] Daniel H O'CONNOR, S Andrew HIRES, Zengcai V GUO et al. « Neural coding during active somatosensation revealed using illusory touch ». In : *Nature neuroscience* 16.7 (2013), p. 958-965 (cf. p. 180).

[O'K76] John O'KEEFE. « Place units in the hippocampus of the freely moving rat ». In : *Experimental neurology* 51.1 (1976), p. 78-109 (cf. p. 17, 29, 37).

[OR93] John O'KEEFE et Michael L RECCE. « Phase relationship between hippocampal place units and the EEG theta rhythm ». In : *Hippocampus* 3.3 (1993), p. 317-330 (cf. p. 17, 37).

[Pal+17] Agostina PALMIGIANO, Theo GEISEL, Fred WOLF et al. « Flexible information routing by transient synchrony ». In : *Nature neuroscience* 20.7 (2017), p. 1014-1022 (cf. p. 41, 42, 65, 91, 123, 148-150, 181, 185, 186).

[PPK05] J Matias PALVA, Satu PALVA et Kai KAILA. « Phase synchrony among neuronal oscillations in the human cortex ». In : *Journal of Neuroscience* 25.15 (2005), p. 3962-3972 (cf. p. 38).

[PP07] Satu PALVA et J Matias PALVA. « New vistas for α-frequency band oscillations ». In : *Trends in neurosciences* 30.4 (2007), p. 150-158 (cf. p. 38).

[Pan+13] Anastasiia PANCHUK, David P ROSIN, Philipp HÖVEL et al. « Synchronization of coupled neural oscillators with heterogeneous delays ». In : *International Journal of Bifurcation and Chaos* 23.12 (2013), p. 1330039 (cf. p. 33).

[PG17] Sofia PANERI et Georgia G GREGORIOU. « Top-down control of visual attention by the prefrontal cortex. Functional specialization and long-range interactions ». In : *Frontiers in neuroscience* 11 (2017), p. 302586 (cf. p. 147).

[PB21] Matthew F PANICHELLO et Timothy J BUSCHMAN. « Shared mechanisms underlie the control of working memory and attention ». In : *Nature* 592.7855 (2021), p. 601-605 (cf. p. 59).

[Pan+10] Stefano PANZERI, Nicolas BRUNEL, Nikos K LOGOTHETIS et al. « Sensory neural codes using multiplexed temporal scales ». In : *Trends in neurosciences* 33.3 (2010), p. 111-120 (cf. p. 180).

[Pan+17] Stefano PANZERI, Christopher D HARVEY, Eugenio PIASINI et al. « Cracking the neural code for sensory perception by combining statistics, intervention, and behavior ». In : *Neuron* 93.3 (2017), p. 491-507 (cf. p. 17, 180).

[Pan+22] Stefano PANZERI, Monica MORONI, Houman SAFAAI et al. « The structures and functions of correlations in neural population codes ». In : *Nature Reviews Neuroscience* 23.9 (2022), p. 551-567 (cf. p. 17, 180, 181).

[Pan+07] Stefano PANZERI, Riccardo SENATORE, Marcelo A MONTEMURRO et al. « Correcting for the sampling bias problem in spike train information measures ». In : *Journal of neurophysiology* 98.3 (2007), p. 1064-1072 (cf. p. 149).

[Pas+08] V PASQUALE, P MASSOBRIO, LL BOLOGNA et al. « Self-organization and neuronal avalanches in networks of dissociated cortical neurons ». In : *Neuroscience* 153.4 (2008), p. 1354-1369 (cf. p. 55).

[PG05] Tatiana PASTERNAK et Mark W GREENLEE. « Working memory in primate sensory systems ». In : *Nature Reviews Neuroscience* 6.2 (2005), p. 97-107 (cf. p. 25).

[Ped+11] Fabian PEDREGOSA, Gaël VAROQUAUX, Alexandre GRAMFORT et al. « Scikit-learn : Machine learning in Python ». In : *the Journal of machine Learning research* 12 (2011), p. 2825-2830 (cf. p. 167).

[Ped+20] Nicola PEDRESCHI, Christophe BERNARD, Wesley CLAWSON et al. « Dynamic core-periphery structure of information sharing networks in entorhinal cortex and hippocampus ». In : *Network Neuroscience* 4.3 (2020), p. 946-975 (cf. p. 57, 58, 150).

[Pen+18] Rodrigo FO PENA, Cesar C CEBALLOS, Vinicius LIMA et al. « Interplay of activation kinetics and the derivative conductance determines resonance properties of neurons ». In : *Physical Review E* 97.4 (2018), p. 042408 (cf. p. 28, 32).

[Pen+19] Rodrigo FO PENA, Vinicius LIMA, Renan O SHIMOURA et al. « Asymmetrical voltage response in resonant neurons shaped by nonlinearities ». In : *Chaos : An Interdisciplinary Journal of Nonlinear Science* 29.10 (2019) (cf. p. 28).

[Pen+15] Yueqing PENG, Sarah GILLIS-SMITH, Hao JIN et al. « Sweet and bitter taste in the brain of awake behaving animals ». In : *Nature* 527.7579 (2015), p. 512-515 (cf. p. 180).

[PB03] Markku PENTTONEN et György BUZSÁKI. « Natural logarithmic relationship between brain oscillators ». In : *Thalamus & Related Systems* 2.2 (2003), p. 145-152 (cf. p. 28, 36).

[PB68] Donald H PERKEL et Theodore H BULLOCK. « Neural coding. » In : *Neurosciences Research Program Bulletin* (1968) (cf. p. 55).

[PNA08] Bijan PESARAN, Matthew J NELSON et Richard A ANDERSEN. « Free choice activates a decision circuit between frontal and parietal cortex ». In : *Nature* 453.7193 (2008), p. 406-409 (cf. p. 91).

[Pes+02] Bijan PESARAN, John S PEZARIS, Maneesh SAHANI et al. « Temporal structure in neuronal activity during working memory in macaque parietal cortex ». In : *Nature neuroscience* 5.8 (2002), p. 805-811 (cf. p. 27, 28, 31).

[Pes+18] Bijan PESARAN, Martin VINCK, Gaute T EINEVOLL et al. « Investigating large-scale brain dynamics using field potential recordings : analysis and interpretation ». In : *Nature neuroscience* 21.7 (2018), p. 903-919 (cf. p. 30).

[Pes19] Luiz PESSOA. « Neural dynamics of emotion and cognition : from trajectories to underlying neural geometry ». In : *Neural Networks* 120 (2019), p. 158-166 (cf. p. 58).

[Pes22] Luiz PESSOA. *The entangled brain : How perception, cognition, and emotion are woven together*. MIT Press, 2022 (cf. p. 18, 19).

[Pet+09] Thomas PETERMANN, Tara C THIAGARAJAN, Mikhail A LEBEDEV et al. « Spontaneous cortical activity in awake monkeys composed of neuronal avalanches ». In : *Proceedings of the National Academy of Sciences* 106.37 (2009), p. 15921-15926 (cf. p. 56).

[Pet+14] Giovanni PETRI, Paul EXPERT, Federico TURKHEIMER et al. « Homological scaffolds of brain functional networks ». In : *Journal of The Royal Society Interface* 11.101 (2014), p. 20140873 (cf. p. 60, 188).

[PA77] Gert PFURTSCHELLER et A ARANIBAR. « Event-related cortical desynchronization detected by power measurements of scalp EEG ». In : *Electroencephalography and clinical neurophysiology* 42.6 (1977), p. 817-826 (cf. p. 38).

[PDS99] Gert PFURTSCHELLER et FH Lopes DA SILVA. « Event-related EEG/MEG synchronization and desynchronization : basic principles ». In : *Clinical neurophysiology* 110.11 (1999), p. 1842-1857 (cf. p. 38).

[PK92] Gert PFURTSCHELLER et Wolfgang KLIMESCH. « Event-related synchronization and desynchronization of alpha and beta waves in a cognitive task ». In : *Induced rhythms in the brain*. Springer, 1992, p. 117-128 (cf. p. 38).

[PSJN96] Gert PFURTSCHELLER, A STANCAK JR et Christa NEUPER. « Post-movement beta synchronization. A correlate of an idling motor area ? » In : *Electroencephalography and clinical neurophysiology* 98.4 (1996), p. 281-293 (cf. p. 39).

[Pie80] John Robinson PIERCE. *An introduction to information theory : symbols, signals & noise*. Courier Corporation, 1980 (cf. p. 50).

[Pik+00] Fenella G PIKE, Ruth S GODDARD, Jillian M SUCKLING et al. *Distinct frequency preferences of different types of rat hippocampal neurones in response to oscillatory input currents*. 2000 (cf. p. 32).

[Pin+20] Edoardo PINZUTI, Patricia WOLLSTADT, Aaron GUTKNECHT et al. « Measuring spectrally-resolved information transfer ». In : *PLoS computational biology* 16.12 (2020), e1008526 (cf. p. 148).

[Pom+22] Marco N POMPILI, Ralitsa TODOROVA, Céline J BOUCLY et al. « Flexible communication between cell assemblies and 'reader'neurons ». In : *BioRxiv* (2022), p. 2022-09 (cf. p. 19).

[Por+15] Alberto PORTA, Mathias BAUMERT, Dirk CYSARZ et al. *Enhancing dynamical signatures of complex systems through symbolic computation*. 2015 (cf. p. 58).

[Pos06] Bradley R POSTLE. « Working memory as an emergent property of the mind and brain ». In : *Neuroscience* 139.1 (2006), p. 23-38 (cf. p. 23, 26).

[PD14] Tobias C POTJANS et Markus DIESMANN. « The cell-type specific cortical microcircuit : relating structure and activity in a full-scale spiking network model ». In : *Cerebral cortex* 24.3 (2014), p. 785-806 (cf. p. 20, 34, 35).

[PS04] Frederic POUILLE et Massimo SCANZIANI. « Routing of spike series by dynamic circuits in the hippocampus ». In : *Nature* 429.6993 (2004), p. 717-723 (cf. p. 150).

[PMW09] Viola PRIESEMANN, Matthias HJ MUNK et Michael WIBRAL. « Subsampling effects in neuronal avalanche distributions recorded in vivo ». In : *BMC neuroscience* 10 (2009), p. 1-20 (cf. p. 56).

[Pri+14] Viola PRIESEMANN, Michael WIBRAL, Mario VALDERRAMA et al. « Spike avalanches in vivo suggest a driven, slightly subcritical brain state ». In : *Frontiers in systems neuroscience* 8 (2014), p. 108 (cf. p. 56).

[PGR06] Emmanuel PROCYK et Patricia S GOLDMAN-RAKIC. « Modulation of dorsolateral prefrontal delay activity during self-organized behavior ». In : *Journal of Neuroscience* 26.44 (2006), p. 11313-11323 (cf. p. 25).

[PGM86] E PUIL, B GIMBARZEVSKY et RM MIURA. « Quantification of membrane properties of trigeminal root ganglion neurons in guinea pigs ». In : *Journal of neurophysiology* 55.5 (1986), p. 995-1016 (cf. p. 32).

[Qui+21] Andrew J QUINN, Vitor Lopes-dos SANTOS, David DUPRET et al. « EMD : empirical mode decomposition and Hilbert-Huang spectral analyses in Python ». In : *Journal of open source software* 6.59 (2021) (cf. p. 43, 44, 167).

[Qui+18] Andrew J QUINN, Diego VIDAURRE, Romesh ABEYSURIYA et al. « Task-evoked dynamic network analysis through hidden Markov modeling ». In : *Frontiers in neuroscience* 12 (2018), p. 603 (cf. p. 44).

[Qui12] Rodrigo Quian QUIROGA. « Spike sorting ». In : *Current Biology* 22.2 (2012), R45-R46 (cf. p. 30).

[Rab+22] Giovanni RABUFFO, Pierpaolo SORRENTINO, Christophe BERNARD et al. « Spontaneous neuronal avalanches as a correlate of access consciousness ». In : *Frontiers in Psychology* 13 (2022), p. 1008407 (cf. p. 59).

[Rag+01] Sridhar RAGHAVACHARI, Michael J KAHANA, Daniel S RIZZUTO et al. « Gating of human theta oscillations by a working memory task ». In : *Journal of Neuroscience* 21.9 (2001), p. 3175-3183 (cf. p. 37).

[RAM98] Gregor RAINER, Wael F ASAAD et Earl K MILLER. « Selective representation of relevant information by neurons in the primate prefrontal cortex ». In : *Nature* 393.6685 (1998), p. 577-579 (cf. p. 25).

[RM02] Gregor RAINER et Earl K MILLER. « Timecourse of object-related neural activity in the primate prefrontal cortex during a short-term memory task ». In : *European Journal of Neuroscience* 15.7 (2002), p. 1244-1254 (cf. p. 25).

[Ray+22] Holly RAYSON, Ranjan DEBNATH, Sanaz ALAVIZADEH et al. « Detection and analysis of cortical beta bursts in developmental EEG data ». In : *Developmental cognitive neuroscience* 54 (2022), p. 101069 (cf. p. 44, 160).

[Ren+10] Alfonso RENART, Jaime DE LA ROCHA, Peter BARTHO et al. « The asynchronous state in cortical circuits ». In : *science* 327.5965 (2010), p. 587-590 (cf. p. 56).

[Ren11] Paul RENDELL. « A universal turing machine in conway's game of life ». In : *2011 International Conference on High Performance Computing & Simulation*. IEEE. 2011, p. 764-772 (cf. p. 48).

[RRW02] Christopher J RENNIE, Peter A ROBINSON et James Joseph WRIGHT. « Unified neurophysical model of EEG spectra and evoked potentials ». In : *Biological cybernetics* 86.6 (2002), p. 457-471 (cf. p. 38).

[Rib+10] Tiago L RIBEIRO, Mauro COPELLI, Fábio CAIXETA et al. « Spike avalanches exhibit universal dynamics across the sleep-wake cycle ». In : *PloS one* 5.11 (2010), e14129 (cf. p. 55).

[RBH03] Magnus JE RICHARDSON, Nicolas BRUNEL et Vincent HAKIM. « From subthreshold to firing-rate resonance ». In : *Journal of neurophysiology* 89.5 (2003), p. 2538-2554 (cf. p. 32).

[Ric+17] Craig G RICHTER, William H THOMPSON, Conrado A BOSMAN et al. « Top-down beta enhances bottom-up gamma ». In : *Journal of Neuroscience* 37.28 (2017), p. 6698-6711 (cf. p. 39).

[Rie+99] Fred RIEKE, David WARLAND, Rob de Ruyter VAN STEVENINCK et al. *Spikes : exploring the neural code*. MIT press, 1999 (cf. p. 19, 55, 57, 180).

[RP12] Adam C RIGGALL et Bradley R POSTLE. « The relationship between working memory storage and elevated activity as measured with functional magnetic resonance imaging ». In : *Journal of Neuroscience* 32.38 (2012), p. 12990-12998 (cf. p. 25).

[RHP80] AJ ROCKEL, Robert W HIORNS et TP POWELL. « The basic uniformity in structure of the neocortex. » In : *Brain : a journal of neurology* 103.2 (1980), p. 221-244 (cf. p. 35).

[RZRG18] R ROMERO-ZALIZ et JF REINOSO-GORDO. « An updated review on watershed algorithms ». In : *Soft computing for sustainability science* (2018), p. 235-258 (cf. p. 168).

[Roo+06] Anita K ROOPUN, Steven J MIDDLETON, Mark O CUNNINGHAM et al. « A beta2-frequency (20–30 Hz) oscillation in nonsynaptic networks of somatosensory cortex ». In : *Proceedings of the National Academy of Sciences* 103.42 (2006), p. 15646-15650 (cf. p. 39).

[Ros+24] Fernando E ROSAS, Bernhard C GEIGER, Andrea I LUPPI et al. « Software in the natural world : A computational approach to emergence in complex multi-level systems ». In : *arXiv preprint arXiv :2402.09090* (2024) (cf. p. 185, 188).

[Ros+19] Fernando E ROSAS, Pedro AM MEDIANO, Michael GASTPAR et al. « Quantifying high-order interdependencies via multivariate extensions of the mutual information ». In : *Physical Review E* 100.3 (2019), p. 032305 (cf. p. 19, 52, 188).

[Ros+20] Fernando E ROSAS, Pedro AM MEDIANO, Henrik J JENSEN et al. « Reconciling emergences : An information-theoretic approach to identify causal emergence in multivariate data ». In : *PLoS computational biology* 16.12 (2020), e1008289 (cf. p. 150).

[Ros+22] Fernando E ROSAS, Pedro AM MEDIANO, Andrea I LUPPI et al. « Disentangling high-order mechanisms and high-order behaviours in complex systems ». In : *Nature Physics* 18.5 (2022), p. 476-477 (cf. p. 188).

[Ros+01] Michael ROSENBLUM, Arkady PIKOVSKY, Jurgen KURTHS et al. « Phase synchronization : from theory to data analysis ». In : *Handbook of biological physics*. T. 4. Elsevier, 2001, p. 279-321 (cf. p. 33).

[RMR06] Sébastien ROUX, William A MACKAY et Alexa RIEHLE. « The pre-movement component of motor cortical local field potentials reflects the level of expectancy ». In : *Behavioural brain research* 169.2 (2006), p. 335-351 (cf. p. 31).

[RBH05] Alex ROXIN, Nicolas BRUNEL et David HANSEL. « Role of delays in shaping spatiotemporal dynamics of neuronal activity in large networks ». In : *Physical review letters* 94.23 (2005), p. 238103 (cf. p. 115, 117, 148).

[RBH06] Alex ROXIN, Nicolas BRUNEL et David HANSEL. « Rate models with delays and the dynamics of large networks of spiking neurons ». In : *Progress of Theoretical Physics Supplement* 161 (2006), p. 68-85 (cf. p. 115, 117, 148).

[SPV07] Yuri B SAALMANN, Ivan N PIGAREV et Trichur R VIDYASAGAR. « Neural mechanisms of visual attention : how top-down feedback highlights relevant locations ». In : *Science* 316.5831 (2007), p. 1612-1615 (cf. p. 39).

[Sab+21] William SABAN, Gal RAZ, Roland H GRABNER et al. « Primitive visual channels have a causal role in cognitive transfer ». In : *Scientific Reports* 11.1 (2021), p. 8759 (cf. p. 114).

[Sal+12] RF SALAZAR, NM DOTSON, SL BRESSLER et al. « Content-specific fronto-parietal synchronization during visual working memory ». In : *Science* 338.6110 (2012), p. 1097-1100 (cf. p. 27, 39, 65, 92).

[Sal+10] Maryam SALEH, Jacob REIMER, Richard PENN et al. « Fast and slow oscillations in human primary motor cortex predict oncoming behaviorally relevant cues ». In : *Neuron* 65.4 (2010), p. 461-471 (cf. p. 39).

[SHH23] Abbaspoor SAMAN, Ahmed T HUSSIN et Kari L HOFFMAN. « Theta-and gamma-band oscillatory uncoupling in the macaque hippocampus ». In : *eLife* 12 (2023) (cf. p. 18, 160).

[SVM00] Maria V SANCHEZ-VIVES et David A MCCORMICK. « Cellular and network mechanisms of rhythmic recurrent activity in neocortex ». In : *Nature neuroscience* 3.10 (2000), p. 1027-1034 (cf. p. 37).

[STL03] A SANDBERG, Jesper TEGNÉR et Anders LANSNER. « A working memory model based on fast Hebbian learning ». In : *Network : Computation in Neural Systems* 14.4 (2003), p. 789 (cf. p. 91, 184).

[SBL11] Roberto SANTANA, Concha BIELZA et Pedro LARRAÑAGA. « Optimizing brain networks topologies using multi-objective evolutionary computation ». In : *Neuroinformatics* 9 (2011), p. 3-19 (cf. p. 94).

[San+23] Andrea SANTORO, Federico BATTISTON, Giovanni PETRI et al. « Higher-order organization of multivariate time series ». In : *Nature Physics* 19.2 (2023), p. 221-229 (cf. p. 59, 60).

[Sau+05] Paul SAUSENG, Wolfgang KLIMESCH, Michael DOPPELMAYR et al. « EEG alpha synchronization and functional coupling during top-down processing in a working memory task ». In : *Human brain mapping* 26.2 (2005), p. 148-155 (cf. p. 36).

[Sch+13] Anna C SCHAPIRO, James L MCCLELLAND, Stephen R WELBOURNE et al. « Why bilateral damage is worse than unilateral damage to the brain ». In : *Journal of cognitive neuroscience* 25.12 (2013), p. 2107-2123 (cf. p. 146).

[Sch+09] René SCHEERINGA, Karl Magnus PETERSSON, Robert OOSTENVELD et al. « Trial-by-trial coupling between EEG and BOLD identifies networks related to alpha and theta EEG power increases during working memory maintenance ». In : *Neuroimage* 44.3 (2009), p. 1224-1238 (cf. p. 38).

[SJA05] Hansjörg SCHERBERGER, Murray R JARVIS et Richard A ANDERSEN. « Cortical local field potential encodes movement intentions in the posterior parietal cortex ». In : *Neuron* 46.2 (2005), p. 347-354 (cf. p. 31).

[Sch+16] Maximilian SCHMIDT, Gleb BEZGIN, Rembrandt BAKKER et al. « From single-cell spiking to large-scale interactions : A multi-scale spiking network model of macaque cortex ». In : *Bernstein Conference 2016*. FZJ-2016-05496. Computational et Systems Neuroscience. 2016 (cf. p. 20).

[SRM23] Robert SCHMIDT, Jonas ROSE et Vignesh MURALIDHARAN. « Transient oscillations as computations for cognition : Analysis, modeling and function ». In : *Current opinion in neurobiology* 83 (2023), p. 102796 (cf. p. 44, 160).

[Sch+22] Matthew T SCHMITZ, Kadellyn SANDOVAL, Christopher P CHEN et al. « The development and evolution of inhibitory neurons in primate cerebrum ». In : *Nature* 603.7903 (2022), p. 871-877 (cf. p. 35).

[Sch+21] Marius SCHNEIDER, Ana Clara BROGGINI, Benjamin DANN et al. « A mechanism for inter-areal coherence through communication based on connectivity and oscillatory power ». In : *Neuron* 109.24 (2021), p. 4050-4067 (cf. p. 41, 91, 187).

[Sch00] Thomas SCHREIBER. « Measuring information transfer ». In : *Physical review letters* 85.2 (2000), p. 461 (cf. p. 51, 123, 136).

[SL09] Charles E SCHROEDER et Peter LAKATOS. « Low-frequency neuronal oscillations as instruments of sensory selection ». In : *Trends in neurosciences* 32.1 (2009), p. 9-18 (cf. p. 39).

[Sch+17] Erich SCHUBERT, Jörg SANDER, Martin ESTER et al. « DBSCAN revisited, revisited : why and how you should (still) use DBSCAN ». In : *ACM Transactions on Database Systems (TODS)* 42.3 (2017), p. 1-21 (cf. p. 167).

[Sch+94] Harald T SCHUPP, Werner LUTZENBERGER, Niels BIRBAUMER et al. « Neurophysiological differences between perception and imagery ». In : *Cognitive Brain Research* 2.2 (1994), p. 77-86 (cf. p. 38).

[SBT17] Philipp SCHWEDHELM, Daniel BALDAUF et Stefan TREUE. « Electrical stimulation of macaque lateral prefrontal cortex modulates oculomotor behavior indicative of a disruption of top-down attention ». In : *Scientific reports* 7.1 (2017), p. 17715 (cf. p. 182).

[SDS15] Arindrajit SEAL, Arunava DAS et Prasad SEN. « Watershed : an image segmentation approach ». In : *International Journal of Computer Science and Information Technologies* 6.3 (2015), p. 2295-2297 (cf. p. 44).

[SEP24] Enrique R SEBASTIAN, Julio ESPARZA et Liset M. de la PRIDA. « Quantifying the distribution of feature values over data represented in arbitrary dimensional spaces ». In : *PLOS Computational Biology* 20.1 (2024), e1011768 (cf. p. 58).

[Seg+63] JP SEGUNDO, GP MOORE, LJ STENSAAS et al. « Sensitivity of neurones in Aplysia to temporal pattern of arriving impulses ». In : *Journal of Experimental Biology* 40.4 (1963), p. 643-667 (cf. p. 55).

[SBB15] Anil K SETH, Adam B BARRETT et Lionel BARNETT. « Granger causality analysis in neuroscience and neuroimaging ». In : *Journal of Neuroscience* 35.8 (2015), p. 3293-3297 (cf. p. 123).

[SDM01] James P SETHNA, Karin A DAHMEN et Christopher R MYERS. « Crackling noise ». In : *Nature* 410.6825 (2001), p. 242-250 (cf. p. 92).

[Sha+07] M SHAFI, Y ZHOU, J QUINTANA et al. « Variability in neuronal activity in primate cortex during working memory tasks ». In : *Neuroscience* 146.3 (2007), p. 1082-1108 (cf. p. 25).

[Sha14] Maoz SHAMIR. « Emerging principles of population coding : in search for the neural code ». In : *Current opinion in neurobiology* 25 (2014), p. 140-148 (cf. p. 181).

[Sha51] Claude E SHANNON. « Prediction and entropy of printed English ». In : *Bell system technical journal* 30.1 (1951), p. 50-64 (cf. p. 46).

[Sha48] Claude Elwood SHANNON. « A mathematical theory of communication ». In : *The Bell system technical journal* 27.3 (1948), p. 379-423 (cf. p. 46, 50, 114).

[Sha84] R SHAW. *The Dripping Faucet as a Model Chaotic System*. 1984 (cf. p. 46, 184).

[ST14] Maxim SHEROZIYA et Igor TIMOFEEV. « Global intracellular slow-wave dynamics of the thalamocortical system ». In : *Journal of Neuroscience* 34.26 (2014), p. 8875-8893 (cf. p. 37).

[She+15] Woodrow L SHEW, Wesley P CLAWSON, Jeff POBST et al. « Adaptation to sensory input tunes visual cortex to criticality ». In : *Nature Physics* 11.8 (2015), p. 659-663 (cf. p. 56).

[She+09] Woodrow L SHEW, Hongdian YANG, Thomas PETERMANN et al. « Neuronal avalanches imply maximum dynamic range in cortical networks at criticality ». In : *Journal of neuroscience* 29.49 (2009), p. 15595-15600 (cf. p. 56).

[She+11] Woodrow L SHEW, Hongdian YANG, Shan YU et al. « Information capacity and transmission are maximized in balanced cortical networks with neuronal avalanches ». In : *Journal of neuroscience* 31.1 (2011), p. 55-63 (cf. p. 56, 184).

[Shi+21] Renan Oliveira SHIMOURA, Rodrigo FO PENA, Vinicius LIMA et al. « Building a model of the brain : from detailed connectivity maps to network organization ». In : *The European Physical Journal Special Topics* 230.14 (2021), p. 2887-2909 (cf. p. 20).

[Shi+17] Hyeyoung SHIN, Robert LAW, Shawn TSUTSUI et al. « The rate of transient beta frequency events predicts behavior across tasks and species ». In : *Elife* 6 (2017), e29086 (cf. p. 20, 44, 160).

[Shi+16] James M SHINE, Patrick G BISSETT, Peter T BELL et al. « The dynamics of functional brain networks : integrated network states during cognitive task performance ». In : *Neuron* 92.2 (2016), p. 544-554 (cf. p. 65, 115).

[SDE12] Markus SIEGEL, Tobias H DONNER et Andreas K ENGEL. « Spectral fingerprints of large-scale neuronal interactions ». In : *Nature Reviews Neuroscience* 13.2 (2012), p. 121-134 (cf. p. 39, 79, 91, 188).

[SED11] Markus SIEGEL, Andreas K ENGEL et Tobias H DONNER. « Cortical network dynamics of perceptual decision-making in the human brain ». In : *Frontiers in human neuroscience* 5 (2011), p. 21 (cf. p. 91).

[SWM09] Markus SIEGEL, Melissa R WARDEN et Earl K MILLER. « Phase-dependent neuronal coding of objects in short-term memory ». In : *Proceedings of the National Academy of Sciences* 106.50 (2009), p. 21341-21346 (cf. p. 27, 39, 91).

[Sil91] Fernando Lopes da SILVA. « Neural mechanisms underlying brain waves : from neural membranes to networks ». In : *Electroencephalography and clinical neurophysiology* 79.2 (1991), p. 81-93 (cf. p. 36).

[Sil13] Fernando Lopes da SILVA. « EEG and MEG : relevance to neuroscience ». In : *Neuron* 80.5 (2013), p. 1112-1128 (cf. p. 28).

[SAC91] Laurie R SILVA, Yael AMITAI et Barry W CONNORS. « Intrinsic oscillations of neocortex generated by layer 5 pyramidal neurons ». In : *Science* 251.4992 (1991), p. 432-435 (cf. p. 38).

[SG95] Wolf SINGER et Charles M GRAY. « Visual feature integration and the temporal correlation hypothesis ». In : *Annual review of neuroscience* 18.1 (1995), p. 555-586 (cf. p. 40).

[SA89] Mark K SINGLEY et John Robert ANDERSON. *The transfer of cognitive skill*. 9. Harvard University Press, 1989 (cf. p. 147).

[SK93] William R SOFTKY et Christof KOCH. « The highly irregular firing of cortical cells is inconsistent with temporal integration of random EPSPs ». In : *Journal of neuroscience* 13.1 (1993), p. 334-350 (cf. p. 34).

[SD93] I SOLTESZ et M DESCHENES. « Low-and high-frequency membrane potential oscillations during theta activity in CA1 and CA3 pyramidal neurons of the rat hippocampus under ketamine-xylazine anesthesia ». In : *Journal of neurophysiology* 70.1 (1993), p. 97-116 (cf. p. 32).

[Sor+23] Pierpaolo SORRENTINO, Emahnuel Troisi LOPEZ, Antonella ROMANO et al. « Brain fingerprint is based on the aperiodic, scale-free, neuronal activity ». In : *NeuroImage* 277 (2023), p. 120260 (cf. p. 44, 56, 92).

[Spa+12] Eelke SPAAK, Mathilde BONNEFOND, Alexander MAIER et al. « Layer-specific entrainment of gamma-band neural activity by the alpha rhythm in monkey visual cortex ». In : *Current biology* 22.24 (2012), p. 2313-2318 (cf. p. 31).

[Spi+08] Rachel L SPINKS, Alexander KRASKOV, Thomas BROCHIER et al. « Selectivity for grasp in local field potential and single neuron activity recorded simultaneously from M1 and F5 in the awake macaque monkey ». In : *Journal of Neuroscience* 28.43 (2008), p. 10961-10971 (cf. p. 39).

[Spo13] Olaf SPORNS. « Network attributes for segregation and integration in the human brain ». In : *Current opinion in neurobiology* 23.2 (2013), p. 162-171 (cf. p. 41, 65).

[Spo16] Olaf SPORNS. *Networks of the Brain*. MIT press, 2016 (cf. p. 19).

[SB16] Olaf SPORNS et Richard F BETZEL. « Modular brain networks ». In : *Annual review of psychology* 67 (2016), p. 613-640 (cf. p. 35).

[SK04] Olaf SPORNS et Rolf KÖTTER. « Motifs in brain networks ». In : *PLoS biology* 2.11 (2004), e369 (cf. p. 94).

[SCM20] Angela STALLONE, Antonio CICONE et Massimo MATERASSI. « New insights and best practices for the successful use of Empirical Mode Decomposition, Iterative Filtering and derived algorithms ». In : *Scientific reports* 10.1 (2020), p. 15161 (cf. p. 44).

[SG11] G Karl STEINKE et Roberto F GALÁN. « Brain rhythms reveal a hierarchical network organization ». In : *PLoS computational biology* 7.10 (2011), e1002207 (cf. p. 36).

[Ste+21] Nicholas A STEINMETZ, Cagatay AYDIN, Anna LEBEDEVA et al. « Neuropixels 2.0 : A miniaturized high-density probe for stable, long-term brain recordings ». In : *Science* 372.6539 (2021), eabf4588 (cf. p. 17).

[SNA93] Mircea STERIADE, Angel NUNEZ et Florin AMZICA. « A novel slow (< 1 Hz) oscillation of neocortical neurons in vivo : depolarizing and hyperpolarizing components ». In : *Journal of neuroscience* 13.8 (1993), p. 3252-3265 (cf. p. 37).

[SBO00] Martin STETTER, Hauke BARTSCH et Klaus OBERMAYER. « A mean-field model for orientation tuning, contrast saturation, and contextual effects in the primary visual cortex ». In : *Biological cybernetics* 82.4 (2000), p. 291-304 (cf. p. 115).

[SS16] Mark STOKES et Eelke SPAAK. « The importance of single-trial analyses in cognitive neuroscience ». In : *Trends in Cognitive Sciences* 20.7 (2016), p. 483-486 (cf. p. 20).

[Sto+13] Mark G STOKES, Makoto KUSUNOKI, Natasha SIGALA et al. « Dynamic coding for cognitive control in prefrontal cortex ». In : *Neuron* 78.2 (2013), p. 364-375 (cf. p. 26, 66).

[SHP17] Bernadette J STOLZ, Heather A HARRINGTON et Mason A PORTER. « Persistent homology of time-dependent functional networks constructed from coupled time series ». In : *Chaos : An Interdisciplinary Journal of Nonlinear Science* 27.4 (2017) (cf. p. 60).

[Sto15] James V STONE. « Information theory : a tutorial introduction ». In : (2015) (cf. p. 50).

[Str+21] Sebastiano STRAMAGLIA, Tomas SCAGLIARINI, Bryan C DANIELS et al. « Quantifying dynamical high-order interdependencies from the o-information : An application to neural spiking dynamics ». In : *Frontiers in Physiology* 11 (2021), p. 595736 (cf. p. 60).

[Str00] Steven H STROGATZ. « From Kuramoto to Crawford : exploring the onset of synchronization in populations of coupled oscillators ». In : *Physica D : Nonlinear Phenomena* 143.1-4 (2000), p. 1-20 (cf. p. 33).

[Str18] Steven H STROGATZ. *Nonlinear dynamics and chaos : with applications to physics, biology, chemistry, and engineering*. CRC press, 2018 (cf. p. 34).

[Stu65] Ch STUMPF. « The fast component in the electrical activity of rabbit's hippocampus ». In : *Electroencephalography and clinical neurophysiology* 18.5 (1965), p. 477-486 (cf. p. 32).

[Suá+24] Laura E SUÁREZ, Agoston MIHALIK, Filip MILISAV et al. « Connectome-based reservoir computing with the conn2res toolbox ». In : *Nature Communications* 15.1 (2024), p. 656 (cf. p. 56).

[SA09] David SUSSILLO et Larry F ABBOTT. « Generating coherent patterns of activity from chaotic neural networks ». In : *Neuron* 63.4 (2009), p. 544-557 (cf. p. 184).

[Sze75] J SZENTAGOTHAI. « The 'module-concept'in cerebral cortex architecture ». In : *Brain research* 95.2-3 (1975), p. 475-496 (cf. p. 35).

[Szu+23] Maciej J SZUL, Sotirios PAPADOPOULOS, Sanaz ALAVIZADEH et al. « Diverse beta burst waveform motifs characterize movement-related cortical dynamics ». In : *Progress in Neurobiology* 228 (2023), p. 102490 (cf. p. 65).

[Szy+11] Francois D SZYMANSKI, Neil C RABINOWITZ, Cesare MAGRI et al. « The laminar and temporal structure of stimulus information in the phase of field potentials of auditory cortex ». In : *Journal of Neuroscience* 31.44 (2011), p. 15787-15801 (cf. p. 31).

[Taa13] Niels A TAATGEN. « The nature and transfer of cognitive skills. » In : *Psychological review* 120.3 (2013), p. 439 (cf. p. 114, 148).

[TB+97] Catherine TALLON-BAUDRY, Olivier BERTRAND, Claude DELPUECH et al. « Oscillatory γ-band (30–70 Hz) activity induced by a visual search task in humans ». In : *Journal of Neuroscience* 17.2 (1997), p. 722-734 (cf. p. 39).

[TB+98] Catherine TALLON-BAUDRY, Olivier BERTRAND, Franck PERONNET et al. « Induced γ-band activity during the delay of a visual short-term memory task in humans ». In : *Journal of Neuroscience* 18.11 (1998), p. 4244-4254 (cf. p. 39).

[TB+04] Catherine TALLON-BAUDRY, Sunita MANDON, Winrich A FREIWALD et al. « Oscillatory synchrony in the monkey temporal lobe correlates with performance in a visual short-term memory task ». In : *Cerebral cortex* 14.7 (2004), p. 713-720 (cf. p. 27).

[Tay+05] K TAYLOR, S MANDON, WA FREIWALD et al. « Coherent oscillatory activity in monkey area v4 predicts successful allocation of attention ». In : *Cerebral Cortex* 15.9 (2005), p. 1424-1437 (cf. p. 39).

[TWK17] Peter N TAYLOR, Yujiang WANG et Marcus KAISER. « Within brain area tractography suggests local modularity using high resolution connectomics ». In : *Scientific reports* 7.1 (2017), p. 39859 (cf. p. 35).

[Teh+06] EJ TEHOVNIK, AS TOLIAS, F SULTAN et al. « Direct and indirect activation of cortical neurons by electrical microstimulation ». In : *Journal of neurophysiology* 96.2 (2006), p. 512-521 (cf. p. 180).

[Tet+10] Christian TETZLAFF, Samora OKUJENI, Ulrich EGERT et al. « Self-organized criticality in developing neuronal networks ». In : *PLoS computational biology* 6.12 (2010), e1001013 (cf. p. 56).

[Tho+02] Alex M THOMSON, David C WEST, Yun WANG et al. « Synaptic connections and small circuits involving excitatory and inhibitory neurons in layers 2–5 of adult rat and cat neocortex : triple intracellular recordings and biocytin labelling in vitro ». In : *Cerebral cortex* 12.9 (2002), p. 936-953 (cf. p. 35).

[TS09] Paul TIESINGA et Terrence J SEJNOWSKI. « Cortical enlightenment : are attentional gamma oscillations driven by ING or PING? » In : *Neuron* 63.6 (2009), p. 727-732 (cf. p. 33).

[Tii+93] HT TIITINEN, J SINKKONEN, K REINIKAINEN et al. « Selective attention enhances the auditory 40-Hz transient response in humans ». In : *Nature* 364.6432 (1993), p. 59-60 (cf. p. 39).

[TES98] Giulio TONONI, Gerald M EDELMAN et Olaf SPORNS. « Complexity and coherency : integrating information in the brain ». In : *Trends in cognitive sciences* 2.12 (1998), p. 474-484 (cf. p. 184).

[TSE94] Giulio TONONI, Olaf SPORNS et Gerald M EDELMAN. « A measure for brain complexity : relating functional segregation and integration in the nervous system. » In : *Proceedings of the National Academy of Sciences* 91.11 (1994), p. 5033-5037 (cf. p. 41).

[TSE96] Giulio TONONI, Olaf SPORNS et Gerald M EDELMAN. « A complexity measure for selective matching of signals by the brain. » In : *Proceedings of the National Academy of Sciences* 93.8 (1996), p. 3422-3427 (cf. p. 54).

[TC98] Christopher TORRENCE et Gilbert P COMPO. « A practical guide to wavelet analysis ». In : *Bulletin of the American Meteorological society* 79.1 (1998), p. 61-78 (cf. p. 43).

[TD17] Jonathan TOUBOUL et Alain DESTEXHE. « Power-law statistics and universal scaling in the absence of criticality ». In : *Physical Review E* 95.1 (2017), p. 012413 (cf. p. 56).

[Tra+96] Roger D TRAUB, Miles A WHITTINGTON, Ian M STANFORD et al. « A mechanism for generation of long-range synchronous fast oscillations in the cortex ». In : *Nature* 383.6601 (1996), p. 621-624 (cf. p. 33).

[Tre96] Anne TREISMAN. « The binding problem ». In : *Current opinion in neurobiology* 6.2 (1996), p. 171-178 (cf. p. 40).

[Tre01] Stefan TREUE. « Neural correlates of attention in primate visual cortex ». In : *Trends in neurosciences* 24.5 (2001), p. 295-300 (cf. p. 120, 138, 139).

[Tsu+07] Yasuhiro TSUBO, Masahiko TAKADA, Alex D REYES et al. « Layer and frequency dependencies of phase response properties of pyramidal neurons in rat motor cortex ». In : *European Journal of Neuroscience* 25.11 (2007), p. 3429-3441 (cf. p. 32).

[Tul+07] Anil M TULADHAR, Niels ter HUURNE, Jan-Mathijs SCHOFFELEN et al. « Parieto-occipital sources account for the increase in alpha activity with working memory load ». In : *Human brain mapping* 28.8 (2007), p. 785-792 (cf. p. 38, 39).

[US10] Peter J UHLHAAS et Wolf SINGER. « Abnormal neural oscillations and synchrony in schizophrenia ». In : *Nature reviews neuroscience* 11.2 (2010), p. 100-113 (cf. p. 32).

[VVABE94] Carl VAN VREESWIJK, LF ABBOTT et G BARD ERMENTROUT. « When inhibition not excitation synchronizes neural firing ». In : *Journal of computational neuroscience* 1 (1994), p. 313-321 (cf. p. 33).

[VVS96] Carl VAN VREESWIJK et Haim SOMPOLINSKY. « Chaos in neuronal networks with balanced excitatory and inhibitory activity ». In : *Science* 274.5293 (1996), p. 1724-1726 (cf. p. 56).

[VV+18] Bram VAN VUGT, Bruno DAGNINO, Devavrat VARTAK et al. « The threshold for conscious report : Signal loss and response bias in visual and frontal cortex ». In : *Science* 360.6388 (2018), p. 537-542 (cf. p. 42).

[Van69] Case H VANDERWOLF. « Hippocampal electrical activity and voluntary movement in the rat ». In : *Electroencephalography and clinical neurophysiology* 26.4 (1969), p. 407-418 (cf. p. 37).

[Van16] André VANDIERENDONCK. « A working memory system with distributed executive control ». In : *Perspectives on Psychological Science* 11.1 (2016), p. 74-100 (cf. p. 65, 183).

[Var+01] Francisco VARELA, Jean-Philippe LACHAUX, Eugenio RODRIGUEZ et al. « The brainweb : phase synchronization and large-scale integration ». In : *Nature reviews neuroscience* 2.4 (2001), p. 229-239 (cf. p. 18, 57, 65).

[Var89] Francisco J VARELA. « Connaître : les sciences cognitives : tendances et perspectives ». In : *(No Title)* (1989) (cf. p. 18).

[Var24] Thomas F VARLEY. « Generalized decomposition of multivariate information ». In : *Plos one* 19.2 (2024), e0297128 (cf. p. 19).

[VB24] Thomas F VARLEY et Joshua BONGARD. « Evolving higher-order synergies reveals a trade-off between stability and information integration capacity in complex systems ». In : *arXiv preprint arXiv :2401.14347* (2024) (cf. p. 54, 188).

[Var+23a] Thomas F VARLEY, Maria POPE, Joshua FASKOWITZ et al. « Multivariate information theory uncovers synergistic subsystems of the human cerebral cortex ». In : *Communications biology* 6.1 (2023), p. 451 (cf. p. 19, 52, 93, 188).

[Var+23b] Thomas F VARLEY, Maria POPE, Maria GRAZIA et al. « Partial entropy decomposition reveals higher-order information structures in human brain activity ». In : *Proceedings of the National Academy of Sciences* 120.30 (2023), e2300888120 (cf. p. 93).

[Vez+21] Julien VEZOLI, Martin VINCK, Conrado Arturo BOSMAN et al. « Brain rhythms define distinct interaction networks with differential dependence on anatomy ». In : *Neuron* 109.23 (2021), p. 3862-3878 (cf. p. 36, 40, 93).

[Vic+11] Raul VICENTE, Michael WIBRAL, Michael LINDNER et al. « Transfer entropy—a model-free measure of effective connectivity for the neurosciences ». In : *Journal of computational neuroscience* 30.1 (2011), p. 45-67 (cf. p. 123).

[Vic+94] Jonathan D VICTOR, Keith PURPURA, Ephraim KATZ et al. « Population encoding of spatial frequency, orientation, and color in macaque V1 ». In : *Journal of neurophysiology* 72.5 (1994), p. 2151-2166 (cf. p. 31).

[Vin+23] Martin VINCK, Cem URAN, Georgios SPYROPOULOS et al. « Principles of large-scale neural interactions ». In : *Neuron* 111.7 (2023), p. 987-1002 (cf. p. 30, 41, 42, 65, 92, 185).

[VA05] Tim P VOGELS et Larry F ABBOTT. « Signal propagation and logic gating in networks of integrate-and-fire neurons ». In : *Journal of neuroscience* 25.46 (2005), p. 10786-10795 (cf. p. 181).

[Vog+24] Nicole VOGES, Vinicius LIMA, Johannes HAUSMANN et al. « Decomposing neural circuit function into information processing primitives ». In : *Journal of Neuroscience* 44.2 (2024) (cf. p. 19, 51, 60, 88, 179).

[VP12] Nicole VOGES et L PERRINET. « Complex dynamics in recurrent cortical networks based on spatially realistic connectivities ». In : *Frontiers in computational neuroscience* 6 (2012), p. 41 (cf. p. 150).

[VCS98] M VOLGUSHEV, M CHISTIAKOVA et W SINGER. « Modification of discharge patterns of neocortical neurons by induced oscillations of the membrane potential ». In : *Neuroscience* 83.1 (1998), p. 15-25 (cf. p. 40).

[VDM94] Christoph VON DER MALSBURG. « The correlation theory of brain function ». In : *Models of neural networks : Temporal aspects of coding and information processing in biological systems*. Springer, 1994, p. 95-119 (cf. p. 57).

[VDMPS10] Christoph VON DER MALSBURG, William A PHILLIPS et Wolf SINGER. *Dynamic coordination in the brain : from neurons to mind*. MIT press, 2010 (cf. p. 18).

[VSS00] Astrid VON STEIN et Johannes SARNTHEIN. « Different frequencies for different scales of cortical integration : from local gamma to long range alpha/theta synchronization ». In : *International journal of psychophysiology* 38.3 (2000), p. 301-313 (cf. p. 36).

[WFP20] Mengni WANG, David J FOSTER et Brad E PFEIFFER. « Alternating sequences of future and past behavior encoded within hippocampal theta oscillations ». In : *Science* 370.6513 (2020), p. 247-250 (cf. p. 185).

[Wan+21] Rong WANG, Mianxin LIU, Xinhong CHENG et al. « Segregation, integration, and balance of large-scale resting brain networks configure different cognitive abilities ». In : *Proceedings of the National Academy of Sciences* 118.23 (2021), e2022288118 (cf. p. 65).

[WR93] X-J WANG et J RINZEL. « Spindle rhythmicity in the reticularis thalami nucleus : synchronization among mutually inhibitory neurons ». In : *Neuroscience* 53.4 (1993), p. 899-904 (cf. p. 33).

[Wan01] Xiao-Jing WANG. « Synaptic reverberation underlying mnemonic persistent activity ». In : *Trends in neurosciences* 24.8 (2001), p. 455-463 (cf. p. 25).

[Wan10] Xiao-Jing WANG. « Neurophysiological and computational principles of cortical rhythms in cognition ». In : *Physiological reviews* 90.3 (2010), p. 1195-1268 (cf. p. 28, 32-34, 88).

[WB96] Xiao-Jing WANG et György BUZSÁKI. « Gamma oscillation by synaptic inhibition in a hippocampal interneuronal network model ». In : *Journal of neuroscience* 16.20 (1996), p. 6402-6413 (cf. p. 31, 33, 34).

[WR92] Xiao-Jing WANG et John RINZEL. « Alternating and synchronous rhythms in reciprocally inhibitory model neurons ». In : *Neural computation* 4.1 (1992), p. 84-97 (cf. p. 33).

[WS98] Duncan J WATTS et Steven H STROGATZ. « Collective dynamics of 'small-world'networks ». In : *nature* 393.6684 (1998), p. 440-442 (cf. p. 34, 183).

[Whe+09] Lewis WHEATON, Esteban FRIDMAN, Stephan BOHLHALTER et al. « Left parietal activation related to planning, executing and suppressing praxis hand movements ». In : *Clinical Neurophysiology* 120.5 (2009), p. 980-986 (cf. p. 38).

[WTJ95] Miles A WHITTINGTON, Roger D TRAUB et John GR JEFFERYS. « Synchronized oscillations in interneuron networks driven by metabotropic glutamate receptor activation ». In : *Nature* 373.6515 (1995), p. 612-615 (cf. p. 33).

[Whi+00] Miles A WHITTINGTON, Roger D TRAUB, Nancy KOPELL et al. « Inhibition-based rhythms : experimental and mathematical observations on network dynamics ». In : *International journal of psychophysiology* 38.3 (2000), p. 315-336 (cf. p. 33).

[Wib+17] Michael WIBRAL, Viola PRIESEMANN, Jim W KAY et al. « Partial information decomposition as a unified approach to the specification of neural goal functions ». In : *Brain and cognition* 112 (2017), p. 25-38 (cf. p. 19, 114, 179, 188).

[WVL14] Michael WIBRAL, Raul VICENTE et Joseph T LIZIER. *Directed information measures in neuroscience*. T. 724. Springer, 2014 (cf. p. 122).

[Wic99] Wayne A WICKELGREN. « Webs, cell assemblies, and chunking in neural nets : introduction. » In : *Canadian Journal of Experimental Psychology/Revue canadienne de psychologie expérimentale* 53.1 (1999), p. 118 (cf. p. 148).

[Wie56] Norbert WIENER. « The theory of prediction ». In : *Modern mathematics for engineers* (1956) (cf. p. 51, 123).

[Wil+58] Maurice V WILKES, David J WHEELER, Stanley GILL et al. *The preparation of programs for an electronic digital computer*. 1958 (cf. p. 146).

[Wil+20] Alex H WILLIAMS, Ben POOLE, Niru MAHESWARANATHAN et al. « Discovering precise temporal patterns in large-scale neural recordings through robust and interpretable time warping ». In : *Neuron* 105.2 (2020), p. 246-259 (cf. p. 43).

[WB10] Paul L WILLIAMS et Randall D BEER. « Nonnegative decomposition of multivariate information ». In : *arXiv preprint arXiv :1004.2515* (2010) (cf. p. 19, 51, 114, 124, 150, 179).

[WC72] Hugh R WILSON et Jack D COWAN. « Excitatory and inhibitory interactions in localized populations of model neurons ». In : *Biophysical journal* 12.1 (1972), p. 1-24 (cf. p. 33, 88).

[Woe04] Carl R WOESE. « A new biology for a new century ». In : *Microbiology and molecular biology reviews* 68.2 (2004), p. 173-186 (cf. p. 20).

[Wol97] Stephen WOLFRAM. *New kind of science*. 1997 (cf. p. 47, 48).

[WF07] Thilo WOMELSDORF et Pascal FRIES. « The role of neuronal synchronization in selective attention ». In : *Current opinion in neurobiology* 17.2 (2007), p. 154-160 (cf. p. 40, 91).

[Wom+06] Thilo WOMELSDORF, Pascal FRIES, Partha P MITRA et al. « Gamma-band synchronization in visual cortex predicts speed of change detection ». In : *Nature* 439.7077 (2006), p. 733-736 (cf. p. 31).

[Wom+07] Thilo WOMELSDORF, Jan-Mathijs SCHOFFELEN, Robert OOSTENVELD et al. « Modulation of neuronal interactions through neuronal synchronization ». In : *science* 316.5831 (2007), p. 1609-1612 (cf. p. 40).

[WH09] Zhaohua WU et Norden E HUANG. « Ensemble empirical mode decomposition : a noise-assisted data analysis method ». In : *Advances in adaptive data analysis* 1.01 (2009), p. 1-41 (cf. p. 166, 167).

[Xin+12] Dajun XING, Yutai SHEN, Samuel BURNS et al. « Stochastic generation of gamma-band activity in primary visual cortex of awake and anesthetized monkeys ». In : *Journal of Neuroscience* 32.40 (2012), 13873-13880a (cf. p. 41).

[XFB23] Yihan XIONG, Pascal FRIES et André M BASTOS. « Which Rhythms Reflect Bottom-Up and Top-Down Processing? » In : *Intracranial EEG : A Guide for Cognitive Neuroscientists*. Springer, 2023, p. 389-414 (cf. p. 39).

[Yan+12] Hongdian YANG, Woodrow L SHEW, Rajarshi ROY et al. « Maximal variability of phase synchrony in cortical networks with neuronal avalanches ». In : *Journal of neuroscience* 32.3 (2012), p. 1061-1072 (cf. p. 56).

[Yge+11] Pierre YGER, Sami EL BOUSTANI, Alain DESTEXHE et al. « Topologically invariant macroscopic statistics in balanced networks of conductance-based integrate-and-fire neurons ». In : *Journal of computational neuroscience* 31.2 (2011), p. 229-245 (cf. p. 150).

[You93] Malcolm P YOUNG. « The organization of neural systems in the primate cerebral cortex ». In : *Proceedings of the Royal Society of London. Series B : Biological Sciences* 252.1333 (1993), p. 13-18 (cf. p. 35).

[Yu+08] Shan YU, Debin HUANG, Wolf SINGER et al. « A small world of neuronal synchrony ». In : *Cerebral cortex* 18.12 (2008), p. 2891-2901 (cf. p. 35).

[Yu+14] Shan YU, Andreas KLAUS, Hongdian YANG et al. « Scale-invariant neuronal avalanche dynamics and the cut-off in size distributions ». In : *PloS one* 9.6 (2014), e99761 (cf. p. 55).

[ZR21] Mickael ZBILI et Sylvain RAMA. « A quick and easy way to estimate entropy and mutual information for neuroscience ». In : *Frontiers in Neuroinformatics* 15 (2021), p. 596443 (cf. p. 68).

[Zha+22] Fan ZHANG, Alessandro DADUCCI, Yong HE et al. « Quantitative mapping of the brain's structural connectivity using diffusion MRI tractography : A review ». In : *Neuroimage* 249 (2022), p. 118870 (cf. p. 35).

[Zha+08] Yan ZHANG, Yonghong CHEN, Steven L BRESSLER et al. « Response preparation and inhibition : the role of the cortical sensorimotor beta rhythm ». In : *Neuroscience* 156.1 (2008), p. 238-246 (cf. p. 38).

[ZR02] Robert S ZUCKER et Wade G REGEHR. « Short-term synaptic plasticity ». In : *Annual review of physiology* 64.1 (2002), p. 355-405 (cf. p. 25).

[ZMD11] Joel ZYLBERBERG, Jason Timothy MURPHY et Michael Robert DEWEESE. « A sparse coding model with synaptically local plasticity and spiking neurons can account for the diverse shapes of V1 simple cell receptive fields ». In : *PLoS computational biology* 7.10 (2011), e1002250 (cf. p. 148).

APPENDICES

A. [Replication] Inter-areal Balanced Amplification Enhances Signal Propagation in a Large-Scale Circuit Model of the Primate Cortex

RESCIENCE C

Replication / Computational Neuroscience

[Re] Inter-areal Balanced Amplification Enhances Signal Propagation in a Large-Scale Circuit Model of the Primate Cortex

Vinicius Lima[1,2], Renan O. Shimoura[3,2], Nilton L. Kamiji[3], Demian Battaglia[1,4], and Antonio C. Roque[1,4]

[1]Aix-Marseille University, Institute for Systems Neuroscience (INS UMR 1106, Inserm), Marseille, France – [2]These authors contributed equally to this work, Gif sur Yvette, France – [3]Department of Physics, School of Philosophy, Sciences and Letters of Ribeirão Preto (FFCLRP), University of São Paulo„ Ribeirao Preto, Brazil – [4]University of Strasbourg Institute for Advanced Studies (USIAS), Strasbourg, France

Edited by
Benoit Girard

Reviewed by
Marcel Stimberg
Stephan Grein

Received
05 May 2023

Published
04 December 2023

DOI
10.5281/zenodo.10257800

1 Introduction

Information processing in the cortex relies on stable and, at the same time, reconfigurable signal propagation among its areas, i.e.: first, the signal is neither attenuated nor amplified as it propagates across the cortical hierarchy of areas; second, the extent to which signal propagate through hierarchically connected regions must be regulated by context. Despite numerous studies done on inter-area signal propagation in the mammalian cortex [1, 2, 3], the underlying mechanisms that could allow a simultaneously reliable and flexible signal transmission are not yet completely understood. In computational neuroscience, many models address this question, however most of them make unrealistic assumptions such as perfect identity of all areas, homogeneity of connection weights across all stages of the hierarchy, and strictly feedforward network architecture, even though cortical networks are rich in recurrent connections and feedback loops [4]. Here we replicate a recent modelling study by Joglekar et. al., [5]. In this work, the authors address the problem of reliable and flexible signal propagation in a large-scale network model embedding a realistic multi-regional connectome. The network structure of the model is prescribed by an empiricaly-determined directed and weighted inter-areal connectivity matrix for the macaque cortex, containing 29 areas distributed across the occipital, temporal, parietal, and frontal lobes [4]. Furthermore, regions have heterogeneous time constants, due to a phenomenological reproduction of varying number of excitatory spines across the cortical hierarchy [6]. The dynamics of network nodes are described initially in terms of a population-level mean-field rate model [7, 8]. In a second part of the article, a spiking network model of leaky integrate-and-fire neurons is used as well to study synchrony modulations within each region. One of the key contributions of Joglekar et. al. [5] study is to reveal the important role of a mechanism named *global balanced amplification (GBA)*. Briefly, this mechanism consists of increasing inter-areal excitation to facilitate signal propagation to different areas, combined simultaneously with an increase of local inhibition to assure network stability. Modulating GBA provides thus a way to enable stable signal propagation or to disable it, thus conditionally switching on or off the access to regions distant from the site of input injection.

Copyright © 2023 V. Lima et al., releusepackageed under a Creative Commons Attribution 4.0 International license.
Correspondence should be addressed to Vinicius Lima (vinicius.lima.cordeiro@gmail.com)
The authors have declared that no competing interests exists.
Code is available at https://github.com/ViniciusLima94/ReScience-Joglekar/tree/master/code..
Data is available at https://github.com/ViniciusLima94/ReScience-Joglekar/tree/master/code/interareal.
Open peer review is available at https://github.com/ReScience/submissions/issues/72.

As mentioned in the Methods section of Joglekar et. al. [5], the original large-scale spiking neuron network was implemented in the Brian 2 simulator [9]. Here, we provide an original implementation of both the rate based, and the spike based model in the NEST simulator [10, 11], which allows parallel execution of the network simulation, making the code particularly easy to run in super-computers. In addition, our implementation of the model also provides an optimized open code for any researcher willing to use or adapt the model for other scientific projects.
The selection of results we have chosen to reproduce provides a rich overview of the main contents of the original paper. We obtained qualitatively similar results and we checked under what conditions their robustness and validity were kept.

Availability of code implementations for the original model

In the original publication, the authors do not link any associated code repository with their implementation of the models described. However, we found a repository with Matlab and Python (Brian 2) scripts in the following address: github.com/xjwanglab/JoglekarEtAl2018_Neuron. Despite the fact that those scripts helped to detect discrepancies and non-specified parameters in the original article, for the spiking model, not all parameters could be directly "plugged-in" into Nest without conversion, and some adjustment was often required in order to obtain the firing rate regimes specified in the original paper, as we elaborated throughout this replication paper.

2 Methods

In this section we describe the models used in the original implementations [5]. We start by briefly presenting the data used to construct the network connectivity, and to estimate the synaptic weights among different cortical regions [4]. Next, we describe the rate based model, and lastly the spiking neuron model. For the last two, we make a bottom-up description, i.e., starting from single population/neuron dynamics, the local network structure, to the large-scale network structure for each model. In this section we focus on the general description of each model, specific parameters will be given in the Results section, since they change depending on the specific replicated result.

2.1 Network connectivity data

To determine the inter-regional connectome and the number of projections originating from each cortical area, the original model uses high-quality retrograde tracing data by Markov et. al., [4], encompassing 29 areas from the macaque cerebral cortex. Restricted to these 29 areas, the connectome is edge-complete, i.e. there are no missing inter-regional connections that have not been characterized [12]. The directed weight from a source to a target area is estimated to be proportional to the Fraction of Labeled Neurons (FLN). The FLN is defined as the number of labeled neurons in a source area divided by the total number of labeled neurons in all source areas. As retrograde tracers are used, the FLN can be considered as an indication of the relative of neurons sending long-range projections from one source area to a target.
In Fig. 1(a) we show the logarithms of the FLN values between areas used for the simulations here reproduced. The delay between regions is estimated using wiring distances between the different regions in the macaque cortex, which are shown in Fig. 1(b), and assuming a propagation velocity of $v = 3.5$ m/s [13]. Finally in Fig. 1(c), we show the hierarchical rank of the different regions in the connectome. The quantities in Fig. 1 are the ones on which later simulations are going to be constructed.
Henceforth, we will denote a pair of cortical areas by the indexes i, and j, in such a way that FLN_{ij} is the FLN from area i to area j. Note that, since the graph given by

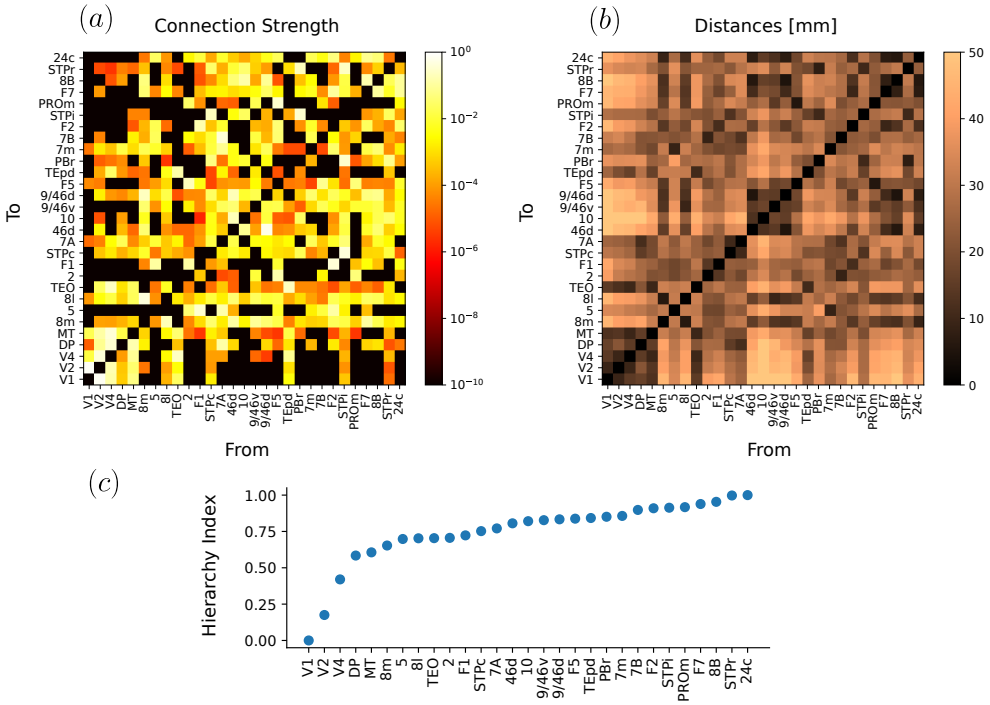

Figure 1. Data from Markov et. al., [4] used to build the large-scale networks. In (a) we show the FLN in logarithmic scale due to the large range of values encountered (non-existent connections are shown in black), in (b) the wiring distance between cortical areas, and in (c) the normalized anatomical hierarchy of each cortical area.

the weighted matrix in Fig. 1(a) is asymmetric, $\text{FLN}_{ij} \neq \text{FLN}_{ji}$. The delay will be represent by the letter D, and $D_{ij} = D_{ji}$ is the delay between area i and j. Similarly, the anatomical hierarchy of area i is denoted by h_i.
The data used to build the network is available with the code related to this article in: github.com/ViniciusLima94/ReScience-Joglekar/blob/master/code/interareal (the original data can be obtained from core-nets.org, however it is necessary to properly organize it in order to be able to run the model; in our repository, all the necessary preprocessing is done).

2.2 Rate based models

Here we describe the rate based model. We reproduce two sets of results from the original paper in which this model is used: namely, Fig. 1, and Fig. 3 from [5].

Population dynamics — The population dynamics of the rate based model is given by Eq. 1

$$\tau_{E,I} \frac{dr_{E,I}(t)}{dt} = -r_{E,I}(t) + \beta_{E,I}\phi[I_{\text{ext}}(t)], \tag{1}$$

where $r(t)$ is the firing rate of each specific population, the sub-index E, I indicates whether the population is excitatory or inhibitory, τ is the time constant, β is the slope of the frequency-current curve, I_{ext} is the net external input which is the sum of synaptic (I_{syn}), injected (I_{inj}), and any other input current, and $\phi[x] = \max(x, 0)$ is a threshold-linear transfer function.

Local circuit — The local circuit is composed of an excitatory and an inhibitory populations, coupled by an excitatory to inhibitory connection ($E \rightarrow I$), and an inhibitory to excitatory connection ($I \rightarrow E$). In addition, each population is connected to itself, via an $E \rightarrow E$ and an $I \rightarrow I$ couplings. The local circuit described is schematized in Fig. 2(a), and can be written as:

$$\begin{aligned} \tau_E \frac{dr_E(t)}{dt} &= -r_E(t) + \beta_E \phi[\omega_{EE} r_E(t) - \omega_{IE} r_I(t) + I_{\text{inj,E}}(t)], \\ \tau_I \frac{dr_I(t)}{dt} &= -r_I(t) + \beta_I \phi[\omega_{EI} r_E(t) - \omega_{II} r_I(t) + I_{\text{inj,I}}(t)], \end{aligned} \tag{2}$$

where ω_{ij} is the local synaptic weight from i to j. $I_{\text{inj,E}}$, and $I_{\text{inj,I}}$ are external currents injected in the excitatory, and inhibitory populations, respectively.

Large-scale circuit — The local dynamics of regions within the large-scale network model follows Eq. 2. However, regions are now heterogeneous and each of them sees its local weights modulated according to the hierarchical rank of each area. Specifically, the components of the local synaptic currents in area i, are given by the following equations:

$$I_{EE}^{\text{local,i}} = \omega_{EE}(1 + \eta h_i) r_E^i, \tag{3}$$

$$I_{IE}^{\text{local,i}} = -\omega_{IE} r_I^i, \tag{4}$$

$$I_{EI}^{\text{local,i}} = \omega_{EI}(1 + \eta h_i) r_E^i \tag{5}$$

$$I_{II}^{\text{local,i}} = -\omega_{II} r_I^i, \tag{6}$$

Intra-regional excitatory currents are increased by a hierarchy dependent gain factor, in which a parameter η multiplies the hierarchical rank index of the considered areas. Consequently, regions with a higher hierarchical order are more excitable.
The long-range synaptic projections are considered to be purely excitatory and their strength are determined by the weighted graph presented in Section 2.1. In practice, if the FLN between area i and j is greater than zero ($\text{FLN}_{ij} > 0$), those areas are connected. The total long-range synaptic currents that the excitatory and inhibitory populations of area i receive are given by Eqs. 7-8.

$$I_{EE}^{lr,i} = \mu_{EE}(1 + \eta h_i) \sum_{\substack{j=0 \\ i \neq j}}^{N_{\text{areas}}} \text{FLN}_{ji} r_E^j, \tag{7}$$

$$I_{EI}^{lr,i} = \mu_{EI}(1 + \eta h_i) \sum_{\substack{j=0 \\ i \neq j}}^{N_{\text{areas}}} \text{FLN}_{ji} r_E^j, \tag{8}$$

where μ represents the long-range synaptic weights, and N_{areas} is the number of cortical areas. Note that the long-range connections are scaled by the hierarchical position of the target regions.
The total current received by the excitatory and inhibitory populations in an area i can be expressed by combining Eqs. 3-8, as follows:

$$I_E^i = I_{EE}^{local,i} + I_{EE}^{lr,i} + I_{IE}^{\text{local,i}} + I_{\text{inj,E}}^i, \tag{9}$$

$$I_I^i = I_{EI}^{local,i} + I_{EI}^{lr,i} + I_{II}^{\text{local,i}} + I_{\text{inj,I}}^i, \tag{10}$$

The transmission delay (D_{ij}) between areas i and j is neglected and considered to be instantaneous ($D_{ij} = 0$, $\forall\, i$ and j), so that no use is made of the tract length matrix of Fig. 1b, but only of the FLN matrix of Fig. 1a and the hierarchical order of Fig. 1c.

2.3 Spiking neuron models

In this section, we describe the spiking neuron network models. Based on them, we reproduced the results of Fig. 5, and Fig. 6 from the original paper.

Single neuron — Neurons were modeled using the leaky integrate-and-fire (LIF) model as follows.

$$\frac{dV(t)}{dt} = -\frac{V(t) - V_{\mathrm{r}}}{\tau_{E,I}} + \frac{I_{\mathrm{ext}}(t)}{C_{E,I}}, \tag{11}$$

where $V(t)$ is the time-dependent membrane potential, V_r is the resting potential, τ is the membrane time constant, and C is the membrane capacitance. The external current is given by $I_{\mathrm{ext}} = I_{\mathrm{syn}} + I_{\mathrm{inj}}$, where I_{syn} is the synaptic, and I_{inj} the injected currents.
A spike is emitted following the spike-and-reset rule in Eq. 12:

$$V(t) \geq V_{\mathrm{th}} \Rightarrow \begin{cases} \text{Spike at time } t \\ V(t + \tau_{\mathrm{ref}}) = V_{\mathrm{reset}}, \end{cases} \tag{12}$$

where V_{th} is the spike threshold, τ_{ref} is the refractory period, and V_{reset} is the reset value of the membrane potential. In Table 1, we show the parameters used for the LIF neuron.

V_{r} [mV]	V_{reset} [mV]	$V(0)$ [mV]	τ_E [ms]	τ_I [ms]	τ_{ref} [ms]	C_E [pA]	C_I [pA]
-70.0	-60.0	-70.0	20.0	10.0	2.0	400.0	200.0

Table 1. Parameters for the LIF neuron model in Eqs. 11-12.

Local circuit — The local circuit in each spiking region is composed of $N = N_E + N_I = 2000$ LIF neurons, where $N_E = 1600$ are excitatory, and $N_I = 400$ are inhibitory. Connections are random and sparse, established with a fixed probability for each pair of neurons set as $p = 0.1$. The synaptic current received by the neuron i is given by:

$$I^i_{\mathrm{syn}} = \sum_j \omega_{ji} \sum_k \delta(t - t^k_j - d), \tag{13}$$

where ω_{ji} is the synaptic weight from neuron j to neuron i, t^k_j is the time of the kth spike from neuron j, and d is the local delay. The input spike-trains are mathematically represented as the sum of Dirac delta terms.
The local synaptic currents are obtained by replacing the rates r_E, and r_I in Eqs. 3-6 with the input spike trains from Eq. 13. The total local synaptic current received by an excitatory neuron in area i is obtained by combining Eqs. 14-15:

$$I^{\mathrm{local,i}}_{EE} = \sum_{j=0}^{N^{\mathrm{pre}}_E} \omega_{EE}(1 + \eta h_i) \sum_k \delta(t - t^k_j - d), \tag{14}$$

$$I^{\mathrm{local,i}}_{IE} = -\sum_{j=0}^{N^{\mathrm{pre}}_I} \omega_{IE} \sum_k \delta(t - t^k_j - d),, \tag{15}$$

and the total local synaptic current received by an inhibitory neuron in area i is given by Eqs. 16-17.

$$I_{EI}^{\text{local,i}} = \sum_{j=0}^{N_E^{\text{pre}}} \omega_{EI}(1+\eta h_i) \sum_k \delta(t - t_j^k - d), \tag{16}$$

$$I_{II}^{\text{local,i}} = -\sum_{j=0}^{N_I^{\text{pre}}} \omega_{II} \sum_k \delta(t - t_j^k - d), \tag{17}$$

In the expression above, N_E^{pre}, and N_I^{pre} are the number of excitatory and inhibitory pre-synaptic neurons, respectively.

Large-scale circuit — Each region is modeled as the local circuit described above. Their long-range synaptic currents received by excitatory and inhibitory neurons in area i from neurons in area j, are given by:

$$I_{EE}^{lr,i} = \sum_{j=0}^{N_E^{\text{pre}}} \mu_{EE}(1+\eta h_i)\text{FLN}_{ji} \sum_k \delta(t - t_j^k - D_{ji}^{'}), \tag{18}$$

$$I_{EI}^{lr,i} = \sum_{j=0}^{N_E^{\text{pre}}} \mu_{EI}(1+\eta h_i)\text{FLN}_{ji} \sum_k \delta(t - t_j^k - D_{ji}^{'}), \tag{19}$$

The delays $D_{ji}^{'}$ are sampled from normal distribution with mean D_{ji}, and standard deviation $0.1D_{ij}$ ($D_{ji}^{'} = \mathcal{N}(D_{ji}, 0.1D_{ji})$). These delays were estimated dividing the tract lengths (Fig. 2b) by the propagation velocity of $v = 3.5$ m/s.
The hierarchical order of the targeted region is scaled via a gain parameter η. All the parameters used in the model of a large-scale circuit described above are given in Table 5.

2.4 Balanced amplification

As we briefly mentioned in Section 1, the models described above were used to study signal propagation in the cortical system. In Joglekar et. al., [5], the mechanism of *balanced amplification*, is hypothesised to contribute to reliable signal propagation through the cortical hierarchy.
For the local circuits, and 2.3.2) this mechanism is refereed to as *local* balanced amplification (LBA), and consists of increasing the recurrent excitation (ω_{EE}), and the lateral inhibition (ω_{IE}). For the large-scale circuits this mechanism is referred to as *global* balanced amplification (GBA), and consists of increasing the long-range $E \to E$ excitation (μ_{EE}), and the local lateral inhibition (ω_{IE}).
These balanced amplification mechanisms, when activated, can achieve two effects: first, through the increase of excitatory couplings, signal transmission among areas is enhanced; and, second, increasing the lateral inhibition within local circuits, network instability is avoided, despite the overall increase in excitation.
In the results we will compare signal propagation in the models above in two alternative regimes, corresponding to two distinct functional states of the brain network: (i) Weak LBA/GBA, and (ii) Strong LBA/GBA. The transition from regime (i) to (ii) is done via increasing ω_{EE}/μ_{EE}, and ω_{IE}, as described above. The parameters used in each regime are specified in the specifically associated results section.

3 Results

In this Section we will present the results we choose to replicate from the original article. These results give an outlook of the mechanism of global balanced amplification

(Section 2.4). In Sections 3.1-3.3 we replicate the result in Figures 1, 3, 5 and 6 from Joglekar et. al. [5]. For each result we also highlight the issues we had replicating it, such as the parameters values not informed in the original publication. The name of those parameters will be coloured red in the parameter Tables 2-5.

3.1 Local Balanced Amplification in an Inhibition-Stabilized Local Circuit

To reproduce a first result in Figure 1 of the original [5] paper, we use the local circuit described by the rate based model of Eq. 2. In Fig. 2(a), we show a schematic representation of this simple circuit. The parameters for the used model are given in Table 2 of this article. All parameters were copied from the original publication, apart from τ_E and τ_I for which we could not find an explicit value in the original publication. However, in line with descriptions and Equation 1 therein, we set $\tau_E = \tau_I = \tau$ and adjusted this common value τ to get figures looking similar to the original ones. The estimated value is the one we report in Table 2, together with the other parameters.
This first result we reproduce exemplify the mechanism of balanced amplification within a local circuit. In Fig. 2(b), we show the evolution of the excitatory rate $r_E(t)$, starting from the initial condition $r_E(0) = 1$, and $r_I(0) = 0$. This initial condition emulates the state in which the E population is already active due to a transient input. The green and violet curves correspond to the E rate evolution in a weak and strong LBA conditions. Note that the response of the system is indeed enhanced in the strong LBA case, leading to evoked activity which has both a stronger peak amplitude and an enhanced transient.

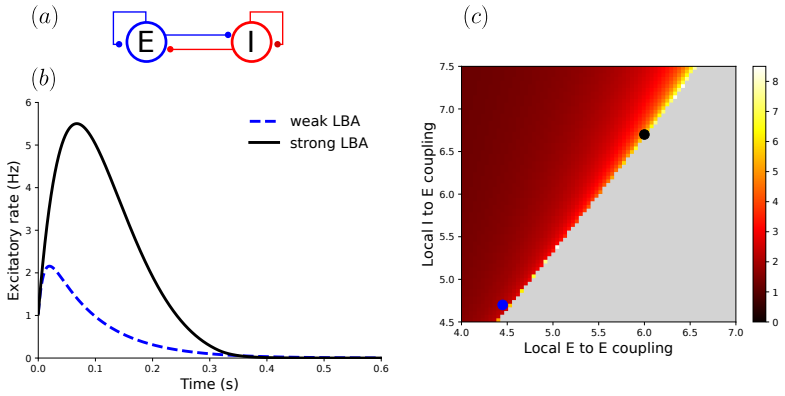

Figure 2. Replication of the result in Figure 1 of the original publication [5]. In (a) we show a schematic depiction of the local circuit used to generate the results, in (b) we show the response rate of the excitatory population after its initial value being set to 1 Hz (emulating application of a brief destabilizing input), for weak (green) and strong (purple) local balanced amplification (LBA). In (c), we show the peak rate of the excitatory population as a function of ω_{EE}, and ω_{IE}, where the green and purple circles indicate the points used to produce the curves in (b) (corresponding, respectively, to the used weak and strong LBA conditions)

To illustrate the mechanism of LBA, in Fig.2(c) we show the peak response of the excitatory population as a function of the internal couplings ω_{EE}, and ω_{IE}. The regions where the excitatory rate diverge are shown in gray. As it can be seen, a high increase of ω_{EE} destabilizes the circuit making its rate explode, however as ω_{IE} increases, larger values of ω_{EE} can be tolerated before triggering a rate instability. Remark that both the weak and strong LBA working points lie at the slightly sub-critical edge of this rate instability. We consider that the replication of this result was successful, despite one of the parameters in Table 2 had to be estimated.

	Weak LBA	Strong LBA
ω_{EI} [pA/Hz]	4.29	
ω_{II} [pA/Hz]	4.71	
β_E	1.00	
β_I	1.00	
$r_E(0)$ [Hz]	1.00	
$r_I(0)$ [Hz]	0.00	
τ [ms]	20.0	30.0
ω_{EE} [pA/Hz]	4.45	6.00
ω_{IE} [pA/Hz]	4.70	6.70

Table 2. Parameters used in Eq. 2 to produce the results in Fig. 2. For the parameters in red we could not find a value in the original publication and we had therefore to guess values allowing the reproduction of the published results. Note that we have used $\tau_E = \tau_I = \tau$.

Missing parameters: τ.

3.2 Global Balanced Amplification in the Large-Scale Model Improves Signal Propagation

Next, we study the propagation of an input pulse in the network composed of 29 cortical areas [4] (Section 2.1), where each node comprises an E and I population of rate based model (Section 2.2). All the parameters used for the model are given in Table 3.
In Fig. 3(a,b) we show a schematic representation of the connection between two cortical areas, for the weak and strong GBA cases. The increase in μ_{EE} and ω_{IE} for the strong GBA conditions is represented by the thickness of the arrows for these connections in Fig. 3(b).
For each area i a background input is inject to the excitatory ($I^i_{BG,E}$) and inhibitory ($I^i_{BG,I}$) populations in order to maintain a background rate of $r_E^{\text{BG}} = 10$ Hz in the first and $r_I^{\text{BG}} = 35$ Hz in the latter. The initial firing rates are set as being equal to the background rate.
To compute $I^i_{BG,E}$ and $I^i_{BG,I}$, first let $\boldsymbol{W}_{EE}$, $\boldsymbol{W}_{IE}$, $\boldsymbol{W}_{EI}$ and $\boldsymbol{W}_{II}$ be square matrices with size N_{areas}. Then, using M^{ij} to denote the element in row i and column j from a given matrix M, we can compute each element from those matrices as:

$$W_{EE}^{ij} \Rightarrow \begin{cases} \mu_{EE}(1+\eta h_i)\text{FLN}_{ji}, \text{ if } i \neq j, \\ -1 + \omega_{EE}(1+\eta h_i), \text{ if } i = j, \end{cases} \tag{20}$$

$$W_{IE}^{ij} \Rightarrow \begin{cases} 0, \text{ if } i \neq j, \\ -\omega_{IE}, \text{ if } i = j, \end{cases} \tag{21}$$

$$W_{EI}^{ij} \Rightarrow \begin{cases} \mu_{EI}(1+\eta h_i)\text{FLN}_{ji}, \text{ if } i \neq j, \\ \omega_{EI}(1+\eta h_i), \text{ if } i = j, \end{cases} \tag{22}$$

and,

$$W_{II}^{ij} \Rightarrow \begin{cases} 0, \text{ if } i \neq j, \\ -1 + \omega_{II}, \text{ if } i = j. \end{cases} \tag{23}$$

Next we define the square matrix $\boldsymbol{A}$ with size $2N_{\text{areas}}$:

$$\boldsymbol{A} = \begin{bmatrix} \boldsymbol{W}_{EE} & \boldsymbol{W}_{IE} \\ \boldsymbol{W}_{EI} & \boldsymbol{W}_{II} \end{bmatrix}, \tag{24}$$

and $\boldsymbol{B}$ a matrix with dimensions $[2N_{\text{areas}}, 1]$, where $B^i = r_E^{\text{BG}}$ for $i < N_{\text{areas}}$, otherwise $B^i = r_I^{\text{BG}}$. The background currents are computed as:

$$\boldsymbol{I}_{BG} = -\boldsymbol{A} \times \boldsymbol{B}, \tag{25}$$

where $\times$ is the matrix multiplication, $I^i_{BG,E}$, and $I^i_{BG,I}$ are given by:

$$\begin{cases} I^i_{BG,E} = I^i_{BG}, \text{ if } i < N_{\text{areas}}, \\ I^{i-N_{\text{areas}}}_{BG,I} = I^i_{BG}, \text{ if } i \geq N_{\text{areas}}. \end{cases} \tag{26}$$

Such procedure lead to determine parameters associated to the steady-state working point of the network. For exact derivation, of Eq. 26 see [5] star methods section.
To simulate the signal propagation, an input is injected in the excitatory population of the primary visual cortex (V1) for $t_{\text{durr}} = 225$ ms, from $t_i = 200$ ms to $t_f = 225$ ms. For

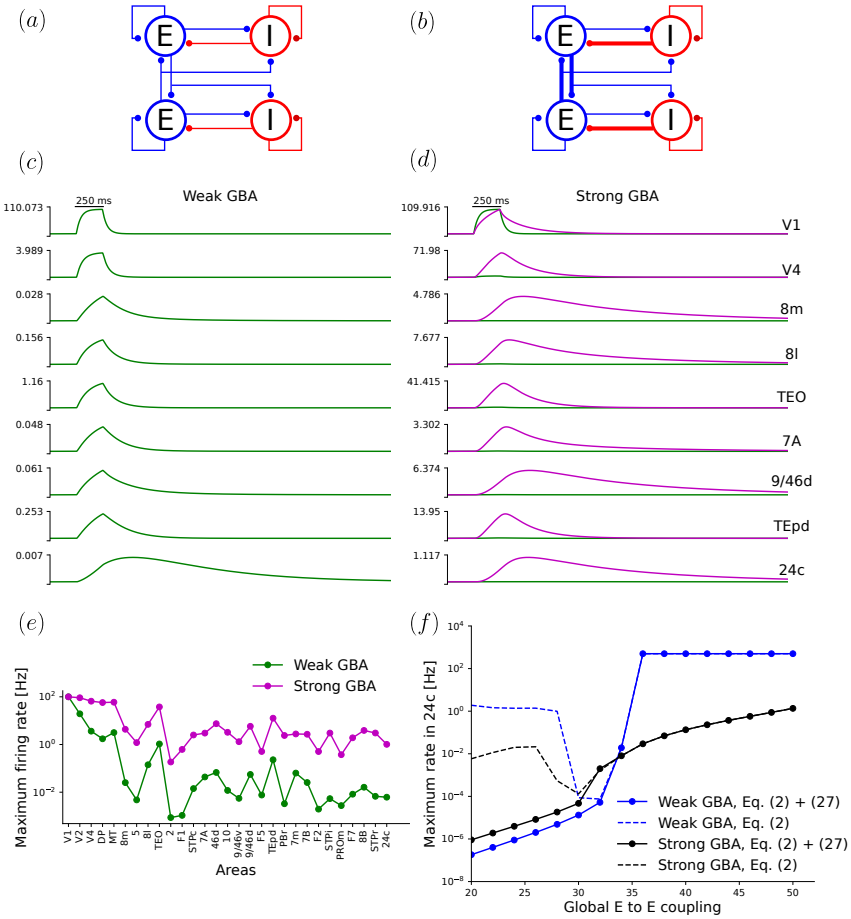

Figure 3. Reproduction of Figure 3 from the original paper [5]. In (a) and (b), we show inter-regional coupling within the large-scale connectome model for the regimes of weak and strong Global Balanced Amplification (GBA). In (c) and (d), we show propagating pulses of response to a stimulus injected in region V1, in regions with increasing hierarchy. Responses in (d) are sustained for longer times in certain regions and stronger in amplitude (the green lines in (d) correspond to the lines in (c), remark the changed vertical time-scale). The increase in peak response in strong vs weak GBA is also visualized for all regions in (e), in (f) we show the maximum excitatory rate at area 24c for weak (blue) and strong (black) GBA, the solid lines correspond to the simulations using the correction given by Eq. 27.

the weak GBA the input injected in V1 was $I^{\mathrm{V1}}_{\mathrm{inj,E}} = 41.90$ pA/Hz and for the strong GBA $I^{\mathrm{V1}}_{\mathrm{inj,E}} = 21.93$ pA/Hz.
The input injected to area V1 is attenuated of factor larger than $10,000$ times as it reaches area 24c in the weak GBA, while for the strong GBA the attenuation is approximately of only 100 times (Fig. 3(c,d)). The enhancement in signal propagation can also be tracked by looking at the peak firing rate in each cortical area after the input was injected in V1. In Fig. 3(e), we show the peak response rate in each region for both the weak and strong GBA regimes. The plot is in logarithmic scale manifesting the large level of boosted propagation to higher hierarchical order areas.
Finally, in Fig. 3(f), we measured the maximum response firing rate in area 24c (highest hierarchical order) as a function of the long-range coupling scale μ_{EE}, the the weak and strong GBA cases. For both conditions, we use the same parameters as for the weak GBA in Fig. 3(c), and the values of μ_{EE} used go from 20 pA/Hz to 50 pA/Hz with a step of 2 pA/Hz. For the strong GBA we have increased ω_{IE} using the following rule: $\omega_{IE} = 19.7 + 0.31\mu_{EE}$, that was set manually based on the ranges used in their Matlab source code (see bellow).
The first result we obtained is shown by the dashed lines in Fig. 3(f). For values of $\mu_{EE} < 30$ pA/Hz, the obtained result diverged from the original one and we obtained greater peak firing rates in area 24c.
We were able to retrieve the original results, shown in solid lines in Fig. 3(f), by introducing the following condition while solving the rate equations numerically:

$$\text{If } r_{E,I}(t) < r^{\mathrm{BG}}_{E,I}, \text{ then } r_{E,I}(t) = r^{\mathrm{BG}}_{E,I}. \tag{27}$$

This condition was not mentioned in the original article. However it was found in the Matlab implementation of the model that we cited in the section "Availability of code implementations for the original model".
Such adjustment guarantees that the firing rates of any population in the model do not go below their baseline activity, causing some of the populations to be effectively "switched off". In absence of this condition, some of the inhibitory populations would become too silent, reducing the overall level of inhibition and thus causing some rates to increase in an unbalanced way (hence the larger peak response rate in area 24c).
The condition in Eq. 27 was not mentioned in the original publication. In order to be able to reproduce this result we made a modification to NEST source code, adding the possibility to set the condition given in Eq. 27 as an option for the rate model available in NEST. This resulted in a pull-request that was integrated as the model "threshold_lin_rate" in NEST from version 3.0 [14]. For this reason it is recommended to use this updated version when attempting to run our simulation codes.
Overall, we were able to replicate the behavior of the reference model. However, concerning the specific result of Fig. 3(f), the original result could be reproduced only adding the ad hoc but reasonable condition in Eq. 27.

3.3 Reliable Signal Propagation in a Spiking Network Model

Next, we continue the analysis of the propagation of an input signal in the large-scale model, but replacing the rate units with the regional spiking network model described in Section 2.3.
We study signal propagation in the spiking large-scale model for two different regimes of the network: (i) asynchronous and (ii) synchronous. In both cases, we perform simulations in both the weak and strong GBA conditions. The parameters for (i) and for (ii) are given in Table 5.
The activity of the network is driven by independent white noise background currents injected in all neurons, and given by Eq. 28.

$$I^{i}_{BG,E,I} = \mu_{V,E,I}\frac{C_{E,I}}{\tau_{E,I}} + \sigma_V \frac{C_{E,I}}{\tau_{E,I}}\frac{1+e^{-dt/\tau_{E,I}}}{1-e^{-dt/\tau_{E,I}}}\xi(t), \tag{28}$$

where μ_V is the average value of the membrane potential, σ_V is the standard deviation of the noise, both in mV, and $\xi(t)$ is a Gaussian variable with zero mean and unit variance. In the original paper, the authors mention that a background input was given to the network in order to maintain the spiking activity of the excitatory population between 0.75 and 1.5 Hz and the inhibitory population between 5 and6 Hz. Although the authors did not specify the background noise parameters, the model equations found in their Brian2 code take the form $dV/dt = f(V) + (\sigma/\tau)\xi(t)$ ("rishimodelpython_brian2_spiking.py"), lines 137 and 141). We converted the values of σ set on their code using Eq. 28. However, some adjustments of the parameters were required to reproduce the specified steady-state rates (Table 4).
To study signal propagation we injected an external current pulse into all excitatory neurons in V1 ($I^{\mathrm{V1}}_{\mathrm{inj,E}}$). In the next two sessions we show the results for the asynchronous and synchronous regimes.

Asynchronous regime — For the asynchronous regime we injected an input pulse $I^{\mathrm{V1}}_{\mathrm{inj,E}}$ for $t_{\mathrm{durr}} = 150$ ms, from $t_i = 500$ ms to $t_f = 650$ ms. For the weak GBA $I^{\mathrm{V1}}_{\mathrm{inj,E}} = 300$ pA, and for the strong GBA $I^{\mathrm{V1}}_{\mathrm{inj,E}} = 126$ pA.
In Fig. 4(a,b) we show the raster plot (only excitatory neurons within each area are shown) for the weak and strong GBA conditions. Our result is very similar to the original one. For the weak GBA condition, the signal propagates to a few areas only along the ventral visual stream: V1, V2, V4, TEO and TEpd. In the strong GBA condition, the response to the input injected in V1 is enhanced in those areas, and other areas are reached as well such as: 7A, 46d, 7m and 7B. The arrival time in each area varies due to the used synaptic inter-areal delays in long-range connections.
To show the propagation of the signal to other areas, in Fig. 4(c) we measure the peak excitatory firing rate between t_i and $t_f + 20$ ms. The maximum firing rates are plot in logarithmic scale and one can observe that they indeed increase for the strong GBA condition, with a near-perfect quantitative matching with the original figure in [5]. The results about signal propagation in the large-scale spiking network model in the asynchronous regime are reproduced in our NEST model.

Synchronous regime — For the synchronous regime we injected an input pulse $I^{\mathrm{V1}}_{\mathrm{inj,E}}$ for $t_{\mathrm{durr}} = 8$ ms, from $t_i = 500$ ms to $t_f = 508$ ms. For the weak GBA $I^{\mathrm{V1}}_{\mathrm{inj,E}} = 200$ pA and for the strong GBA $I^{\mathrm{V1}}_{\mathrm{inj,E}} = 200$ pA.
We performed the same analyses as for the asynchronous case. In Fig. 5(a,b) we show the raster plot for the weak and strong GBA conditions. Qualitatively we got a result very similar to the original one, even though the maximum response rate per regions in Fig. 5(c) had some quantitative differences. Notably, the response amplification we obtained for hierarchically-intermediate regions as STPc, 7a, 46d and 10 was less strong than in the original model and we did not observe substantial amplification in the highest order regions as STPr and 24c. In general, all rates we obtained in early regions (V1, V2, V4, DP, MT) were stronger than expected.
We report in Fig. 5 a simulation with a good semi-quantitative match with the original results. However, we also noticed that the network is highly sensitive to the random seed used to initialize the simulation and this sensibility on initial conditions may explain the quantitative deviations between our response profile and the one shown in the original paper. It is important to note that NEST assigns different seeds to each thread used to simulate the network, therefore, using a different number of threads when running a parallel situation might change the result, making even more difficult to obtain

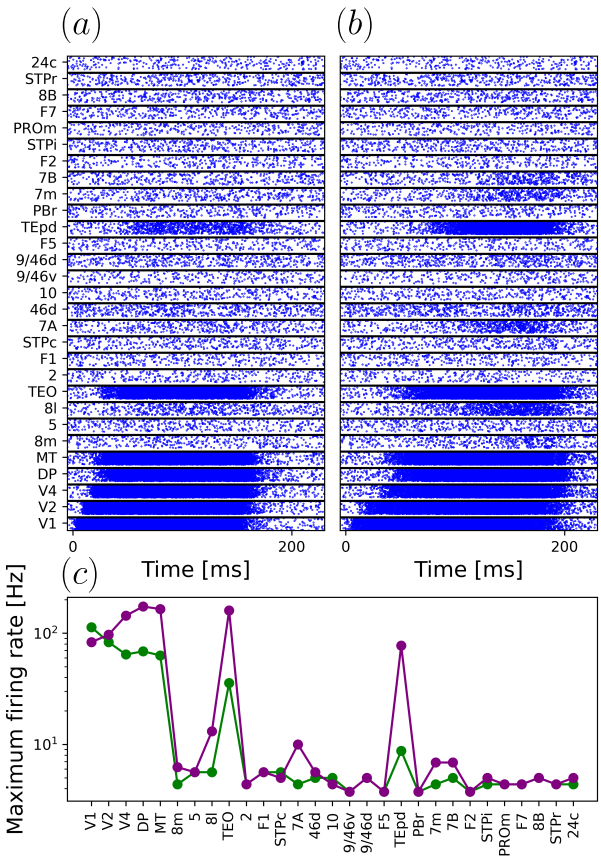

Figure 4. Signal propagation in the large-scale spiking neuron network in the asynchronous regime. In (a) we show the network response to a stimulus applied to V1 ($I^{\mathrm{V1}}_{\mathrm{inj,E}} = 300$ pA) during 150 ms in the weak GBA. In (b) we show the same but for the strong GBA condition ($I^{\mathrm{V1}}_{\mathrm{inj,E}} = 126$ pA). In (c) we show the peak response rate in each region along the cortical hierarchy, after the stimulus injection in V1 for the weak (green), and strong GBA (purple) conditions.

exactly the same raster when repeating the simulation multiple times (for our simulation we have used 20 threads). Furthermore, we noticed the same phenomenon when running the original Brian 2 code for this model (data not shown), which suggests this is not an issue of incorrectly fitting parameters but rather an intrinsic property of the model. Additionally, we noticed that in the authors' script the seed was fixed ("rishimodelpython_brian2_spiking.py", lines 30-32).

Further investigations revealed that the network activity depends on the state set for the random number generator. For Figs. 4-5, we run the simulations for a range of random seed values to obtain the expected results. However, changing their values could generate an unstable network. Especially, for the strong GBA and synchronous case, activity can become epileptic-like in some high-order regions, as shown in an example simulation in Fig. 6. Conversely, this dependence on initial conditions can generate instances in which the network is in a less excitable state, as a consequence activity may not reach areas such as PROm. In other cases, activity will reach even area 24c, without divergence of firing rates, if the network is in a slightly more excitable state.

This suggests, that the synchronous network may be sitting close to a rate instability. Tuning the system to be slightly subcritical is crucial for access to high-hierarchical

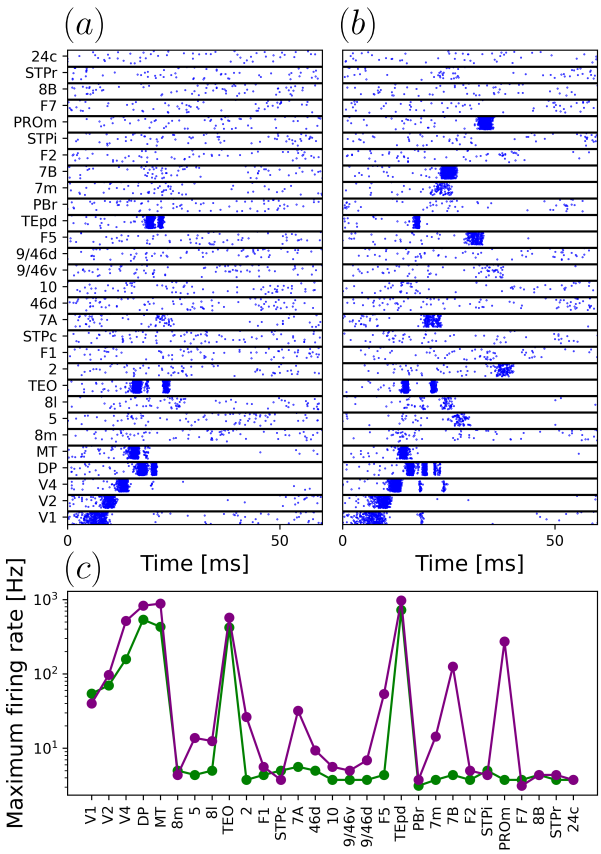

Figure 5. Signal propagation in the large-scale spiking neuron network in the synchronous regime. In (a) we show the network's response to a stimulus applied to V1 ($I^{\mathrm{V1}}_{\mathrm{inj,E}} = 200$ pA) during 8 ms in the weak GBA condition. In (b) we show the same but for the strong GBA condition ($I^{\mathrm{V1}}_{\mathrm{inj,E}} = 200$ pA). In (c), we show the peak frequency in each area after the stimulus injection in V1 for the weak (green), and strong GBA (purple) conditions.

order regions to take place, as an effect of enhanced GBA. However, we may have been using a too narrow safety margin, or an exceedingly strong input pulse. The simulations we show have been done with parameter choices providing the best a posteriori match we could find between reproduced and original simulations. However, some parameters had to be guessed, as previously mentioned, since we could not find where they are explicitly informed in the original paper, which makes our attempts of reproduction more complication as systematic parameter search in such a large-scale spiking model is beyond reach (or, anyway, too carbon-costly).

Notice that some in some early sensory regions (V1 to MT) the peak rates are an order of magnitude stronger than in the original paper. However, even considering that some key information to reproduce the model was missing (see Section 3.4) the main qualitative features of the original results (amplification and selective access to high-order ventral stream regions) are reproduced, we consider that, even in the synchronous regime, we have successfully reproduced the nature of results in the original paper.For

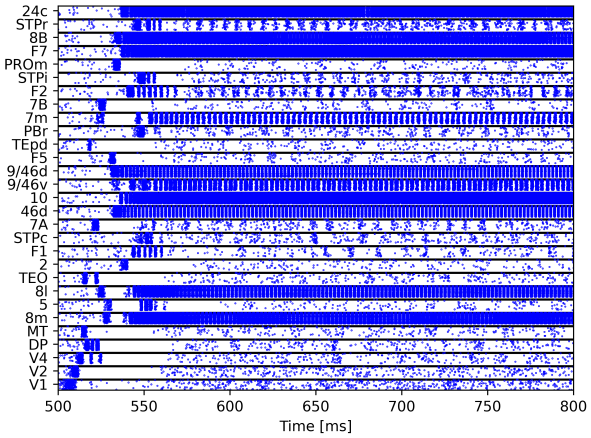

Figure 6. Raster plot for the synchronous regime network with strong GBA condition, with all parameters as in Fig. 5, but with a different choice of random seeds for the parallel simulation. This example raster manifests that, depending on the seed used, the network may become exceedingly unstable.

3.4 Important information needed during replication

In this section we list some information and parameter values that were needed to replicate the results, but were not found in the original article.

- The time constants τ_E and τ_I defined for the rate based model in Eq. 2 and used for the weak and strong GBA were not informed. For this work we made the approximation that $\tau = \tau_E = \tau_I$ and then we adjusted them by hand. The values that better fit the expected results are presented in Table 2.
- The values of ω_{IE} used for the strong GBA in Fig. 3(f) were not cited in the main reference and we estimated it by considering that ω_{IE} increases linearly with μ_{EE}: $\omega_{IE} = 19.7 + \alpha\mu_{EE}$, where 19.7 is the ω_{IE} used for the weak GBA and the parameter α was adjusted in order to obtain a result close to the original one. The value of α that gave the best approximation we could find was $\alpha \approx 0.31$.
- Another important information to reproduce the Figure 3 from the Joglekar et al. (2018) is the fact that we can only obtain the expected results if we include the minimum activity condition defined in Eq. 27 when solving the Eq. 2. However, this detail was not mentioned in the original article. In Fig. 3(f) we show the difference of the results by considering or not the condition defined in Eq. 27.
- The background noise needed to activate the spiking network model were not given in details in the reference article. The only information found were the mean firing rate ranges in the absence of input which are: 0.75 to 1.5 Hz for the excitatory population; and 5 to 6 Hz for the inhibitory population. To try to obtain these firing rates we used, by simplicity, white noise background currents independently injected into every neuron, as described by Eq. 28 (the average firing rates of the network in the absence of stimuli are shown in Table 4 for each condition, all the values are in the range cited in the original publication). The parameters of this white noise currents were adjusted manually (systematic optimization out of reach for such a massive model) and the values are presented in Table 5.
- Considering the approximations made for the spiking network model, we found that rate instabilities could eventually be induced by specific choices of seeds for

generating random numbers. And that in some conditions, the peak firing rate of some areas could reach one order of magnitude more than the ones reported in the original paper. This sensitivity is particularly evident in simulations conducted in the high synchrony, strong GBA case. As we shown in Fig. 4 and 5 we were nevertheless able to replicate the results of Figures 5 and 6 from Joglekar et al. (2018). However, simulations were unstable for some random seeds.

- The results obtained may depend on both the Python and Nest version used, since the RNG algorithms and C compiler used by NEST can influence the results. Since the number of threads used to run the code also changes the seeds assigned to each parallel executer, this can also impact on the results resulting in slightly different outcomes.

4 Conclusion

Using the NEST simulator to re-implement the original model we were able to reproduce the main results of the original article [5], at least in their qualitative essence and, often, also in precise quantitative match. In general, our results confirm the validity of the central concepts of the original paper, notably about the role of balanced amplification mechanisms in enhancing signal propagation while guaranteeing network stability.
In our replication, we also pointed some difficulties to reproduce the original model. All of them suggest that the "sweet spot" needed for strong LBA and GBA to properly work is more difficult than estimated to obtain, as variations in the exact rate of specific regions and transient loss of E/I balance within them could compromise the delicate equilibrium between excitatory boosting and inhibitory stabilization. Thus, from our reproduction attempts, we also learn that it may be important for physiological networks to embed regulatory mechanisms that help maintaining the network operation point close to this desired sweet-spot. Such role may be played for instance by neuromodulatory or homeostatic plasticity processes [15, 16], not included in simple mechanistic models as the one we reproduce here.
In this context in which a careful fine tuning seems to be needed for perfect functionality, we suffered particularly of the lack of information about some of the parameters (or, at least, of our unsuccessful attempts to find this information). We do not exclude thus that with other, more adapted parameter choices the robustness of GBA-mediated signal propagation gets further strengthened.

5 Acknowledgements

DB acknowledges the organizers of the Latin American School on Computational Neuroscience (LASCON VIII, Sao Paulo, Brazil), since the idea of performing this replication was born during discussions in the context of this school where he had kindly been invited. DB and VL are supported by the Maria Skłodowska-Curie action program of the European Union under the Innovative Training Network "iConn" (H2020 ITN 859937). R.O.S. thanks financial support from São Paulo Research Foundation (FAPESP), grant 2017/07688-9. This study was financed in part by the Coordenação de Aperfeiçoamento de Pessoal de Nível Superior - Brasil (CAPES) - Finance Code 001. ACR is supported by the São Paulo Research Foundation (FAPESP) grant 2013/07699-0 (CEPID NeuroMat) and by Brazilian National Council for Scientific and Technological Development (CNPq) Research Productivity Grant 303359/2022-6. N.L.K. thanks financial support from São Paulo Research Foundation (FAPESP), grant 2016/03855-5.

References

1. M. C. van Rossum, G. G. Turrigiano, and S. B. Nelson. "Fast propagation of firing rates through layered networks of noisy neurons." In: **Journal of neuroscience** 22.5 (2002), pp. 1956–1966. DOI: 10.1523/JNEUROSCI.22-05-01956.2002. URL: https://doi.org/10.1523/JNEUROSCI.22-05-01956.2002.
2. A. Kumar, S. Rotter, and A. Aertsen. "Conditions for propagating synchronous spiking and asynchronous firing rates in a cortical network model." In: **Journal of neuroscience** 28.20 (2008), pp. 5268–5280. DOI: 10.1523/JNEUROSCI.2542-07.2008. URL: http://dx.doi.org/10.1523/JNEUROSCI.2542-07.2008.
3. A. Kumar, S. Rotter, and A. Aertsen. "Spiking activity propagation in neuronal networks: reconciling different perspectives on neural coding." In: **Nature reviews neuroscience** 11.9 (2010), pp. 615–627. DOI: 10.1038/nrn2886. URL: http://dx.doi.org/10.1038/nrn2886.
4. N. T. Markov, M. Ercsey-Ravasz, A. Ribeiro Gomes, C. Lamy, L. Magrou, J. Vezoli, P. Misery, A. Falchier, R. Quilodran, M. Gariel, et al. "A weighted and directed interareal connectivity matrix for macaque cerebral cortex." In: **Cerebral cortex** 24.1 (2014), pp. 17–36. DOI: 10.1093/cercor/bhs270. URL: http://dx.doi.org/%2010.1093/cercor/bhs270.
5. M. R. Joglekar, J. F. Mejias, G. R. Yang, and X.-J. Wang. "Inter-areal balanced amplification enhances signal propagation in a large-scale circuit model of the primate cortex." In: **Neuron** 98.1 (2018), pp. 222–234. DOI: 10.1016/j.neuron.2018.02.031. URL: http://dx.doi.org/10.1016/j.neuron.2018.02.031.
6. G. Elston. "Specialization of the Neocortical Pyramidal Cell during Primate Evolution." In: **Evolution of Nervous Systems**. Ed. by J. H. Kaas. Oxford: Academic Press, 2007, pp. 191–242. DOI: 10.1016/B0-12-370878-8/00164-6. URL: http://dx.doi.org/10.1016/B0-12-370878-8/00164-6.
7. R. Chaudhuri, K. Knoblauch, M.-A. Gariel, H. Kennedy, and X.-J. Wang. "A large-scale circuit mechanism for hierarchical dynamical processing in the primate cortex." In: **Neuron** 88.2 (2015), pp. 419–431. DOI: 10.1016/j.neuron.2015.09.008. URL: http://dx.doi.org/10.1016/j.neuron.2015.09.008.
8. J. F. Mejias, J. D. Murray, H. Kennedy, and X. J. Wang. "Feedforward and feedback frequency-dependent interactions in a large-scale laminar network of the primate cortex." In: **Sci. Adv,** 2 (2016), e1601335. DOI: 10.1126/sciadv.1601335. URL: http://dx.doi.org/10.1126/sciadv.1601335.
9. M. Stimberg, R. Brette, and D. F. Goodman. "Brian 2, an intuitive and efficient neural simulator." In: **Elife** 8 (2019). DOI: 10.7554/eLife.47314. URL: http://dx.doi.org/10.7554/eLife.47314.
10. M.-O. Gewaltig and M. Diesmann. "Nest (neural simulation tool)." In: **Scholarpedia** 2.4 (2007), p. 1430.
11. J. Jordan, R. Deepu, J. Mitchell, J. M. Eppler, S. Spreizer, J. Hahne, E. Thomson, I. Kitayama, A. Peyser, T. Fardet, et al. **NEST 2.18. 0**. Tech. rep. Jülich Supercomputing Center, 2019.
12. N. T. Markov et al. "The role of long-range connections on the specificity of the macaque interareal cortical network." English. In: **Proceedings of the National Academy of Sciences of the United States of America** 110.13 (Mar. 2013), p. 5187 5192. DOI: 10.1073/pnas.1218972110.
13. H. A. Swadlow. "Efferent neurons and suspected interneurons in S-1 forelimb representation of the awake rabbit: receptive fields and axonal properties." In: **Journal of Neurophysiology** 63.6 (1990), pp. 1477–1498. DOI: 10.1152/jn.1990.63.6.1477. URL: http://dx.doi.org/10.1152/jn.1990.63.6.1477.
14. J. Hahne et al. **NEST 3.0**. Version 3.0. June 2021. DOI: 10.5281/zenodo.4739103. URL: https://doi.org/10.5281/zenodo.4739103.
15. J. M. Shine. "Neuromodulatory Influences on Integration and Segregation in the Brain." In: **Trends in Cognitive Sciences** 23.7 (2019), pp. 572–583. DOI: 10.1016/j.tics.2019.04.002.
16. P. J. Sjöström, G. G. Turrigiano, and S. B. Nelson. "Rate, timing, and cooperativity jointly determine cortical synaptic plasticity." eng. In: **Neuron** 32.6 (Dec. 2001), pp. 1149–1164. DOI: 10.1016/s0896-6273(01)00542-6.

	Weak GBA	Strong GBA
ω_{EI} [pA/Hz]	12.5	
ω_{II} [pA/Hz]	12.5	
ω_{EE} [pA/Hz]	24.3	
μ_{EI} [pA/Hz]	25.3	
β_E/β_I	0.066/0.351	
r_E^{BG}/r_I^{BG} [Hz]	10/35	
$r_E(0)/r_I(0)$ [Hz]	10/35	
τ_E/τ_I[ms]	20/10	
η	0.68	
τ_i/τ_f [ms]	200/225	
ω_{IE} [pA/Hz]	19.7	25.2
μ_{EE} [pA/Hz]	33.7	51.5
$I_{inj,E}^{V1}$ [pA/Hz]	41.90	21.93

Table 3. Parameters used for the large-scale rate based model described in Section 2.2.3, to produce the results in Fig. 3.

Weak GBA		
Firing rate [Hz]	Asynchronous	Synchronous
Excitatory	1.30	0.83
Inhibitory	5.59	5.62
Strong GBA		
Excitatory	1.49	0.82
Inhibitory	5.99	5.52

Table 4. Average firing rate for each cell population type and each network state.

	Asynchronous		Synchronous	
	Weak GBA	Strong GBA	Weak GBA	Strong GBA
ω_{EI} [mV]	0.075		0.3	
ω_{II} [mV]	0.075		0.3	
ω_{EE} [mV]	0.01		0.04	
μ_{EI} [mV]	0.19/4		0.19	
d [ms]	2.0		2.0	
η	4.0		4.0	
$\mu_{V,E}$ [mV]	284.0		308.0	320.0
$\mu_{V,I}$ [mV]	314.0		280.0	
σ_V [mV]	2.12		2.12	
t_{durr} [ms]	150.0		8.0	
ω_{IE} [mV]	0.0375	0.05	0.56	0.98
μ_{EE} [mV]	0.0375	0.05	0.16	0.25
$I_{\text{inj,E}}^{\text{V1}}$ [pA]	300	126	200	200

Table 5. Parameters used for the spiking neuron networks in the asynchronous , and synchronous regimes , and for strong, and weak GBA for both regimes. For the parameters indicated in red, we could not find corresponding values in the original paper, therefore we had to estimate their values to guarantee a semi-quantitative matching between our reproduced and the original results. Systematic optimization is out-of-reach for such a complex large-scale spiking model.
Missing parameters: $\mu_{V,E}$, $\mu_{V,I}$, σ_V.

B. Frites : A Python package for functional connectivity analysis and group-level statistics of neurophysiological data

---

The Journal of Open Source Software

Frites: A Python package for functional connectivity analysis and group-level statistics of neurophysiological data

Etienne Combrisson [1], **Ruggero Basanisi** [1], **Vinicius Lima Cordeiro** [1,2], **Robin A. A Ince** [3], **and Andrea Brovelli** [1]

1 Institut de Neurosciences de la Timone, Aix Marseille Université, UMR 7289 CNRS, 13005, Marseille, France **2** Institut de Neurosciences des Systèmes, Aix-Marseille Université, UMR 1106 Inserm, 13005, Marseille, France **3** Institute of Neuroscience and Psychology, University of Glasgow, Glasgow, UK

DOI: 10.21105/joss.03842

Software

- Review
- Repository
- Archive

Editor: Marie E. Rognes

Reviewers:

- @madvn
- @travisbthomp

Submitted: 21 September 2021
Published: 11 November 2022

License
Authors of papers retain copyright and release the work under a Creative Commons Attribution 4.0 International License (CC BY 4.0).

Summary

The field of cognitive computational neuroscience addresses open questions regarding the complex relation between cognitive functions and the dynamic coordination of neural activity over large-scale and hierarchical brain networks. State-of-the-art approaches involve the characterization of brain regions and inter-areal interactions that participate in cognitive processes (Battaglia & Brovelli, 2020). More precisely, the study of cognitive brain networks underlies linking local neural activity or interactions between brain regions to experimental variables, such as sensory stimuli or behavioral responses. The relation between the brain data and external variables might take complex forms (e.g. non-linear relationships) with strong variations across brain regions and participants. Therefore, powerful measures of information are required to detect complex relations and the statistical relevance at the population level should be able to adapt to the inter subject variability.

Statement of need

`Frites` (*Framework for Information Theoretical analysis of Electrophysiological data and Statistics*) is an open-source Python package, designed for researchers and students with little programming knowledge and working on the discovery of cognitive brain networks using neurophysiological data. It combines in a single framework information-based analyses of neurophysiological recordings and group-level statistical inference that can adapt to the inherent variability across participants. The measures of information and the group-level statistics functionalities are wrapped into high-level workflows. In addition, `Frites` also includes several measures of functional connectivity (FC) for measuring pairwise interactions between brain regions. To the best of our knowledge, `Frites` is the only Python software combining information-theoretical approaches with flexible group-level analyses for the discovery of cognitive brain networks.

Supported neurophysiological recordings and link with other softwares

`Frites` is suitable for the analysis of continuous and multi-channel neurophysiological data, encompassing non-invasive recordings with uniform spatial sampling (e.g., M/EEG data) such as invasive and spatially sparse recordings, such as intracranial EEG or Local Field Potentials (LFPs). The package supports standard `NumPy` array inputs (Harris et al., 2020), neuro-oriented objects from the `MNE-Python` software (Gramfort et al., 2013), but also multi-dimensional labelled `Xarray` objects (Hoyer & Hamman, 2017).

Measures of information and group-level statistics

Frites is equipped with a set of information theoretic tools for the analysis of interactions between brain signals and their relation with experimental task-related variables. By default, Frites is using the Gaussian Copula Mutual-Information (Ince et al., 2017) to study the relation between either local brain activity, cross-frequency coupling (Combrisson et al., 2020) or inter-areal FC with experimental variables (i.e., cognitive tasks). For what concerns FC, the toolbox allows the estimate of dynamic (i.e., time-resolve) (Brovelli et al., 2017), undirected (e.g., mutual information) and directed (e.g., Granger causality) FC on a single-trial basis (Brovelli et al., 2015). The networks built from the FC can then be further analyzed using graph-theoretical approaches from the Brain Connectivity Toolbox (Rubinov & Sporns, 2010). Nevertheless, Frites is not limited to the included estimators as the definition of custom ones is also supported, such as IDTxl kernel methods (Wollstadt et al., 2019), infotheory information decomposition (Candadai & Izquierdo, 2019) or scikit-learn cross-validated classifiers (Pedregosa et al., 2011). The estimated information can then be combined with the group-level statistics for the identification of feature-specific networks. While Frites is strongly oriented toward neuroscience applications, the estimators of information are agnostic to data types and can therefore be applied to different fields.

For statistical inferences, the package integrates a non-parametric permutation-based statistical framework (Maris & Oostenveld, 2007) to perform group-level inferences on non-negative measures of information. The toolbox includes different methods that cope with multiple-comparison correction problems, such as test- and cluster-wise p-value corrections. The implemented framework also supports both fixed- and random-effect models to adapt to inter-individuals and inter-sessions variability (Combrisson et al., 2022).

Workflows

Frites provides a set of workflows that integrate several analysis steps. Those workflows take as inputs the neural data coming from single or multi-participants (or single / multi sessions), estimate the amount of information shared between the brain data and the external variable, at each brain region and time bins, and finally perform network-level statistical inference, corrected for multiple comparisons. Those high-level workflows are particularly useful for users with no or little programming knowledge as all of those steps can be performed in a very few lines of code, with standard inputs like MNE-Python epochs.

Performance

Several computations implemented in the workflows, such as permutation tests, are computationally demanding. To decrease computing time, the core functions for information measures exploit a NumPy tensor-based implementation or can be accelerated using the Numba compiler (Lam et al., 2015). Then, Frites natively supports parallel processing using the Joblib package.

Acknowledgements

EC and AB were supported by the PRC project "CausaL" (ANR-18-CE28-0016). This project/research has received funding from the European Union's Horizon 2020 Framework Programme for Research and Innovation under the Specific Grant Agreement No. 945539 (Human Brain Project SGA3). RB acknowledges support through a PhD Scholarship awarded by the Neuroschool. This work has received support from the French government under the Programme Investissements d'Avenir, Initiative d'Excellence d'Aix-Marseille Université via A*Midex (AMX-19-IET-004) and ANR (ANR-17-EURE-0029) funding. RAAI was supported by the Wellcome Trust [214120/Z/18/Z]. VLC is supported by a scholarship from the European

Union's Horizon 2020 research and innovation programme under the Marie Sk lodowska-Curie grant agreement No 859937.

References

Battaglia, D., & Brovelli, A. (2020). Functional connectivity and neuronal dynamics: Insights from computational methods. *The Cognitive Neurosciences*. https://doi.org/10.7551/mitpress/11442.001.0001

Brovelli, A., Badier, J.-M., Bonini, F., Bartolomei, F., Coulon, O., & Auzias, G. (2017). Dynamic Reconfiguration of Visuomotor-Related Functional Connectivity Networks. *The Journal of Neuroscience*, *37*(4), 839–853. https://doi.org/10.1523/JNEUROSCI.1672-16.2016

Brovelli, A., Chicharro, D., Badier, J.-M., Wang, H., & Jirsa, V. (2015). Characterization of Cortical Networks and Corticocortical Functional Connectivity Mediating Arbitrary Visuomotor Mapping. *The Journal of Neuroscience*, *35*(37), 12643–12658. https://doi.org/10.1523/jneurosci.4892-14.2015

Candadai, M., & Izquierdo, E. J. (2019). Infotheory: A c++/python package for multivariate information theoretic analysis. *arXiv Preprint arXiv:1907.02339*. https://doi.org/10.21105/joss.01609

Combrisson, E., Allegra, M., Basanisi, R., Ince, R. A. A., Giordano, B. L., Bastin, J., & Brovelli, A. (2022). Group-level inference of information-based measures for the analyses of cognitive brain networks from neurophysiological data. *NeuroImage*, *258*, 119347. https://doi.org/10.1016/j.neuroimage.2022.119347

Combrisson, E., Nest, T., Brovelli, A., Ince, R. A. A., Soto, J. L. P., Guillot, A., & Jerbi, K. (2020). Tensorpac: An open-source Python toolbox for tensor-based phase-amplitude coupling measurement in electrophysiological brain signals. *PLoS Computational Biology*, *16*(10), e1008302. https://doi.org/10.1371/journal.pcbi.1008302

Gramfort, A., Luessi, M., Larson, E., Engemann, D. A., Strohmeier, D., Brodbeck, C., Goj, R., Jas, M., Brooks, T., Parkkonen, L., & Hämäläinen, M. S. (2013). MEG and EEG data analysis with MNE-Python. *Frontiers in Neuroscience*, *7*(267), 1–13. https://doi.org/10.3389/fnins.2013.00267

Harris, C. R., Millman, K. J., Walt, S. J. van der, Gommers, R., Virtanen, P., Cournapeau, D., Wieser, E., Taylor, J., Berg, S., Smith, N. J., & others. (2020). Array programming with NumPy. *Nature*, *585*(7825), 357–362.

Hoyer, S., & Hamman, J. (2017). Xarray: ND labeled arrays and datasets in Python. *Journal of Open Research Software*, *5*(1). https://doi.org/10.5334/jors.148

Ince, R. A. A., Giordano, B. L., Kayser, C., Rousselet, G. A., Gross, J., & Schyns, P. G. (2017). A statistical framework for neuroimaging data analysis based on mutual information estimated via a gaussian copula: Gaussian Copula Mutual Information. *Human Brain Mapping*, *38*(3), 1541–1573. https://doi.org/10.1002/hbm.23471

Lam, S. K., Pitrou, A., & Seibert, S. (2015). Numba: A LLVM-based Python JIT compiler. *Proceedings of the Second Workshop on the LLVM Compiler Infrastructure in HPC*, 1–6. https://doi.org/10.1145/2833157.2833162

Maris, E., & Oostenveld, R. (2007). Nonparametric statistical testing of EEG- and MEG-data. *Journal of Neuroscience Methods*, *164*(1), 177–190. https://doi.org/10.1016/j.jneumeth.2007.03.024

Pedregosa, F., Varoquaux, G., Gramfort, A., Michel, V., Thirion, B., Grisel, O., Blondel, M., Prettenhofer, P., Weiss, R., Dubourg, V., Vanderplas, J., Passos, A., Cournapeau, D.,

Brucher, M., Perrot, M., & Duchesnay, E. (2011). Scikit learn : Machine Learning in Python. *Journal of Machine Learning Research*, *12*, 2825–2830.

Rubinov, M., & Sporns, O. (2010). Complex network measures of brain connectivity: Uses and interpretations. *Neuroimage*, *52*(3), 1059–1069. https://doi.org/10.1016/j.neuroimage.2009.10.003

Wollstadt, P., Lizier, J. T., Vicente, R., Finn, C., Martinez-Zarzuela, M., Mediano, P., Novelli, L., & Wibral, M. (2019). IDTxl: The information dynamics toolkit xl: A python package for the efficient analysis of multivariate information dynamics in networks. *Journal of Open Source Software*, *4*(34), 1081. https://doi.org/10.21105/joss.01081